THE LATTICE MODEL OF PARTICLE TRANSPORT THROUGH NANO-CHANNELS

A DISSERTATION

SUBMITTED TO THE

DEPARTMENT OF PHYSICS

ADDIS ABABA UNIVERSITY

IN PARTIAL FULFILMENT

OF THE REQUIREMENT FOR THE

DEGREE OF DOCTOR OF PHILOSOPHY

IN

PHYSICS

BY

YITAGESU ELFAGD

ADDIS ABABA, ETHIOPIA

June 2014

ADDIS ABABA UNIVERSITY

DEPARTMENT OF PHYSICS

THE LATTICE MODEL OF PARTICLE TRANSPORT THROUGH NANO-CHANNELS

by

Yitagesu Elfagd

Approved by the the Examination Committee

Chairman: _____

External Examiner: _____

Internal Examiner: _____

Research Supervisor: _____

DECLARATION

I the undersigned declare that this PhD dissertation is my original work and has not been presented for a degree in any other university, and that all sources of material used for the dissertation have been duly acknowledged.

Author: ———————————————————-

Yitagesu Elfagd

This PhD dissertation has been submitted for examination with my approval as university advisor.

Research Supervisor: ———————————————————

Dr. Mulugeta Bekele

Place: Department of Physics, Addis Ababa University

Date: June 2014

TO MY

LORD

SAVIOR

STRENGTH

SHEPHERD

MOTIVATOR

TEACHER

JESUS CHRIST

Contents

List of Figures

Abstract

When membranes channels are very narrow so that their average diameters are comparable to the average size of the permeating particles, then two particles can't pass each other inside the channel. These molecular-sized channels are usually referred to as **nano-channels**. The research work presented in this thesis deals with the modeling of nano-channels, description of their transport properties and the channel gating mechanisms. As particles permeate through nano-channels, they interact with multiple weakly attractive and repulsive sites on the wall of the nano-channel, where the attractive sites act as potential wells and the repulsive sites act as potential barriers. In this thesis, the potential energy landscape of the internal wall of the entire length of the nano-channel is modeled as a spatial distribution of potential wells and potential barriers. Moreover, we considered the potential wells as the lattice sites of a one dimensional lattice with s lattice sites and particles permeating through nano-channels spend more time in the vicinity of these potential well sites. We assumed that between these potential wells, there are particle repelling sites or potential barriers that must be hopped by the permeating particles. Thus, the height of the potential barrier between the potential wells or lattice sites controls the rate of particle transport through nano-channels. The phenomenon of particle transport or diffusion through nano-channels is modeled as hopping of particles between nearest neighbor potential wells across the intervening potential barriers.

The occupation numbers that denote the lattice sites in the emitter and collector baths are η_e and η_c and the channel sites are η_i, where $i = 1, 2, ..., s$ with s denoting the total number of lattice sites. The average value of these internal and external occupation numbers lies in the range between zero and one. In

this work, we employ the discrete or lattice model of particle transport through nano-channels, which employs the Master equation formulation of the rate equations that describe the time rate of change of the average values of the occupation numbers associated with each lattice site. The effects of the potential barriers between the potential wells are taken into account via the forward and backward transition rates. These transition rates describe the rate of forward and backward hopping of a particle sitting at a given potential well across the intervening potential barriers.

In the first chapter, we have proposed a simple lattice model of nano-channels and simple expressions for the total rate at which particle are injected into and out of the nano-channel at the two end sites. In chapter two, starting from the Master equation of the rate equations and employing the steady state assumption and the mean filed approximation of the effective transition rates for both the internal and external sites, we have derived a general expression of the average particle flux through a nano-channel at steady state. The expression of the average particle flux is a multi variable function. That is, $J = J(n_e, n_c, \eta_e, \eta_c, \gamma_e, \gamma_c, \eta_1, ..., \eta_s, \gamma_1, ..., \gamma_s, k_e^+, k_c^-, k_1^-, ..., k_s^-, k_1^+, ..., k_s^+)$, where $\gamma_i = 1 - \eta_i$. The nano-channel is characterized by the channel parameters $\eta_1, ..., \eta_s, \gamma_1, ..., \gamma_s$, $k_1^-, ..., k_s^-$, $k_1^+, ..., k_s^+$. The effects of the emitter bath is taken into account via the bath parameters $n_e, \eta_e, \gamma_e, k_e^+$ and that of the collector bath via the bath parameters $n_c, \eta_c, \gamma_c, k_c^-$. In chapter three and four, we have presented a detailed description of the properties of a nano-channel with one and two internal potential wells, respectively.

Our results show that the average particle flux through a nano-channel as a function of Δn, for the specified values of the other parameters, is a rapidly increasing function of Δn for small and intermediate values. When $\Delta n = 0$, the average flux has a minimum value and as Δn increases to large values, the average particle flux through a nano-channel with both one and two internal potential wells increases slowly and finally enters into the saturation region in which it no longer increase as the concentration gradient increases. For most cases, the range of the concentration gradient in which the average particle flux becomes saturated lies between $1.0\ M$ and $10\ M$ for the specified values of the other parameters. Moreover, the average particle flux approaches more rapidly

to its saturation value when the external potential well V_e is occupied and the external potential well V_c is empty. The average particle flux as a function of Δn, through a nano-channel with a single internal potential well is greater than the average particle flux through a nano-channel with two internal potential wells, that is $J_1(\Delta n|\eta_e,\eta_c) > J_2(\Delta n|\eta_e,\eta_c)$.

Moreover, the average particle flux through a nano-channel, with one and two internal potential wells, as a function of the external occupation number η_e, for the specified values of the other parameters, is a rapidly increasing function of η_e for small values of η_e, usually $\eta_e \approx 0.2$ and after that it becomes saturated. When $\eta_e = 0$, the optimized particle flux assumes a minimum value and the nano-channel is in the inactivated state. When $\eta_e = 1$ the nano-channel becomes fully activated and as a result the average flux approaches a maximum positive value. Thus, η_e acts as a gating variable that controls the direction and magnitude of particle transport through a nano-channel. Moreover, the average particle flux as a function of η_c, for the specified values of the other parameters, approaches to a maximum positive value as $\eta_c \to 0$ and decreases as η_c increases and finally as $\eta_c \to 1$, the flux decreases to a small negative value. When $\eta_c = 0$, the average particle flux has a maximum positive value and the nano-channel is in the fully activated state and when $\eta_c = 1$ the nano-channel becomes fully inactivated and as a result the flux approaches a small negative value. Therefore, η_c also acts as a gating variable that controls the magnitude and direction of particle transport through a nano-channel.

In this thesis, we have also shown that the average values of the occupation numbers of the internal potential wells as a function of Δn, for the specified values of the other parameters, are rapidly increasing functions of Δn for small and intermediate values. When $\Delta n \to 0$, the average occupation numbers have small positive values and as Δn increases to large values, the average occupation numbers of the internal potential wells of a nano-channel with both one and two internal potential wells increase slowly and finally approach the saturation region in which they no longer increase as the concentration gradient increases. For most cases, the range of the concentration gradient in which these average occupation numbers become saturated lies between $1.0\ M$ and $10\ M$ for the specified values of the other parameters. Moreover, the average occupa-

tion numbers approach more rapidly to the saturation value when the external potential wells V_e and V_c are occupied. For a nano-channel with two internal potential wells, the average occupation number as functions of Δn of the internal potential well V_1 is greater than the average occupation number of the internal potential well V_2, that is $\eta_{12}(\Delta n|\eta_e,\eta_c) > \eta_{22}(\Delta n|\eta_e,\eta_c)$.

The average value of the occupation number of the internal potential well V_1 increases more rapidly as η_e increases and slowly as η_c increases. Similarly, the average value of the occupation number of the internal potential well V_2 increases more rapidly as η_c increases and slowly as η_e increases. As the average value of the occupation number of V_1 increases, the average value of the occupation number of V_2 also increases, and vice versa. The average value of the occupation number of V_1 increases as the values of the normalized potential barriers u_1^-, u_1^+ and u_2^+ increase and as u_e^+, u_2^- and u_c^- decrease. Similarly, the average value of the occupation number of V_2 increases as the values of the normalized potential barriers u_2^-, u_2^+ and u_1^- increase and as u_e^+, u_1^+ and u_c^- decrease.

ACKNOWLEDGMENTS

Throughout the long journey of this PhD work my heavenly father Jesus Christ is the source of my motivation, enthusiasm and determination. I have encountered so many obstacles during this long journey. But all the time my lord Jesus Christ encourages, motivates and enlightens me. Whenever I think of Him I become renewed and energized. I also get some Heavenly power and guidance. During those dark and difficult times He enlightens my eyes and fills me with His power. There is no word to express His help care and love for me. It surpasses our little mind and the expression of our language. The only thing I can say is what is written in the holy scripture: **I will praise You forever, Because You have done it; And in the presence of Your saints I will wait on Your name, for it is good**. PSALM 52: 9.

I am extremely grateful to Addis Ababa University for sponsoring me to do my PhD research here in Ethiopia. I am grateful for the financial support and all other assistances that I received from the University. May God Bless Addis Ababa University.

I would like to express my sincere thanks to my supervisor Dr. Mulugeta Bekele for his limitless and invaluable effort in guiding and supervising this work. I am very impressed by his friendly approach, continues encouragement, patience and stimulating guidance, his wide knowledge, enthusiasm for research and generosity of time towards students. I gained a lot of knowledge and experience from fruitful discussions I had with him. He gave me great academic freedom in my research which I hope will help me to gradually establish independent research ability. To work with him is really a great pleasure. I am hopeful that my relation with him will unfold through time. May God Bless him with His Heavenly Blessings.

I would also like to express my sincere thanks to Prof. Joanny. I traveled to Paris two times for one month and started my research work presented in this thesis. During my short time at the Curie Institute in Paris, I worked with Prof. Joanny, who facilitated and arranged all the financial and facilities for my research. In addition to this I have done my work intensively during this short

time and I had discussion with Prof. Joanny everyday. I am very impressed by his friendly approach, continues encouragement, patience and stimulating guidance, his wide knowledge, enthusiasm for research and generosity of time towards students. I gained a lot of knowledge and experience from fruitful discussions I had with him. To work with him is really a great pleasure. I am hopeful that my relation with him will unfold through time. I would also like to thank the Foundation Pierre-Gilles de Gennes for Research (FPGG). It is the FPGG who covered all the financial support for my visit to Curie Institute. May God Bless Prof. Joanny and DeGennes foundation with His Heavenly Blessings.

I would also like to express my gratitude to Physics department of Addis Ababa University particularly to the special colleagues who have served as the department chairmen during the period of my PhD study; Dr. Tilahun Tesfaye, Dr Gizaw Mengistu, Dr Lemi Demeyu, Dr. Belayneh Mesfin for the support and encouragement. I would also like to thank W/ro. Tselat Adinew, the secretary of the department of physics for her friendly approach, encouragement and providing me all the facilities that I needed from the department for my work. I would also like to thank all the staff members of the department of physics for friendly approach and love. May God Bless you with His Heavenly Blessings.

I would also like to thank Dr Tatek Yergou and His PhD student Solomon for the fruitful discussions that I had with them. During our discussions, they provided me with some useful ideas that helped me plot the graphs at the final stage of the research work. May God Bless you with His Heavenly Blessings.

At the last, but certainly not the least I am deeply indebted to my precious family. May God Bless you with His Heavenly Blessings.

Yitagesu Elfagd, Addis Ababa, Ethiopia

June 2014

1

MODEL AND THEORY OF NANO-CHANNELS

1.1 Introduction

The protein channels of cellular membranes support and regulate the fluxes of various ionic and metabolic molecules that are critical for proper cell functioning Ref. (1; 2; 3; 4). When the Protein channels embedded in membranes are very narrow so that their average diameters are comparable to the average size of the molecules that permeate through these molecular sized channels, then two particles can't pass each other inside the channel. These molecular-sized or nano-sized channels are usually referred to as **nano-channels** or **molecular-channels** or **one-dimensional channels**. In this thesis, we preferred to use the term nano-channels to describe these molecular sized protein channels embedded in lipid bilayer membranes. The possible translational collective modes of motion of the permeating particles inside these nano-channels are constrained to be along the longitudinal direction, that is along the length of the nano-channel and are blocked in the transverse direction. Thus, the possible collective excitations inside these nano-channels are the longitudinal collective translational motion of particles, which give rise to the single file nature of the translocation of the particles through the nano-channel. A simple model of the structure of a lipid bilayer membrane and the surrounding aqueous solution is available in literatures, in particular in Ref. (16; 17; 18; 19; 20). One simple structure taken from the internet is shown in Fig. 1.1.

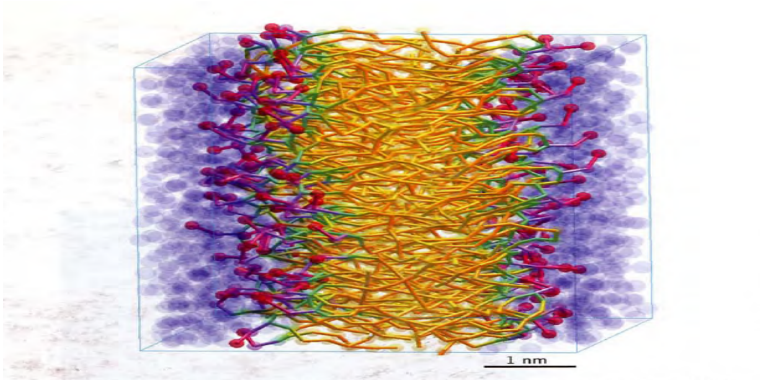

Fig. 1.1: A simple model of the three dimensional structural of a lipid bilayer membrane and the surrounding aqueous solution

In most biological cells, the intracellular solution (ICS) and extracellular solution (ECS) are separated by LBLM. The gross two dimensional structure of the ICS, LBLM and ECS system is shown in Fig. 1.2.

Fig. 1.2: A simple gross model of the two dimensional structure of the LBLM, ECS and ICS

The extracellular solution (ECS), considered as the emitter bath, has two domains, the bulk and the interfacial domains. The bulk domain of the ECS, denoted by ECBS in Fig. 1.2, the component that is far away from the outer surface of LBLM, is the homogeneous and unpolarized component of the ECS that acts as the source of particles. The interfacial domain of the ECS, denoted by ECPS in Fig. 1.2, the component that is in the vicinity of the outer surface of the LBLM, is the inhomogeneous and polarized component. Similarly, the intracellular solution (ICS), considered as the collector bath, has two domains, the bulk and the interfacial domains. The bulk domain of the ICS, denoted by ICBS in Fig. 1.2,

the component that is far away from the inner surface of the LBLM, is the homogeneous and unpolarized component of the ICS that acts as the sink of particles. The interfacial domain of the ICS, denoted by ICPS in Fig. 1.2, the component that is in the vicinity of the inner surface of the LBLM, is the inhomogeneous and polarized component.

Moreover, a gross model of the structure of LBLM, ECS and ICS system when nano-channels are embedded in the LBLM is shown in Fig. 1.3.

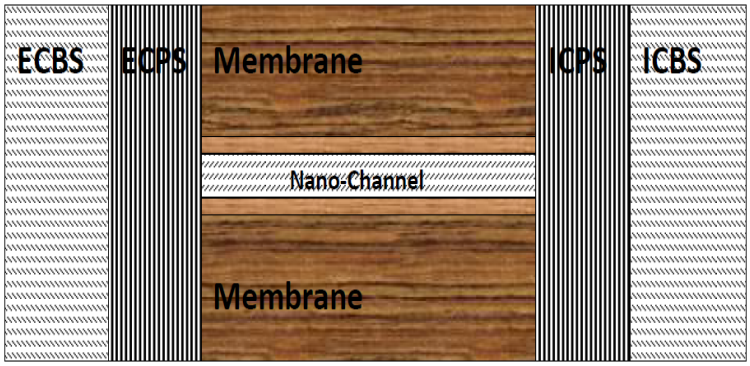

Fig. 1.3: A simple gross model of the Structure of ECS, LBLM and ICS system when nano-channels are embedded in the LBLM

It is known that the structure of protein channels of cell membranes is very complex, and it is reasonable to suggest that the corresponding free-energy potential of interaction has a very rough landscape. Recent molecular dynamics simulations of glycerol translocation through aquaglyceroporin GlpF have calculated a PMF that shows several relatively weak $(2-6\,\kappa_B T)$ but strongly localized narrow wells as shown in Ref. (4). Similar profiles of the PMF are also discussed in Ref. (8). We consider a molecular sized channel neglecting structural details and molecular composition. That is, a random potential of mean force profile along the internal path of particles through nano-channels, without considering the specificity and composition of the nano-channel, can be employed to develop a general model and theory that can describe the most important features of particle transport through nano-channels. A general landscape of the potential of the mean force along the length of a nano-channel is shown in Fig. 1.4.

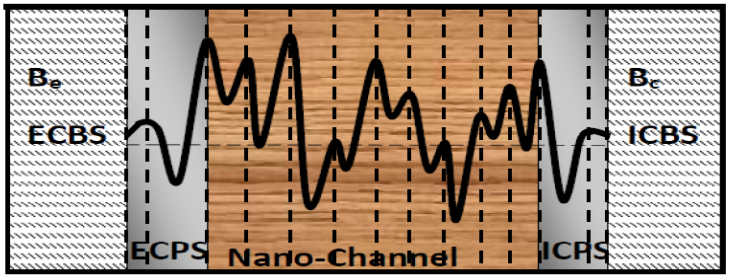

Fig. 1.4: Landscape of the potential of mean force along the length of a typical nano-channel

Fig. 1.4 shows that the landscape of the potential of the mean force along the internal path of particles through nano-channels is very complex. As can be seen from Fig. 1.4, the entire internal path of particles through a nano-channel is equivalent to an array of potential wells and potential barriers, in which the heights of the potential barriers and the depths of the potential wells aren't uniform, but are randomly distributed along the internal path of particles through the nano-channel. The potential wells or potential minima or trap centers are particle attracting or binding sites on the internal wall of the nano-channel and the potential barriers or potential maxima are particle repelling sites on the internal wall of the nano-channel. As particles permeate through nano-channels, they interact with these attractive and repulsive sites on the internal wall of the nano-channel. They also interact with water molecules and other constituent particles of the aqueous solution. These interaction potential energies are collectively described by the potential of mean forces (PMF). The landscape of the PMF of nano-channels is generally asymmetric with multiple weakly attractive and repulsive sites. Thus, the landscape of the PMF is modeled as a spatial distribution of potential wells and potential barriers. The energies of these potential wells and potential barriers and the distances between them aren't uniformly distributed. Moreover, the heights of the potential barriers and the depths of the potential wells are also randomly distributed.

In the general model of the PMF shown in Fig. 1.4, we have assumed the existence of two external potential wells situated in ECPS and ICPS, which play the role of gating variables of nano-channels as we will show in chapter four and five. In the next section we will formulate the lattice model of nano-channels.

1.2 One Dimensional Lattice Model of Nano-Channels

As the potential of mean force profile along the length of the nano-channel shown in Fig. 1.4 and in Ref. (4; 8), which is just an array of potential wells and potential barriers, suggest, it is possible to divide the whole length L of the nano-channel into s energetically inequivalent and none-uniformly spaced cells, whose centers coincide with the bottom of the potential wells on the landscape of PMF, are considered as the lattice sites of a one dimensional lattice. Nano-channels are therefore represented by a one dimensional lattice, which is considered as an irregular lattice as there is no periodic distribution of the locations of the potential wells and the potential barriers along the landscape of the one dimensional potential profile. Moreover, the total number of lattice sites of the one dimensional lattice representing a nano-channel is equal to the total number of potential wells on the landscape of the PMF along the internal path of particles through the nano-channel. Therefore, in the lattice model description of particle transport through nano-channels, the attractive sites on the internal wall of the nano-channel are considered as the lattice sites of a one dimensional lattice and the repulsive sites between the neighboring attractive sites are modeled as potential barriers, across which particles hop during their translocation through the nano-channel. As Fig. 1.4 shows, there are s internal lattice sites, associated with the s potential wells of the nano-channel, and two external lattice sites, associated with the polarized portions of the two baths, and as a result the one dimensional lattice representing nano-channels has $s+2$ lattice sites. The collective system consisting of the Nano-Channel, the emitter bath and the collector bath is shown in Fig. 1.5. The nano-channel is considered as an open system coupled to two particle reservoirs, the emitter bath and the collector bath B_c, with densities n_e and n_c, respectively. The bulk portion of the ECS (B_e) acts as the source of particles and the interfacial portion of the ECS is represented by the prominent potential well V_e as shown in Fig. 1.5, situated just at the center of ECPS. The bulk portion of the ICS (B_c) acts as the sink of particles and the interfacial portion of the ICS is represented by the prominent potential well V_c as shown in Fig. 1.5, situated just at the center of ICPS.

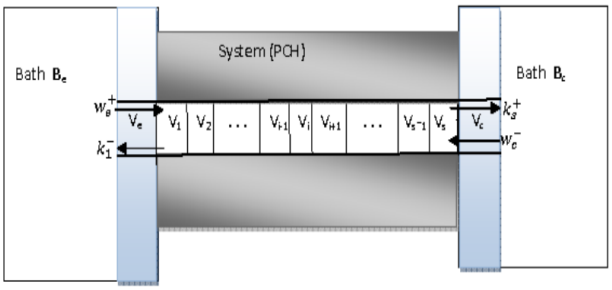

Fig. 1.5: A simple one dimensional lattice representing nano-channels coupled to the emitter bath and collector bath via its left and right boundary sites, V_1 and V_s, respectively.

The remaining s internal sites of the one dimensional lattice are represented by the s cells V_i, where $i = 1, 2, ..., s$ labels the sites of the local potential wells. The nano-channel is coupled to B_e via V_1, situated at the left end $(x = 0)$, and to B_c via V_s, situated at the right end $(x = L)$. The system therefore corresponds to diffusion of particles through an open medium between two particle reservoirs with different densities. The emitter bath is connected to the nano-channel via V_e which is in direct contact with V_1 and the collector bath is coupled to the nano-channel via V_c which is in direct contact with V_s.

The states of both internal and external lattice sites at any time t are described by the binary variables, $\eta_i(t)$, which correspond to the occupation number of the lattice site V_i at time t, where i labels the sites of the internal and external potential wells. The only interaction between particles is a hard-core repulsion that prevents more than one particle occupying the same lattice site at the same time. This is the so-called totally asymmetric exclusion process Ref. (3), where exclusion effects preclude more than one particle at any site. Therefore, each occupation number $\eta_i = 1$ if the $i - th$ site is occupied by a single particle and $\eta_i = 0$ if the site is vacant. The nano-channel is therefore an open and is thus driven system with stationary none-equilibrium states, as particles enter and leave the nano-channel via the two end sites, which act as boundaries between the nano-channel and the two baths, at different rates.

1.3 The hopping Mode of Particle Transport Through Nano-Channels

There are two models of particle transport through nano-channels, the discrete and continuum modes of motion, (2; 3; 4; 5; 6; 7; 8; 9). The discreet mode of motion of particles through nano-channels involves hopping of particles across the potential barrier separating the potential wells, which are the lattice sites of the one dimensional lattice representing nano-channels. That is, the diffusive mode of motion of neutral particles through nano-channels is modeled as hopping of particles over a one dimensional lattice. This model utilizes the Master equation to describe the rate of change of the average value of the occupation numbers of the lattice sites. Diffusion on a topologically disordered lattice structure isn't yet well developed. A molecule sitting at a localized potential well hops across the intervening potential barrier to a neighboring vacant potential well with the assistance of a phonon or another dynamical excitation. After staying there for a while, it hops again to another nearest neighbor vacant potential well. The assistance of other degrees of freedom will make the motion of molecules stochastic. Therefore, instead of the continuum model, the Fokker-Planck description, it is sensible to study the dynamics of Particle transport through nano-channels coupled to emitter and collector baths using the lattice model of particle transport through nano-channels, that is in terms of the Master equation.

The motion of particles inside nano-channels can be decomposed into two components. The first one is the local fluctuation mode of motion of particles in the local potential wells. The second mode of motion involves hopping of particles across the potential barrier between nearest neighbor vacant potential wells. When the height of the potential barrier separating two nearest neighbor potential wells is high compared to thermal energy, these jumps are rare and take place on time scales very much greater than the time scales for local fluctuations. Thus, when the temperature T isn't too large, the probability distribution function of the particles is concentrated only around these local potential wells. Because the particles spend most of their time around these minima, the mean dwell time at these sites is large. In other words, the potential minima

are the sites at which the particles reside for long periods of time, making occasional jumps to neighboring sites. The time spent during hopping is negligible compared to the dwell time in the potential wells. In our analysis we consider the local fluctuations about the potential minima to be always in equilibrium on the longer time scale of hopping.

The dynamics of a particle on the longer time scale is thus hopping between the nearest neighbor sites with nonuniform jump rates. We thus specify the state of the lattice site V_i at time t by its occupancy number $\eta_i(t)$. This state changes when particles jump from one site to another site and thus $\eta_i(t)$ is a stochastic process. The state is stochastic because its change due to hopping across the potential barrier between nearest neighbor potential wells is driven by the random thermal motion and other collective excitations (phonon), that are created and annihilated randomly. Thus, we arrive at diffusion of particles on a disordered one dimensional lattice structure with nonuniform jump rates characterizing the hopping mode of conduction of particles through nano-channels, where transport of molecules through nano-channels takes place by hopping of particles across the potential barrier between an array of potential wells distributed along the length of the internal wall of the nano-channel.

1.4 Model of the Transition Rates Describing Hopping Mode Motion of Particles Through Nano-Channels

The transition rates between the nearest neighbor lattice sites of the nano-channel are different for different sites and in different directions which means that the barrier height energies of the potential barriers separating the potential wells are nonuniformly distributed along the internal particle path through the nano-channel. The non-uniformity of the the transition rates arises from two factors, from the nonuniform distribution of the distance between the potential wells and from the nonuniformly distribution of the heights of the potential barriers and the depths of the potential wells along the internal particle path through the nano-channel.

The diffusive motion of particles through nano-channels involves a process in which a particle jumps from one site V_i to nearest neighbor vacant site $V_{i\pm1}$ with a certain transition rate. As the particle number density of the permeating

particles in the emitter bath B_e increases, the occupancy of the the external lattice site V_e increases and thus the mean residence time or the average time that the site is being vacant decreases as n_e increases. In other words, as n_e increases, η_e increases but $\gamma_e = 1 - \eta_e$ decreases. Similarly, as the particle number density n_c increases, η_c increases but $\gamma_c = 1 - \eta_c$ decreases, which means that the mean residence time that V_c is being vacant decreases as n_c increases. Therefore, the increase in the density of the permeating particles in the vicinity of V_e and V_c will enhance the frequency of the jump rates to V_1 and V_s, respectively.

At the two boundary sites of the nano-channel, the dynamics is modified to mimic the coupling with the reservoirs. Since the nano-channel is coupled to B_e and B_c via V_1 and V_s, respectively, it exchanges particles with the reservoirs at different rates and thus the total number of particles inside the nano-channel is not conserved. During each time interval dt, a particle sitting at V_e, where $\eta_e = 1$, hops to V_1 when V_1 is vacant so that $\eta_1 = 0$ and vice versa. Let us consider the following notations:

$$\begin{aligned} V_i &= V_i(1) \qquad \text{when site } V_i \text{ is occupied and thus } \eta_i = 1 \\ V_i &= V_i(0) \qquad \text{when site } V_i \text{ is vacant and thus } \eta_i = 0 \end{aligned} \tag{1.1}$$

In terms of the above notations, the elementary hopping processes occurring across the potential barrier between the sites V_e and V_1 can be described by a simple elementary process of the form:

$$V_e(1) + V_1(0) \rightleftharpoons V_e(0) + V_1(1) \tag{1.2}$$

During the forward elementary reaction (from left to right), a particle hops from V_e to V_1 at the intrinsic rate constant k_e^+ and during the reverse elementary reaction, a particle hops from V_1 to V_e at the intrinsic rate constant k_1^-. The intrinsic transition rate k_e^+ is given in units of $(\mu M)^{-1}s^{-1}$ and n_e is given in units of μM so that the product $k_e^+ n_e$ has the dimension of s^{-1}. Therefore, the average particle flux through the nano-channel has the dimension of s^-.

The possible values of the transition rates that we will employ in the graphical analysis of this work are chosen based on the works of Ref. [(1; 2)], where we have added additional factors as would be shown below. Based on the work of Anatoly B. Kolomeisky [(2)], a particle enters the nano-channel from the emitter

bath with concentration c_1 with the rate $u_0 = k_{on}c_1$ and from the collector bath with concentration c_2 with the rate $w_0 = k_{on}c_2$, where $k_{on} = 15(\mu M)^{-1}s^{-1}$. Moreover, a particle leaves the nano-channel to the emitter bath and collector bath with the rates $w_1 = k_{off}$ and $u_N = k_{off}$), respectively, with $k_{off} = \approx 500s^{-}$. For the internal sites, it was assumed that a particle at site $j(j = 1, 2, 3, ..., s)$ jumps to the right (left) with the rate $u_j(w_j)$ where $u_j = w_j = \alpha$, with $\alpha \approx 500s^{-}$.

The total transition rate from V_e to V_1 would be highly influenced by the concentration of particles in B_e. We incorporate this fact into the dynamics by the assumption that a particle hops from B_e to V_1 only if it occupies V_e. It is sensible to assume that the total nearest neighbor assisted jump rate from V_e to V_1 is proportional to n_e, η_e and γ_1. Therefore, the total rate at which particles are injected from the emitter bath B_e into V_1, denoted by $\Omega_e^+(n_e, \eta_e, \gamma_1)$, that takes the above fact into account can be written as:

$$\Omega_e^+(n_e, \eta_e, \gamma_1, k_e^+) = n_e\eta_e\gamma_1 k_e^+ \tag{1.3}$$

where we have introduced the following variables for convenience.

$$\begin{aligned}\gamma_i &= 1 - \eta_i \\ \gamma_e &= 1 - \eta_e \\ \gamma_c &= 1 - \eta_c\end{aligned} \tag{1.4}$$

where $i = 1, 2, ..., s$, with s being the number of internal potential wells. Thus, the expression of the transition rates in Eq. (1.3) and Eq. (1.6) is slightly different from those used in Ref. (1; 2).

Moreover, during each time interval dt, a particle occupying site V_c (when $\eta_c = 1$ and thus V_c is the donor site) hops to the vacant site V_s (when $\eta_s = 0$ and thus V_s is an acceptor site) and vice versa. The elementary hopping processes across the potential barrier between the sites V_c and V_s can also be described by the elementary reaction of the form:

$$V_c(0) + V_s(1) \rightleftharpoons V_c(1) + V_s(0) \tag{1.5}$$

During the forward elementary reaction (from left to right), a particle hops from V_s to V_c at the intrinsic rate constant k_s^+ and during the reverse elementary reaction, a particle hops from V_c to V_s at the intrinsic rate constant k_c^-. We also

assume that the total nearest neighbor assisted jump rate from V_c to V_s is proportional to n_c, η_c and γ_s. Therefore, the total rate at which particles are injected from the collector bath B_c into V_s, denoted by $\Omega_c^+(n_c, \eta_c, \gamma_s)$, that takes the above fact into account can be written as:

$$\Omega_c^+(n_c, \eta_c, \gamma_s, k_c^-) = n_c \eta_c \gamma_s k_c^- \tag{1.6}$$

For the internal channel sites, we assume the following elementary reaction.

$$\begin{aligned} V_i(1) + V_{i+1}(0) &\rightleftharpoons V_i(0) + V_{i+1}(1) \quad \text{for the jump process between } V_i \text{ and } V_{i+1} \\ V_i(0) + V_{i-1}(1) &\rightleftharpoons V_i(1) + V_{i-1}(0) \quad \text{for the jump process between } V_i \text{ and } V_{i-1} \end{aligned} \tag{1.7}$$

During the forward elementary reaction (from left to right), a particle at the donor site $V_i(1)$, where $\eta_i = 1$ jumps to its right neighbor acceptor site $V_{i+1}(0)$, where $\eta_{i+1} = 0$, with a site dependent intrinsic jump rate k_i^+ and during the reverse elementary reaction, a particle at the donor site $V_{i+1}(1)$, where $\eta_{i+1} = 1$, jumps to its left neighbor acceptor site $V_i(0)$, where $\eta_i = 0$, with the intrinsic jump rate k_{i+1}^-. We have similar description for the second elementary reaction. Thus, a particle at a given site hops to its right or left neighbor site provided that the donor site is occupied and the acceptor site is empty. Therefore the total transition rates for the internal sites are given by:

$$\begin{aligned} \Omega_i^+(\eta_i, \gamma_{i+1}, k_i^+) &= \eta_i \gamma_{i+1} k_i^+ \qquad \text{from } V_i \text{ to } V_{i+1} \\ \Omega_i^-(\eta_i, \gamma_{i-1}, k_i^-) &= \eta_i \gamma_{i-1} k_i^- \qquad \text{from } V_i \text{ to } V_{i-1} \end{aligned} \tag{1.8}$$

In our model, the transition rates are more general which can be modified to include different additional factors. Moreover, we assumed that the intrinsic transition rates don't depend on the occupation numbers of the lattice sites. Except these modifications of the effective transition rates, our model is more general and can be applied for any system. In the next section we will discuss these concepts in more detail.

1.5 Specification of the Range of the Possible Values of the Transition Rates

The intrinsic transition rates k_e^+ and k_c^- are given in units of $(\mu M)^{-1} s^{-1}$ and the concentrations n_e and n_c are given in units of μM so that the products $k_e^+ n_e$ and

$k_c^- n_c$ have the dimensions of s^{-1} and as a result the average particle flux through the nano-channel has the dimension of s^-. The dimension of both k_i^+ and k_i^- is s^{-1}.

From the experiments on maltodextrin translocation through maltoporin channels , in Ref. (2) the following values are used for the external and internal transition rates.

$$\begin{aligned} k_e^+ &= 15 \times 10^6 M^{-1} s^{-1} = 15(\mu M)^{-1} s^{-1} \\ k_c^- &= 15 \times 10^6 M^{-1} s^{-1} = 15(\mu M)^{-1} s^{-1} \\ k_1^+ &= k_2^+ = ... = k_s^+ = 500 s^- \\ k_1^- &= k_2^- = ... = k_s^- = 500 s^- \end{aligned} \tag{1.9}$$

On the other hand, from the experiments on maltodextrin translocation through maltoporin channels, in Ref. (1) the following numerical values are used for zero potential difference, with an experimental error of $\approx \pm 10$ percent.

$$k_e^+ = 8.6 \times 10^6 M^{-1} s^{-1} = 8.6(\mu M)^{-1} s^{-1} \tag{1.10}$$

For the other transition rate at zero voltage they have obtained:

$$k_c^- = 2.2 \times 10^6 M^{-1} s^{-1} \tag{1.11}$$

with an experimental error of $\approx \pm(20-25)$ percent. From Ref. (1), for a channel with a single internal site, there is only a single thermodynamic binding constant at zero voltage that is given by:

$$\begin{aligned} K &= \frac{k_e^+}{k_1^-} = \frac{k_c^-}{k_1^+} \\ K &= \frac{k_e^+ + k_c^-}{k_1^- + k_1^+} \\ K &= \frac{k_{on}}{k_{off}} \end{aligned} \tag{1.12}$$

where they defined the parameters:

$$\begin{aligned} k_{on} &= k_e^+ + k_c^- \\ k_{off} &= k_1^- + k_1^+ \end{aligned} \tag{1.13}$$

K has two values, the smaller and the larger one:

$$K = 3.0 \times 10^4$$
$$K = 1.7 \times 10^4 \tag{1.14}$$

Moreover, at zero voltage, they employed the relations:

$$k_{off} = 340 \quad \text{when} \quad K = 3.0 \times 10^4$$
$$k_{off} = 580 \quad \text{when} \quad K = 1.7 \times 10^4 \tag{1.15}$$

Employing these results, they also obtained the following relations :

$$k_1^- = 0.796 \times k_{off} = 270.64 \quad \text{when} \quad k_{off} = 340$$
$$k_1^- = 0.796 \times k_{off} = 461.68 \quad \text{when} \quad k_{off} = 580$$
$$k_1^+ = 0.204 \times k_{off} = 69.36 \quad \text{when} \quad k_{off} = 340$$
$$k_1^+ = 0.204 \times k_{off} = 118.32 \quad \text{when} \quad k_{off} = 580 \tag{1.16}$$

According to model used by Ref. (1), the values of the transition rates lie in the range:

$$270.64 < k_1^- < 461.68$$
$$69.36 < k_1^+ < 118.32 \tag{1.17}$$

Therefore, as the above result shows, the bath transition rates in units of $(\mu M)^{-1}s^{-1}$ have values in the ranges specified below.

$$1 < k_e^+ < 15$$
$$1 < k_c^- < 15 \tag{1.18}$$

Moreover, the internal transition rates in units of s^{-1} have values in the ranges specified below.

$$0 < k_1^- < 500$$
$$0 < k_1^+ < 500 \tag{1.19}$$

In this research work, we have calculated the average particle flux through the nano-channel for the following fixed ranges of the average values of the occu-

pation numbers of the internal and external potential wells.

$$
\begin{aligned}
0 < \eta_e < 1 \\
0 < \eta_i < 1 \\
0 < \eta_c < 1 \\
0 < \gamma_e < 1 \\
0 < \gamma_i < 1 \\
0 < \gamma_c < 1
\end{aligned}
\tag{1.20}
$$

where $i = 1, 2, ..., s$, with s being the number of internal potential wells.

2

FORMULATION OF THE DYNAMICS OF PARTICLE TRANSPORT THROUGH NANO-CHANNELS

2.1 The Master Equation Description of the Time Evolution of the Occupation Numbers of the Lattice Sites

The translocation of particles through nano-channels is a dynamic process in which the average values of the occupation numbers of the channel and bath lattice sites change with time as the occupation probability of these sites change with time. We employ the Master equation to describe the essential features of the hopping mode of motion of molecules through nano-channels embedded in LBLM, Ref. (4; 5; 7; 8; 9; 10; 11; 12; 13) and (42; 43; 44; 45; 46; 47; 48). The averaging process is taken over all the possible values of the bath and channel parameters in their specified ranges. We assume that the hopping mode of motion of particles through nano-channels take place only between nearest neighbor sites as the probability of long range hopping is negligible. Therefore, the total transition rates into the particular site i from V_{i-1} and V_{i+1} and the total transitions out of i into V_{i-1} and V_{i+1} is given by the master equation, Ref. (7; 9; 10; 11).

$$\begin{aligned}\frac{d\langle\eta_i\rangle}{dt} &= \langle\Omega^+_{i-1} + \Omega^-_{i+1} - \Omega^+_i - \Omega^-_i\rangle \\ \frac{d\langle\eta_i\rangle}{dt} &= \langle\Omega^+_{i-1}\rangle + \langle\Omega^-_{i+1}\rangle - \langle\Omega^+_i\rangle - \langle\Omega^-_i\rangle \end{aligned} \tag{2.1}$$

Upon substituting the expressions of the total transition rates defined in Eq. (1.8) into Eq. (2.1), we get

$$\frac{d\langle\eta_i\rangle}{dt} = \langle\eta_{i-1}(1-\eta_i)\rangle k_{i-1}^{+} + \langle\eta_{i+1}(1-\eta_i)\rangle k_{i+1}^{-} - \\ - \langle\eta_i(1-\eta_{i-1})\rangle k_i^{-} - \langle\eta_i(1-\eta_{i+1})\rangle k_i^{+} \tag{2.2}$$

We can rewrite Eq. (2.2) in a more familiar form:

$$\frac{d\langle\eta_i\rangle}{dt} = \langle\eta_{i-1}(1-\eta_i)\rangle k_{i-1}^{+} - \langle\eta_i(1-\eta_{i-1})\rangle k_i^{-} - \\ - [\langle\eta_i(1-\eta_{i+1})\rangle k_i^{+} - \langle\eta_{i+1}(1-\eta_i)\rangle k_{i+1}^{-}] \tag{2.3}$$

The Master equation for the rate of change of the average value of the occupation number of V_1 is:

$$\frac{d\langle\eta_1\rangle}{dt} = \langle n_e\eta_e(1-\eta_1)\rangle k_e^{+} - \langle\eta_1(1-\eta_e)\rangle k_1^{-} - \\ - [\langle\eta_1(1-\eta_2)\rangle k_1^{+} - \langle\eta_2(1-\eta_1)\rangle k_2^{-}] \tag{2.4}$$

The Master equation for the rate of change of the average value of the occupation number of V_s is:

$$\frac{d\langle\eta_s\rangle}{dt} = \langle\eta_{s-1}(1-\eta_s)\rangle k_{s-1}^{+} - \langle\eta_s(1-\eta_{s-1})\rangle k_s^{-} - \\ - [\langle\eta_s(1-\eta_c)\rangle k_s^{+} - \langle n_c\eta_c(1-\eta_s)\rangle k_c^{-}] \tag{2.5}$$

2.2 The Average Particle Flux Through a Nano-Channel at Steady State

These equation are the familiar continuity equations associated with each site in the nano-channel. We make the assumption that the particle flux from the emitter bath to the collector bath is positive. Therefore, the average current associated with the hopping mode of motion of particles through a nano-channel is:

$$J_i = \langle\eta_i(1-\eta_{i+1})\rangle k_i^{+} - \langle\eta_{i+1}(1-\eta_i)\rangle k_{i+1}^{-} \quad \text{between } V_i \text{ and } V_{i+1} \\ J_e = \langle n_e\eta_e(1-\eta_1)\rangle k_e^{+} - \langle\eta_1(1-\eta_e)\rangle k_1^{-} \quad \text{between } V_e \text{ and } V_1 \\ J_c = \langle\eta_s(1-\eta_c)\rangle k_s^{+} - \langle n_c\eta_c(1-\eta_s)\rangle k_c^{-} \quad \text{between } V_s \text{ and } V_c \tag{2.6}$$

In terms of the γ variables defined in Eq. (1.4), the expression in Eq. (2.6) becomes:

$$\begin{aligned} J_i &= \langle \eta_i \gamma_{i+1} \rangle k_i^+ - \langle \gamma_i \eta_{i+1} \rangle k_{i+1}^- \quad \text{from } V_i \text{ to } V_{i+1} \\ J_e &= \langle n_e \eta_e \gamma_1 \rangle k_e^+ - \langle \eta_1 \gamma_e \rangle k_1^- \quad \text{from } V_e \text{ to } V_1 \\ J_c &= \langle \eta_s \gamma_c \rangle k_s^+ - \langle n_c \eta_c \gamma_s \rangle k_c^- \quad \text{from } V_s \text{ to } V_c \end{aligned} \tag{2.7}$$

In the first expression of Eq. (2.7), the average value of the occupation number of the lattice sites of the nano-channel is coupled to the occupation numbers its nearest neighbor lattice sites. Moreover, in the second and third expression of Eq. (2.7) the average values of the particle number densities in emitter and collector baths are coupled to occupation numbers of the leftmost and rightmost lattice sites of the nano-channel, respectively. Solving such coupled equations is difficult and thus we are forced to make some simplifying assumption so as to decouple these equations. We must decouple the correlation of the occupation numbers so as to solve the problem exactly and propose some decoupling mechanisms so as to find a more manageable expression of the average particle flux. At steady state, particles can't accumulate in the local potential wells and thus the average particle flux across each potential barrier between nearest neighbor potential wells must be the same.

2.3 The Mean Field Approximation of the Steady State Particle Flux Through Nano-Channels

At steady state, particles can't accumulate in the local potential energy wells and thus the average current across each potential energy barrier between the nearest potential well sites must be the same. Therefore, the first assumption is the *steady state assumption*, which states that:

$$J_e = J_1 = J_2 = ... = J_s = J_c = J = \text{constant} \tag{2.8}$$

The second assumption is the *Mean field approximation*, as discussed in Ref. (10). The mean field approximation consists of factorizing the two site correlation, that is we impose the condition of uncorrelated occupancy of the lattice sites of the nano-Channel at Steady State. Therefore, the assumption of uncor-

related occupancy of the lattice sites the nano-channel becomes:

$$\langle \eta_i \gamma_{i+1} \rangle = \langle \eta_i \rangle \langle \gamma_{i+1} \rangle \tag{2.9}$$

In the third assumption, we assume that the occupation numbers of the external potential wells V_e and V_c and the internal potential wells V_1 and V_s are uncorrelated with the particle number densities of the emitter and collector baths, respectively. That is, the correlation among the three numbers in Eq. (2.7) can be decoupled. Therefore:

$$\begin{aligned} \langle n_e \eta_e \eta_1 \rangle &= \langle n_e \rangle \langle \eta_e \rangle \langle \eta_1 \rangle \\ \langle n_c \eta_c \eta_s \rangle &= \langle n_c \rangle \langle \eta_c \rangle \langle \eta_s \rangle \end{aligned} \tag{2.10}$$

Employing the assumptions stated in Eq. (2.8), Eq. (2.9) and Eq. (2.10), the expressions of the steady state average particle flux through the nano-channel given in Eq. (2.7) becomes:

$$\begin{aligned} J &= \langle \eta_i \rangle \langle \gamma_{i+1} \rangle k_i^+ - \langle \eta_{i+1} \rangle \langle \gamma_i \rangle k_{i+1}^- \quad \text{from } V_i \text{ to } V_{i+1} \\ J &= \langle \eta_e \rangle \langle n_e \rangle \langle \gamma_1 \rangle k_e^+ - \langle \eta_1 \rangle \langle \gamma_e \rangle k_1^- \quad \text{from } V_e \text{ to } V_1 \\ J &= \langle \eta_s \rangle \langle \gamma_c \rangle k_s^+ - \langle \eta_c \rangle \langle n_c \rangle \langle \gamma_s \rangle k_c^- \quad \text{from } V_s \text{ to } V_c \end{aligned} \tag{2.11}$$

As a result of the mean field approximation, the transition rates become linearized. Therefore, as one can see from Eq. (2.11), the effective linearized transition rates can be defined as:

$$\begin{aligned} \omega_i^+ &= \langle \gamma_{i+1} \rangle k_i^+ \quad \text{from } V_i \text{ to } V_{i+1} \\ \omega_i^- &= \langle \gamma_{i-1} \rangle k_i^- \quad \text{from } V_i \text{ to } V_{i-1} \\ \omega_e^+ &= \langle n_e \rangle \langle \gamma_1 \rangle k_e^+ \quad \text{from } V_e \text{ to } V_1 \\ \omega_c^- &= \langle n_c \rangle \langle \gamma_s \rangle k_c^- \quad \text{from } V_c \text{ to } V_s \end{aligned} \tag{2.12}$$

Employing the linearized effective transition rates in Eq. (2.12), the expression of the net average particle flux across the potential energy barrier between the potential wells V_e and V_1 becomes:

$$J = \langle \eta_e \rangle \omega_e^+ - \langle \eta_1 \rangle \omega_1^- \tag{2.13}$$

The expressions of the net average particle flux across the potential energy barrier between the potential energy wells V_s and V_c becomes:

$$J = \langle \eta_s \rangle \omega_s^+ - \langle \eta_c \rangle \omega_c^- \tag{2.14}$$

The expressions of the net average particle flux across the potential energy barrier between the potential energy wells V_i and V_{i+1} becomes:

$$J = \langle \eta_i \rangle \omega_i^+ - \langle \eta_{i+1} \rangle \omega_{i+1}^- \qquad \text{for } 1 \leq i \leq s-1 \tag{2.15}$$

Thus, employing Eq. (2.15), the expression of the average particle flux across the potential energy barrier between V_1 to V_2 is:

$$J = \langle \eta_1 \rangle \omega_1^+ - \langle \eta_2 \rangle \omega_2^- \tag{2.16}$$

Solving Eq. (2.16) for $\langle \eta_1 \rangle$ and then substituting the resulting expression into Eq. (2.13), one can get the following expression for the average current.

$$J = \frac{\omega_1^+}{\omega_1^-}[\langle \eta_e \rangle \omega_e^+ - J] - \langle \eta_2 \rangle \omega_2^- \tag{2.17}$$

Thus, after some rearrangement of Eq. (2.17), we get:

$$J = \frac{\omega_e^+ \left[\langle \eta_e \rangle - \frac{\omega_1^- \omega_2^-}{\omega_e^+ \omega_1^+} \langle \eta_2 \rangle \right]}{1 + \frac{\omega_1^-}{\omega_1^+}} \tag{2.18}$$

The average particle flux across the potential energy barrier between V_2 and V_3 is:

$$J = \frac{\omega_e^+ \left[\langle \eta_e \rangle - \frac{\omega_1^- \omega_2^- \omega_3^-}{\omega_e^+ \omega_1^+ \omega_2^+} \langle \eta_3 \rangle \right]}{1 + \frac{\omega_1^-}{\omega_1^+} + \frac{\omega_1^- \omega_2^-}{\omega_1^+ \omega_2^+}} \tag{2.19}$$

By repeating the above procedure for the net average particle flux across each potential barrier, we finally get general the expression of the net average particle flux across the potential barrier between V_{s-1} and V_s:

$$J = \omega_e^+ \left[\frac{\langle \eta_e \rangle - \prod_{i=1}^{s} \left\{ \frac{\omega_i^-}{\omega_{i-1}^+} \right\} \langle \eta_s \rangle}{1 + \sum_{i=1}^{s-1} \prod_{r=1}^{i} \left\{ \frac{\omega_r^-}{\omega_r^+} \right\}} \right] \tag{2.20}$$

We repeat the same procedure for the average particle flux across the potential energy barrier between V_s and V_{s+1} and get the following general expression for the average current.

$$J = \omega_e^+ \left[\frac{\langle \eta_e \rangle - \prod_{i=1}^{s+1} \left\{ \frac{\omega_i^-}{\omega_{i-1}^+} \right\} \langle \eta_s \rangle}{1 + \sum_{i=1}^{s-1} \prod_{r=1}^{i} \left\{ \frac{\omega_r^-}{\omega_r^+} \right\}} \right] \tag{2.21}$$

Since $V_{s+1} = V_c$ and $V_0 = V_e$, we have that:

$$\begin{aligned} \omega_0^+ &= \omega_e^+ \\ \omega_{s+1}^- &= \omega_c^- \end{aligned} \tag{2.22}$$

Using the definitions in Eq. (2.22), we can rearrange the Eq. (2.21) and get:

$$J = \frac{\left[\omega_e^+ \langle \eta_e \rangle - \prod_{i=1}^{s} \left\{ \frac{\omega_i^-}{\omega_i^+} \right\} \omega_c^- \langle \eta_c \rangle \right]}{1 + \sum_{i=1}^{s} \prod_{r=1}^{i} \left\{ \frac{\omega_r^-}{\omega_r^+} \right\}} \tag{2.23}$$

Using the definitions of the effective transition rates given in Eq. (2.12), the ratio of the effective transition rates in Eq. (2.23) can be rewritten as:

$$\prod_{i=1}^{s} \frac{\omega_i^-}{\omega_i^+} = \frac{\langle \gamma_e \rangle \langle \gamma_1 \rangle}{\langle \gamma_s \rangle \langle \gamma_c \rangle} \prod_{i=1}^{s} \frac{k_i^-}{k_i^+} \tag{2.24}$$

Upon substituting Eq. (2.24) and (2.12) into Eq. (2.23), the expression of the average particle flux through the nano-channel becomes:

$$J = \frac{\langle \gamma_1 \rangle}{\langle \gamma_c \rangle} \left\{ \frac{\langle n_e \rangle \langle \eta_e \rangle \langle \gamma_c \rangle k_e^+ - \prod_{i=1}^{s} \left[\frac{k_i^-}{k_i^+} \right] \langle n_c \rangle \langle \eta_c \rangle \langle \gamma_e \rangle k_c^-}{1 + \sum_{i=1}^{s} \prod_{r=1}^{i} \frac{\omega_r^-}{\omega_r^+}} \right\} \tag{2.25}$$

The product of the ratio of the intrinsic jump rates is a constant and can be represented by a constant parameter μ_s that is defined by:

$$\mu_s = \prod_{i=1}^{s} \left[\frac{k_i^-}{k_i^+} \right] \tag{2.26}$$

Using Eq. (2.26) into Eq. (2.25), we get:

$$J = \frac{\langle \gamma_1 \rangle}{\langle \gamma_c \rangle} \left\{ \frac{\langle n_e \rangle \langle \eta_e \rangle \langle \gamma_c \rangle k_e^+ - \mu_s \langle n_c \rangle \langle \eta_c \rangle \langle \gamma_e \rangle k_c^-}{1 + \sum_{i=1}^{s} \prod_{r=1}^{i} \frac{\omega_r^-}{\omega_r^+}} \right\} \tag{2.27}$$

Let us use the following notations of the mean values of the variables for convenience.

$$\begin{aligned}
\langle n_e \rangle &= n_e; \\
\langle n_c \rangle &= n_c; \\
\langle \eta_e \rangle &= \eta_e; \\
\langle \eta_c \rangle &= \eta_c; \\
\langle \gamma_e \rangle &= \gamma_e; \\
\langle \gamma_c \rangle &= \gamma_c
\end{aligned} \tag{2.28}$$

Moreover, the expression in the denominator of Eq. (2.27) can defined by:

$$\chi_s = \sum_{i=1}^{s} \prod_{r=1}^{i} \frac{\omega_r^-}{\omega_r^+} \tag{2.29}$$

Using the notation given in Eq. (2.28) and (2.29) into Eq. (2.27), the general expression of the average particle flux at steady state becomes:

$$J = \frac{\gamma_1}{\gamma_c} \left[\frac{n_e \eta_e \gamma_c k_e^+ - \mu_s n_c \eta_c \gamma_e k_c^-}{1 + \chi_s} \right] \tag{2.30}$$

In the general expression of the average particle flux given in Eq. (2.30) the term in the numerator depends on the properties of the two baths, that is, it depends on the emitter bath variables $n_e, \eta_e, \gamma_e, k_e^+$ and on the collector bath variables $n_c, \eta_c, \gamma_c, k_c^-$. The expression of χ_s consists of the sets of the occupation numbers of the lattice sites of the nano-channel, that is $(\gamma_1, \gamma_2, ..., \gamma_s)$. It also takes into account the possible potential profile of the entire particle path along the length of the channel through the set of the parameters $(k_1^\pm, k_2^\pm, ..., k_s^\pm)$. It also depends on products of the ratio of the backward and forward transition rates. In the following section we will discuss the expressions of the parameters χ_s and μ_s and the average particle flux J as a function of the intrinsic transition rates, the δ and β parameters and the occupation numbers of the channel and bath sites.

2.4 Expression of the the Average Particle Flux in Terms of δ and β Parameters

The parameters χ_s and μ_s in Eq. (2.30) are the channel parameters that characterize the nature of the nano-channel, where μ_s depends on $k_1^\pm, k_2^\pm, ..., k_s^\pm$ and χ_s

depends on $k_1^{\pm}, k_2^{\pm}, ..., k_s^{\pm}$, $\gamma_e, \gamma_1, \gamma_2, ..., \gamma_s, \gamma_c$. We can rewrite the expression of χ_s defined in Eq. (2.29) as follows:

$$\chi_s = \sum_{i=1}^{s} \prod_{r=1}^{i} \frac{\omega_r^-}{\omega_r^+} = \sum_{i=1}^{s} \prod_{r=1}^{i} \frac{k_r^-}{k_r^+} \frac{\langle \gamma_{r-1} \rangle}{\langle \gamma_{r+1} \rangle}$$

$$\chi_s = \frac{\gamma_e \gamma_1}{\gamma_1 \gamma_2} \frac{k_1^-}{k_1^+} + \frac{\gamma_e \gamma_1}{\gamma_2 \gamma_3} \frac{k_1^- k_2^-}{k_1^+ k_2^+} + \frac{\gamma_e \gamma_1}{\gamma_3 \gamma_4} \frac{k_1^- k_2^- k_3^-}{k_1^+ k_2^+ k_3^+} + ... + \frac{\gamma_e \gamma_1}{\gamma_s \gamma_c} \prod_{i=1}^{s} \frac{k_i^-}{k_i^+} \tag{2.31}$$

Using Eq. (2.26) and Eq. (2.31) into Eq. (2.30), we can rewrite the average particle flux in another form:

$$J_s = \frac{\frac{n_e \eta_e k_e^+}{\gamma_e} - \left[\frac{k_1^- k_2^- ... k_s^-}{k_1^+ k_2^+ ... k_s^+}\right] \left[\frac{n_c \eta_c k_c^-}{\gamma_c}\right]}{\frac{1}{\gamma_e \gamma_1} + \frac{k_1^-}{k_1^+} \frac{1}{\gamma_1 \gamma_2} + \frac{k_1^- k_2^-}{k_1^+ k_2^+} \frac{1}{\gamma_2 \gamma_3} + ... + \frac{k_1^- k_2^- ... k_{s-1}^-}{k_1^+ k_2^+ ... k_{s-1}^+} \frac{1}{\gamma_{s-1} \gamma_s} + \frac{k_1^- k_2^- ... k_s^-}{k_1^+ k_2^+ ... k_s^+} \frac{1}{\gamma_s \gamma_c}} \tag{2.32}$$

Based on the forms of Eq. (2.31) and Eq. (2.32), let us define a new channel parameter δ_i:

$$\delta_i = \frac{k_i^-}{k_i^+} \tag{2.33}$$

where the parameter δ_i is the ratio of the backward and forward transition rates from a given site. Using Eq. (2.33) into Eq. (2.26), we get:

$$\mu_s = \prod_{i=1}^{s} \delta_i \tag{2.34}$$

Therefore, the parameter μ_s depends on $\delta_1, \delta_2, \delta_3, ..., \delta_s$. We can rewrite the second expression in Eq. (2.31) in terms of the set of parameters $\{\delta_i\}$ as:

$$\chi_s = \gamma_e \gamma_1 \left[\frac{\delta_1}{\gamma_1 \gamma_2} + \frac{\delta_1 \delta_2}{\gamma_2 \gamma_3} + \frac{\delta_1 \delta_1 \delta_3}{\gamma_3 \gamma_4} + ... + \frac{\delta_1 \delta_2 \delta_3 ... \delta_{s-1}}{\gamma_{s-1} \gamma_s} + \frac{\delta_1 \delta_2 \delta_3 ... \delta_s}{\gamma_s \gamma_c} \right] \tag{2.35}$$

Therefore, using Eq. (2.34) and Eq. (2.35) into Eq. (2.30), the expression of the average particle flux through the nano-channel with s internal sites becomes:

$$J_s = \frac{n_e \eta_e \gamma_c k_e^+ - (\delta_1 \delta_2 ... \delta_s) n_c \eta_c \gamma_e k_c^-}{\gamma_e \gamma_c \left[\frac{1}{\gamma_e \gamma_1} + \frac{\delta_1}{\gamma_1 \gamma_2} + \frac{\delta_1 \delta_2}{\gamma_2 \gamma_3} + \frac{\delta_1 \delta_1 \delta_3}{\gamma_3 \gamma_4} + ... + \frac{\delta_1 \delta_2 \delta_3 ... \delta_{s-1}}{\gamma_{s-1} \gamma_s} + \frac{\delta_1 \delta_2 \delta_3 ... \delta_s}{\gamma_s \gamma_c} \right]} \tag{2.36}$$

We can further simplify Eq. (2.36) and get:

$$J_s = \frac{\left[\frac{n_e \eta_e k_e^+}{\gamma_e}\right] - (\delta_1 \delta_2 ... \delta_s) \left[\frac{n_c \eta_c k_c^-}{\gamma_c}\right]}{\frac{1}{\gamma_e \gamma_1} + \frac{\delta_1}{\gamma_1 \gamma_2} + \frac{\delta_1 \delta_2}{\gamma_2 \gamma_3} + \frac{\delta_1 \delta_1 \delta_3}{\gamma_3 \gamma_4} + ... + \frac{\delta_1 \delta_2 \delta_3 ... \delta_{s-1}}{\gamma_{s-1} \gamma_s} + \frac{\delta_1 \delta_2 \delta_3 ... \delta_s}{\gamma_s \gamma_c}} \tag{2.37}$$

As Eq. (2.37) shows, the first term in the numerator depends only on the properties of the emitter bath, the second term on the properties of the nano-channel and the third term on the properties of the collector bath. After some rearrangement of Eq. (2.32), we get:

$$J_s = \frac{\frac{n_e \eta_e k_e^+}{k_1^- \gamma_e} - \left[\frac{k_2^-}{k_1^+}\frac{k_3^-}{k_2^+}\frac{k_4^-}{k_3^+}\cdots\frac{k_s^-}{k_{s-1}^+}\right]\left[\frac{n_c \eta_c k_c^-}{k_s^+ \gamma_c}\right]}{\frac{1}{k_1^- \gamma_e \gamma_1} + \frac{1}{k_1^+ \gamma_1 \gamma_2} + \left[\frac{k_2^-}{k_1^+}\right]\frac{1}{k_2^+ \gamma_2 \gamma_3} + \left[\frac{k_2^-}{k_1^+}\frac{k_3^-}{k_2^+}\right]\frac{1}{k_3^+ \gamma_3 \gamma_4} + ... + \left[\frac{k_2^-}{k_1^+}\frac{k_3^-}{k_2^+}\frac{k_4^-}{k_3^+}\cdots\frac{k_s^-}{k_{s-1}^+}\right]\frac{1}{k_s^+ \gamma_s \gamma_c}} \tag{2.38}$$

Based on the form of Eq. (2.38), let us define another channel parameter:

$$\beta_i = \frac{k_{i+1}^-}{k_i^+} \tag{2.39}$$

where the parameter β_i is the ratio of the backward and forward transition rates across a given potential barrier between two neighboring sites. Therefore, using the definition in Eq. (2.39) into Eq. (2.38), we get:

$$J_s = \frac{\left[\frac{n_e \eta_e}{\gamma_e}\right]\frac{k_e^+}{k_1^-} - \beta_1\beta_2\beta_3...\beta_{s-1}\left[\frac{n_c \eta_c}{\gamma_c}\right]\frac{k_c^-}{k_s^+}}{\frac{1}{k_1^- \gamma_e \gamma_1} + \frac{1}{k_1^+ \gamma_1 \gamma_2} + \frac{\beta_1}{k_2^+ \gamma_2 \gamma_3} + \frac{\beta_1\beta_2}{k_3^+ \gamma_3 \gamma_4} + ... + \frac{\beta_1\beta_2\beta_3...\beta_{s-2}}{k_{s-1}^+ \gamma_{s-1} \gamma_s} + \frac{\beta_1\beta_2\beta_3...\beta_{s-1}}{k_s^+ \gamma_s \gamma_c}} \tag{2.40}$$

We have now presented a general formulation of particle transport across a membrane that separates two baths facilitated by nano-channels. We have derived two similar expression of the average particle flux through a nano-channel, that are described in terms of the δ and β parameters as shown in Eq. (2.37) and Eq. (2.40). These two forms of the expression of the particle flux are more general and can be applied to any nano-channel, where the effects of the channel structure are taken into account by the set of the channel parameters.

$$\sigma_c = (\eta_1, \eta_2, ..., \eta_s, \gamma_1, \gamma_2, ..., \gamma_s, k_1^+, k_2^+, ..., k_s^+, k_1^-, k_2^-, ..., k_s^-) \tag{2.41}$$

These parameters characterize the nano-channel as they depend on the nature of the nano-channel. The effects of the two baths are taken into account by the set of bath parameters.

$$\sigma_b = (n_e, n_c, \eta_e, \eta_c, \gamma_e, \gamma_c, k_e^+, k_c^-) \tag{2.42}$$

To make progress in the analytical and numerical analysis, we make some assumptions that simplify the general expression of the average particle current given in Eq. (2.37) and Eq. (2.40).

2.5 Approximations and Assumptions of the Bath and Channel Parameters

2.5.1 The Permeability Coefficient of Membrane Transport Facilitated by Nano-Channels

As the form of the general expressions of the average particle flux through a nano-channel with s internal sites in Eq. (2.37) and Eq. (2.40) suggests, we impose the following constraint equation that couples the channel parameters to the emitter and collector bath parameters.

$$\begin{aligned}\frac{k_e^+\eta_e}{k_1^-\gamma_e} &= \beta_1\beta_2\beta_3...\beta_{s-1}\left[\frac{k_c^-\eta_c}{k_s^+\gamma_c}\right] \\ \frac{k_e^+\eta_e}{\gamma_e} &= \delta_1\delta_2\delta_3...\delta_s\left[\frac{k_c^-\eta_c}{\gamma_c}\right]\end{aligned} \tag{2.43}$$

The expression on the left consists of the parameters that couple the emitter bath to the nano-channel and the expression on the right in the square bracket consists of the parameters that couple the collector bath with the nano-channel. Upon using the first constraint equation in Eq. (2.43) into Eq. (2.40), we get the following expression after some rearrangement:

$$J_s = \left[\frac{k_e^+\eta_e}{k_1^-\gamma_e}\right]\left[\frac{1}{\frac{1}{k_1^-\gamma_e\gamma_1}+\frac{1}{k_1^+\gamma_1\gamma_2}+\frac{\beta_1}{k_2^+\gamma_2\gamma_3}+\frac{\beta_1\beta_2}{k_3^+\gamma_3\gamma_4}+...+\frac{\beta_1\beta_2\beta_3...\beta_{s-2}}{k_{s-1}^+\gamma_{s-1}\gamma_s}+\frac{\beta_1\beta_2\beta_3...\beta_{s-1}}{k_s^+\gamma_s\gamma_c}}\right](n_e-n_c) \tag{2.44}$$

where s denotes that the nano-channel has s internal sites. The concentration gradient of the permeating particles between the emitter and collector baths is defined as:

$$\Delta n = n_e - n_c \tag{2.45}$$

Therefore, using Eq. (2.45) into Eq. (2.44), we get:

$$J_s = \left[\frac{k_e^+\eta_e}{k_1^-\gamma_e}\right]\left[\frac{1}{\frac{1}{k_1^-\gamma_e\gamma_1}+\frac{1}{k_1^+\gamma_1\gamma_2}+\frac{\beta_1}{k_2^+\gamma_2\gamma_3}+\frac{\beta_1\beta_2}{k_3^+\gamma_3\gamma_4}+...+\frac{\beta_1\beta_2\beta_3...\beta_{s-2}}{k_{s-1}^+\gamma_{s-1}\gamma_s}+\frac{\beta_1\beta_2\beta_3...\beta_{s-1}}{k_s^+\gamma_s\gamma_c}}\right]\Delta n \tag{2.46}$$

We can rewrite Eq. (2.46) in the conventional law of permeation as:

$$J_s = P_s \Delta n \tag{2.47}$$

Now Eq (2.47) is similar to the standard form of the equation of permeation of particles across a membrane and as a result the parameter P_s is interpreted as the average permeability coefficient associated with particle transport across a membrane, in which the permeation is facilitated by a nano-channel with s-site. By comparing Eq. (2.46) and Eq. (2.47), the average permeability coefficient associated with particle transport through nano-channels is defined as:

$$P_s = \left[\frac{k_e^+ \eta_e}{k_1^- \gamma_e}\right] \left[\frac{1}{\frac{1}{k_1^- \gamma_e \gamma_1} + \frac{1}{k_1^+ \gamma_1 \gamma_2} + \frac{\beta_1}{k_2^+ \gamma_2 \gamma_3} + \frac{\beta_1 \beta_2}{k_3^+ \gamma_3 \gamma_4} + ... + \frac{\beta_1 \beta_2 \beta_3 ... \beta_{s-2}}{k_{s-1}^+ \gamma_{s-1} \gamma_s} + \frac{\beta_1 \beta_2 \beta_3 ... \beta_{s-1}}{k_s^+ \gamma_s \gamma_c}}\right] \tag{2.48}$$

The permeability coefficient characterizes the permeation ability of particles across a membrane facilitated by membrane spanning nano-channels. The permeability coefficient depends on the structure and properties of the nano-channel and also on the properties of the regions ECPS, via η_e, γ_e, k_e^+, and ICPS via γ_c. As one can see from Eq. 2.48, the average permeability coefficient depends on the following set of bath and channel parameters:

$$P_s = P_s(\eta_e, \eta_1, \eta_2, ..., \eta_s, \eta_c, k_e^+, k_1^+, k_2^+, ..., k_s^+, k_1^-, k_2^-, ..., k_s^-, k_c^-) \tag{2.49}$$

When the transition rates k_e^+ and k_c^- are expressed in units of $M^{-1}s^{-1}$, where M refers to mole and s refers to second, the permeability coefficient is also given in units of $M^{-1}s^{-1}$ and when k_e^+ and k_c^- are expressed in units of $(\mu M)^{-1}s^{-1}$, where μM refers to micro-moles, the permeability coefficient is also given in units of $(\mu M)^{-1}s^{-1}$ so that the particle flux is in units of s^{-1}.

Moreover, using the first constraint equation in Eq. 2.43 into Eq. (2.48) can also be rearranged and can be defined in terms of the δ parameters as:

$$P_s = \left[\frac{k_e^+ \eta_e}{\gamma_e}\right] \left[\frac{1}{\frac{1}{\gamma_e \gamma_1} + \frac{\delta_1}{\gamma_1 \gamma_2} + \frac{\delta_1 \delta_2}{\gamma_2 \gamma_3} + ... + \frac{\delta_1 \delta_2 \delta_3 ... \delta_{s-1}}{\gamma_{s-1} \gamma_s} + \frac{\delta_1 \delta_2 \delta_3 ... \delta_s}{\gamma_s \gamma_c}}\right] \tag{2.50}$$

The expressions of the permeability coefficients defined in Eq (2.48) and in Eq. (2.50) are equivalent as one can be reduced to the other by some rearrangement

of the transition rates. Therefore, both Eq (2.48) and in Eq. (2.50) can be expressed in terms of the transition rates as:

$$P_s = \left[\frac{k_e^+\eta_e}{\gamma_e}\right]\left[\frac{1}{\frac{1}{\gamma_e\gamma_1}+\frac{k_1^-}{k_1^+}\frac{1}{\gamma_1\gamma_2}+\frac{k_1^-k_2^-}{k_1^+k_2^+}\frac{1}{\gamma_2\gamma_3}+\frac{k_1^-k_2^-k_3^-}{k_1^+k_2^+k_3^+}\frac{1}{\gamma_3\gamma_4}+...+\frac{k_1^-k_2^-...k_s^-}{k_1^+k_2^+...k_s^+}\frac{1}{\gamma_s\gamma_c}}\right] \tag{2.51}$$

2.6 Equality of the δ and β Parameters

Let us assume that all the δ parameters are equal. That is:

$$\delta_1 = \delta_2 = \delta_3 = ... = \delta_s = \delta \tag{2.52}$$

This means that the ratios of the forward to backward transition rates from each lattice site are equal. Upon substituting Eq. (2.52) into Eq. (2.37), we get:

$$J_s = \frac{\frac{n_e\eta_e k_e^+}{\gamma_e} - \frac{\delta^s n_c\eta_c k_c^-}{\gamma_c}}{\frac{1}{\gamma_e\gamma_1}+\frac{\delta}{\gamma_1\gamma_2}+\frac{\delta^2}{\gamma_2\gamma_3}+\frac{\delta^3}{\gamma_3\gamma_4}+...+\frac{\delta^{s-1}}{\gamma_{s-1}\gamma_s}+\frac{\delta^s}{\gamma_s\gamma_c}} \tag{2.53}$$

Upon substituting Eq. (2.52) into Eq. (2.50), the expression of average permeability coefficient becomes:

$$P_s = \frac{\eta_e k_e^+}{\gamma_e}\left[\frac{1}{\frac{1}{\gamma_e\gamma_1}+\frac{\delta}{\gamma_1\gamma_2}+\frac{\delta^2}{\gamma_2\gamma_3}+\frac{\delta^3}{\gamma_3\gamma_4}+...+\frac{\delta^{s-1}}{\gamma_{s-1}\gamma_s}+\frac{\delta^s}{\gamma_s\gamma_c}}\right] \tag{2.54}$$

Let us also assume that all the β parameters are equal. That is:

$$\beta_1 = \beta_2 = \beta_3 = ... = \beta_s = \beta \tag{2.55}$$

This means that the ratios of the forward to backward transition rates across each potential barrier in the nano-channel are equal. Upon substituting Eq. (2.55) into Eq. (2.40), the expression of the average particle flux becomes:

$$J_s = \frac{\left[\frac{n_e\eta_e}{\gamma_e}\right]\frac{k_e^+}{k_1^-} - \beta^{s-1}\left[\frac{n_c\eta_c}{\gamma_c}\right]\frac{k_c^-}{k_s^+}}{\frac{1}{k_1^-\gamma_e\gamma_1}+\frac{1}{k_1^+\gamma_1\gamma_2}+\frac{\beta}{k_2^+\gamma_2\gamma_3}+\frac{\beta^2}{k_3^+\gamma_3\gamma_4}+...+\frac{\beta^{s-2}}{k_{s-1}^+\gamma_{s-1}\gamma_s}+\frac{\beta^{s-1}}{k_s^+\gamma_s\gamma_c}} \tag{2.56}$$

Upon substituting Eq. (2.55) into Eq. (2.48), the expression of average permeability coefficient becomes:

$$P_s = \left[\frac{k_e^+\eta_e}{k_1^-\gamma_e}\right]\left[\frac{1}{\frac{1}{k_1^-\gamma_e\gamma_1}+\frac{1}{k_1^+\gamma_1\gamma_2}+\frac{\beta}{k_2^+\gamma_2\gamma_3}+\frac{\beta^2}{k_3^+\gamma_3\gamma_4}+...+\frac{\beta^{s-2}}{k_{s-1}^+\gamma_{s-1}\gamma_s}+\frac{\beta^{s-1}}{k_s^+\gamma_s\gamma_c}}\right] \tag{2.57}$$

As Eq. (2.57) suggests, let us assume that all the forward transition rates, except k_s^+, are equal, that is:

$$k_1^+ = k_2^+ = ... = k_{s-1}^+ = k_f \tag{2.58}$$

Therefore, upon combining Eq. (2.58) and Eq. (2.55), we get that all the backward transition rates, except k_1^-, are also equal. That is:

$$k_2^- = k_3^- = ... = k_s^- = k_b \tag{2.59}$$

Using Eq. (2.58) into Eq. (2.56), we get:

$$J_s = \frac{\left[\frac{n_e\eta_e}{\gamma_e}\right]\frac{k_e^+}{k_1^-} - \beta^{s-1}\left[\frac{n_c\eta_c}{\gamma_c}\right]\frac{k_c^-}{k_s^+}}{\frac{1}{k_1^-\gamma_e\gamma_1} + \frac{1}{k_f}\left\{\frac{1}{\gamma_1\gamma_2} + \frac{\beta}{\gamma_2\gamma_3} + \frac{\beta^2}{\gamma_3\gamma_4} + ... + \frac{\beta^{s-2}}{\gamma_{s-1}\gamma_s}\right\} + \frac{\beta^{s-1}}{k_s^+\gamma_s\gamma_c}} \tag{2.60}$$

Moreover, using Eq. (2.58) into Eq. (2.57), we get:

$$P_s = \left[\frac{k_e^+\eta_e}{k_1^-\gamma_e}\right]\left[\frac{1}{\frac{1}{k_1^-\gamma_e\gamma_1} + \frac{1}{k_f}\left\{\frac{1}{\gamma_1\gamma_2} + \frac{\beta}{\gamma_2\gamma_3} + \frac{\beta^2}{\gamma_3\gamma_4} + ... + \frac{\beta^{s-2}}{\gamma_{s-1}\gamma_s}\right\} + \frac{\beta^{s-1}}{k_s^+\gamma_s\gamma_c}}\right] \tag{2.61}$$

2.7 Equality of the Occupation Numbers of the Internal Potential Wells

We also assume that the occupation numbers of all the internal lattice sites of the nano-channel are equal. That is:

$$\begin{aligned}\eta_1 &= \eta_2 = \eta_3 = ... = \eta_s = \eta \\ \gamma_1 &= \gamma_2 = \gamma_3 = ... = \gamma_s = \gamma = 1 - \eta\end{aligned} \tag{2.62}$$

Using Eq. (2.62) into Eq. (2.53), the expression of the average particle flux becomes:

$$\begin{aligned}J_s &= \frac{\frac{n_e\eta_e k_e^+}{\gamma_e} - \frac{\delta^s n_c\eta_c k_c^-}{\gamma_c}}{\frac{1}{\gamma_e\gamma} + \frac{\delta}{\gamma^2} + \frac{\delta^2}{\gamma^2} + \frac{\delta^3}{\gamma^2} + ... + \frac{\delta^{s-1}}{\gamma^2} + \frac{\delta^s}{\gamma\gamma_c}} \\ J_s &= \frac{\frac{n_e\eta_e k_e^+}{\gamma_e} - \frac{\delta^s n_c\eta_c k_c^-}{\gamma_c}}{\frac{1}{\gamma}\left(\frac{1}{\gamma_e} - \frac{1}{\gamma}\right) + \frac{\delta^s}{\gamma}\left(\frac{1}{\gamma_c} - \frac{1}{\gamma}\right) + \frac{1}{\gamma^2}(1 + \delta + \delta^2 + \delta^3 + ... + \delta^{s-1} + \delta^s)} \\ J_s &= \gamma^2\left[\frac{\frac{n_e\eta_e k_e^+}{\gamma_e} - \frac{\delta^s n_c\eta_c k_c^-}{\gamma_c}}{\frac{\gamma-\gamma_e}{\gamma_e} + \frac{\delta^s(\gamma-\gamma_c)}{\gamma_c} + (1 + \delta + \delta^2 + \delta^3 + ... + \delta^s)}\right]\end{aligned} \tag{2.63}$$

Using Eq. (2.62) into Eq. (2.54), the expression of the average permeability coefficient becomes:

$$P_s = \frac{k_e^+ \eta_e}{\gamma_e}\left[\frac{1}{\frac{1}{\gamma}(\frac{1}{\gamma_e}-\frac{1}{\gamma})+\frac{\delta^s}{\gamma}(\frac{1}{\gamma_c}-\frac{1}{\gamma})+\frac{1}{\gamma^2}(1+\delta+\delta^2+\delta^3+...+\delta^s)}\right]$$
$$P_s = \frac{\gamma^2 k_e^+ \eta_e}{\gamma_e}\left[\frac{1}{\frac{\gamma-\gamma_e}{\gamma_e}+\frac{\delta^s(\gamma-\gamma_c)}{\gamma_c}+(1+\delta+\delta^2+\delta^3+...+\delta^s)}\right] \tag{2.64}$$

Similarly, using Eq. (2.62) into Eq. (2.60), the expression of the average particle flux becomes:

$$J_s = \frac{\left[\frac{n_e\eta_e}{\gamma_e}\right]\frac{k_e^+}{k_1^-} - \beta^{s-1}\left[\frac{n_c\eta_c}{\gamma_c}\right]\frac{k_c^-}{k_s^+}}{\frac{1}{k_1^-\gamma_e\gamma}+\frac{1}{k_f\gamma^2}\left\{1+\beta+\beta^2+...+\beta^{s-2}\right\}+\frac{\beta^{s-1}}{k_s^+\gamma\gamma_c}}$$
$$J_s = \gamma\frac{\left[\frac{n_e\eta_e}{\gamma_e}\right]\frac{k_e^+}{k_1^-} - \beta^{s-1}\left[\frac{n_c\eta_c}{\gamma_c}\right]\frac{k_c^-}{k_s^+}}{\frac{1}{k_1^-\gamma_e}+\frac{1}{k_f\gamma}\left\{1+\beta+\beta^2+...+\beta^{s-2}\right\}+\frac{\beta^{s-1}}{k_s^+\gamma_c}} \tag{2.65}$$

Moreover, using Eq. (2.62) into Eq. (2.61), the expression of the average permeability coefficient becomes:

$$P_s = \left[\frac{k_e^+\eta_e}{k_1^-\gamma_e}\right]\left[\frac{1}{\frac{1}{k_1^-\gamma_e\gamma}+\frac{1}{k_f\gamma^2}\left\{1+\beta+\beta^2+...+\beta^{s-2}\right\}+\frac{\beta^{s-1}}{k_s^+\gamma\gamma_c}}\right]$$
$$P_s = \left[\frac{\gamma k_e^+\eta_e}{k_1^-\gamma_e}\right]\left[\frac{1}{\frac{1}{k_1^-\gamma_e}+\frac{1}{k_f\gamma}\left\{1+\beta+\beta^2+...+\beta^{s-2}\right\}+\frac{\beta^{s-1}}{k_s^+\gamma_c}}\right] \tag{2.66}$$

When the parameter δ is small compared to one, we can retain only the first order terms for the sum in the denominator of Eq. (2.63) and Eq. (2.64). That is:

$$1+\delta+\delta^2+\delta^3+...+\delta^s \approx 1+\delta \qquad \text{when}\, \delta \ll 1 \tag{2.67}$$

Therefore, using the approximation in Eq. (2.67), the expression of the average particle flux in Eq. (2.63) becomes:

$$J_s = \gamma^2\left[\frac{\frac{n_e\eta_e k_e^+}{\gamma_e} - \frac{\delta^s n_c\eta_c k_c^-}{\gamma_c}}{\frac{\gamma-\gamma_e}{\gamma_e}+\frac{\delta^s(\gamma-\gamma_c)}{\gamma_c}+(1+\delta)}\right] \tag{2.68}$$

Moreover, using Eq. (2.67) into Eq. (2.64), the expression of the average permeability coefficient becomes:

$$P_s = \frac{\gamma^2 k_e^+\eta_e}{\gamma_e}\left[\frac{1}{\frac{\gamma-\gamma_e}{\gamma_e}+\frac{\delta^s(\gamma-\gamma_c)}{\gamma_c}+(1+\delta)}\right] \tag{2.69}$$

Similarly when the parameter β is small compared to one, we can retain only the first order terms for the sum in the denominator of Eq. (2.65) and Eq. (2.66). That is:

$$1+\beta+\beta^2+\beta^3+...+\beta^s \approx 1+\beta \qquad \text{when } \beta \ll 1 \tag{2.70}$$

Thus, using Eq. (2.70) into Eq. (2.65), the expression of the average particle flux becomes:

$$J_s = \frac{\left[\frac{n_e\eta_e}{\gamma_e}\right]\frac{k_e^+}{k_1^-} - \beta^{s-1}\left[\frac{n_c\eta_c}{\gamma_c}\right]\frac{k_c^-}{k_s^+}}{\frac{1}{k_1^-\gamma_e\gamma}+\frac{1}{k_f\gamma^2}\{1+\beta\}+\frac{\beta^{s-1}}{k_s^+\gamma\gamma_c}} \tag{2.71}$$

Moreover, using Eq. (2.70) into Eq. (2.66), the expression of the average permeability coefficient becomes.

$$P_s = \left[\frac{k_e^+\eta_e}{k_1^-\gamma_e}\right]\left[\frac{1}{\frac{1}{k_1^-\gamma_e\gamma}+\frac{1}{k_f\gamma^2}\{1+\beta\}+\frac{\beta^{s-1}}{k_s^+\gamma\gamma_c}}\right] \tag{2.72}$$

When the forward and backward transition rates from each lattice site are equal, that is, $k_j^- = k_j^+$, then $\delta = 1$ and as a result we get:

$$1+\delta+\delta^2+\delta^3+...+\delta^s = s+1 \qquad \text{when } \delta = 1 \tag{2.73}$$

Using Eq. (2.73) into Eq. (2.63), we get:

$$J_s = \gamma^2\left[\frac{\frac{n_e\eta_e k_e^+}{\gamma_e} - \frac{n_c\eta_c k_c^-}{\gamma_c}}{\frac{\gamma-\gamma_e}{\gamma_e}+\frac{(\gamma-\gamma_c)}{\gamma_c}+s+1}\right] \tag{2.74}$$

Using Eq. (2.73) into Eq. (2.64), we get:

$$P_s = \frac{\gamma^2 k_e^+\eta_e}{\gamma_e}\left[\frac{1}{\frac{\gamma-\gamma_e}{\gamma_e}+\frac{(\gamma-\gamma_c)}{\gamma_c}+1+s}\right] \tag{2.75}$$

When the forward and backward transition rates across each potential barrier in the nano-channel are equal, that is, $k_{j+1}^- = k_j^+$, then $\beta = 1$ and as a result we have:

$$1+\beta+\beta^2+\beta^3+...+\beta^{s-2} = s-1 \qquad \text{when } \beta = 1 \tag{2.76}$$

Using Eq. (2.76) into Eq. (2.65), we get:

$$J_s = \gamma \frac{\left[\frac{n_e\eta_e}{\gamma_e}\right]\frac{k_e^+}{k_1^-} - \left[\frac{n_c\eta_c}{\gamma_c}\right]\frac{k_c^-}{k_s^+}}{\frac{1}{k_1^-\gamma_e} + \frac{s-1}{k_f\gamma} + \frac{1}{k_s^+\gamma_c}} \tag{2.77}$$

Moreover, using Eq. (2.76) into Eq. (2.66), we get:

$$P_s = \left[\frac{\gamma k_e^+\eta_e}{k_1^-\gamma_e}\right]\left[\frac{1}{\frac{1}{k_1^-\gamma_e} + \frac{s-1}{k_f\gamma} + \frac{1}{k_s^+\gamma_c}}\right] \tag{2.78}$$

Moreover, when s is very large and $\delta < 1$, the sum in the denominators of Eq. (2.63) and Eq. (2.64) can be represented by a geometric series. That is:

$$\begin{aligned} &\sum_{j=0}^{\infty}\delta^j \to \frac{1}{1-\delta}, \quad \text{when s is large and } \delta < 1 \\ &\frac{\delta^s(\gamma-\gamma_c)}{\gamma_c} \to 0, \quad \text{when s is large, } \delta < 1 \text{ and } \frac{\gamma-\gamma_c}{\gamma_c} < 1 \end{aligned} \tag{2.79}$$

Therefore, using Eq. (2.79) into Eq. (2.63), we get:

$$J_s = \gamma^2\left[\frac{\frac{n_e\eta_e k_e^+}{\gamma_e} - \frac{\delta^s n_c\eta_c k_c^-}{\gamma_c}}{\frac{\gamma-\gamma_e}{\gamma_e} + \frac{1}{1-\delta}}\right] \tag{2.80}$$

Therefore, using Eq. (2.79) into Eq. (2.64), we get:

$$P_s = \frac{\gamma^2 k_e^+\eta_e}{\gamma_e}\left[\frac{1}{\frac{\gamma-\gamma_e}{\gamma_e} + \frac{1}{1-\delta}}\right] \tag{2.81}$$

Furthermore, when s is very large and $\beta < 1$, the sum in the denominators of Eq. (2.65) and Eq. (2.66) can be represented by a geometric series. That is:

$$\begin{aligned} &\sum_{j=0}^{\infty}\beta^j \to \frac{1}{1-\beta}, \quad \text{when s is large and } \beta < 1 \\ &\frac{\beta^{s-1}}{k_s^+\gamma_c} \to 0, \quad \text{when s is large, } \beta < 1 \text{ and } \frac{1}{k_s^+\gamma_c} < 1 \end{aligned} \tag{2.82}$$

Therefore, using Eq. (2.82) into Eq. (2.65), we get:

$$J_s = \left[\frac{\gamma n_e\eta_e k_e^+}{k_1^-\gamma_e}\right]\left[\frac{1}{\frac{1}{k_1^-\gamma_e} + \frac{1}{k_f\gamma}\left\{\frac{1}{1-\beta}\right\}}\right] \tag{2.83}$$

Therefore, using Eq. (2.82) into Eq. (2.66), we get:

$$P_s = \left[\frac{\gamma k_e^+\eta_e}{k_1^-\gamma_e}\right]\left[\frac{1}{\frac{1}{k_1^-\gamma_e} + \frac{1}{k_f\gamma}\left\{\frac{1}{1-\beta}\right\}}\right] \tag{2.84}$$

2.8 Expression of the δ Parameters in terms of the Equilibrium Values

We assumed that the forward and backward transition rates and hence the delta and beta parameters are independent of the occupation numbers of the lattice sites of the nano-channel and also independent of the concentrations of the permeating particles in the two baths. Therefore, we can express the δ and β parameters in terms of the equilibrium values of the particle number densities and occupation numbers of the two end sites. The average particle flux through the nano-channel vanishes at equilibrium even in the presence of a concentration gradient between the two baths. This is so because the average current depends not only on the concentration gradient between the two baths but also on the occupation numbers of the two external sites, on the occupation numbers of the s internal sites and on the two jump rates from the two baths to the nano-channel via the two end sites. We can write this functional dependence as:

$$J_s = J(n_e, n_c, \eta_e, \eta_c, k_e^+, k_c^-, \gamma_e, \gamma_1, \gamma_2, ..., \gamma_s, \gamma_c, k_1^-, k_2^-, ..., k_s^-, k_1^+, k_2^+, ..., k_s^+) \quad (2.85)$$

Thus, employing the condition that the average current can vanish if the expression in the numerator of Eq. (2.37) is zero for a finite value of the expression in the denominator, we can determine the expression of the product of the δ parameters in the square bracket in Eq. (2.37). We can solve for the product of the δ parameters by setting the expression in the numerator of Eq. (2.37) to zero. That is:

$$\mu_s = \delta_1\delta_2...\delta_s = \frac{n_e^o}{n_c^o}\frac{\eta_e^o}{\eta_c^o}\frac{\gamma_c^o}{\gamma_e^o}\frac{k_e^+}{k_c^-} \quad (2.86)$$

where the superscript o denotes the values assumed by these parameters when the system is in equilibrium, that is, when there is no net flux through the nano-channel. Therefore, using Eq. (2.86) into Eq. (2.37), the expression of the average particle flux through the nano-channel becomes:

$$J_s = \frac{\frac{n_e\eta_e k_e^+}{\gamma_e} - \left[\frac{n_e^o}{n_c^o}\frac{\eta_e^o}{\eta_c^o}\frac{\gamma_c^o}{\gamma_e^o}\frac{k_e^+}{k_c^-}\right]\left[\frac{n_c\eta_c k_c^-}{\gamma_c}\right]}{\frac{1}{\gamma_e\gamma_1} + \frac{\delta_1}{\gamma_1\gamma_2} + \frac{\delta_1\delta_2}{\gamma_2\gamma_3} + \frac{\delta_1\delta_1\delta_3}{\gamma_3\gamma_4} + ... + \frac{\delta_1\delta_2\delta_3...\delta_{s-1}}{\gamma_{s-1}\gamma_s} + \frac{\delta_1\delta_2\delta_3...\delta_s}{\gamma_s\gamma_c}} \quad (2.87)$$

We can rearrange Eq. (2.87) in another form as:

$$J_s = \frac{n_e^o \eta_e^o k_e^+}{\gamma_e^o} \left[\frac{\frac{\frac{n_e}{n_e^o}\frac{\eta_e}{\eta_e^o}}{\frac{\gamma_e}{\gamma_e^o}} - \frac{\frac{n_c}{n_c^o}\frac{\eta_c}{\eta_c^o}}{\frac{\gamma_c}{\gamma_c^o}}}{\frac{1}{\gamma_e\gamma_1} + \frac{\delta_1}{\gamma_1\gamma_2} + \frac{\delta_1\delta_2}{\gamma_2\gamma_3} + \frac{\delta_1\delta_1\delta_3}{\gamma_3\gamma_4} + ... + \frac{\delta_1\delta_2\delta_3...\delta_{s-1}}{\gamma_{s-1}\gamma_s} + \frac{\delta_1\delta_2\delta_3...\delta_s}{\gamma_s\gamma_c}} \right] \tag{2.88}$$

We now define the following normalized bath and channel parameters.

$$\begin{aligned}
\rho_e &= \frac{n_e}{n_e^o}; \\
\rho_c &= \frac{n_c}{n_c^o}; \\
\nu_e &= \frac{\eta_e}{\eta_e^o}; \\
\nu_1 &= \frac{\eta_1}{\eta_1^o}; \\
\nu_s &= \frac{\eta_s}{\eta_s^o}; \\
\nu_c &= \frac{\eta_c}{\eta_c^o}; \\
\lambda_e &= \frac{\gamma_e}{\gamma_e^o}; \\
\lambda_c &= \frac{\gamma_c}{\gamma_c^o}
\end{aligned} \tag{2.89}$$

Using Eq. (2.89) into Eq. (2.88), we get:

$$J_s = \frac{n_e^o \eta_e^o k_e^+}{\gamma_e^o} \left[\frac{\frac{\rho_e\nu_e}{\lambda_e} - \frac{\rho_c\nu_c}{\lambda_c}}{\frac{1}{\gamma_e\gamma_1} + \frac{\delta_1}{\gamma_1\gamma_2} + \frac{\delta_1\delta_2}{\gamma_2\gamma_3} + \frac{\delta_1\delta_1\delta_3}{\gamma_3\gamma_4} + ... + \frac{\delta_1\delta_2\delta_3...\delta_{s-1}}{\gamma_{s-1}\gamma_s} + \frac{\delta_1\delta_2\delta_3...\delta_s}{\gamma_s\gamma_c}} \right] \tag{2.90}$$

Moreover, Eq. (2.90) can be rewritten in a more convenient way.

$$J_s = \frac{\rho_e\nu_e n_e^o \eta_e^o k_e^+}{\lambda_e\gamma_e^o} \left[\frac{1 - \frac{\rho_c\nu_c\lambda_e}{\rho_e\nu_e\lambda_c}}{\frac{1}{\gamma_e\gamma_1} + \frac{\delta_1}{\gamma_1\gamma_2} + \frac{\delta_1\delta_2}{\gamma_2\gamma_3} + \frac{\delta_1\delta_1\delta_3}{\gamma_3\gamma_4} + ... + \frac{\delta_1\delta_2\delta_3...\delta_{s-1}}{\gamma_{s-1}\gamma_s} + \frac{\delta_1\delta_2\delta_3...\delta_s}{\gamma_s\gamma_c}} \right] \tag{2.91}$$

The average particle flux injected from the emitter bath into the nano-channel via its leftmost site is:

$$\begin{aligned}
J &= n_e\eta_e\gamma_1 k_e^+ - \eta_1\gamma_e k_1^- \\
J &= \rho_e\nu_e\gamma_1 n_e^o\eta_e^o k_e^+ \left[1 - \frac{\eta_1\gamma_e k_1^-}{\rho_e\nu_e\gamma_1 n_e^o\eta_e^o k_e^+} \right]
\end{aligned} \tag{2.92}$$

At steady state the average particle flux has the same value across each potential barrier of the nano-channel. Therefore, employing this property, we can equate

the two expressions of the average particle fluxes in Eq. (2.91) and Eq. 2.92 so as to get the expression of the factor in the denominator of Eq. (2.91).

$$\frac{1}{\frac{1}{\gamma_e\gamma_1}+\frac{\delta_1}{\gamma_1\gamma_2}+\frac{\delta_1\delta_2}{\gamma_2\gamma_3}+\frac{\delta_1\delta_1\delta_3}{\gamma_3\gamma_4}+...+\frac{\delta_1\delta_2\delta_3...\delta_{s-1}}{\gamma_{s-1}\gamma_s}+\frac{\delta_1\delta_2\delta_3...\delta_s}{\gamma_s\gamma_c}}=\gamma_1\lambda_e\gamma_e^o\left[\frac{1-\frac{\eta_1\gamma_e k_1^-}{\rho_e\nu_e\gamma_1 n_e^o\eta_e^o k_e^+}}{1-\frac{\rho_c\nu_c\lambda_e}{\rho_e\nu_e\lambda_c}}\right] \tag{2.93}$$

Now if the second term in the denominator of the expression on the right hand side of Eq. (2.93) is small compared to one, then we can expand it using Taylor's series and retain only the first order terms and neglect higher order terms. That is:

$$\frac{1}{\frac{1}{\gamma_e\gamma_1}+\frac{\delta_1}{\gamma_1\gamma_2}+\frac{\delta_1\delta_2}{\gamma_2\gamma_3}+\frac{\delta_1\delta_1\delta_3}{\gamma_3\gamma_4}+...+\frac{\delta_1\delta_2\delta_3...\delta_{s-1}}{\gamma_{s-1}\gamma_s}+\frac{\delta_1\delta_2\delta_3...\delta_s}{\gamma_s\gamma_c}}= \gamma_1\lambda_e\gamma_e^o\left[1-\frac{\eta_1\gamma_e k_1^-}{\rho_e\nu_e\gamma_1 n_e^o\eta_e^o k_e^+}\right]\left[1+\frac{\rho_c\nu_c\lambda_e}{\rho_e\nu_e\lambda_c}\right] \tag{2.94}$$

Upon substituting Eq. (2.94) into Eq. (2.91), after some rearrangement we get:

$$J=\rho_e\nu_e\gamma_1 n_e^o\eta_e^o k_e^+\left[1-\frac{\eta_1\gamma_e k_1^-}{\rho_e\nu_e\gamma_1 n_e^o\eta_e^o k_e^+}\right]\left[1-\left\{\frac{\rho_c\nu_c\lambda_e}{\rho_e\nu_e\lambda_c}\right\}^2\right] \tag{2.95}$$

2.9 Expression of the β Parameters in terms of the Equilibrium Values

Following the same arguments as we did in the previous section, employing the condition that the average current can vanish if the expression in the numerator of Eq. (2.40) is zero for a finite value of the expression in the denominator, we can determine the expression of the product of the beta parameters in the square bracket in Eq. (2.40). We can solve for the product of the beta parameters by setting the expression in the numerator of Eq. (2.40) to zero. That is:

$$\mu_s=\beta_1\beta_2...\beta_{s-1}=\frac{n_e^o}{n_c^o}\frac{\eta_e^o}{\eta_c^o}\frac{\gamma_c^o}{\gamma_e^o}\frac{k_e^+}{k_c^-}\frac{k_s^+}{k_1^-} \tag{2.96}$$

where the superscript o denotes the values assumed by these parameters when the system is in equilibrium, that is, when there is no net flux through the nano-

channel. Therefore, using Eq. (2.96) into Eq. (2.40), we get:

$$J_s = \frac{k_e^+}{k_1^-}\left[\frac{\frac{n_e\eta_e}{\gamma_e} - \left[\frac{n_e^o}{n_c^o}\frac{\eta_e^o}{\eta_c^o}\frac{\gamma_c^o}{\gamma_e^o}\right]\left[\frac{n_c\eta_c}{\gamma_c}\right]}{\frac{1}{k_1^-\gamma_e\gamma_1} + \frac{1}{k_1^+\gamma_1\gamma_2} + \frac{\beta_1}{k_2^+\gamma_2\gamma_3} + \frac{\beta_1\beta_2}{k_3^+\gamma_3\gamma_4} + ... + \frac{\beta_1\beta_2\beta_3...\beta_{s-2}}{k_{s-1}^+\gamma_{s-1}\gamma_s} + \frac{\beta_1\beta_2\beta_3...\beta_{s-1}}{k_s^+\gamma_s\gamma_c}}\right] \tag{2.97}$$

We can rearrange Eq. (2.97) as:

$$J_s = \frac{n_e^o\eta_e^o k_e^+}{\gamma_e^o k_1^-}\left[\frac{\frac{n_e}{n_e^o}\frac{\eta_e}{\eta_e^o}\frac{\gamma_e^o}{\gamma_e} - \frac{n_c}{n_c^o}\frac{\eta_c}{\eta_c^o}\frac{\gamma_c^o}{\gamma_c}}{\frac{1}{k_1^-\gamma_e\gamma_1} + \frac{1}{k_1^+\gamma_1\gamma_2} + \frac{\beta_1}{k_2^+\gamma_2\gamma_3} + \frac{\beta_1\beta_2}{k_3^+\gamma_3\gamma_4} + ... + \frac{\beta_1\beta_2\beta_3...\beta_{s-2}}{k_{s-1}^+\gamma_{s-1}\gamma_s} + \frac{\beta_1\beta_2\beta_3...\beta_{s-1}}{k_s^+\gamma_s\gamma_c}}\right] \tag{2.98}$$

Employing the notation in Eq. (2.89), Eq. (2.98) becomes:

$$J_s = \frac{n_e^o\eta_e^o k_e^+}{\gamma_e^o k_1^-}\left[\frac{\frac{\rho_e\nu_e}{\lambda_e} - \frac{\rho_c\nu_c}{\lambda_c}}{\frac{1}{k_1^-\gamma_e\gamma_1} + \frac{1}{k_1^+\gamma_1\gamma_2} + \frac{\beta_1}{k_2^+\gamma_2\gamma_3} + \frac{\beta_1\beta_2}{k_3^+\gamma_3\gamma_4} + ... + \frac{\beta_1\beta_2\beta_3...\beta_{s-2}}{k_{s-1}^+\gamma_{s-1}\gamma_s} + \frac{\beta_1\beta_2\beta_3...\beta_{s-1}}{k_s^+\gamma_s\gamma_c}}\right] \tag{2.99}$$

This equation can also be written as:

$$J_s = \frac{\rho_e\nu_e}{\lambda_e}\frac{n_e^o\eta_e^o k_e^+}{\gamma_e^o k_1^-}\left[\frac{1 - \frac{\rho_c\nu_c\lambda_e}{\rho_e\nu_e\lambda_c}}{\frac{1}{k_1^-\gamma_e\gamma_1} + \frac{1}{k_1^+\gamma_1\gamma_2} + \frac{\beta_1}{k_2^+\gamma_2\gamma_3} + \frac{\beta_1\beta_2}{k_3^+\gamma_3\gamma_4} + ... + \frac{\beta_1\beta_2\beta_3...\beta_{s-2}}{k_{s-1}^+\gamma_{s-1}\gamma_s} + \frac{\beta_1\beta_2\beta_3...\beta_{s-1}}{k_s^+\gamma_s\gamma_c}}\right] \tag{2.100}$$

The average particle flux injected from the emitter bath into the leftmost site of the nano-channel is given by Eq. (2.92). At steady state the average particle flux has the same value across each potential barrier between neighboring potential wells of the nano-channel. Therefore, employing this property, we can equate Eq. (2.92) to Eq. (2.100) so as to get the same expression of the average particle current at steady state, that is Eq. (2.95).

$$J_s = \rho_e\nu_e\gamma_1 n_e^o\eta_e^o k_e^+\left[1 - \frac{\eta_1\gamma_e k_1^-}{\rho_e\nu_e\gamma_1 n_e^o\eta_e^o k_e^+}\right]\left[1 - \left\{\frac{\rho_c\nu_c\lambda_e}{\rho_e\nu_e\lambda_c}\right\}^2\right] \tag{2.101}$$

2.10 The Assumption of Uniform Average Particle Flux Across Each Potential Barrier at Steady State

The expression of χ_s defined in Eq. (2.29) can be rewritten as:

$$\chi_s = \gamma_e\gamma_1\left[\sum_{i=1}^{s-1}\frac{1}{\gamma_i\gamma_{i+1}}\prod_{r=1}^{i}\frac{k_r^-}{k_r^+}+\frac{1}{\gamma_s\gamma_c}\prod_{r=1}^{s}\frac{k_r^-}{k_r^+}\right]$$
$$\chi_s = \frac{\gamma_e\gamma_1}{\gamma_s\gamma_c}\left[\sum_{i=1}^{s-1}\frac{\gamma_s\gamma_c}{\gamma_i\gamma_{i+1}}\prod_{r=1}^{i}\frac{k_r^-}{k_r^+}+\prod_{r=1}^{s}\frac{k_r^-}{k_r^+}\right] \tag{2.102}$$

Moreover, we assume that the average particle current across each potential barrier between neighboring potential energy wells is zero at equilibrium. Thus, for the potential energy barrier between the sites V_i and V_{i+1} we have:

$$\eta_e^o = \prod_{r=1}^{i+1}\frac{\omega_r^-}{\omega_{r-1}^+}\eta_i^o$$
$$\eta_e^o = \frac{\gamma_e^o\eta_{i+1}^o k_{i+1}^-}{n_e^o\gamma_{i+1}^o k_e^+}\prod_{r=1}^{i}\frac{k_r^-}{k_r^+} \tag{2.103}$$

Solving for the product of the ratio of the jump rates in Eq. (2.103), we get

$$\prod_{r=1}^{i}\frac{k_r^-}{k_r^+} = \frac{\gamma_{i+1}^o}{\gamma_e^o}\frac{n_e^o\eta_e^o}{\eta_{i+1}^o}\frac{k_e^+}{k_{i+1}^-}$$
$$\prod_{r=1}^{s}\frac{k_r^-}{k_r^+} = \frac{\gamma_c^o}{\gamma_e^o}\frac{n_e^o\eta_e^o}{n_c^o\eta_c^o}\frac{k_e^+}{k_c^-} \tag{2.104}$$

Upon substituting Eq. (2.104) into Eq. (2.102), we get:

$$\chi_s = \frac{\gamma_e\gamma_1}{\gamma_s\gamma_c}\left[\sum_{i=1}^{s-1}\frac{\gamma_s\gamma_c}{\gamma_i\gamma_{i+1}}\frac{\gamma_{i+1}^o}{\gamma_e^o}\frac{n_e^o\eta_e^o}{\eta_{i+1}^o}\frac{k_e^+}{k_{i+1}^-}+\frac{\gamma_c^o}{\gamma_e^o}\frac{n_e^o\eta_e^o}{n_c^o\eta_c^o}\frac{k_e^+}{k_c^-}\right]$$
$$\chi_s = \frac{\gamma_e\gamma_1 n_e^o\eta_e^o k_e^+}{\gamma_e^o}\left[\sum_{i=1}^{s-1}\left\{\frac{\gamma_{i+1}^o}{\gamma_i\gamma_{i+1}\eta_{i+1}^o k_{i+1}^-}\right\}+\frac{\gamma_c^o}{\gamma_s\gamma_c n_c^o\eta_c^o k_c^-}\right] \tag{2.105}$$

We can now write the above expression as:

$$\chi_s = av_s \tag{2.106}$$

where we have defined that:

$$a = \frac{\gamma_e\gamma_1 n_e^o\eta_e^o k_e^+}{\gamma_e^o}$$
$$v_s = \sum_{i=1}^{s-1}\left\{\frac{\gamma_{i+1}^o}{\gamma_i\gamma_{i+1}\eta_{i+1}^o k_{i+1}^-}\right\}+\frac{\gamma_c^o}{\gamma_s\gamma_c n_c^o\eta_c^o k_c^-} \tag{2.107}$$

Now using Eq. (2.106) and (2.86) into (2.30), we get:

$$J_s = \frac{\gamma_1}{\gamma_c}\left[\frac{n_e\eta_e\gamma_c k_e^+ - \left[\frac{n_e^o}{n_c^o}\frac{\eta_e^o}{\eta_c^o}\frac{\gamma_c^o}{\gamma_e^o}\frac{k_e^+}{k_c^-}\right] n_c\eta_c\gamma_e k_c^-}{1+a\upsilon_s}\right] \tag{2.108}$$

The expression in Eq. (2.108) can be written as:

$$J_s = n_e\eta_e k_e^+\gamma_1\left[\frac{1-\frac{n_e^o}{n_e}\frac{\eta_e^o}{\eta_e}\frac{\gamma_c^o}{\gamma_c}\frac{n_c}{n_c^o}\frac{\eta_c}{\eta_c^o}\frac{\gamma_e}{\gamma_e^o}}{1+a\upsilon_s}\right] \tag{2.109}$$

Using the definitions of the gamma variables in Eq. (1.4) into Eq. (2.109), we get:

$$J_s = n_e\eta_e k_e^+(1-\eta_1)\left[\frac{1-\frac{n_e^o}{n_e}\frac{\eta_e^o}{\eta_e}\frac{(1-\eta_c^o)}{(1-\eta_c)}\frac{n_c}{n_c^o}\frac{\eta_c}{\eta_c^o}\frac{(1-\eta_e}{(1-\eta_e^o}}{1+a\upsilon_s}\right] \tag{2.110}$$

Let us define the following variables for convenience

$$\begin{aligned}\nu_e^o &= \frac{1}{\eta_e^o};\\ \nu_1^o &= \frac{1}{\eta_1^o};\\ \nu_s^o &= \frac{1}{\eta_s^o};\\ \nu_c^o &= \frac{1}{\eta_c^o}\end{aligned} \tag{2.111}$$

Using the definitions given in Eq. (2.89) and (2.111) into Eq. (2.110), we get:

$$J_s = \rho_e\nu_e(\nu_1^o-\nu_1)n_e^o\eta_e^o\eta_1^o k_e^+\left[\frac{1-\frac{\rho_c\nu_c}{\rho_e\nu_e}\frac{\nu_e-\nu_e^o}{\nu_c-\nu_c^o}\frac{\nu_c^o-1}{\nu_e^o-1}}{1+av_s}\right] \tag{2.112}$$

At steady state the average current must be the same across each potential barrier traversed by the particles. Therefore, using the definitions given in Eq. (2.89) and (2.111) into Eq. (2.92), we get the expression of the average particle flux across the potential barrier between the sites V_e and V_1.

$$J_s = \rho_e\nu_e(\nu_1^o-\nu_1)n_e^o\eta_e^o\eta_1^o k_e^+\left[1-\frac{\nu_1(\nu_e-\nu_e^o)k_1^-}{\rho_e\nu_e(\nu_1-\nu_1^o)n_e^o k_e^+}\right] \tag{2.113}$$

By equating Eq. (2.112) and (2.113), we get the expression of the term in the denominator of Eq. (2.112).

$$\frac{1}{1+av_s} = \frac{1-\frac{\nu_1(\nu_e-\nu_e^o)k_1^-}{\rho_e\nu_e(\nu_1-\nu_1^o)n_e^o k_e^+}}{1-\frac{\rho_c\nu_c}{\rho_e\nu_e}\frac{\nu_e-\nu_e^o}{\nu_c-\nu_c^o}\frac{\nu_c^o-1}{\nu_e^o-1}} \tag{2.114}$$

Now for small values of the second expression in the denominator of Eq. (2.114), we can expand it using Taylor's series and retain only the first order terms and neglect higher order terms:

$$\frac{1}{1+av_s} = \left[1 - \frac{\nu_1(\nu_e - \nu_e^o)k_1^-}{\rho_e\nu_e(\nu_1 - \nu_1^o)n_e^o k_e^+}\right]\left[1 + \frac{\rho_c\nu_c}{\rho_e\nu_e}\frac{\nu_e - \nu_e^o}{\nu_c - \nu_c^o}\frac{\nu_c^o - 1}{\nu_e^o - 1}\right] \tag{2.115}$$

Upon substituting Eq. (2.115) into Eq. (2.112), we get the following expression of the average particle flux after some rearangement:

$$\begin{aligned} J_s = \rho_e\nu_e(\nu_1^o - \nu_1)n_e^o\eta_e^o\eta_1^o k_e^+ \left[1 - \frac{\nu_1(\nu_e - \nu_e^o)k_1^-}{\rho_e\nu_e(\nu_1 - \nu_1^o)n_e^o k_e^+}\right] \\ \left[1 - \left\{\frac{\rho_c\nu_c}{\rho_e\nu_e}\frac{\nu_e - \nu_e^o}{\nu_c - \nu_c^o}\frac{\nu_c^o - 1}{\nu_e^o - 1}\right\}^2\right] \end{aligned} \tag{2.116}$$

We can also have another similar expression of the average particle flux at steady state following the same procedures. As stated previously, during the derivation of Eq. (2.116), the average particle flux is assumed to have the same value across each potential barrier traversed by the particle. Thus, the average particle flux across the potential barrier between the sites V_s and V_c is:

$$J_s = \eta_s\gamma_c k_s^+ - n_c\eta_c\gamma_s k_c^- \tag{2.117}$$

Using the definitions given in Eq. (2.89) and (2.111) into Eq. (2.117), we get:

$$\begin{aligned} J_s &= -n_c\eta_c\gamma_s k_c^- \left[1 - \frac{\eta_s\gamma_c k_s^+}{n_c\eta_c\gamma_s k_c^-}\right] \\ J_s &= -\rho_c\nu_c(\nu_s^o - \nu_s)n_c^o\eta_c^o\eta_s^o k_c^- \left[1 - \frac{(\nu_c^o - \nu_c)\nu_s k_s^+}{\rho_c\nu_c(\nu_s^o - \nu_s)n_c^o k_c^-}\right] \end{aligned} \tag{2.118}$$

By equating Eq. (2.112) and (2.118), we get another expression of the term in the denominator of equation 2.112:

$$\frac{1}{1+av_s} = -\left[\frac{\rho_c\nu_c(\nu_s^o - \nu_s)n_c^o\eta_c^o\eta_s^o k_c^-}{\rho_e\nu_e(\nu_1^o - \nu_1)n_e^o\eta_e^o\eta_1^o k_e^+}\right]\left[\frac{1 - \frac{(\nu_c^o - \nu_c)\nu_s k_s^+}{\rho_c\nu_c(\nu_s^o - \nu_s)n_c^o k_c^-}}{1 - \frac{\rho_c\nu_c}{\rho_e\nu_e}\frac{\nu_e - \nu_e^o}{\nu_c - \nu_c^o}\frac{\nu_c^o - 1}{\nu_e^o - 1}}\right] \tag{2.119}$$

Now for small values of the second term in the denominator of Eq. (2.119), we can expand it using Taylor's series and retain only the first order terms and neglect the higher order terms.

$$\frac{1}{1+av_s} = -\left[\frac{\rho_c\nu_c(\nu_s^o - \nu_s)n_c^o\eta_c^o\eta_s^o k_c^-}{\rho_e\nu_e(\nu_1^o - \nu_1)n_e^o\eta_e^o\eta_1^o k_e^+}\right]\left[1 - \frac{\nu_s(\nu_c^o - \nu_c)k_s^+}{\rho_c\nu_c(\nu_s^o - \nu_s)n_c^o k_c^-}\right]\left[1 + \frac{\rho_c\nu_c}{\rho_e\nu_e}\frac{\nu_e - \nu_e^o}{\nu_c - \nu_c^o}\frac{\nu_c^o - 1}{\nu_e^o - 1}\right] \tag{2.120}$$

Upon substituting Eq. (2.120) into Eq. (2.112), we get the following general expression of the average particle flux at steady state after some rearrangement:

$$J_s = \rho_c \nu_c (\nu_s - \nu_s^o) n_c^o \eta_c^o \eta_s^o k_c^- \left[1 - \frac{\nu_s(\nu_c^o - \nu_c)k_s^+}{\rho_c \nu_c (\nu_s^o - \nu_s) n_c^o k_c^-}\right] \left[1 - \left\{\frac{\rho_c \nu_c}{\rho_e \nu_e} \frac{\nu_e - \nu_e^o}{\nu_c - \nu_c^o} \frac{\nu_c^o - 1}{\nu_e^o - 1}\right\}^2\right] \tag{2.121}$$

The average particle fluxes given by the expressions in Eq. (2.95), (2.101), (2.116) and (2.121) are simply the average particle flux through a nano-channel with a single internal site with a small perturbation term that is less than one. That is, the second terms on the right hand side are considered as small perturbations to the particle flux through a nano-channel with a single internal site. In the next chapter we will optimize the average particle flux at steady state with respect to the bath and channel parameters.

3

DESCRIPTION OF THE PROPERTIES OF A NANO-CHANNEL WITH A SINGLE INTERNAL POTENTIAL WELL

3.1 The Average Particle Flux Through a Nano-channel with a Single Internal Potential Well and its Average Occupation Number

Using the notations in Eq. (2.28) into Eq. (2.11), we get the following expressions of the average particle flux through a nano-channel:

$$\begin{aligned} J &= n_e\eta_e\gamma_1 k_e^+ - \eta_1\gamma_e k_1^- \qquad \text{from } V_e \text{ to } V_1 \\ J &= \eta_i\gamma_{i+1}k_i^+ - \eta_{i+1}\gamma_i k_{i+1}^- \quad \text{from } V_i \text{ to } V_{i+1} \\ J &= \eta_s\gamma_c k_s^+ - n_c\eta_c\gamma_s k_c^- \qquad \text{from } V_s \text{ to } V_c \end{aligned} \tag{3.1}$$

The average particle flux across each potential energy barrier along the internal wall of the nano-channel given in Eq. (3.1) is more general and is difficult to solve. Therefore, in this chapter we consider a particular case in which the nano-channel has only one internal potential well, that is $s = 1$. Therefore, in the following section, we present a detailed analysis of a nano-channel which has a single internal potential well, whose potential of mean force profile is shown in Fig. 3.1.

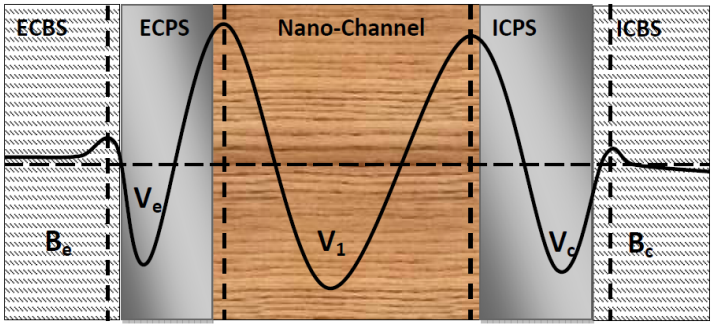

Fig. 3.1: A simple model of the one dimensional profile of the PMF of a nano-channel with a single internal potential well embedded in LBLM

The expression of the net average particle flux across the potential energy barrier between the potential wells V_e and V_1 is given by the first expression in Eq. 3.1.

$$J = n_e \eta_e \gamma_1 k_e^+ - \eta_1 \gamma_e k_1^- \tag{3.2}$$

One can now solve Eq. (3.2) for η_1 and get the following expression of η_1 as a function of the average particle flux J.

$$\eta_1 = \frac{n_e \eta_e k_e^+ - J}{n_e \eta_e k_e^+ + \gamma_e k_1^-} \tag{3.3}$$

The expressions of the net average particle flux across the potential energy barrier between the potential wells V_1 and V_c is given by the third expression in Eq. 3.1.

$$J = \eta_1 \gamma_c k_1^+ - n_c \eta_c \gamma_1 k_c^- \tag{3.4}$$

Upon substituting the expression of γ_1 given in Eq. 1.4 into Eq. 3.4, we get:

$$J = \eta_1 [\gamma_c k_1^+ + n_c \eta_c k_c^-] - n_c \eta_c k_c^- \tag{3.5}$$

Upon substituting the expression of η_1 in Eq. 3.3 into Eq. 3.5, we get the expressions of the net average particle flux through the nano-channel with a single internal potential well:

$$J = \frac{n_e \eta_e \gamma_c k_e^+ k_1^+ - n_c \eta_c \gamma_e k_1^- k_c^-}{n_e \eta_e k_e^+ + \gamma_e k_1^- + \gamma_c k_1^+ + n_c \eta_c k_c^-} \tag{3.6}$$

Therefore, upon substituting the expression of the average particle flux in Eq. 3.6 into Eq. 3.3, we get the expression of the average occupation number of the potential well V_1:

$$\eta_1 = \frac{(n_e\eta_e k_e^+)^2 + \gamma_e k_1^-[n_e\eta_e k_e^+ + n_c\eta_c k_c^-] + n_e n_c \eta_e \eta_c k_e^+ k_c^-}{(n_e\eta_e k_e^+)^2 + n_e\eta_e k_e^+[2\gamma_e k_1^- + \gamma_c k_1^+ + n_c\eta_c k_c^-] + \gamma_e k_1^-[\gamma_e k_1^- + \gamma_c k_1^+ + n_c\eta_c k_c^-]} \tag{3.7}$$

We define the concentration gradient between the emitter and collector baths as follows:

$$\Delta n = n_e - n_c \tag{3.8}$$

The concentrations of the two baths are expressed in units of ***micro-moles***, denoted by μM. For convenience we set the concentration of the collector bath to be one micro-moles, that is $n_c = 1\mu M$ and as a result one can express the concentration of the emitter bath in terms of the concentration gradient Δn between the two baths. That is:

$$n_e = 1 + \Delta n \quad \text{when } n_c = 1\mu M \tag{3.9}$$

Using Eq. 1.4 and Eq. 3.9 into Eq. 3.6, we get the following general expression of the average particle flux through a nano-channel with a single internal potential well as a function of the concentration gradient Δn.

$$J = \frac{k_e^+ k_1^+ \eta_e(1-\eta_c) - k_1^- k_c^- \eta_c(1-\eta_e) + k_e^+ k_1^+ \eta_e(1-\eta_c)\Delta n}{k_e^+\eta_e + k_1^-(1-\eta_e) + k_1^+(1-\eta_c) + k_c^-\eta_c + k_e^+\eta_e\Delta n} \tag{3.10}$$

Moreover, upon substituting Eq. 1.4 and Eq. 3.9 into Eq. 3.7, we get the general expression of the average occupation number of the internal potential well V_1 in terms of the concentration gradient Δn.

$$\begin{aligned}\eta_1 = {} & \{(k_e^+\eta_e)^2(1+\Delta n)^2 + k_e^+\eta_e[k_1^-(1-\eta_e) + k_c^-\eta_c](1+\Delta n) + k_1^- k_c^-\eta_c(1-\eta_e)\}/ \\ & \{(k_e^+\eta_e)^2(1+\Delta n)^2 + k_e^+\eta_e[2k_1^-(1-\eta_e) + k_1^+(1-\eta_c) + k_c^-\eta_c](1+\Delta n) + \\ & k_1^-(1-\eta_e)[k_1^-(1-\eta_e) + k_1^+(1-\eta_c) + k_c^-\eta_c]\}\end{aligned} \tag{3.11}$$

The transition rates depend on the potential of mean force profile along the internal wall of the nano-channel. We take this fact into account by defining the

transition rates in terms of the height of the potential energy barriers between the potential energy wells.

$$
\begin{aligned}
k_e^+ &= \nu_e^+ \exp(-u_e^+) \\
k_c^- &= \nu_c^- \exp(-u_c^-) \\
k_j^- &= \nu_j^- \exp(-u_j^-) \\
k_j^+ &= \nu_j^+ \exp(-u_j^+)
\end{aligned} \tag{3.12}
$$

where we have defined the normalized energies u_j^- and u_j^+ as follows:

$$
\begin{aligned}
u_e^+ &= \beta E_e^+ = \frac{E_e^+}{k_B T} \\
u_c^- &= \beta E_c^- = \frac{E_c^-}{k_B T} \\
u_j^- &= \beta E_j^- = \frac{E_j^-}{k_B T} \\
u_j^+ &= \beta E_j^+ = \frac{E_j^+}{k_B T}
\end{aligned} \tag{3.13}
$$

where T is the absolute temperature, k_B is the Boltzmann constant, E_j^- and E_j^+ are the heights of the potential energy barrier in the backward and forward directions from the potential energy well V_j, respectively. Moreover, the coefficients in Eq. 3.12, have values which are given in Eq. 1.9. That is:

$$
\begin{aligned}
\nu_e^+ &= 15 \times 10^6 M^{-1} s^{-1} = 15\ (\mu M)^{-1} s^{-1} \\
\nu_c^- &= 15 \times 10^6 M^{-1} s^{-1} = 15\ (\mu M)^{-1} s^{-1} \\
\nu_1^+ &= \nu_2^+ = ... = \nu_s^+ = 500\ s^- \\
\nu_1^- &= \nu_2^- = ... = \nu_s^- = 500\ s^-
\end{aligned} \tag{3.14}
$$

Upon substituting the expressions in Eq. 3.12 into Eq. 3.10, we get:

$$
\begin{aligned}
&J = \{\nu_e^+ \nu_1^+ \eta_e (1-\eta_c) \exp(-[u_e^+ + u_1^+]) - \nu_1^- \nu_c^- \eta_c (1-\eta_e) \exp(-[u_1^- + u_c^-]) + \\
&\nu_e^+ \nu_1^+ \eta_e (1-\eta_c) \exp(-[u_e^+ + u_1^+]) \Delta n\} / \\
&\{\nu_e^+ \eta_e \exp(-u_e^+) + \nu_1^- (1-\eta_e) \exp(-u_1^-) + \nu_1^+ (1-\eta_c) \exp(-u_1^+) + \nu_c^- \eta_c \exp(-u_c^-) + \\
&\nu_e^+ \eta_e \exp(-u_e^+) \Delta n\}
\end{aligned} \tag{3.15}
$$

Upon substituting the expressions in Eq. 3.12 into Eq. 3.11, we get:

$$\eta_1 = \{(\nu_e^+\eta_e)^2(1+\Delta n)^2\exp(-2u_e^+) + \nu_e^+\eta_e\exp(-u_e^+)[\nu_1^-(1-\eta_e)\exp(-u_1^-)+$$
$$\nu_c^-\eta_c\exp(-u_c^-)](1+\Delta n) + \nu_1^-\nu_c^-\eta_c(1-\eta_e)\exp(-[u_1^- + u_c^-])\}/$$
$$\{(\nu_e^+\eta_e)^2\exp(-2u_e^+)(1+\Delta n)^2 + \nu_e^+\eta_e\exp(-u_e^+)[2\nu_1^-(1-\eta_e)\exp(-u_1^-)+$$
$$\nu_1^+(1-\eta_c)\exp(-u_1^+) + \nu_c^-\eta_c\exp(-u_c^-)](1+\Delta n) + \nu_1^-(1-\eta_e)\exp(-u_1^-)[\nu_1^-(1-\eta_e)\exp(-u_1^-)+$$
$$\nu_1^+(1-\eta_c)\exp(-u_1^+) + \nu_c^-\eta_c\exp(-u_c^-)]\} \tag{3.16}$$

In the next section, we consider cases where the heights of the potential energy barriers between the neighboring potential energy wells are different and we will plot the variation of the average particle flux through the nano-channel as a function of the concentration gradient between the emitter and collector baths and discuss the properties that can be extracted from the plot.

3.2 Discussion of the Average Particle Flux Through a Nano-Channel with a Single Internal Potential Well

3.2.1 The Average Particle Flux Through a Nano-Channel as a Function of the Concentration Gradient when the Potential Barriers are Twice of Thermal Energy

In this section we will present a detailed description of the average particle flux through a nano-channel with a single internal potential well and two external potential wells as a function of the concentration gradient between the emitter and collector baths when the potential barriers are twice of the thermal energy k_BT. Taking this fact into account, we will plot the variation of the average particle flux through the nano-channel as a function of the concentration gradient and discuss some of its important properties.

Using $\eta_c = 0$, $u_e^+ = 2$, $u_1^- = 2$, $u_1^+ = 2$, $u_c^- = 2$ and the values the transition rates specified in Eq. 3.14 into Eq. 3.15, we have plotted the variation of the average particle flux J through a nano-channel with a single internal potential well as a function of concentration gradient Δn in units of μM for five different values of η_e, that is $\eta_e = 0, \eta_e = 0.25, \eta_e = 0.5, \eta_e = 0.75, \eta_e = 1.0$ on the same graph as shown in Fig. 3.2.

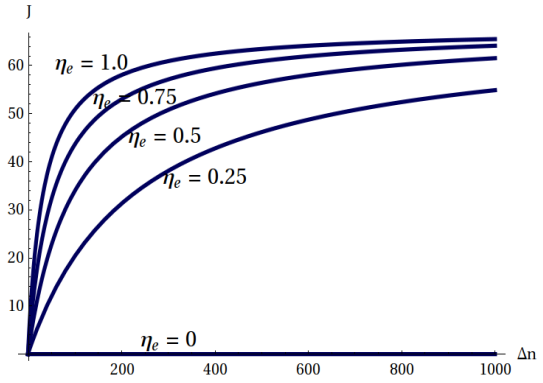

Fig. 3.2: Plot of J as a function of the concentration gradient Δn in units of μM when $s = 1$, $n_c = 1.0\ \mu M$, $\eta_c = 0$, $\nu_e^+ = \nu_c^- = 15\,(\mu M)^{-1}s^{-1}, \nu_1^- = \nu_1^+ = 500\,s^{-1}$, $u_e^+ = 2$, $u_1^- = 2$, $u_1^+ = 2$, $u_c^- = 2$ for the values $\eta_e = 0, \eta_e = 0.25, \eta_e = 0.5, \eta_e = 0.75, \eta_e = 1.0$

Using $\eta_c = 0.5$, $u_e^+ = 2, u_1^- = 2, u_1^+ = 2, u_c^- = 2$ and the values of the transition rates specified in Eq. 3.14 into Eq. 3.15, we have plotted the variation of the average particle flux J through a nano-channel with a single internal potential well as a function of concentration gradient Δn in units of μM for five different values of η_e, that is $\eta_e = 0, \eta_e = 0.25, \eta_e = 0.5, \eta_e = 0.75, \eta_e = 1.0$ on the same graph as shown in Fig. 3.3.

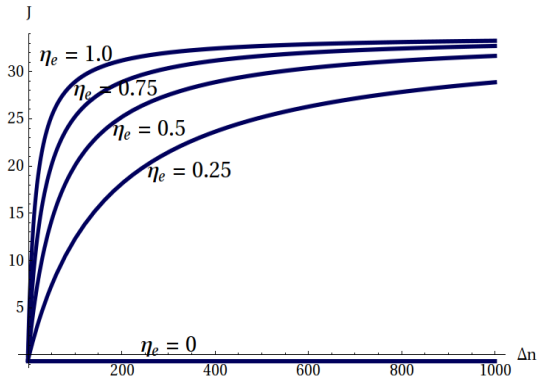

Fig. 3.3: Plot of J as a function of the concentration gradient Δn in units of μM when $s = 1$, $n_c = 1.0\,\mu M$, $\eta_c = 0.5$, $\nu_e^+ = \nu_c^- = 15\,(\mu M)^{-1}s^{-1}, \nu_1^- = \nu_1^+ = 500\,s^{-1}$, $u_e^+ = 2$, $u_1^- = 2$, $u_1^+ = 2$, $u_c^- = 2$ for the values $\eta_e = 0, \eta_e = 0.25, \eta_e = 0.5, \eta_e = 0.75, \eta_e = 1.0$

Using $\eta_c = 1.0$, $u_e^+ = 2, u_1^- = 2, u_1^+ = 2, u_c^- = 2$ and the values of the transition rates specified in Eq. 3.14 into Eq. 3.15, we have plotted the variation of the average particle flux J through a nano-channel with a single internal site as a function of concentration gradient Δn in units of μM for five different values of η_e, that is $\eta_e = 0, \eta_e = 0.25, \eta_e = 0.5, \eta_e = 0.75, \eta_e = 1.0$ on the same graph as shown in Fig. 3.4.

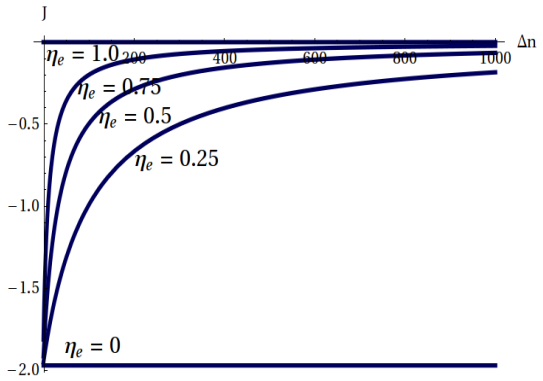

Fig. 3.4: Plot of J as a function of the concentration gradient Δn in units of μM when $s = 1$, $n_c = 1.0\,\mu M$, $\eta_c = 1.0$, $\nu_e^+ = \nu_c^- = 15\,(\mu M)^{-1}s^{-1}, \nu_1^- = \nu_1^+ = 500\,s^{-1}$, $u_e^+ = 2$, $u_1^- = 2$, $u_1^+ = 2$, $u_c^- = 2$ for the values $\eta_e = 0, \eta_e = 0.25, \eta_e = 0.5, \eta_e = 0.75, \eta_e = 1.0$

For the given values of η_e and η_c, the average particle flux through a nano-channel with a single internal potential well as a function of the concentration gradient Δn is denoted by $J_1(\Delta n|\eta_e, \eta_c)$. Since we have assumed that the concentration of the permeating particles in the collector bath to be $n_c = 1.0\,\mu M$, the maximum negative value of the concentration gradient is $\Delta n = -1.0\,\mu M$. Using these notations and assumptions, we see from Fig. 3.2 to Fig. 3.4 that $J_1(\Delta n|\eta_e = 0, \eta_c) < J_1(\Delta n|\eta_e = 0.25, \eta_c) < J_1(\Delta n|\eta_e = 0.5, \eta_c) < J_1(\Delta n|\eta_e = 0.75, \eta_c) < J_1(\Delta n|\eta_e = 1.0, \eta_c)$ for all possible values of Δn and η_c. That is, for the given values of Δn and η_c in their respective ranges, the average particle flux through a nano-channel with a single internal potential well increases as the average value of η_e increases.

The average particle flux through the nano-channel is zero even in the presence of a large concentration gradient between the two baths when $\eta_e = \eta_c = 0$ and $\eta_e = \eta_c = 1.0$ as shown in Fig. 3.2 and Fig. 3.4, respectively. The average particle flux through the nano-channel assumes negative values when $\eta_c = 1.0$ for all possible values of Δn and η_e as shown in Fig. 3.4. When $\Delta n = -1.0\,\mu M$ and $\eta_e = 1.0$, the average particle flux through the nano-channel is zero for all possible values of η_c and for all other values of η_e the flux is negative and its magnitude increases as η_c increases and we have the maximum negative flux when $\eta_c = 1.0$. Moreover, $J_1(\Delta n = -1.0\mu M|\eta_e, \eta_c = 0) \to 0$ for all possible values of η_e.

For small values of Δn, the average particle flux through the nano-channel increases rapidly as Δn increases and then it increases slowly and finally saturates to a constant value for large values of Δn. For a given value of η_c, the rate of approach of the average flux as a function of Δn to the saturation value is different for different values of η_e. That is, the flux saturates more quickly at a small value of Δn when $\eta_e = 1.0$ and as η_e decreases from its maximum value of one to zero, the concentration gradient at which the flux becomes saturated increases from the smallest value, which occurs when $\eta_e = 1.0$ to the largest one, which occurs when $\eta_e = 0$. In other words, for a given value of η_c, the value of Δn at which the flux saturates increases as η_e decreases from one to zero. For a given value of η_c, the average flux associated with different values of η_e converge to each other as $\Delta n \rightarrow -1.0\,\mu M$ and then diverge from each other as Δn increases to intermediate values and finally the flux associated with different values of η_e saturates to the same maximum positive value as Δn increases to large values. The saturation values of the average particle flux associated with different values of η_c are: $J_1^{sat}(\Delta n \rightarrow 10M|\eta_e > 0, \eta_c = 0) \rightarrow 67.6676\,s^{-1}$, $J_1^{sat}(\Delta n \rightarrow 10M|\eta_e > 0, \eta_c = 0.5) \rightarrow 33.8338\,s^{-1}$, $J_1^{sat}(\Delta n \rightarrow 10M|\eta_e > 0, \eta_c = 0.95) \rightarrow 3.38338\,s^{-1}$ and $J_1^{sat}(\Delta n \rightarrow 10M|\eta_e > 0, \eta_c = 1.0) \rightarrow 0$ for all possible values of η_e in the range $0 < \eta_e < 1.0$.

Therefore, the average flux attains a maximum positive value when $\eta_c = 0$ and $\eta_e = 1.0$ for for large values of Δn. Therefore, when $\eta_c = 0$, the mean residence time of a particle at the potential well V_c is negligible and as result the occupation probability of V_c is almost zero. Moreover, as $\eta_e \rightarrow 1$, the mean residence time of a particle at the potential well V_e is large and as result the occupation probability of this site is almost one. This means that the average particle flux through the nano-channel attains a maximum positive value when V_c is empty, that is $\eta_c = 0$, and when V_e is occupied, that is $\eta_e = 1$.

Using $\eta_e = 0$, $u_e^+ = 2, u_1^- = 2, u_1^+ = 2, u_c^- = 2$ and the values of the transition rates specified in Eq. 3.14 into Eq. 3.15, we have plotted the variation of the average particle flux J through a nano-channel with a single internal site as a function of concentration gradient Δn in units of μM for five different values of η_c, that is $\eta_c = 0, \eta_c = 0.25, \eta_c = 0.5, \eta_c = 0.75, \eta_c = 1.0$ on the same graph as shown in Fig. 3.5.

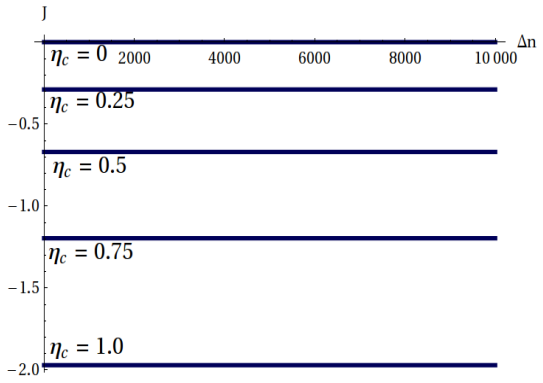

Fig. 3.5: Plot of J as a function of the concentration gradient Δn in units of μM when $s = 1$, $n_c = 1.0\,\mu M$, $\eta_e = 0$, $\nu_e^+ = \nu_c^- = 15\,(\mu M)^{-1}s^{-1}, \nu_1^- = \nu_1^+ = 500\,s^{-1}$, $u_e^+ = 2$, $u_1^- = 2$, $u_1^+ = 2$, $u_c^- = 2$ for the values $\eta_c = 0, \eta_c = 0.25, \eta_c = 0.5, \eta_c = 0.75, \eta_c = 1.0$

Using $\eta_e = 0.1$, $u_e^+ = 2, u_1^- = 2, u_1^+ = 2, u_c^- = 2$ and the values of the transition rates specified in Eq. 3.14 into Eq. 3.15, we have plotted the variation of the average particle flux J through a nano-channel with a single internal site as a function of concentration gradient Δn in units of μM for five different values of η_c, that is $\eta_c = 0, \eta_c = 0.25, \eta_c = 0.5, \eta_c = 0.75, \eta_c = 1.0$ on the same graph as shown in Fig. 3.6.

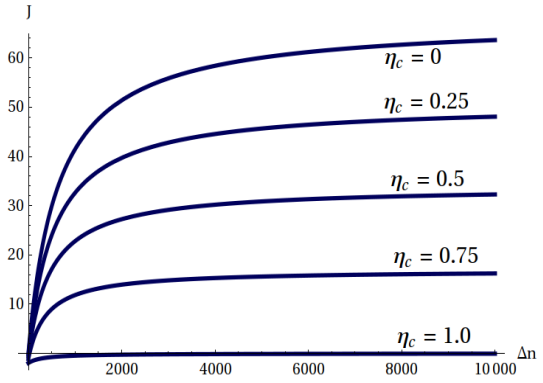

Fig. 3.6: Plot of J as a function of the concentration gradient Δn in units of μM when $s = 1$, $n_c = 1.0\,\mu M$, $\eta_e = 0.1$, $\nu_e^+ = \nu_c^- = 15\,(\mu M)^{-1}s^{-1}, \nu_1^- = \nu_1^+ = 500\,s^{-1}$, $u_e^+ = 2$, $u_1^- = 2$, $u_1^+ = 2$, $u_c^- = 2$ for the values $\eta_c = 0, \eta_c = 0.25, \eta_c = 0.5, \eta_c = 0.75, \eta_c = 1.0$

Using $\eta_e = 0.5$, $u_e^+ = 2, u_1^- = 2, u_1^+ = 2, u_c^- = 2$ and the values of the transition rates specified in Eq. 3.14 into Eq. 3.15, we have plotted the variation of the

average particle flux J through a nano-channel with a single internal site as a function of concentration gradient Δn in units of μM for five different values of η_c, that is $\eta_c = 0, \eta_c = 0.25, \eta_c = 0.5, \eta_c = 0.75, \eta_c = 1.0$ on the same graph as shown in Fig. 3.7.

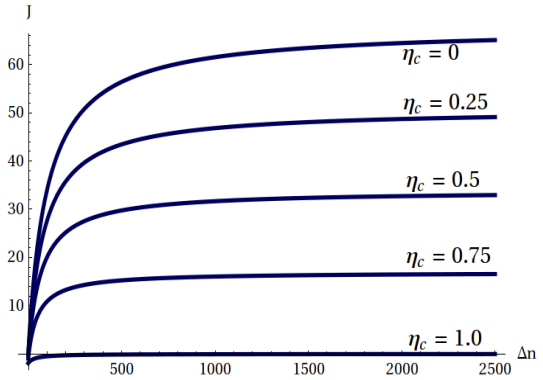

Fig. 3.7: Plot of J as a function of the concentration gradient Δn in units of μM when $s = 1$, $n_c = 1.0\,\mu M$, $\eta_e = 0.5$, $\nu_e^+ = \nu_c^- = 15\,(\mu M)^{-1}s^{-1}, \nu_1^- = \nu_1^+ = 500\,s^{-1}$, $u_e^+ = 2$, $u_1^- = 2$, $u_1^+ = 2$, $u_c^- = 2$ for the values η_c, that is $\eta_c = 0, \eta_c = 0.25, \eta_c = 0.5, \eta_c = 0.75, \eta_c = 1.0$

Using $\eta_e = 1.0$, $u_e^+ = 2, u_1^- = 2, u_1^+ = 2, u_c^- = 2$ and the values of the transition rates specified in Eq. 3.14 into Eq. 3.15, we have plotted the variation of the average particle flux J through a nano-channel with a single internal site as a function of concentration gradient Δn in units of μM for five different values of η_c, that is $\eta_c = 0, \eta_c = 0.25, \eta_c = 0.5, \eta_c = 0.75, \eta_c = 1.0$ on the same graph as shown in Fig. 3.8.

As Fig. 3.5 shows, when $\eta_e = 0$, the average particle flux through the nano-channel assumes constant negative values that don't change as the concentration gradient increases and its magnitude increases as η_c increases. When $\eta_e = 0$, the average particle flux associated with different values of η_c is: $J_1(\Delta n|\eta_e = 0, \eta_c = 0) \to 0$, $J_1(\Delta n|\eta_e = 0, \eta_c = 0.25) \to -0.288767\,s^{-1}$, $J_1(\Delta n|\eta_e = 0, \eta_c = 0.5) \to -0.669977\,s^{-1}$, $J_1(\Delta n|\eta_e = 0, \eta_c = 0.75) \to -1.19648\,s^{-1}$ and $J_1(\Delta n|\eta_e = 0, \eta_c = 1.0) \to -1.9709\,s^{-1}$ for all possible values of Δn. Moreover, the average particle flux through the nano-channel assumes negative values when $\eta_c = 1.0$ and $0 \leq \eta_e < 1.0$ and positive values when $\eta_e = 1.0$ and $0 \leq \eta_c < 1.0$ for all possible values of Δn as shown in Fig. 3.8.

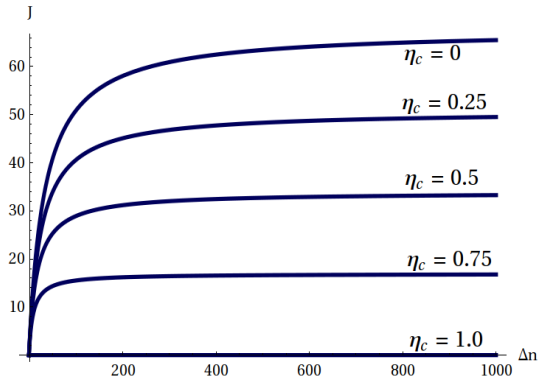

Fig. 3.8: Plot of J as a function of the concentration gradient Δn in units of μM when $s = 1$, $n_c = 1.0\,\mu M$, $\eta_e = 1.0$, $\nu_e^+ = \nu_c^- = 15\,(\mu M)^{-1}s^{-1}, \nu_1^- = \nu_1^+ = 500\,s^{-1}$, $u_e^+ = 2$, $u_1^- = 2$, $u_1^+ = 2$, $u_c^- = 2$ for the values $\eta_c = 0, \eta_c = 0.25, \eta_c = 0.5, \eta_c = 0.75, \eta_c = 1.0$

As the figures from Fig. 3.5 to Fig. 3.8 show, for a given value of η_e, the average particle flux through the nano-channel assumes a maximum value when $\eta_c = 0$ and a minimum value when $\eta_c = 1.0$. That is, $J_1(\Delta n|\eta_e, \eta_c = 0) > J_1(\Delta n|\eta_e, \eta_c = 0.25) > J_1(\Delta n|\eta_e, \eta_c = 0.5) > J_1(\Delta n|\eta_e, \eta_c = 0.75) > J_1(\Delta n|\eta_e, \eta_c = 1.0)$ for all possible values of Δn and η_e. The average particle flux through the nano-channel is zero even in the presence of a large concentration gradient between the two baths when $\eta_e = \eta_c = 0$ and $\eta_e = \eta_c = 1.0$ as shown in Fig. 3.5 and Fig. 3.8, respectively. When $\Delta n = -1.0\,\mu M$ and $\eta_e = 1.0$, the average particle flux through the nano-channel is zero for all possible values of η_c in the range $0 \leq \eta_c \leq 1.0$. For small values of Δn, the average flux increases rapidly as Δn increases and then it increases slowly and finally it saturates to a constant value for large values of Δn.

Moreover, the value of the concentration gradient at which the average particle flux through the nano-channel becomes saturated increases from the least value, which occurs when $\eta_c = 1.0$, to the largest value which occurs when $\eta_c = 0$, for all possible values of η_e. That is, $J_1(\Delta n|\eta_e, \eta_c = 1.0)$ saturates first at a small value of Δn and $J_1(\Delta n|\eta_e, \eta_c = 0)$ saturates last at a large value of Δn for any value of η_e. Moreover, as η_e increases, the value of Δn at which the flux saturates decreases as one can see in the Fig. 3.5 to Fig. 3.8. All the fluxes shown in the figures from Fig. 3.5 to Fig. 3.8 saturate to the same maximum positive values which are the same as those shown in the figures from Fig. 3.2 to Fig.

3.4. That is, $J_1^{sat}(\Delta n \to 10M|\eta_e > 0, \eta_c = 0) \to 67.6676\, s^{-1}$, $J_1^{sat}(\Delta n \to 10M|\eta_e > 0, \eta_c = 0.25) \to 50.7507\, s^{-1}$, $J_1^{sat}(\Delta n \to 10M|\eta_e > 0, \eta_c = 0.5) \to 33.8338\, s^{-1}$, $J_1^{sat}(\Delta n \to 10M|\eta_e > 0, \eta_c = 0.75) \to 16.9169\, s^{-1}$ and $J_1^{sat}(\Delta n \to 10M|\eta_e > 0, \eta_c = 1.0) \to 0$ for all possible values of η_e in the range $0 < \eta_e < 1.0$. Therefore, for the given values of Δn and η_e in their respective ranges, the average particle flux through a nano-channel with a single internal potential well decreases as the average value of η_c increases.

Using $\eta_e = 0.1$, $\eta_c = 0.1$, $u_1^- = 2, u_1^+ = 2, u_c^- = 2$ and the values of the transition rates specified in Eq. 3.14 into Eq. 3.15, we have plotted the variation of the average particle flux J through a nano-channel with a single internal potential well as a function of concentration gradient Δn in units of μM for four different values of u_e^+, that is $u_e^+ \approx 0, u_e^+ = 1.0, u_e^+ = 2.0, u_e^+ = 3.0$ on the same graph as shown in Fig. 3.9.

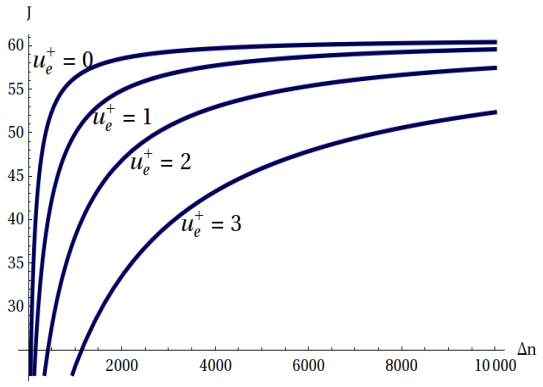

Fig. 3.9: Plot of J as a function of the concentration gradient Δn in units of μM when $s = 1$, $n_c = 1.0\ \mu M$, $\eta_e = 0.1$, $\eta_c = 0.1$, $\nu_e^+ = \nu_c^- = 15\,(\mu M)^{-1} s^{-1}, \nu_1^- = \nu_1^+ = 500\, s^{-1}$, $u_1^- = 2$, $u_1^+ = 2$, $u_c^- = 2$, $u_e^+ = 2, u_1^- = 2, u_1^+ = 2, u_c^- = 2$ for the values $u_e^+ \approx 0, u_e^+ = 1.0, u_e^+ = 2.0, u_e^+ = 3.0$

Using $\eta_e = 0.95$, $\eta_c = 0.95$, $u_1^- = 2, u_1^+ = 2, u_c^- = 2$ and the values of the transition rates specified in Eq. 3.14 into Eq. 3.15, we have plotted the variation of the average particle flux J through a nano-channel with a single internal potential well as a function of concentration gradient Δn in units of μM for four different values of u_e^+, that is $u_e^+ \approx 0, u_e^+ = 1.0, u_e^+ = 2.0, u_e^+ = 3.0$ on the same graph as shown in Fig. 3.10.

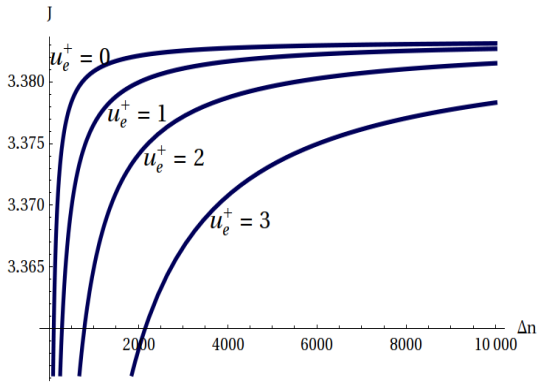

Fig. 3.10: Plot of J as a function of the concentration gradient Δn in units of μM when $s = 1$, $n_c = 1.0\,\mu M$, $\eta_e = 0.95$, $\eta_c = 0.95$, $\nu_e^+ = \nu_c^- = 15\,(\mu M)^{-1}s^{-1}, \nu_1^- = \nu_1^+ = 500\,s^{-1}$, $u_e^+ = 2, u_1^- = 2, u_1^+ = 2, u_c^- = 2$ for the values $u_e^+ \approx 0, u_e^+ = 1.0, u_e^+ = 2.0, u_e^+ = 3.0$

Using $\eta_e = 1$, $\eta_c = 0$, $u_1^- = 2, u_1^+ = 2, u_c^- = 2$ and the values of the transition rates specified in Eq. 3.14 into Eq. 3.15, we have plotted the variation of the average particle flux J through a nano-channel with a single internal potential well as a function of concentration gradient Δn in units of μM for four different values of u_e^+, that is $u_e^+ \approx 0, u_e^+ = 1.0, u_e^+ = 2.0, u_e^+ = 3.0$ on the same graph as shown in Fig. 3.11.

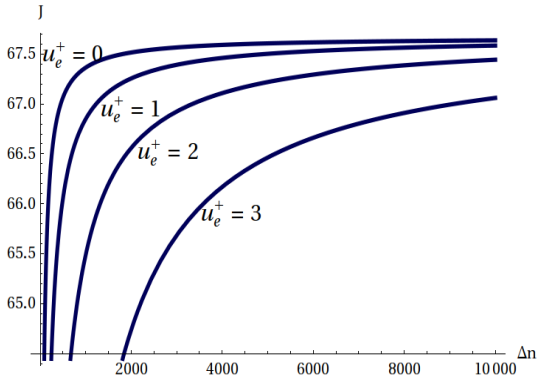

Fig. 3.11: Plot of J as a function of the concentration gradient Δn in units of μM when $s = 1$, $n_c = 1.0\,\mu M$, $\eta_e = 1.0$, $\eta_c = 0$, $\nu_e^+ = \nu_c^- = 15\,(\mu M)^{-1}s^{-1}, \nu_1^- = \nu_1^+ = 500\,s^{-1}$, $u_e^+ = 2, u_1^- = 2, u_1^+ = 2, u_c^- = 2$ for the values $u_e^+ \approx 0, u_e^+ = 1.0, u_e^+ = 2.0, u_e^+ = 3.0$

Using $\eta_e = 0.5$, $\eta_c = 0.5$, $u_e^+ = 2, u_1^+ = 2, u_c^- = 2$ and the values of the transition rates specified in Eq. 3.14 into Eq. 3.15, we have plotted the variation of the

average particle flux J through a nano-channel with a single internal potential well as a function of concentration gradient Δn in units of μM for four different values of u_1^-, that is $u_1^- \approx 0, u_1^- = 1.0, u_1^- = 2.0, u_1^- = 3.0$ on the same graph as shown in Fig. 3.12.

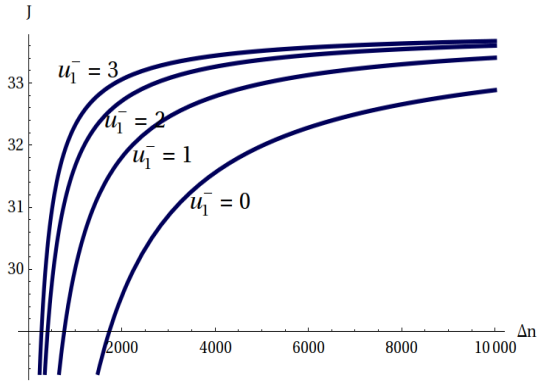

Fig. 3.12: Plot of J as a function of the concentration gradient Δn in units of μM when $s = 1$, $n_c = 1.0\,\mu M$, $\eta_e = 0.5$, $\eta_c = 0.5$, $\nu_e^+ = \nu_c^- = 15\,(\mu M)^{-1}s^{-1}, \nu_1^- = \nu_1^+ = 500\,s^{-1}$, $u_e^+ = 2, u_1^- = 2, u_1^+ = 2, u_c^- = 2$ for the values $u_1^- \approx 0, u_1^- = 1.0, u_1^- = 2.0, u_1^- = 3.0$

Using $\eta_e = 0.5$, $\eta_c = 0.5$, $u_e^+ = 2, u_1^- = 2, u_c^- = 2$ and the values of the transition rates specified in Eq. 3.14 into Eq. 3.15, we have plotted the variation of the average particle flux J through a nano-channel with a single internal potential well as a function of concentration gradient Δn in units of μM for four different values of u_e^+, that is $u_1^+ \approx 0, u_1^+ = 1.0, u_1^+ = 2.0, u_1^+ = 3.0$ on the same graph as shown in Fig. 3.13.

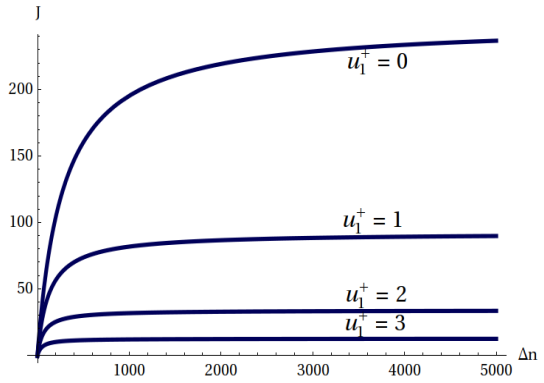

Fig. 3.13: Plot of J as a function of the concentration gradient Δn in units of μM when $s = 1$, $n_c = 1.0\,\mu M$, $\eta_e = 0.5$, $\eta_c = 0.5$, $\nu_e^+ = \nu_c^- = 15\,(\mu M)^{-1}s^{-1}, \nu_1^- = \nu_1^+ = 500\,s^{-1}$, $u_e^+ = 2, u_1^- = 2, u_1^+ = 2, u_c^- = 2$ for the values $u_1^+ \approx 0, u_1^+ = 1.0, u_1^+ = 2.0, u_1^+ = 3.0$

Using $\eta_e = 0.5$, $\eta_c = 0.5$, $u_e^+ = 2, u_1^- = 2, u_1^+ = 2$ and the values of the transition rates specified in Eq. 3.14 into Eq. 3.15, we have plotted the variation of the average particle flux J through a nano-channel with a single internal potential well as a function of concentration gradient Δn in units of μM for four different values of u_c^-, that is $u_c^- \approx 0, u_c^- = 1.0, u_c^- = 2.0, u_c^- = 3.0$ on the same graph as shown in Fig. 3.14.

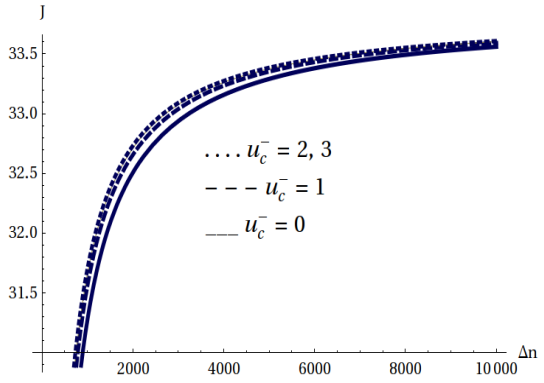

Fig. 3.14: Plot of J as a function of the concentration gradient Δn in units of μM when $s = 1$, $n_c = 1.0\,\mu M$, $\eta_e = 0.5$, $\eta_c = 0.5$, $\nu_e^+ = \nu_c^- = 15\,(\mu M)^{-1}s^{-1}, \nu_1^- = \nu_1^+ = 500\,s^{-1}$, $u_e^+ = 2, u_1^- = 2, u_1^+ = 2, u_c^- = 2$ for the values $u_c^- \approx 0, u_c^- = 1.0, u_c^- = 2.0, u_c^- = 3.0$

As one can see in Fig. 3.9 to Fig. 3.11 and in Fig. 3.13, the average particle flux as a function of Δn through a nano-channel with a single internal potential well

decreases as the height of the normalized potential barriers u_e^+ and u_1^+ increase from values that are nearly zero to higher values. The average flux approaches the saturation values more quickly when u_e^+ is small than when u_e^+ is large but the flux approaches the saturation value more quickly when u_1^+ is large than when u_1^+ is small. The average particle flux associated with different values of u_e^+ saturate to the same maximum positive value but the average particle flux associated with different values of u_1^+ saturate to the different maximum positive values as Δn increases to large positive values. Therefore, for all possible values of u_e^+, we see that $J_1^{sat}(\Delta n \rightarrow 10M|\eta_e = 0.1, \eta_c = 0.1) \rightarrow 60.9008\, s^{-1}$, $J_1^{sat}(\Delta n \rightarrow 10M|\eta_e = 0.95, \eta_c = 0.95) \rightarrow 3.38338\, s^{-1}$, $J_1^{sat}(\Delta n \rightarrow 10M|\eta_e = 1.0, \eta_c = 0) \rightarrow 67.6676\, s^{-1}$, $J_1^{sat}(\Delta n \rightarrow 10M|\eta_e = 0, \eta_c = 1.0) \rightarrow -1.9709\, s^{-1}$. Moreover, we see that $J_1^{sat}(\Delta n \rightarrow 10M|\eta_e = 0.1, \eta_c = 0.1, u_1^+ = 0) \rightarrow 449.999\, s^{-1}$, $J_1^{sat}(\Delta n \rightarrow 10M|\eta_e = 0.1, \eta_c = 0.1, u_1^+ = 1) \rightarrow 165.546\, s^{-1}$, $J_1^{sat}(\Delta n \rightarrow 10M|\eta_e = 0.1, \eta_c = 0.1, u_1^+ = 2) \rightarrow 60.9008\, s^{-1}$, $J_1^{sat}(\Delta n \rightarrow 10M|\eta_e = 0.1, \eta_c = 0.1, u_1^+ = 3) \rightarrow 22.4042\, s^{-1}$.

However, the average particle flux as a function of Δn through a nano-channel with a single internal potential well increases as the height of the normalized potential barriers u_1^- and u_c^- increase from values that are nearly zero to higher values as shown in Fig. 3.12 and in Fig. 3.14. The average particle flux associated with the different values of u_1^- and u_c^- saturate to the same maximum positive value as Δn increases to large positive values, that is, $J_1^{sat}(\Delta n \rightarrow 10M|\eta_e = 0.1, \eta_c = 0.1, u_1^-) = J_1^{sat}(\Delta n \rightarrow 10M|\eta_e = 0.1, \eta_c = 0.1, u_c^-) \rightarrow 60.9009\, s^{-1}$ for all possible values of u_1^- and u_c^-.

3.2.2 The Average Particle Flux Through a Nano-Channel as a Function of the Average Occupation number of the External Potential Wells when the Potential Barriers are Twice of Thermal Energy

Using the positive concentration gradient $\Delta n = 1000\ \mu M$, $u_e^+ = 2, u_1^- = 2, u_1^+ = 2, u_c^- = 2$ and the values of the transition rates specified in Eq. 3.14 into Eq. 3.15, we have plotted the variation of the average particle flux J through a nano-channel with a single internal potential well as a function of η_c for five different values of η_e, that is, $\eta_e = 0, \eta_e = 0.25, \eta_e = 0.5, \eta_e = 0.75, \eta_e = 1.0$ on the same graph as shown in Fig. 3.15.

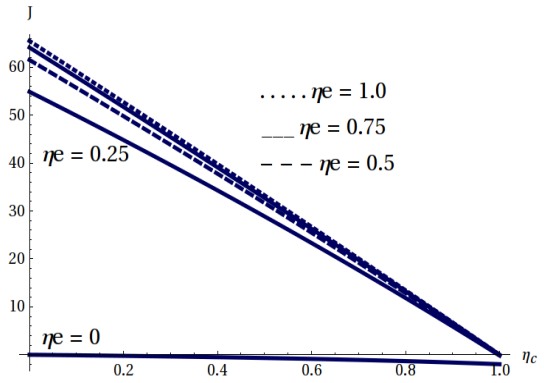

Fig. 3.15: Plot of J as a function of η_c when $s = 1$, $\Delta n = 1000\ \mu M$, $n_c = 1.0\ \mu M$, $\nu_e^+ = \nu_c^- = 15\,(\mu M)^{-1}s^{-1}, \nu_1^- = \nu_1^+ = 500\,s^{-1}$, $u_e^+ = 2, u_1^- = 2, u_1^+ = 2, u_c^- = 2$ for the values $\eta_e = 0, \eta_e = 0.25, \eta_e = 0.5, \eta_e = 0.75, \eta_e = 1.0$

Using the positive concentration gradient $\Delta n = 50\ \mu M$, $u_e^+ = 2, u_1^- = 2, u_1^+ = 2, u_c^- = 2$ and the values of the transition rates specified in Eq. 3.14 into Eq. 3.15, we have plotted the variation of the average particle flux J through a nano-channel with a single internal potential well as a function of η_c for five different values of η_e, that is, $\eta_e = 0, \eta_e = 0.25, \eta_e = 0.5, \eta_e = 0.75, \eta_e = 1.0$ on the same graph as shown in Fig. 3.16.

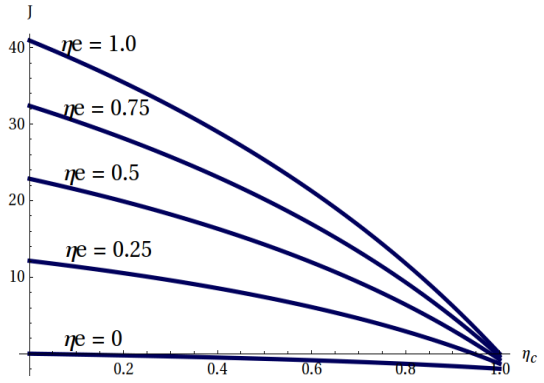

Fig. 3.16: Plot of J as a function of η_c when $s = 1$, $\Delta n = 50\,\mu M$, $n_c = 1.0\,\mu M$, $\nu_e^+ = \nu_c^- = 15\,(\mu M)^{-1}s^{-1}, \nu_1^- = \nu_1^+ = 500\,s^{-1}$, $u_e^+ = 2, u_1^- = 2, u_1^+ = 2, u_c^- = 2$ for the values $\eta_e = 0, \eta_e = 0.25, \eta_e = 0.5, \eta_e = 0.75, \eta_e = 1.0$

When there is a positive concentration gradient of $\Delta n = 1000\ \mu M$ the average particle flux as a function of η_c approaches to slightly different maximum positive values as $\eta_c \to 0$ and to slightly different maximum negative values as $\eta_c \to 1.0$ as shown in Fig. 3.15. For the given values of Δn and η_e, the average

flux decreases as η_c increases from zero to one. The average particle fluxes associated with different values of η_e are far apart from each other as $\eta_c \to 0$ and assume the values: $J_1(\Delta n = 1000\ \mu M|\eta_e = 0, \eta_c \to 0) \to 0$, $J_1(\Delta n = 1000\ \mu M|\eta_e = 0.25, \eta_c \to 0) \to 54.876 s^{-1}$, $J_1(\Delta n = 1000\ \mu M|\eta_e = 0.5, \eta_c \to 0) \to 61.5216 s^{-1}$, $J_1(\Delta n = 1000\ \mu M|\eta_e = 0.75, \eta_c \to 0) \to 64.1096 s^{-1}$ and $J_1(\Delta n = 1000\ \mu M|\eta_e = 1.0, \eta_c \to 0) \to 65.4869 s^{=1}$. The fluxes converge to each other as $\eta_c \to 1.0$ and assume the values: $J_1(\Delta n = 1000\ \mu M|\eta_e = 0, \eta_c \to 1.0) \to -1.9709 s^{-1}$, $J_1(\Delta n = 1000\ \mu M|\eta_e = 0.25, \eta_c \to 1.0) \to -0.183713 s^{-1}$, $J_1(\Delta n = 1000\ \mu M|\eta_e = 0.5, \eta_c \to 1.0) \to -0.0652952 s^{-1}$, $J_1(\Delta n = 1000\ \mu M|\eta_e = 0.75, \eta_c \to 1.0) \to -0.0222567 s^{-1}$ and $J_1(\Delta n = 1000\ \mu M|\eta_e = 1.0, \eta_c \to 1.0) \to 0$. Moreover, the fluxes assume the values $J_1(\Delta n = 1000\ \mu M|\eta_e = 1.0, \eta_c) > 0$ and $J_1(\Delta n = 1000\ \mu M|\eta_e = 0, \eta_c) < 0$ for all possible values of η_c.

Using zero concentration gradient $\Delta n = 0$, $u_e^+ = 2, u_1^- = 2, u_1^+ = 2, u_c^- = 2$ and the values of the transition rates specified in Eq. 3.14 into Eq. 3.15, we have plotted the variation of the average particle flux J through a nano-channel with a single internal potential well as a function of η_c for five different values of η_e, that is $\eta_e = 0, \eta_e = 0.25, \eta_e = 0.5, \eta_e = 0.75, \eta_e = 1.0$ on the same graph as shown in Fig. 3.17.

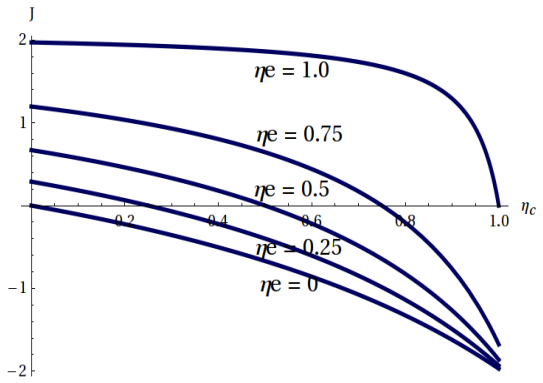

Fig. 3.17: Plot of J as a function of η_c when $s = 1$, $\Delta n = 0$, $n_c = 1.0\,\mu M$, $\nu_e^+ = \nu_c^- = 15\,(\mu M)^{-1} s^{-1}, \nu_1^- = \nu_1^+ = 500\,s^{-1}$, $u_e^+ = 2, u_1^- = 2, u_1^+ = 2, u_c^- = 2$ for the values $\eta_e = 0, \eta_e = 0.25, \eta_e = 0.5, \eta_e = 0.75, \eta_e = 1.0$

When $\Delta n = 0$, the average particle flux as a function of η_c obey that $J_1(\Delta n = 0|\eta_e = 1.0, \eta_c) > J_1(\Delta n = 0|\eta_e = 0.75, \eta_c) > J_1(\Delta n = 0|\eta_e = 0.5, \eta_c) > J_1(\Delta n = 0|\eta_e = 0.25, \eta_c) > J_1(\Delta n = 0|\eta_e = 1.0, \eta_c)$ and approach to different maximum

positive values as $\eta_c \to 0$, that is, $J_1(\Delta n = 0|\eta_e = 0, \eta_c \to 0) \to 0$, $J_1(\Delta n = 0|\eta_e = 0.25, \eta_c \to 0) \to 0.288767$, $J_1(\Delta n = 0|\eta_e = 0.5, \eta_c \to 0) \to 0.669977$, $J_1(\Delta n = 0|\eta_e = 0.75, \eta_c \to 0) \to 1.19648$, $J_1(\Delta n = 0|\eta_e = 1.0, \eta_c \to 0) \to 1.9709$. Moreover, the average particle flux as a function of η_c approach to different maximum negative values, that is, $J_1(\Delta n = 0|\eta_e = 0, \eta_c \to 1.0) \to -1.9709$, $J_1(\Delta n = 0|\eta_e = 0.25, \eta_c \to 1.0) \to -1.93336$, $J_1(\Delta n = 0|\eta_e = 0.5, \eta_c \to 1.0) \to -1.86241$, $J_1(\Delta n = 0|\eta_e = 0.75, \eta_c \to 1.0) \to -1.67771$, $J_1(\Delta n = 0|\eta_e = 1.0, \eta_c \to 1.0) \to 0$. When $\Delta n = 0$, the average particle flux through the nano-channel is positive if $J_1(\Delta n = 0|\eta_e = 0.25, \eta_c < 0.25) > 0$, $J_1(\Delta n = 0|\eta_e = 0.5, \eta_c < 0.5) > 0$, $J_1(\Delta n = 0|\eta_e = 0.75, \eta_c < 0.75) > 0$. Moreover, $J_1(\Delta n = 0|\eta_e = 0, \eta_c) < 0$ and $J_1(\Delta n = 0|\eta_e = 1, 0, \eta_c) > 0$ for all possible values of η_c in the range $0 \leq \eta_c \leq 1.0$.

Using the negative concentration gradient $\Delta n = -1.0\ \mu M$, $u_e^+ = 2, u_1^- = 2, u_1^+ = 2, u_c^- = 2$ and the values of the transition rates specified in Eq. 3.14 into Eq. 3.15, we have plotted the variation of the average particle flux J through a nano-channel with a single internal potential well as a function of η_c for five different values of η_e, that is $\eta_e = 0, \eta_e = 0.25, \eta_e = 0.5, \eta_e = 0.75, \eta_e = 1.0$ on the same graph as shown in Fig. 3.18.

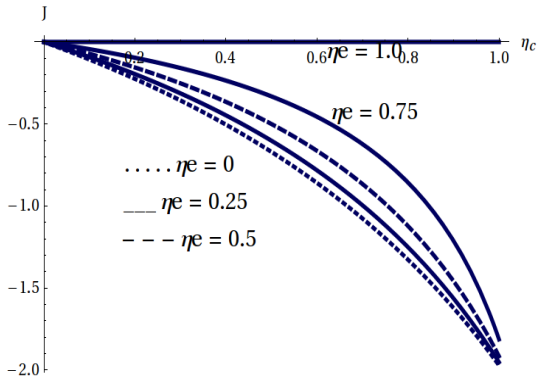

Fig. 3.18: Plot of J as a function of η_c when $s = 1$, $\Delta n = -1.0\ \mu M$, $n_c = 1.0\,\mu M$, $\nu_e^+ = \nu_c^- = 15\,(\mu M)^{-1}s^{-1}, \nu_1^- = \nu_1^+ = 500\,s^{-1}$, $u_e^+ = 2, u_1^- = 2, u_1^+ = 2, u_c^- = 2$ for the values $\eta_e = 0, \eta_e = 0.25, \eta_e = 0.5, \eta_e = 0.75, \eta_e = 1.0$

When the concentration gradient has the maximum possible negative value, that is, $\Delta n = -1.0\ \mu M$, Fig. 3.18 shows that the average particle flux through the nano-channel as a function of η_c is zero when $\eta_e = 1.0$ for all possible values of η_c in the range $0 \leq \eta_c \leq 1.0$ and is negative for all possible values of η_e in the

range $0 \leq \eta_e < 1.0$ in the entire range $0 \leq \eta_c \leq 1.0$. When $\Delta n = -1.0\ \mu M$, the average particle flux is zero when $\eta_c = 0$ for all possible values of η_e and as $\eta_c \to 1.0$, the average particle flux as a function of η_c approach to different maximum negative values, that is, $J_1(\Delta n = -1.0\ \mu M|\eta_e = 0, \eta_c \to 1.0) \to -1.9709 s^{-1}$, $J_1(\Delta n = -1.0\ \mu M|\eta_e = 0.25, \eta_c \to 1.0) \to -1.95195 s^{-1}$, $J_1(\Delta n = -1.0\ \mu M|\eta_e = 0.5, \eta_c \to 1.0) \to -1.91512 s^{-1}$, $J_1(\Delta n = -1.0\ \mu M|\eta_e = 0.75, \eta_c \to 1.0) \to -1.81253 s^{-1}$, $J_1(\Delta n = -1.0\ \mu M|\eta_e = 1.0, \eta_c \to 1.0) \to 0$.

Using the positive concentration gradient $\Delta n = 2500\ \mu M$, $u_e^+ = 2, u_1^- = 2, u_1^+ = 2, u_c^- = 2$ and the values of the transition rates specified in Eq. 3.14 into Eq. 3.15, we have plotted the variation of the average particle flux J through a nano-channel with a single internal potential well as a function of η_e for five different values of η_c, that is $\eta_c = 0, \eta_c = 0.25, \eta_c = 0.5, \eta_c = 0.75, \eta_c = 1.0$ on the same graph as shown in Fig. 3.19.

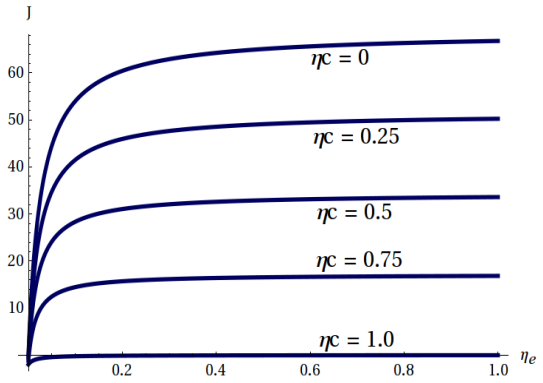

Fig. 3.19: Plot of J as a function of η_e when $s = 1$, $\Delta n = 2500\ \mu M$, $n_c = 1.0\,\mu M$, $\nu_e^+ = \nu_c^- = 15\,(\mu M)^{-1} s^{-1}, \nu_1^- = \nu_1^+ = 500\,s^{-1}$, $u_e^+ = 2, u_1^- = 2, u_1^+ = 2, u_c^- = 2$ for the values $\eta_c = 0, \eta_c = 0.25, \eta_c = 0.5, \eta_c = 0.75, \eta_c = 1.0$

Using the positive concentration gradient $\Delta n = 35\ \mu M$, $u_e^+ = 2, u_1^- = 2, u_1^+ = 2, u_c^- = 2$ and the values of the transition rates specified in Eq. 3.14 into Eq. 3.15, we have plotted the variation of the average particle flux J through a nano-channel with a single internal potential well as a function of η_e for five different values of η_c, that is $\eta_c = 0, \eta_c = 0.25, \eta_c = 0.5, \eta_c = 0.75, \eta_c = 1.0$ on the same graph as shown in Fig. 3.20.

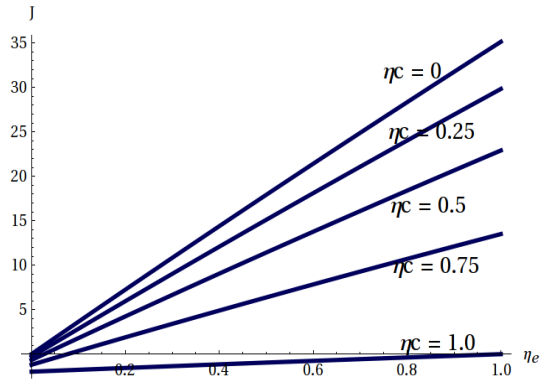

Fig. 3.20: Plot of J as a function of η_e when $s = 1$, $\Delta n = 35\ \mu M$, $n_c = 1.0\,\mu M$, $\nu_e^+ = \nu_c^- = 15\,(\mu M)^{-1}s^{-1}, \nu_1^- = \nu_1^+ = 500\,s^{-1}$, $u_e^+ = 2, u_1^- = 2, u_1^+ = 2, u_c^- = 2$ for the values $\eta_c = 0, \eta_c = 0.25, \eta_c = 0.5, \eta_c = 0.75, \eta_c = 1.0$

When $\Delta n = 2500\ \mu M$ and $\Delta n = 35\ \mu M$ the average particle flux approach to slightly different negative values as $\eta_e \to 0$ and and assume the values: $J_1^{sat}(\Delta n = 2500\ \mu M|\eta_e \to 1.0, \eta_c = 0) \to 0$, $J_1^{sat}(\Delta n = 2500\ \mu M|\eta_e \to 1.0, \eta_c = 0.25) \to -0.288767s^{-1}$, $J_1^{sat}(\Delta n = 2500\ \mu M|\eta_e \to 1.0, \eta_c = 0.5) \to -0.669977s^{-1}$, $J_1^{sat}(\Delta n = 2500\ \mu M|\eta_e \to 1.0, \eta_c = 0.75) \to -1.19648s^{-1}$, $J_1^{sat}(\Delta n = 2500\ \mu M|\eta_e \to 1.0, \eta_c = 1.0) \to -1.9709s^{-1}$. The fluxes diverge from each other and saturate to different maximum negative values as $\eta_e \to 1.0$, that is, $J_1^{sat}(\Delta n = 2500\ \mu M|\eta_e \to 1.0, \eta_c = 0) \to 66.7776$, $J_1^{sat}(\Delta n = 2500\ \mu M|\eta_e \to 1.0, \eta_c = 0.25) \to 50.2435$, $J_1^{sat}(\Delta n = 2500\ \mu M|\eta_e \to 1.0, \eta_c = 0.5) \to 33.6032$, $J_1^{sat}(\Delta n = 2500\ \mu M|\eta_e \to 1.0, \eta_c = 0.75) \to 16.8557$, $J_1^{sat}(\Delta n = 2500 \mu M|\eta_e \to 1.0, \eta_c = 1.0) \to 0$. Moreover, when $\Delta n \approx 35\ \mu M$ the average particle flux increases almost linearly as η_c increases and approach to different maximum positive values as $\eta_c \to 1.0$. Moreover, the average particle flux assumes the values when $J_1^{sat}(\Delta n = 2500\ \mu M|\eta_e, \eta_c \to 0) > 0$ and $J_1^{sat}(\Delta n = 2500\ \mu M|\eta_e, \eta_c \to 1.0) < 0$ for all possible values of η_e.

Using zero concentration gradient $\Delta n = 0$, $u_e^+ = 2, u_1^- = 2, u_1^+ = 2, u_c^- = 2$ and the values of the transition rates specified in Eq. 3.14 into Eq. 3.15, we have plotted the variation of the average particle flux J through a nano-channel with a single internal potential well as a function of η_e for five different values of η_c, that is $\eta_c = 0, \eta_c = 0.25, \eta_c = 0.5, \eta_c = 0.75, \eta_c = 1.0$ on the same graph as shown in Fig. 3.21.

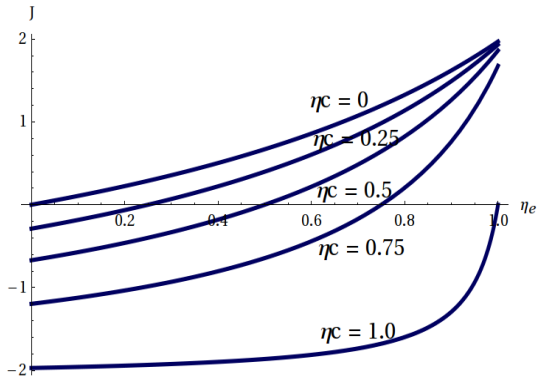

Fig. 3.21: Plot of J as a function of η_e when $s = 1$, $\Delta n = 0$, $n_c = 1.0\,\mu M$, $\nu_e^+ = \nu_c^- = 15\,(\mu M)^{-1}s^{-1}, \nu_1^- = \nu_1^+ = 500\,s^{-1}$, $u_e^+ = 2, u_1^- = 2, u_1^+ = 2, u_c^- = 2$ for the values $\eta_c = 0, \eta_c = 0.25, \eta_c = 0.5, \eta_c = 0.75, \eta_c = 1.0$

When $\Delta n = 0$, the average particle flux as a function of η_e obey that $J_1(\Delta n = 0|\eta_e, \eta_c = 0) > J_1(\Delta n = 0|\eta_e, \eta_c = 0.25) > J_1(\Delta n = 0|\eta_e, \eta_c = 0.5) > J_1(\Delta n = 0|\eta_e, \eta_c = 0.75) > J_1(\Delta n = 0|\eta_e, \eta_c = 1.0)$ and approach to different negative values as $\eta_e \to 0$, that is, $J_1(\Delta n = 0|\eta_c = 0, \eta_e \to 0) \to 0$, $J_1(\Delta n = 0|\eta_c = 0.25, \eta_e \to 0) \to -0.288767$, $J_1(\Delta n = 0|\eta_c = 0.5, \eta_e \to 0) \to -0.669977$, $J_1(\Delta n = 0|\eta_c = 0.75, \eta_e \to 0) \to -1.19648$, $J_1(\Delta n = 0|\eta_c = 1.0, \eta_e \to 0) \to -1.9709$. Moreover, the average particle flux as a function of η_e approach to different maximum positive values, that is, $J_1(\Delta n = 0|\eta_c = 0, \eta_e \to 1.0) \to 1.9709$, $J_1(\Delta n = 0|\eta_c = 0.25, \eta_e \to 1.0) \to 1.93336$, $J_1(\Delta n = 0|\eta_c = 0.5, \eta_e \to 1.0) \to 1.86241$, $J_1(\Delta n = 0|\eta_c = 0.75, \eta_e \to 1.0) \to 1.67771$, $J_1(\Delta n = 0|\eta_c = 1.0, \eta_e \to 1.0) \to 0$. When $\Delta n = 0$, the average particle flux through the nano-channel is positive if $J_1(\Delta n = 0|\eta_c = 0.25, \eta_e > 0.25) > 0$, $J_1(\Delta n = 0|\eta_c = 0.5, \eta_e > 0.5) > 0$, $J_1(\Delta n = 0|\eta_c = 0.75, \eta_e > 0.75) > 0$. Moreover, $J_1(\Delta n = 0|\eta_c = 0, \eta_e) > 0$ and $J_1(\Delta n = 0|\eta_c = 1, 0, \eta_e) < 0$ for all possible values of η_e in the range $0 \leq \eta_e \leq 1.0$.

Using the maximum negative concentration gradient, that is, $\Delta n = -1.0\ \mu M$, $u_e^+ = 2, u_1^- = 2, u_1^+ = 2, u_c^- = 2$ and the values of the transition rates specified in Eq. 3.14 into Eq. 3.15, we have plotted the variation of the average particle flux J through a nano-channel with a single internal potential well as a function of η_e for five different values of η_c, that is $\eta_c = 0, \eta_c = 0.25, \eta_c = 0.5, \eta_c = 0.75, \eta_c = 1.0$ on the same graph as shown in Fig. 3.22.

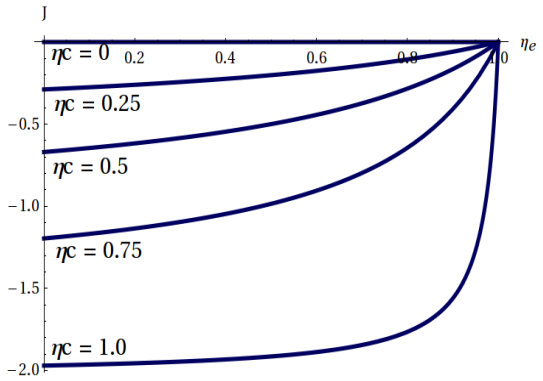

Fig. 3.22: Plot of J as a function of η_e when $s = 1$, $\Delta n = -1.0\,\mu M$, $n_c = 1.0\,\mu M$, $\nu_e^+ = \nu_c^- = 15\,(\mu M)^{-1}s^{-1}, \nu_1^- = \nu_1^+ = 500\,s^{-1}$, $u_e^+ = 2, u_1^- = 2, u_1^+ = 2, u_c^- = 2$ for the values $\eta_c = 0, \eta_c = 0.25, \eta_c = 0.5, \eta_c = 0.75, \eta_c = 1.0$

When $\Delta n = -1.0\ \mu M$, Fig. 3.22 shows that the average particle flux through the nano-channel as a function of η_e is zero when $\eta_c = 0$ for all possible values of η_e in the range $0 \leq \eta_e \leq 1.0$ and is negative for all possible values of η_c in the range $0 < \eta_c \leq 1.0$ in the entire range $0 \leq \eta_e \leq 1.0$. When $\Delta n = -1.0\ \mu M$, the average particle flux is zero when $\eta_e = 1.0$ for all possible values of η_c and as $\eta_e \to 0$, the average particle flux as a function of η_e approach to different maximum negative values, that is, $J_1(\Delta n = -1.0\ \mu M|\eta_c = 0, \eta_e \to 0) \to 0$, $J_1(\Delta n = -1.0\ \mu M|\eta_c = 0.25, \eta_e \to 0) \to -0.288767 s^{-1}$, $J_1(\Delta n = -1.0\ \mu M|\eta_c = 0.5, \eta_e \to 0) \to -0.669977 s^{-1}$, $J_1(\Delta n = -1.0\ \mu M|\eta_c = 0.75, \eta_e \to 0) \to -1.19648 s^{-1}$, $J_1(\Delta n = -1.0\ \mu M|\eta_c = 1.0, \eta_e \to 0) \to -1.9709 s^{-1}$.

Using $\eta_e = 0$, $u_e^+ = 2, u_1^- = 2, u_1^+ = 2, u_c^- = 2$ and the values of the transition rates specified in Eq. 3.14 into Eq. 3.15, we have plotted the variation of the average particle flux J through a nano-channel with a single internal potential well as a function of η_c for five different values of the concentration gradient Δn in units of μM, that is $\Delta n = -1.0, \Delta n = 0, \Delta n = 35, \Delta n = 100, \Delta n = 500, \Delta n = 1000$ on the same graph as shown in Fig. 3.23.

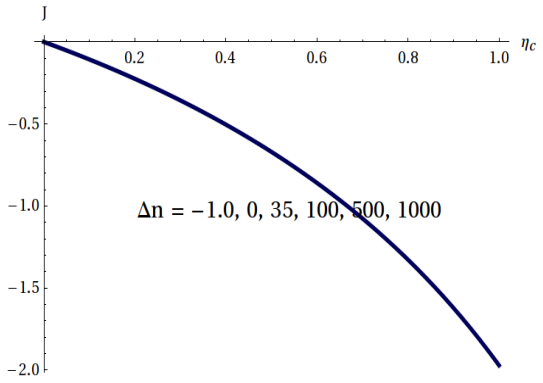

Fig. 3.23: Plot of J as a function of η_c when $s = 1$, $n_c = 1.0\,\mu M$, $\eta_e = 0$, $\nu_e^+ = \nu_c^- = 15\,(\mu M)^{-1}s^{-1}, \nu_1^- = \nu_1^+ = 500\,s^{-1}$, $u_e^+ = 2, u_1^- = 2, u_1^+ = 2, u_c^- = 2$ for the values $\Delta n = -1.0, \Delta n = 0, \Delta n = 35, \Delta n = 100, \Delta n = 500, \Delta n = 1000$

Using $\eta_e = 0.001$, $u_e^+ = 2, u_1^- = 2, u_1^+ = 2, u_c^- = 2$ and the values of the transition rates specified in Eq. 3.14 into Eq. 3.15, we have plotted the variation of the average particle flux J through a nano-channel with a single internal potential well as a function of η_c for five different values of the concentration gradient Δn in units of μM, that is $\Delta n = -1.0, \Delta n = 0, \Delta n = 35, \Delta n = 100, \Delta n = 500, \Delta n = 1000$ on the same graph as shown in Fig. 3.24.

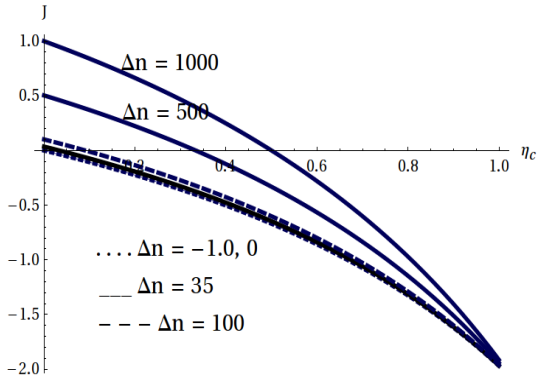

Fig. 3.24: Plot of J as a function of η_c when $s = 1$, $n_c = 1.0\,\mu M$, $\eta_e = 0.001$, $\nu_e^+ = \nu_c^- = 15\,(\mu M)^{-1}s^{-1}, \nu_1^- = \nu_1^+ = 500\,s^{-1}$, $u_e^+ = 2, u_1^- = 2, u_1^+ = 2, u_c^- = 2$ for the values $\Delta n = -1.0, \Delta n = 0, \Delta n = 35, \Delta n = 100, \Delta n = 500, \Delta n = 1000$

Using $\eta_e = 1.0$, $u_e^+ = 2, u_1^- = 2, u_1^+ = 2, u_c^- = 2$ and the values of the transition rates specified in Eq. 3.14 into Eq. 3.15, we have plotted the variation of the average particle flux through a nano-channel with a single internal potential well as a function of η_c for five different values of the concentration gradient Δn in

units of μM, that is $\Delta n = -1.0, \Delta n = 0, \Delta n = 35, \Delta n = 100, \Delta n = 500, \Delta n = 1000$ on the same graph as shown in Fig. 3.25.

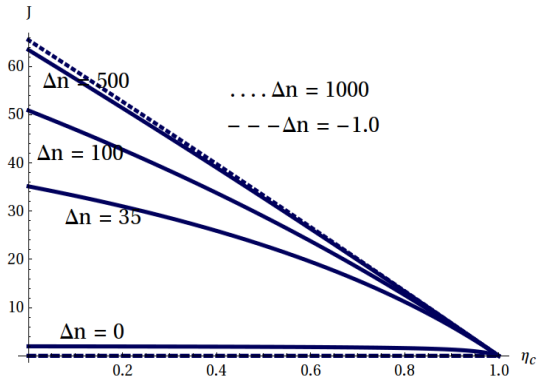

Fig. 3.25: Plot of J as a function of η_c when $s = 1$, $n_c = 1.0\,\mu M$, $\eta_e = 1.0$, $\nu_e^+ = \nu_c^- = 15\,(\mu M)^{-1}s^{-1}, \nu_1^- = \nu_1^+ = 500\,s^{-1}$, $u_e^+ = 2, u_1^- = 2, u_1^+ = 2, u_c^- = 2$ for the values $\Delta n = -1.0, \Delta n = 0, \Delta n = 35, \Delta n = 100, \Delta n = 500, \Delta n = 1000$

When $\eta_e = 0$, as shown in Fig. 3.23 the average particle flux is negative in the entire range $0 \leq \eta_c \leq 1$ and has the same value for all possible values of Δn. As η_e increases the flux associated with different values of Δn become separated from each other, that is, the distance between them increases and the flux increases in the positive direction and finally the flux associated with all possible values of Δn becomes totally positive as $\eta_c \to 1.0$. Moreover, $J_1(\Delta n = -1.0\ \mu M|\eta_c, \eta_e) < J_1(\Delta n = 0|\eta_c, \eta_e) < J_1(\Delta n = 35\ \mu M|\eta_c, \eta_e) < J_1(\Delta n = 100\ \mu M|\eta_c, \eta_e) < J_1(\Delta n = 500\ \mu M|\eta_c, \eta_e) < J_1(\Delta n = 1000\ \mu M|\eta_c, \eta_e)$ for all possible values of η_e and η_c. The average particle flux assumes a maximum value when $\eta_c \to 0$ for all possible values of η_e and Δn and then decreases as η_c increases and finally become minimum when $\eta_c = 1.0$.

Using $\eta_c = 0$, $u_e^+ = 2, u_1^- = 2, u_1^+ = 2, u_c^- = 2$ and the values of the transition rates specified in Eq. 3.14 into Eq. 3.15, we have plotted the variation of the average particle flux J through a nano-channel with a single internal potential well as a function of η_e for five different values of the concentration gradient Δn in units of μM, that is $\Delta n = -1.0, \Delta n = 0, \Delta n = 35, \Delta n = 100, \Delta n = 500, \Delta n = 1000$ on the same graph as shown in Fig. 3.26.

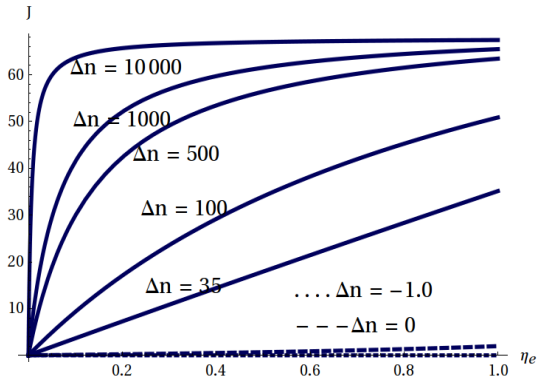

Fig. 3.26: Plot of J as a function of η_e when $s = 1$, $n_c = 1.0\,\mu M$, $\eta_c = 0$, $\nu_e^+ = \nu_c^- = 15\,(\mu M)^{-1}s^{-1}, \nu_1^- = \nu_1^+ = 500\,s^{-1}$, $u_e^+ = 2, u_1^- = 2, u_1^+ = 2, u_c^- = 2$ for the values $\Delta n = -1.0, \Delta n = 0, \Delta n = 35, \Delta n = 100, \Delta n = 500, \Delta n = 1000$

Using $\eta_c = 1.0$, $u_e^+ = 2, u_1^- = 2, u_1^+ = 2, u_c^- = 2$ and the values of the transition rates specified in Eq. 3.14 into Eq. 3.15, we have plotted the variation of the average particle flux through a nano-channel with a single internal potential well as a function of η_e for five different values of the concentration gradient Δn in units of μM, that is $\Delta n = -1.0, \Delta n = 0, \Delta n = 35, \Delta n = 100, \Delta n = 500, \Delta n = 1000$ on the same graph as shown in Fig. 3.27.

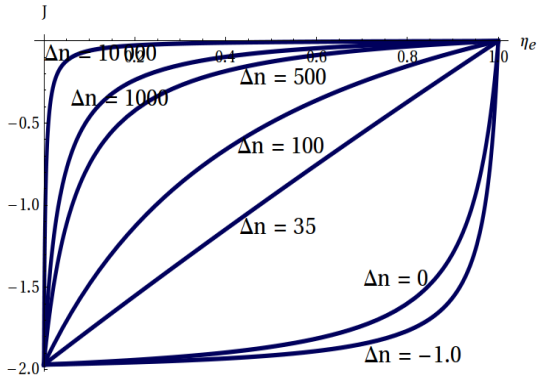

Fig. 3.27: Plot of J as a function of η_e when $s = 1$, $n_c = 1.0\,\mu M$, $\eta_c = 1.0$, $\nu_e^+ = \nu_c^- = 15\,(\mu M)^{-1}s^{-1}, \nu_1^- = \nu_1^+ = 500\,s^{-1}$, $u_e^+ = 2, u_1^- = 2, u_1^+ = 2, u_c^- = 2$ for the values $\Delta n = -1.0, \Delta n = 0, \Delta n = 35, \Delta n = 100, \Delta n = 500, \Delta n = 1000$

When $\eta_c = 1.0$, as shown in Fig. 3.27 the average particle flux is negative in the entire range $0 \leq \eta_e \leq 1$ and the flux increases almost linearly when $\Delta n = 35\mu M$ for all possible values of η_e. The fluxes associated with the possible values of Δn converge to each other as $\eta_e \to 0$ and $\eta_e \to 1.0$ and as η_e increases

to intermediate values the flux associated with different values of Δn diverge from each other, that is, the distance between them increases. Moreover, the magnitudes of the fluxes associated with different values of Δn obey $|J_1(\Delta n = -1.0\ \mu M|\eta_c, \eta_e)| < |J_1(\Delta n = 0|\eta_c, \eta_e)| < |J_1(\Delta n = 35\ \mu M|\eta_c, \eta_e)| < |J_1(\Delta n = 100\ \mu M|\eta_c, \eta_e)| < |J_1(\Delta n = 500\ \mu M|\eta_c, \eta_e)| < |J_1(\Delta n = 1000\ \mu M|\eta_c, \eta_e)|$ for all possible values of η_e and η_c.

3.2.3 Conclusion

1. Therefore, for the given values of Δn and η_e in their respective ranges, the average particle flux through a nano-channel with a single internal potential well decreases as the average value of η_c increases.

2. The average particle flux through the nano-channel is zero even in the presence of a large concentration gradient between the two baths when $\eta_e = \eta_c = 0$ and $\eta_e = \eta_c = 1.0$ and average particle flux through the nano-channel assumes negative values when $\eta_c = 1.0$ for all possible values of Δn and η_e.

3. The average particle flux associated with different values of u_e^+ saturate to the same maximum positive value but the average particle flux associated with different values of u_1^+ saturate to the different maximum positive values as Δn increases to large positive values.

4. The average flux approaches the saturation values more quickly when u_e^+ is small than when u_e^+ is large but the flux approaches the saturation value more quickly when u_1^+ is large than when u_1^+ is small.

5. The average particle flux associated with the different values of u_1^- and u_c^- saturate to the same maximum positive value as Δn increases to large positive values,

3.3 Discussion of the Average Occupation Number of a Nano-Channel with a Single Internal Potential Well

In this section, we will present a detailed description of the average occupation number of the internal potential well V_1 of a nano-channel with a single internal potential well and two external potential wells as a function of the concentration gradient between the emitter and collector baths and as a function of the occupation number of the external potential wells when the height of the potential barriers is twice of the thermal energy k_BT. Taking this fact into account, we will plot the variation of the average occupation number of the internal potential well as a function of the concentration gradient and the occupation number of the external potential wells.

3.3.1 The Average Occupation Number of the Internal Potential Well of a Nano-channel as a Function of the Concentration Gradient

Using $\eta_c = 0$, $u_e^+ = 2, u_1^- = 2, u_1^+ = 2, u_c^- = 2$ and the values of the transition rates specified in Eq. 3.14 into Eq. 3.16, we have plotted the variation of the average occupation number η_1 of the internal potential well V_1 of a nano-channel with a single internal potential well as a function of the concentration gradient Δn in units of μM for five different values of η_e, that is, $\eta_e = 0, \eta_e = 0.25, \eta_e = 0.5, \eta_e = 0.75, \eta_e = 1.0$ on the same graph as shown in Fig. 3.28.

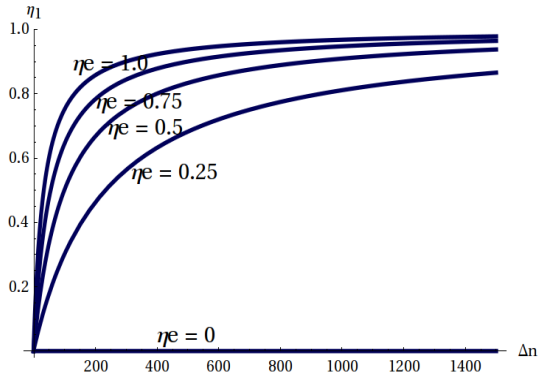

Fig. 3.28: Plot of η_1 as a function of the concentration gradient Δn in units of μM when $s = 1$, $n_c = 1.0\mu M$, $\eta_c = 0$, $\nu_e^+ = \nu_c^- = 15\,(\mu M)^{-1}s^{-1}, \nu_1^- = \nu_1^+ = 500\,s^{-1}$, $u_e^+ = 2, u_1^- = 2, u_1^+ = 2, u_c^- = 2$ for five different values $\eta_e = 0, \eta_e = 0.25, \eta_e = 0.5, \eta_e = 0.75, \eta_e = 1.0$

Using $\eta_c = 0.5$, $u_e^+ = 2, u_1^- = 2, u_1^+ = 2, u_c^- = 2$ and the values of the transition rates specified in Eq. 3.14 into Eq. 3.16, we have plotted the variation of the average value of the occupation number η_1 of the internal potential well of the nano-channel with a single internal potential well as a function of the concentration gradient Δn in units of μM for five different values of η_e, that is $\eta_e = 0, \eta_e = 0.25, \eta_e = 0.5, \eta_e = 0.75, \eta_e = 1.0$ on the same graph as shown in Fig. 3.29.

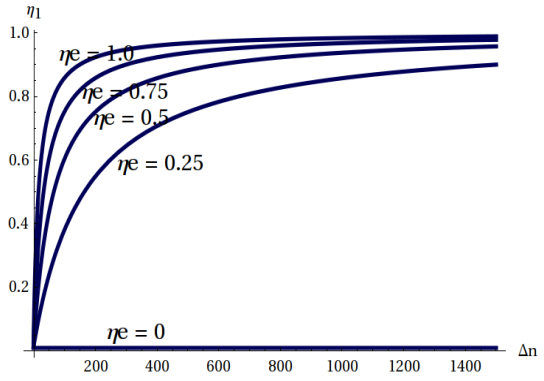

Fig. 3.29: Plot of η_1 as a function of the concentration gradient Δn in units of μM when $s = 1$, $n_c = 1.0\mu M$, $\eta_c = 0.5$,$\nu_e^+ = \nu_c^- = 15\,(\mu M)^{-1}s^{-1}, \nu_1^- = \nu_1^+ = 500\,s^{-1}$, $u_e^+ = 2, u_1^- = 2, u_1^+ = 2, u_c^- = 2$ for five different values $\eta_e = 0, \eta_e = 0.25, \eta_e = 0.5, \eta_e = 0.75, \eta_e = 1.0$

Using $\eta_c = 1.0$, $u_e^+ = 2, u_1^- = 2, u_1^+ = 2, u_c^- = 2$ and the values of the tran-

sition rates specified in Eq. 3.14 into Eq. 3.16, we have plotted the variation of the average value of the occupation number η_1 of the internal potential well of the nano-channel with a single internal potential well as a function of the concentration gradient Δn in units of μM for five different values of η_e, that is $\eta_e = 0, \eta_e = 0.25, \eta_e = 0.5, \eta_e = 0.75, \eta_e = 1.0$ on the same graph as shown in Fig. 3.30.

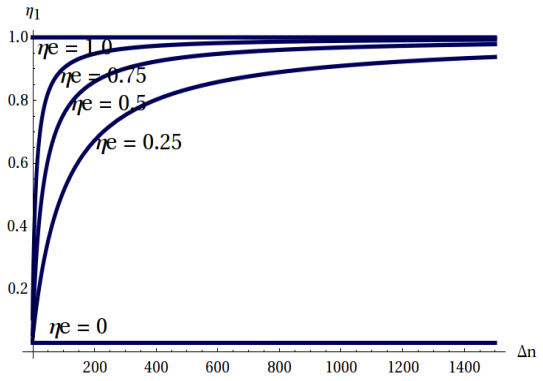

Fig. 3.30: Plot of η_1 as a function of the concentration gradient Δn in units of μM when $s = 1$, $n_c = 1.0\mu M$, $\eta_c = 1.0$, $\nu_e^+ = \nu_c^- = 15\,(\mu M)^{-1}s^{-1}, \nu_1^- = \nu_1^+ = 500\,s^{-1}$, $u_e^+ = 2, u_1^- = 2, u_1^+ = 2, u_c^- = 2$ for five different values $\eta_e = 0, \eta_e = 0.25, \eta_e = 0.5, \eta_e = 0.75, \eta_e = 1.0$

For the given values of η_e and η_c, the average occupation number of the internal potential well of a nano-channel as a function of Δn is denoted by $\eta_1(\Delta n|\eta_e, \eta_c)$. Fig. 3.28 to Fig. 3.30 show that $\eta_1(\Delta n|\eta_e = 0, \eta_c) < \eta_1(\Delta n|\eta_e = 0.25, \eta_c) < \eta_1(\Delta n|\eta_e = 0.5, \eta_c) < \eta_1(\Delta n|\eta_e = 0.75, \eta_c) < \eta_1(\Delta n|\eta_e = 1.0, \eta_c)$ for all possible values of Δn and η_c. The average value of the occupation number assumes the values $\eta_1(\Delta n|\eta_e, \eta_c) = 1.0$ when $\eta_e = 1.0$ and $\eta_c = 1.0$ and $\eta_1(\Delta n|\eta_e, \eta_c) = 0$ when $\eta_e = 0$ and $\eta_c = 0$ for all possible values of Δn. Moreover, $\eta_1(\Delta n \to 10M|\eta_e, \eta_c) \to 1.0$ for all possible values of $\eta_e > 0$ and η_c and $\eta_1(\Delta n|\eta_e = 1.0, \eta_c)$ approaches its saturation or maximum positive value more rapidly than other possible values. For small values of Δn, that is, $\Delta n < 400\mu M$ the average occupation number of V_1 of the nano-channel increases very rapidly as Δn increases and then it increases slowly and finally as Δn increases to large values, $\eta_1(\Delta n|\eta_e, \eta_c)$ saturates to its maximum constant value $\eta_1(\Delta n|\eta_e, \eta_c) \to 1.0$.

For a given value of η_c, the rate of approach of $\eta_1(\Delta n|\eta_e,\eta_c)$ as a function of Δn to the saturation value is different for different values of η_e. That is, $\eta_1(\Delta n|\eta_e,\eta_c)$ saturates more quickly at a small value of Δn when $\eta_e = 1.0$ and as η_e decreases from one to zero, the value of Δn at which $\eta_1(\Delta n|\eta_e,\eta_c)$ becomes saturated increases from the smallest value, which occurs when $\eta_e = 1.0$ to the largest one, which occurs when $\eta_e = 0$. In other words, for a given value of η_c, the value of Δn at which $\eta_1(\Delta n|\eta_e,\eta_c)$ saturates increases as η_e decreases from one to zero. For a given value of η_c, the average value of $\eta_1(\Delta n|\eta_e,\eta_c)$ associated with different values of η_e converge to each other as $\Delta n \rightarrow -1.0\,\mu M$ and then diverge from each other as Δn increases to intermediate values and finally the average value of $\eta_1(\Delta n|\eta_e,\eta_c)$ associated with different values of η_e saturates to the same maximum value $\eta_1(\Delta n|\eta_e,\eta_c) \rightarrow 1.0$ as Δn increases to large values.

Therefore, the average value of $\eta_1(\Delta n|\eta_e,\eta_c)$ attains its maximum value of one when $\eta_c = 1.0$ and $\eta_e = 1.0$ at a very small value of Δn as shown in Fig. 3.30. Therefore, when $\eta_c = 1.0$, the mean residence time of a particle at the potential well V_c is large and as result the occupation probability of V_c is almost one. Moreover, as $\eta_e \rightarrow 1.0$, the mean residence time of a particle at the potential well V_e is large and as result the occupation probability of this site is almost one. This means that the average value of $\eta_1(\Delta n|\eta_e,\eta_c)$ attains its maximum value when V_c is occupied, that is $\eta_c = 1.0$, and when V_e is occupied, that is $\eta_e = 1$.

Using $\eta_e = 0$, $u_e^+ = 2, u_1^- = 2, u_1^+ = 2, u_c^- = 2$ and the values of the transition rates specified in Eq. 3.14 into Eq. 3.16, we have plotted the variation of the average value of the occupation number η_1 of the internal potential well of a nano-channel with a single internal potential well as a function of the concentration gradient Δn in units of μM for five different values of η_c, that is $\eta_c = 0, \eta_c = 0.25, \eta_c = 0.5, \eta_c = 0.75, \eta_c = 1.0$ on the same graph as shown in Fig. 3.31.

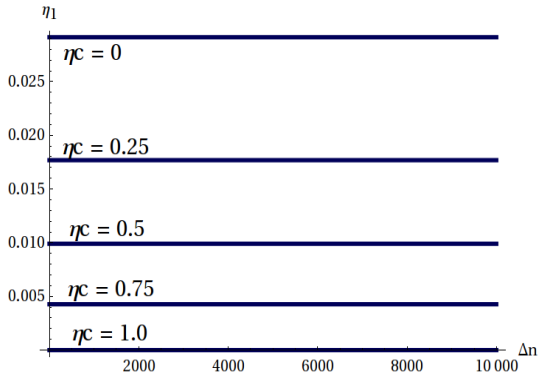

Fig. 3.31: Plot of η_1 as a function of the concentration gradient Δn in units of μM when $s = 1$, $n_c = 1.0\mu M$, $\eta_e = 0$, $\nu_e^+ = \nu_c^- = 15\,(\mu M)^{-1}s^{-1}, \nu_1^- = \nu_1^+ = 500\,s^{-1}$, $u_e^+ = 2, u_1^- = 2, u_1^+ = 2, u_c^- = 2$ for five different values $\eta_c = 0, \eta_c = 0.25, \eta_c = 0.5, \eta_c = 0.75, \eta_c = 1.0$

Using $\eta_e = 0.5$, $u_e^+ = 2, u_1^- = 2, u_1^+ = 2, u_c^- = 2$ and the values of the transition rates specified in Eq. 3.14 into Eq. 3.16, we have plotted the variation of the average value of the occupation number η_1 of the internal potential well of a nano-channel with a single internal potential well as a function of the concentration gradient Δn in units of μM for five different values of η_c, that is $\eta_c = 0, \eta_c = 0.25, \eta_c = 0.5, \eta_c = 0.75, \eta_c = 1.0$ on the same graph as shown in Fig. 3.32.

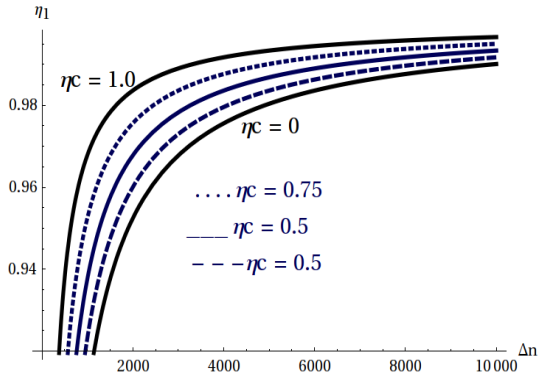

Fig. 3.32: Plot of η_1 as a function of the concentration gradient Δn in units of μM when $s = 1$, $n_c = 1.0\mu M$, $\eta_e = 0.5$, $\nu_e^+ = \nu_c^- = 15\,(\mu M)^{-1}s^{-1}, \nu_1^- = \nu_1^+ = 500\,s^{-1}$, $u_e^+ = 2, u_1^- = 2, u_1^+ = 2, u_c^- = 2$ for five different values $\eta_c = 0, \eta_c = 0.25, \eta_c = 0.5, \eta_c = 0.75, \eta_c = 1.0$

Using $\eta_e = 1.0$, $u_e^+ = 2, u_1^- = 2, u_1^+ = 2, u_c^- = 2$ and the values of the transi-

tion rates specified in Eq. 3.14 into Eq. 3.16, we have plotted the variation of the average value of the occupation number η_1 of the internal potential well of a nano-channel with a single internal potential well as a function of the concentration gradient Δn in units of μM for five different values of η_c, that is $\eta_c = 0, \eta_c = 0.25, \eta_c = 0.5, \eta_c = 0.75, \eta_c = 1.0$ on the same graph as shown in Fig. 3.33.

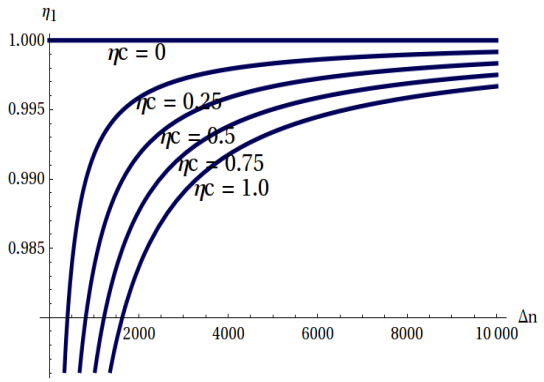

Fig. 3.33: Plot of η_1 as a function of the concentration gradient Δn in units of μM when $s = 1$, $n_c = 1.0\mu M$, $\eta_e = 1.0$, $\nu_e^+ = \nu_c^- = 15\,(\mu M)^{-1}s^{-1}, \nu_1^- = \nu_1^+ = 500\,s^{-1}$, $u_e^+ = 2, u_1^- = 2, u_1^+ = 2, u_c^- = 2$ for five different values $\eta_c = 0, \eta_c = 0.25, \eta_c = 0.5, \eta_c = 0.75, \eta_c = 1.0$

As shown in Fig. 3.31, for the given values of η_c, the average value of $\eta_1(\Delta n|\eta_e = 0, \eta_c)$ as a function of Δn assumes small constant values that don't change as Δn increases. The plots shown in Fig. 3.31 to Fig. 3.33 show that: $\eta_1(\Delta n|\eta_e, \eta_c = 0) < \eta_1(\Delta n|\eta_e, \eta_c = 0.25) < \eta_1(\Delta n|\eta_e, \eta_c = 0.5) < \eta_1(\Delta n|\eta_e, \eta_c = 0.75) < \eta_1(\Delta n|\eta_e, \eta_c = 1.0)$ for all possible values of Δn and η_e. Moreover, $\eta_1(\Delta n|\eta_e, \eta_c) = 1.0$ when $\eta_e = 1.0$ and $\eta_c = 1.0$ and $\eta_1(\Delta n|\eta_e, \eta_c) = 0$ when $\eta_e = 0$ and $\eta_c = 0$ for all possible values of Δn. Furthermore, $\eta_1(\Delta n \to 10M|\eta_e, \eta_c) \to 1.0$ for all possible values of $\eta_e > 0$ and η_c and $\eta_1(\Delta n|\eta_e, \eta_c = 1.0)$ approaches its saturation value more rapidly. For small values of Δn, that is, $\Delta n < 4000\mu M$ the average occupation number of V_1 of the nano-channel increases very rapidly as Δn increases and then it increases slowly and finally as Δn increases to large values, $\eta_1(\Delta n|\eta_e, \eta_c)$ saturates to its maximum constant value $\eta_1(\Delta n|\eta_e, \eta_c) \to 1.0$.

Using $\eta_e = 0.1$, $\eta_c = 0.1$, $u_1^- = 2, u_1^+ = 2, u_c^- = 2$ and the values of the transition rates specified in Eq. 3.14 into Eq. 3.16, we have plotted the variation of the average occupation number η_1 of the internal potential well V_1 of a nano-channel with a single internal site as a function of concentration gradient Δn in

units of μM for four different values of u_e^+, that is $u_e^+ \approx 0, u_e^+ = 1.0, u_e^+ = 2.0, u_e^+ = 3.0$ on the same graph as shown in Fig. 3.34.

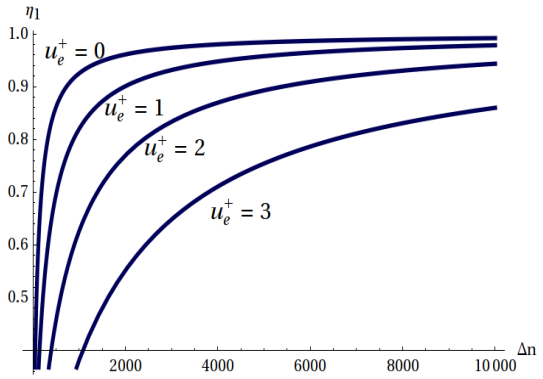

Fig. 3.34: Plot of η_1 as a function of the concentration gradient Δn in units of μM when $s = 1$, $n_c = 1.0\,\mu M$, $\eta_e = 0.1$, $\eta_c = 0.1$, $\nu_e^+ = \nu_c^- = 15\,(\mu M)^{-1}s^{-1}, \nu_1^- = \nu_1^+ = 500\,s^{-1}$, $u_e^+ = 2, u_1^- = 2, u_1^+ = 2, u_c^- = 2$ for the values $u_e^+ \approx 0, u_e^+ = 1.0, u_e^+ = 2.0, u_e^+ = 3.0$

Using $\eta_e = 0.95$, $\eta_c = 0.95$, $u_e^+ = 2, u_1^- = 2, u_1^+ = 2, u_c^- = 2$ and the values of the transition rates specified in Eq. 3.14 into Eq. 3.16, we have plotted the variation of the average Occupation Number η_1 of the internal Potential Well of a nano-channel with a single internal site as a function of concentration gradient Δn in units of μM for four different values of u_e^+, that is $u_e^+ \approx 0, u_e^+ = 1.0, u_e^+ = 2.0, u_e^+ = 3.0$ on the same graph as shown in Fig. 3.35.

Using $\eta_e = 1$, $\eta_c = 0$, $u_e^+ = 2, u_1^- = 2, u_1^+ = 2, u_c^- = 2$ and the values of the transition rates specified in Eq. 3.14 into Eq. 3.16, we have plotted the variation of the average Occupation Number η_1 of the internal Potential Well of a nano-channel with a single internal site as a function of concentration gradient Δn in units of μM for four different values of u_e^+, that is $u_e^+ \approx 0, u_e^+ = 1.0, u_e^+ = 2.0, u_e^+ = 3.0$ on the same graph as shown in Fig. 3.36.

Using $\eta_e = 0$, $\eta_c = 1.0$, $u_e^+ = 2, u_1^- = 2, u_1^+ = 2, u_c^- = 2$ and the values of the transition rates specified in Eq. 3.14 into Eq. 3.16, we have plotted the variation of the average Occupation Number η_1 of the internal Potential Well of a nano-channel with a single internal site as a function of concentration gradient Δn in units of μM for four different values of u_e^+, that is $u_e^+ \approx 0, u_e^+ = 1.0, u_e^+ = 2.0, u_e^+ = 3.0$ on the same graph as shown in Fig. 3.37.

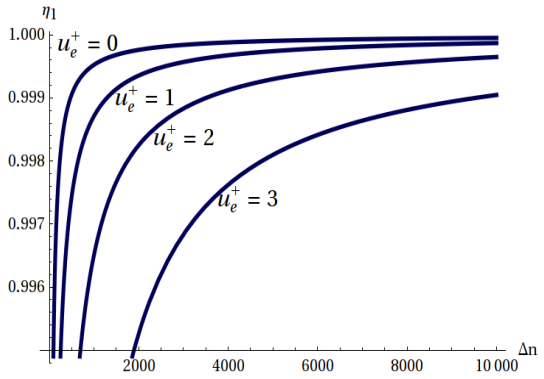

Fig. 3.35: Plot of η_1 as a function of the concentration gradient Δn in units of μM when $s = 1$, $n_c = 1.0\,\mu M$, $\eta_e = 0.95$, $\eta_c = 0.95$, $\nu_e^+ = \nu_c^- = 15\,(\mu M)^{-1}s^{-1}$, $\nu_1^- = \nu_1^+ = 500\,s^{-1}$, $u_e^+ = 2, u_1^- = 2, u_1^+ = 2, u_c^- = 2$ for the values: $u_e^+ \approx 0, u_e^+ = 1.0, u_e^+ = 2.0, u_e^+ = 3.0$

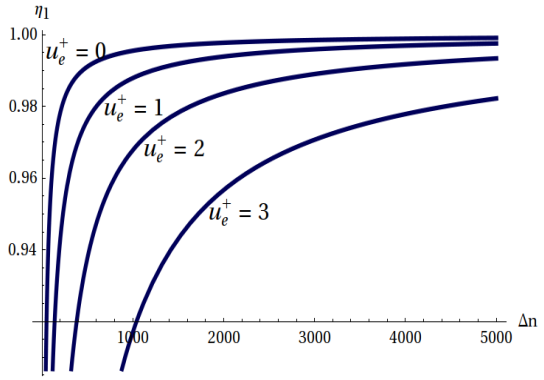

Fig. 3.36: Plot of η_1 as a function of the concentration gradient Δn in units of μM when $s = 1$, $n_c = 1.0\,\mu M$, $\eta_e = 1.0$, $\eta_c = 0$, $\nu_e^+ = \nu_c^- = 15\,(\mu M)^{-1}s^{-1}$, $\nu_1^- = \nu_1^+ = 500\,s^{-1}$, $u_e^+ = 2, u_1^- = 2, u_1^+ = 2, u_c^- = 2$ for the values: $u_e^+ \approx 0, u_e^+ = 1.0, u_e^+ = 2.0, u_e^+ = 3.0$

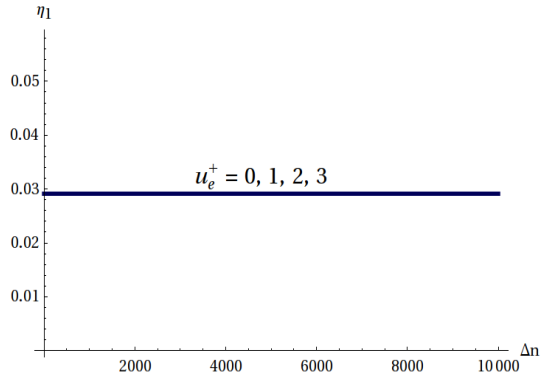

Fig. 3.37: Plot of η_1 as a function of the concentration gradient Δn in units of μM when $s = 1$, $n_c = 1.0\,\mu M$, $\eta_e = 0$, $\eta_c = 1.0$, $\nu_e^+ = \nu_c^- = 15\,(\mu M)^{-1}s^{-1}, \nu_1^- = \nu_1^+ = 500\,s^{-1}$, $u_e^+ = 2, u_1^- = 2, u_1^+ = 2, u_c^- = 2$ for the values: $u_e^+ \approx 0, u_e^+ = 1.0, u_e^+ = 2.0, u_e^+ = 3.0$

Using $\eta_e = 1.0$, $\eta_c = 1.0$, $u_e^+ = 2, u_1^- = 2, u_1^+ = 2, u_c^- = 2$ and the values of the transition rates specified in Eq. 3.14 into Eq. 3.16, we have plotted the variation of the average Occupation Number η_1 of the internal Potential Well of a nano-channel with a single internal site as a function of concentration gradient Δn in units of μM for four different values of u_e^+, that is $u_e^+ \approx 0, u_e^+ = 1.0, u_e^+ = 2.0, u_e^+ = 3.0$ on the same graph as shown in Fig. 3.38.

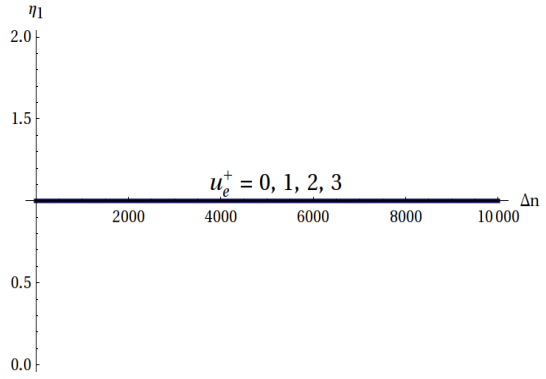

Fig. 3.38: Plot of η_1 as a function of the concentration gradient Δn in units of μM when $s = 1$, $n_c = 1.0\,\mu M$, $\eta_e = 1.0$, $\eta_c = 1.0$, $\nu_e^+ = \nu_c^- = 15\,(\mu M)^{-1}s^{-1}, \nu_1^- = \nu_1^+ = 500\,s^{-1}$, $u_e^+ = 2, u_1^- = 2, u_1^+ = 2, u_c^- = 2$ for the values: $u_e^+ \approx 0, u_e^+ = 1.0, u_e^+ = 2.0, u_e^+ = 3.0$

As shown in Fig. 3.37, the average value of $\eta_1(\Delta n|\eta_e, \eta_c, u_e^+)$ as a function of Δn assumes the same constant values when $\eta_1(\Delta n|\eta_e = 0, \eta_c = 1.0, u_e^+) = 0.0291262$

and $\eta_1(\Delta n|\eta_e = 1.0, \eta_c = 1.0, u_e^+) = 1.0$ that don't change as Δn increases for each possible value of u_e^+. Fig. 3.34 to Fig. 3.36 show the property that: $\eta_1(\Delta n|\eta_e, \eta_c, u_e^+ \approx 0) > \eta_1(\Delta n|\eta_e, \eta_c, u_e^+ \approx 1.0) > \eta_1(\Delta n|\eta_e, \eta_c, u_e^+ \approx 2.0) > \eta_1(\Delta n|\eta_e, \eta_c, u_e^+ \approx 3.0)$ for all possible values of Δn, η_e and η_c. Moreover, $\eta_1(\Delta n|\eta_e, \eta_c, u_e^+)$ approaches its saturation value more rapidly when u_e^+ is small, that is $u_e^+ \approx 0$ than when u_e^+ assumes higher values. Therefore, as the normalized potential barrier u_e^+ increases, the transition rate from the external potential well V_e to the internal potential well V_1 decreases and as result the occupation probability of V_1 is small, which means that the average value of the occupation number η_1 of V_1 of a nano-channel with a single internal potential wells decreases.

Using $\eta_e = 0.5$, $\eta_c = 0.5$, $u_e^+ = 2, u_1^- = 2, u_1^+ = 2, u_c^- = 2$ and the values of the transition rates specified in Eq. 3.14 into Eq. 3.16, we have plotted the variation of the average Occupation Number η_1 of the internal Potential Well of a nano-channel with a single internal site as a function of concentration gradient Δn in units of μM for four different values of u_1^-, that is $u_1^- \approx 0, u_1^- = 1.0, u_1^- = 2.0, u_1^- = 3.0$ on the same graph as shown in Fig. 3.39.

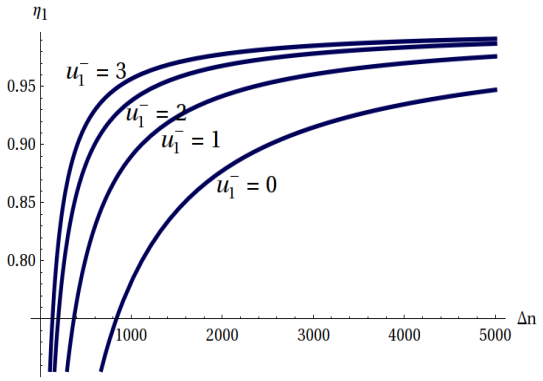

Fig. 3.39: Plot of η_1 as a function of the concentration gradient Δn in units of μM when $s = 1$, $n_c = 1.0\,\mu M$, $\eta_e = 0.5$, $\eta_c = 0.5$, $\nu_e^+ = \nu_c^- = 15\,(\mu M)^{-1}s^{-1}, \nu_1^- = \nu_1^+ = 500\,s^{-1}$, $u_e^+ = 2, u_1^- = 2, u_1^+ = 2, u_c^- = 2$ for the values: $u_1^- \approx 0, u_1^- = 1.0, u_1^- = 2.0, u_1^- = 3.0$

Using $\eta_e = 0.5$, $\eta_c = 0.5$, $u_e^+ = 2, u_1^- = 2, u_1^+ = 2, u_c^- = 2$ and the values of the transition rates specified in Eq. 3.14 into Eq. 3.16, we have plotted the variation of the average Occupation Number η_1 of the internal Potential Well of a nano-channel with a single internal site as a function of concentration gradient Δn in

units of μM for four different values of u_e^+, that is $u_1^+ \approx 0, u_1^+ = 1.0, u_1^+ = 2.0, u_1^+ = 3.0$ on the same graph as shown in Fig. 3.40.

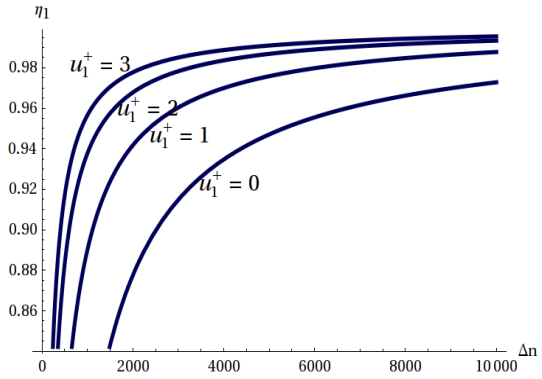

Fig. 3.40: Plot of η_1 as a function of the concentration gradient Δn in units of μM when $s = 1$, $n_c = 1.0\,\mu M$, $\eta_e = 0.5$, $\eta_c = 0.5$, $\nu_e^+ = \nu_c^- = 15\,(\mu M)^{-1}s^{-1}, \nu_1^- = \nu_1^+ = 500\,s^{-1}$, $u_e^+ = 2, u_1^- = 2, u_1^+ = 2, u_c^- = 2$ for the values $u_1^+ \approx 0, u_1^+ = 1.0, u_1^+ = 2.0, u_1^+ = 3.0$

Using $\eta_e = 0.5$, $\eta_c = 0.5$, $u_e^+ = 2, u_1^- = 2, u_1^+ = 2, u_c^- = 2$ and the values of the transition rates specified in Eq. 3.14 into Eq. 3.16, we have plotted the variation of the average Occupation Number η_1 of the internal Potential Well of a nano-channel with a single internal site as a function of concentration gradient Δn in units of μM for four different values of u_c^-, that is $u_c^- \approx 0, u_c^- = 1.0, u_c^- = 2.0, u_c^- = 3.0$ on the same graph as shown in Fig. 3.41.

The average value of $\eta_1(\Delta n|\eta_e, \eta_c)$ becomes large when u_1^- and u_1^+ assume large values as shown in Fig. 3.39 and Fig. 3.40, respectively. That is, when u_1^- and u_1^+ assume large values the escape rate from the internal potential well V_1 is small and as a result the mean residence time of a particle in V_1 becomes large, which in turn imply that the occupation probability of V_1 by a particle increases and thus the average value of $\eta_1(\Delta n|\eta_e, \eta_c)$ increases as u_1^- and u_1^+ increase. The average value of $\eta_1(\Delta n|\eta_e, \eta_c)$ saturates more quickly to its maximum value when u_1^- and u_1^+ assume large values. Moreover, the average value of $\eta_1(\Delta n|\eta_e, \eta_c)$ assumes the same value for each possible value of u_c^- as shown in Fig. 3.41.

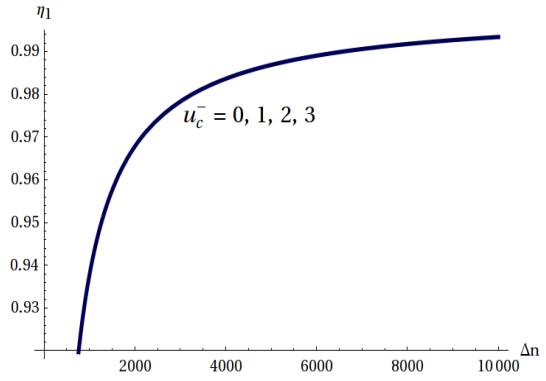

Fig. 3.41: Plot of η_1 as a function of the concentration gradient Δn in units of μM when $s = 1$, $n_c = 1.0\,\mu M$, $\eta_e = 0.5$, $\eta_c = 0.5$, $\nu_e^+ = \nu_c^- = 15\,(\mu M)^{-1}s^{-1}, \nu_1^- = \nu_1^+ = 500\,s^{-1}$, $u_e^+ = 2, u_1^- = 2, u_1^+ = 2, u_c^- = 2$ for the values: $u_c^- \approx 0, u_c^- = 1.0, u_c^- = 2.0, u_c^- = 3.0$

3.3.2 The Average Occupation Number of the Internal Potential Well as a Function of the the Average Occupation Number of the External Potential Wells when the Potential Barriers are Twice of Thermal Energy

Using the positive concentration gradient $\Delta n = 1\ M$, $u_e^+ = 2, u_1^- = 2, u_1^+ = 2, u_c^- = 2$ and the transition rates in Eq. 3.14 into Eq. 3.16, we have plotted the variation of the average occupation number η_1 of the internal potential well V_1 as a function of η_c for five possible values of η_e, that is $\eta_e = 0, \eta_e = 0.25, \eta_e = 0.5, \eta_e = 0.75, \eta_e = 1.0$ on the same graph as shown in Fig. 3.42.

The average value of η_1 associated with all non-zero values of η_e coincide with each other and assume almost the same saturation value of one when Δn assumes large values, in particular as $\Delta n \to 1M$. As Δn decreases to small values, in particular as $\Delta n \to 1M$, the average value of η_1 associated with all non-zero values of η_e separate from each other and assume different values and become almost parallel to each other as shown in Fig. 3.43.

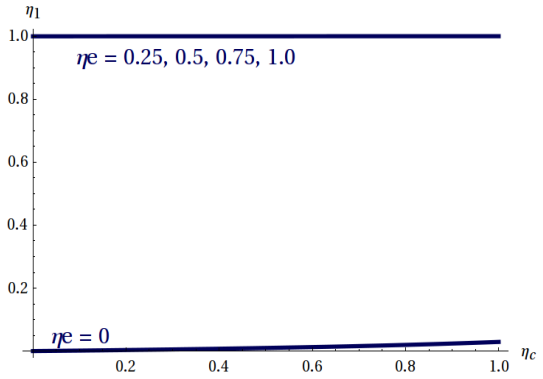

Fig. 3.42: Plot of η_1 as a function of η_c when $s = 1$, $\Delta n = 1000000\ \mu M$, $n_c = 1.0\mu M$, $\nu_e^+ = \nu_c^- = 15\,(\mu M)^{-1}s^{-1}, \nu_1^- = \nu_1^+ = 500\,s^{-1}$, $u_e^+ = 2, u_1^- = 2, u_1^+ = 2, u_c^- = 2$ for five values of η_e, that is: $\eta_e = 0, \eta_e = 0.25, \eta_e = 0.5, \eta_e = 0.75, \eta_e = 1.0$

Using positive concentration gradient $\Delta n = 250\ \mu M$, $u_e^+ = 2, u_1^- = 2, u_1^+ = 2, u_c^- = 2$ and the transition rates in Eq. 3.14 into Eq. 3.16, we have plotted the variation of the average occupation number η_1 of the internal potential well V_1 as a function of η_c for five possible values of η_e, that is $\eta_e = 0, \eta_e = 0.25, \eta_e = 0.5, \eta_e = 0.75, \eta_e = 1.0$ on the same graph as shown in Fig. 3.43.

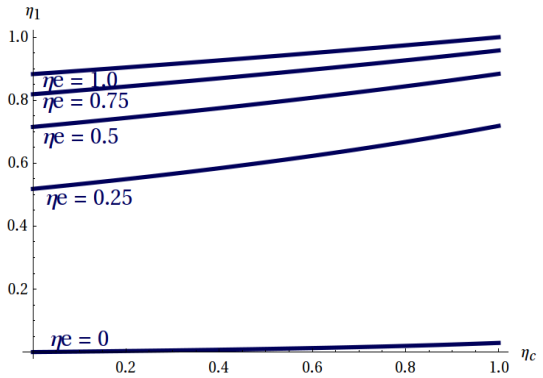

Fig. 3.43: Plot of η_1 as a function of η_c when $s = 1$, $\Delta n = 250\ \mu M$, $n_c = 1.0\mu M$, $\nu_e^+ = \nu_c^- = 15\,(\mu M)^{-1}s^{-1}, \nu_1^- = \nu_1^+ = 500\,s^{-1}$, $u_e^+ = 2, u_1^- = 2, u_1^+ = 2, u_c^- = 2$ for five values of η_e, that is: $\eta_e = 0, \eta_e = 0.25, \eta_e = 0.5, \eta_e = 0.75, \eta_e = 1.0$

Using zero concentration gradient $\Delta n = 0$, $u_e^+ = 2, u_1^- = 2, u_1^+ = 2, u_c^- = 2$ and the transition rates in Eq. 3.14 into Eq. 3.16, we have plotted the variation of the average occupation number η_1 of the internal potential well V_1 as a function of η_c for five possible values of η_e, that is $\eta_e = 0, \eta_e = 0.25, \eta_e = 0.5, \eta_e = 0.75, \eta_e = 1.0$ on the same graph as shown in Fig. 3.44.

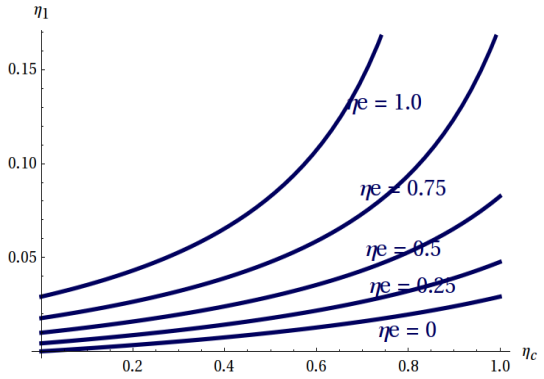

Fig. 3.44: Plot of η_1 as a function of η_c when $s = 1$, $\Delta n = 0$, $n_c = 1.0\mu M$, $\nu_e^+ = \nu_c^- = 15\,(\mu M)^{-1}s^{-1}, \nu_1^- = \nu_1^+ = 500\,s^{-1}$, $u_e^+ = 2, u_1^- = 2, u_1^+ = 2, u_c^- = 2$ for five values of η_e, that is: $\eta_e = 0, \eta_e = 0.25, \eta_e = 0.5, \eta_e = 0.75, \eta_e = 1.0$

When $\Delta n = 0$, the average occupation number η_1 as a function of η_c obey that $\eta_1(\Delta n = 0|\eta_e = 1.0, \eta_c) > \eta_1(\Delta n = 0|\eta_e = 0.75, \eta_c) > \eta_1(\Delta n = 0|\eta_e = 0.5, \eta_c) > \eta_1(\Delta n = 0|\eta_e = 0.25, \eta_c) > \eta_1(\Delta n = 0|\eta_e = 0, \eta_c)$. The average value of η_1 approach to different minimum values as $\eta_c \to 0$, that is, $\eta_1(\Delta n = 0|\eta_e = 0, \eta_c \to 0) \to 0$, $\eta_1(\Delta n = 0|\eta_e = 0.25, \eta_c \to 0) \to 0.00426743$, $\eta_1(\Delta n = 0|\eta_e = 0.5, \eta_c \to 0) \to 0.00990099$, $\eta_1(\Delta n = 0|\eta_e = 0.75, \eta_c \to 0) \to 0.0176817$, $\eta_1(\Delta n = 0|\eta_e = 1.0, \eta_c \to 0) \to 0.0291262$. Moreover, the average occupation number η_1 as a function of η_c approach to different maximum values, that is, $\eta_1(\Delta n = 0|\eta_e = 0, \eta_c \to 1.0) \to 0.0291262$, $\eta_1(\Delta n = 0|\eta_e = 0.25, \eta_c \to 1.0) \to 0.047619$, $\eta_1(\Delta n = 0|\eta_e = 0.5, \eta_c \to 1.0) \to 0.0825688$, $\eta_1(\Delta n = 0|\eta_e = 0.75, \eta_c \to 1.0) \to 0.173554$, $\eta_1(\Delta n = 0|\eta_e = 1.0, \eta_c \to 1.0) \to 1.0$.

Using negative concentration gradient $\Delta n = -1.0\ \mu M$, $u_e^+ = 2, u_1^- = 2, u_1^+ = 2, u_c^- = 2$ and the transition rates in Eq. 3.14 into Eq. 3.16, we have plotted the variation of the average occupation number η_1 of the internal potential well V_1 as a function of η_c for five possible values of η_e, that is $\eta_e = 0, \eta_e = 0.25, \eta_e = 0.5, \eta_e = 0.75, \eta_e = 1.0$ on the same graph as shown in Fig. 3.45.

When $\Delta n = -1.0\ \mu M$, the average occupation number η_1 as a function of η_c obey that $\eta_1(\Delta n = -1.0\ \mu M|\eta_e = 0.99, \eta_c) > \eta_1(\Delta n = -1.0\ \mu M|\eta_e = 0.75, \eta_c) > \eta_1(\Delta n = -1.0\ \mu M|\eta_e = 0.5, \eta_c) > \eta_1(\Delta n = -1.0\ \mu M|\eta_e = 0, \eta_c)$. The average value of η_1 approach to the same minimum zero value as $\eta_c \to 0$. Moreover, the average value of η_1 approach to different maximum values, that is,

$\eta_1(\Delta n = -1.0\ \mu M|\eta_e = 0, \eta_c \to 1.0) \to 0.0291262$, $\eta_1(\Delta n = -1.0\ \mu M|\eta_e = 0.5, \eta_c \to 1.0) \to 0.0566038$, $\eta_1(\Delta n = -1.0\ \mu M|\eta_e = 0.75, \eta_c \to 1.0) \to 0.107143$, $\eta_1(\Delta n = -1.0\ \mu M|\eta_e = 1.0, \eta_c \to 1.0) \to 0.75$.

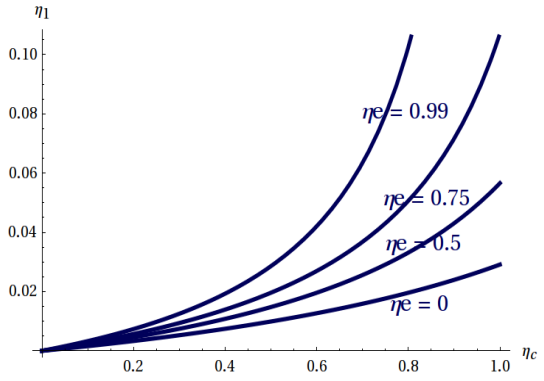

Fig. 3.45: Plot of η_1 as a function of η_c when $s = 1$, $\Delta n = -1.0\ \mu M$, $n_c = 1.0\mu M$, $\nu_e^+ = \nu_c^- = 15\,(\mu M)^{-1}s^{-1}, \nu_1^- = \nu_1^+ = 500\,s^{-1}$, $u_e^+ = 2, u_1^- = 2, u_1^+ = 2, u_c^- = 2$ for five values of η_e, that is: $\eta_e = 0, \eta_e = 0.25, \eta_e = 0.5, \eta_e = 0.75, \eta_e = 1.0$

Using the positive concentration gradient $\Delta n = 10000\ \mu M$,$u_e^+ = 2, u_1^- = 2, u_1^+ = 2, u_c^- = 2$ and the transition rates in Eq. 3.14 into Eq. 3.16, we have plotted the variation of the average occupation number η_1 of the internal potential well V_1 as a function of η_e for five possible values of η_c, that is $\eta_c = 0, \eta_c = 0.25, \eta_c = 0.5, \eta_c = 0.75, \eta_c = 1.0$ on the same graph as shown in Fig. 3.46.

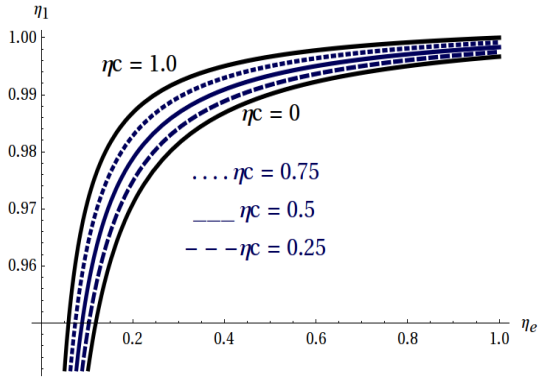

Fig. 3.46: Plot of η_1 as a function of η_e when $s = 1$, $\Delta n = 10000\ \mu M$, $n_c = 1.0\mu M$, $\nu_e^+ = \nu_c^- = 15\,(\mu M)^{-1}s^{-1}, \nu_1^- = \nu_1^+ = 500\,s^{-1}$, $u_e^+ = 2, u_1^- = 2, u_1^+ = 2, u_c^- = 2$ for five values of η_c, that is: $\eta_c = 0, \eta_c = 0.25, \eta_c = 0.5, \eta_c = 0.75, \eta_c = 1.0$

For a given value of $\Delta n = 10000\ \mu M$ and η_c in their respective ranges, the average occupation number η_1 a nano-channel with a single internal potential

well increases as the average value of η_e increases. When $\Delta n = 10000\ \mu M$ the average value of η_1 approach to slightly different minimum values as $\eta_e \rightarrow 0$, that is, $\eta_1(\Delta n = 10000\ \mu M|\eta_e \rightarrow 0, \eta_c = 0) \rightarrow 0$, $\eta_1(\Delta n = 10000\ \mu M|\eta_e \rightarrow 0, \eta_c = 0.25) \rightarrow 0.00426743$, $\eta_1(\Delta n = 10000\ \mu M|\eta_e \rightarrow 0, \eta_c = 0.5) \rightarrow 0.00990099$, $\eta_1(\Delta n = 10000\ \mu M|\eta_e \rightarrow 0, \eta_c = 0.75) \rightarrow 0.0176817$, $\eta_1(\Delta n = 10000\ \mu M|\eta_e \rightarrow 0, \eta_c = 1.0) \rightarrow 0.0291262$ and diverge from each other as η_e increases to intermediate values and finally saturate to the same maximum values of one as $\eta_e \rightarrow 1.0$.

Using zero concentration gradient $\Delta n = 0$, $u_e^+ = 2, u_1^- = 2, u_1^+ = 2, u_c^- = 2$ and the transition rates in Eq. 3.14 into Eq. 3.16, we have plotted the variation of the average occupation number η_1 of the internal potential well V_1 as a function of η_e for five possible values of η_c, that is $\eta_c = 0, \eta_c = 0.25, \eta_c = 0.5, \eta_c = 0.75, \eta_c = 1.0$ on the same graph as shown in Fig. 3.47. When $\Delta n = 0$, the average value of η_1 as a function of η_e obey that $\eta_1(\Delta n = 0|\eta_e, \eta_c = 1.0) > \eta_1(\Delta n = 0|\eta_e, \eta_c = 0.75) > \eta_1(\Delta n = 0|\eta_e, \eta_c = 0.5) > \eta_1(\Delta n = 0|\eta_e, \eta_c = 0.25) > \eta_1(\Delta n = 0|\eta_e, \eta_c = 0)$.

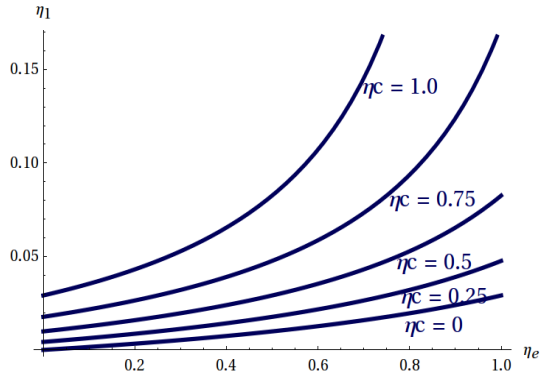

Fig. 3.47: Plot of η_1 as a function of η_e when $s = 1$, $\Delta n = 0$, $n_c = 1.0\mu M$, $\nu_e^+ = \nu_c^- = 15\,(\mu M)^{-1}s^{-1}, \nu_1^- = \nu_1^+ = 500\,s^{-1}$, $u_e^+ = 2, u_1^- = 2, u_1^+ = 2, u_c^- = 2$ for five values of η_c, that is: $\eta_c = 0, \eta_c = 0.25, \eta_c = 0.5, \eta_c = 0.75, \eta_c = 1.0$

The average value of η_1 approach to different minimum values as $\eta_e \rightarrow 0$, that is, $\eta_1(\Delta n = 0|\eta_c = 0, \eta_e \rightarrow 0) \rightarrow 0$, $\eta_1(\Delta n = 0|\eta_c = 0.25, \eta_e \rightarrow 0) \rightarrow 0.00426743$, $\eta_1(\Delta n = 0|\eta_c = 0.5, \eta_e \rightarrow 0) \rightarrow 0.00990099$, $\eta_1(\Delta n = 0|\eta_c = 0.75, \eta_e \rightarrow 0) \rightarrow 0.0176817$, $\eta_1(\Delta n = 0|\eta_c = 1.0, \eta_e \rightarrow 0) \rightarrow 0.0291262$. Moreover, the average value of η_1 approach to different maximum values as $\eta_e \rightarrow 1.0$, that is, $\eta_1(\Delta n = 0|\eta_c = 0, \eta_e \rightarrow 1.0) \rightarrow 0.0291262$, $\eta_1(\Delta n = 0|\eta_c = 0.25, \eta_e \rightarrow 1.0) \rightarrow 0.047619$, $\eta_1(\Delta n =$

$0|\eta_c = 0.5, \eta_e \rightarrow 1.0) \rightarrow 0.0825688$, $\eta_1(\Delta n = 0|\eta_c = 0.75, \eta_e \rightarrow 1.0) \rightarrow 0.173554$, $\eta_1(\Delta n = 0|\eta_c = 1.0, \eta_e \rightarrow 1.0) \rightarrow 1.0$.

Using negative concentration gradient $\Delta n = -1.0\ \mu M$, $u_e^+ = 2, u_1^- = 2, u_1^+ = 2, u_c^- = 2$ and the transition rates in Eq. 3.14 into Eq. 3.16, we have plotted the variation of the average occupation number η_1 of the internal potential well V_1 as a function of η_e for five possible values of η_c, that is $\eta_c = 0, \eta_c = 0.25, \eta_c = 0.5, \eta_c = 0.75, \eta_c = 1.0$ on the same graph as shown in Fig. 3.48. We see that η_1 approach to different minimum values as $\eta_e \rightarrow 0$, that is, $\eta_1(\Delta n = -1.0\mu M|\eta_c = 0, \eta_e \rightarrow 0) \rightarrow 0$, $\eta_1(\Delta n = -1.0\mu M|\eta_c = 0.25, \eta_e \rightarrow 0) \rightarrow 0.00426743$, $\eta_1(\Delta n = -1.0\mu M|\eta_c = 0.5, \eta_e \rightarrow 0) \rightarrow 0.00990099$, $\eta_1(\Delta n = -1.0\mu M|\eta_c = 0.75, \eta_e \rightarrow 0) \rightarrow 0.0176817$, $\eta_1(\Delta n = -1.0\mu M|\eta_c = 1.0, \eta_e \rightarrow 0) \rightarrow 0.0291262$. Moreover, η_1 approach to different maximum values as $\eta_e \rightarrow 1.0$, that is, $\eta_1(\Delta n = -1.0\mu M|\eta_c = 0, \eta_e \rightarrow 1.0) \rightarrow 0$, $\eta_1(\Delta n = -1.0\mu M|\eta_c = 0.25, \eta_e \rightarrow 1.0) \rightarrow 0.00990099$, $\eta_1(\Delta n = -1.0\mu M|\eta_c = 0.5, \eta_e \rightarrow 1.0) \rightarrow 0.0291262$, $\eta_1(\Delta n = -1.0\mu M|\eta_c = 0.75, \eta_e \rightarrow 1.0) \rightarrow 0.0825688$, $\eta_1(\Delta n = -1.0\mu M|\eta_c = 1.0, \eta_e \rightarrow 1.0) \rightarrow 1.0$.

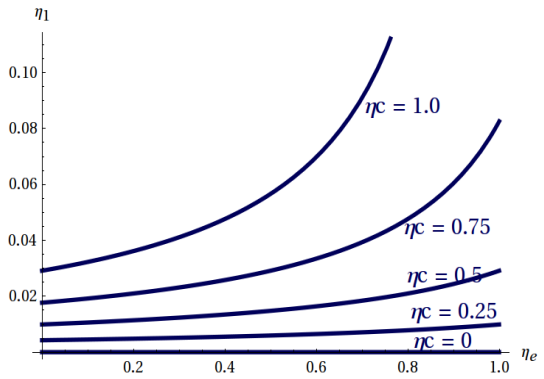

Fig. 3.48: Plot of η_1 as a function of η_e when $s = 1$, $\Delta n = -1.0\ \mu M$, $n_c = 1.0\mu M$, $\nu_e^+ = \nu_c^- = 15\,(\mu M)^{-1}s^{-1}, \nu_1^- = \nu_1^+ = 500\,s^{-1}$, $u_e^+ = 2, u_1^- = 2, u_1^+ = 2, u_c^- = 2$ for five values of η_c, that is $\eta_c = 0, \eta_c = 0.25, \eta_c = 0.5, \eta_c = 0.75, \eta_c = 1.0$

Using $\eta_e = 0$, $u_e^+ = 2, u_1^- = 2, u_1^+ = 2, u_c^- = 2$ and the values of the transition rates specified in Eq. 3.14 into Eq. 3.16, we have plotted the variation of the average occupation number η_1 of a nano-channel with a single internal potential well as a function of η_c for five different values of the concentration gradient Δn in units of μM, that is $\Delta n = -1.0, \Delta n = 0, \Delta n = 35, \Delta n = 100, \Delta n = 500, \Delta n = 1000, \Delta n = 10000$ on the same graph as shown in Fig. 3.49.

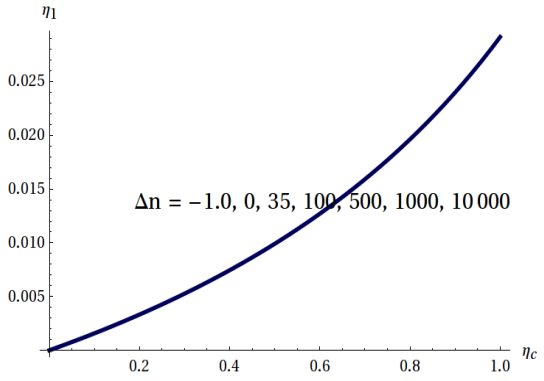

Fig. 3.49: Plot of η_1 as a function of η_c when $s = 1$, $n_c = 1.0\,\mu M$, $\eta_e = 0$, $\nu_e^+ = \nu_c^- = 15\,(\mu M)^{-1}s^{-1}, \nu_1^- = \nu_1^+ = 500\,s^{-1}$, $u_e^+ = 2, u_1^- = 2, u_1^+ = 2, u_c^- = 2$ for the values of Δn in units of μM: $\Delta n = -1.0, \Delta n = 0, \Delta n = 35, \Delta n = 100, \Delta n = 500, \Delta n = 1000, \Delta n = 10000$

Using $\eta_e = 0.5$, $u_e^+ = 2, u_1^- = 2, u_1^+ = 2, u_c^- = 2$ and the values of the transition rates specified in Eq. 3.14 into Eq. 3.16, we have plotted the variation of the average occupation number η_1 of a nano-channel with a single internal potential well as a function of η_c for five different values of the concentration gradient Δn in units of μM, that is $\Delta n = -1.0, \Delta n = 0, \Delta n = 35, \Delta n = 100, \Delta n = 500, \Delta n = 1000, \Delta n = 10000$ on the same graph as shown in Fig. 3.50.

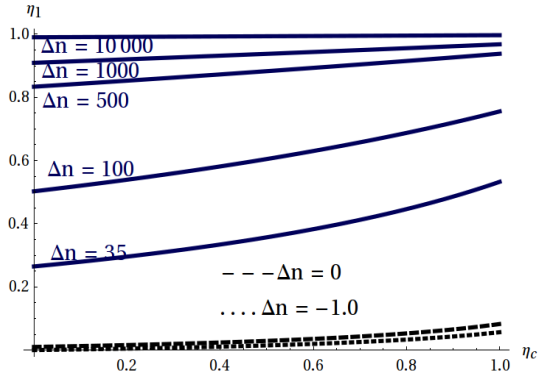

Fig. 3.50: Plot of η_1 as a function of η_c when $s = 1$, $n_c = 1.0\ \mu M$, $\eta_e = 0.5$, $\nu_e^+ = \nu_c^- = 15\,(\mu M)^{-1}s^{-1}, \nu_1^- = \nu_1^+ = 500\,s^{-1}$, $u_e^+ = 2, u_1^- = 2, u_1^+ = 2, u_c^- = 2$ for the values of Δn in units of μM: $\Delta n = -1.0, \Delta n = 0, \Delta n = 35, \Delta n = 100, \Delta n = 500, \Delta n = 1000, \Delta n = 10000$

Using $\eta_e = 1.0$, $u_e^+ = 2, u_1^- = 2, u_1^+ = 2, u_c^- = 2$ and the values of the transition rates specified in Eq. 3.14 into Eq. 3.16, we have plotted the variation of the av-

erage occupation number η_1 of a nano-channel with a single internal potential well as a function of η_c for five different values of the concentration gradient Δn in units of μM, that is $\Delta n = -0.99, \Delta n = 0, \Delta n = 35, \Delta n = 100, \Delta n = 500, \Delta n = 1000, \Delta n = 10000$ on the same graph as shown in Fig. 3.51.

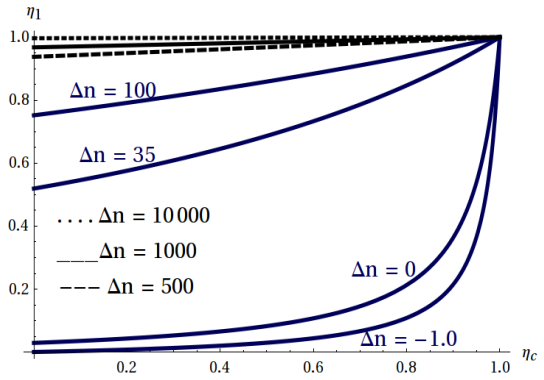

Fig. 3.51: Plot of η_1 as a function of η_c when $s = 1$, $n_c = 1.0\ \mu M$, $\eta_e = 1.0$, $\nu_e^+ = \nu_c^- = 15\,(\mu M)^{-1}s^{-1}, \nu_1^- = \nu_1^+ = 500\,s^{-1}$, $u_e^+ = 2, u_1^- = 2, u_1^+ = 2, u_c^- = 2$ for the values of Δn in units of μM: $\Delta n = -0.99, \Delta n = 0, \Delta n = 35, \Delta n = 100, \Delta n = 500, \Delta n = 1000, \Delta n = 10000$

The average value of η_1 as a function of η_c associated with different values of Δn coincide with each other in the entire range $0 \leq \eta_c \leq 1.0$ when $\eta_e = 0$ and assume the value $\eta_1 = 0.0291262$ when $\eta_c = 1.0$ as one can see in Fig. 3.49. The average value of η_1 associated with different values of Δn separate from each other as η_e increases and finally when $\eta_e = 1.0$, the average value of η_1 associated with different values of Δn approach to different values as $\eta_c \to 0$, that is, $\eta_1(\Delta n = -0.99\ \mu M|\eta_e = 1.0, \eta_c \to 0) \to 0.00029991$, $\eta_1(\Delta n = 0|\eta_e = 1.0, \eta_c \to 0) \to 0.0291262$, $\eta_1(\Delta n = 35\ \mu M|\eta_e = 1.0, \eta_c \to 0) \to 0.519231$, $\eta_1(\Delta n = 100\ \mu M|\eta_e = 1.0, \eta_c \to 0) \to 0.751861$, $\eta_1(\Delta n = 500\ \mu M|\eta_e = 1.0, \eta_c \to 0) \to 0.937617$, $\eta_1(\Delta n = 1000\ \mu M|\eta_e = 1.0, \eta_c \to 0) \to 0.967773$ and $\eta_1(\Delta n = 10000\ \mu M|\eta_e = 1.0, \eta_c \to 0) \to 0.996678$. As η_c increases the values of η_1 associated with the different values of Δn approach to each other and finally all of them converge to the same saturation value of $\eta_1 = 1.0$ when $\eta_c \to 1.0$ as shown in Fig. 3.51.

Using $\eta_c = 0$, $u_e^+ = 2, u_1^- = 2, u_1^+ = 2, u_c^- = 2$ and the values of the transition rates specified in Eq. 3.14 into Eq. 3.16, we have plotted the variation of the average occupation number η_1 of a nano-channel with a single internal potential well as a function of η_e for five different values of the concentration gradient Δn

in units of μM, that is $\Delta n = -0.99, \Delta n = 0, \Delta n = 35, \Delta n = 100, \Delta n = 500, \Delta n = 1000, \Delta n = 10000$ on the same graph as shown in Fig. 3.52.

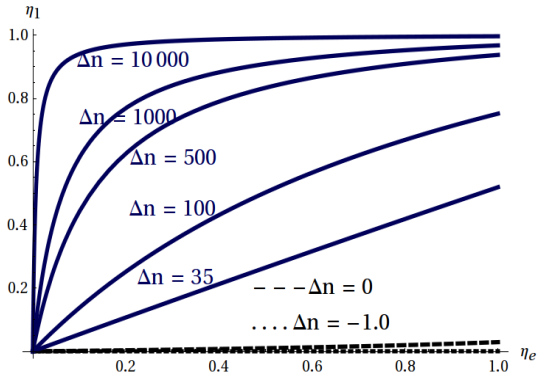

Fig. 3.52: Plot of η_1 as a function of η_e when $s = 1$, $n_c = 1.0\ \mu M$, $\eta_c = 0$, $\nu_e^+ = \nu_c^- = 15\,(\mu M)^{-1}s^{-1}, \nu_1^- = \nu_1^+ = 500\,s^{-1}$, $u_e^+ = 2, u_1^- = 2, u_1^+ = 2, u_c^- = 2$ for the values of Δn in units of μM: $\Delta n = -0.99, \Delta n = 0, \Delta n = 35, \Delta n = 100, \Delta n = 500, \Delta n = 1000, \Delta n = 10000$

Using $\eta_c = 1.0$, $u_e^+ = 2, u_1^- = 2, u_1^+ = 2, u_c^- = 2$ and the values of the transition rates specified in Eq. 3.14 into Eq. 3.16, we have plotted the variation of the average occupation number η_1 of a nano-channel with a single internal potential well as a function of η_e for five different values of the concentration gradient Δn in units of μM, that is $\Delta n = -1.0, \Delta n = 0, \Delta n = 35, \Delta n = 100, \Delta n = 500, \Delta n = 1000, \Delta n = 10000$ on the same graph as shown in Fig. 3.53.

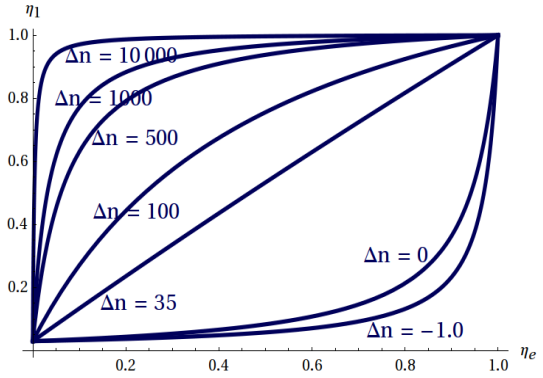

Fig. 3.53: Plot of η_1 as a function of η_e when $s = 1$, $n_c = 1.0\ \mu M$, $\eta_c = 1.0$, $\nu_e^+ = \nu_c^- = 15\,(\mu M)^{-1}s^{-1}, \nu_1^- = \nu_1^+ = 500\,s^{-1}$, $u_e^+ = 2, u_1^- = 2, u_1^+ = 2, u_c^- = 2$ for the values of Δn in units of μM: $\Delta n = -1.0, \Delta n = 0, \Delta n = 35, \Delta n = 100, \Delta n = 500, \Delta n = 1000, \Delta n = 10000$

The average value of η_1 as a function of η_e, $\eta_1(\Delta n = 35\ \mu M|\eta_e, \eta_c)$, increases linearly as η_e increases for each possible value of η_c as one can see from Fig. 3.52 and Fig. 3.53. The average value of η_1 as a function of η_e associated with different values of Δn coincide with each other and assume the value $\eta_1 = 0$ as $\eta_e \rightarrow 0$ and then as η_e increases to intermediate values the deviation between the values of η_1 associated with different values of Δn becomes maximum and then as $\eta_e \rightarrow 1.0$ they converge to each other and assume the same saturation value of $\eta_1 = 1.0$ as one can see in Fig. 3.53. When $\eta_c = 0$, the average value of η_1 associated with different values of Δn approach to different values as $\eta_e \rightarrow 1.0$, that is, $\eta_1(\Delta n = -0.99\ \mu M|\eta_c = 0, \eta_e \rightarrow 1.0) \rightarrow 0.00029991$, $\eta_1(\Delta n = 0|\eta_c = 0, \eta_e \rightarrow 1.0) \rightarrow 0.0291262$, $\eta_1(\Delta n = 35\ \mu M|\eta_c = 0, \eta_e \rightarrow 1.0) \rightarrow 0.519231$, $\eta_1(\Delta n = 100\ \mu M|\eta_c = 0, \eta_e \rightarrow 1.0) \rightarrow 0.751861$, $\eta_1(\Delta n = 500\ \mu M|\eta_c = 0, \eta_e \rightarrow 1.0) \rightarrow 0.937617$, $\eta_1(\Delta n = 1000\ \mu M|\eta_c = 0, \eta_e \rightarrow 1.0) \rightarrow 0.967773$ and $\eta_1(\Delta n = 10000\ \mu M|\eta_c = 0, \eta_e \rightarrow 1.0) \rightarrow 0.996678$.

4

DESCRIPTION OF THE PROPERTIES OF A NANO-CHANNEL WITH TWO INTERNAL POTENTIAL WELLS

4.1 Expressions of the Average Particle Flux and Average Occupation Numbers of the Internal Potential Wells of a Nano-Channel With Two Internal Potential Wells

In this section, we will derive the exact and general expressions of the average particle flux and the average occupation numbers and present a detailed analysis and discussion a nano-channel which has two internal potential wells, denoted by V_1 and V_2, and two external potential wells, denoted by V_e and V_c, as shown in Fig. 4.1, which is a course-grained model of the profile of the potential of mean force along the internal wall of the nano-channel.

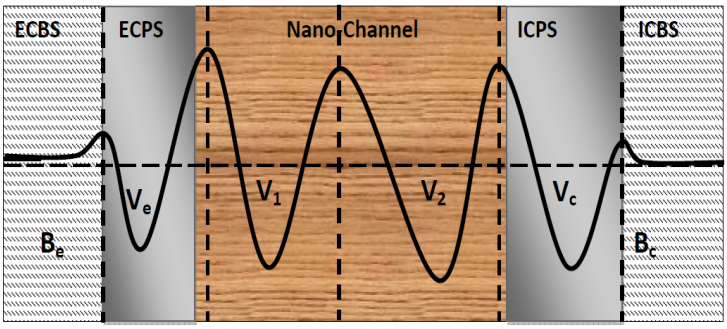

Fig. 4.1: A one dimensional course-grained model of the potential of mean force profile along the internal wall of a nano-channel with two internal potential wells embedded in LBLM

Using the expression of the average particle flux across the potential energy barrier between the potential wells V_e and V_1 given in Eq. (3.2), we have expressed the average occupation number η_1 of the the potential well V_1 as a function of the the average particle flux as shown in Eq. (3.3). That is, from Eq. (3.3), the expressions of η_1 and γ_1 are given by:

$$\begin{aligned} \eta_1 &= \frac{n_e\eta_e k_e^+ - J}{n_e\eta_e k_e^+ + \gamma_e k_1^-} \\ \gamma_1 &= \frac{\gamma_e k_1^- + J}{n_e\eta_e k_e^+ + \gamma_e k_1^-} \end{aligned} \tag{4.1}$$

Moreover, the average particle flux across the potential energy barrier between the potential wells V_1 and V_2 is given by the second expression in Eq. (3.1).

$$J = \eta_1\gamma_2 k_1^+ - \eta_2\gamma_1 k_2^- \tag{4.2}$$

One can now solve Eq. (4.2) so as to get the following expression of η_2 as a function of the average particle flux J.

$$\eta_2 = \frac{\eta_1 k_1^+ - J}{\eta_1 k_1^+ + \gamma_1 k_2^-} \tag{4.3}$$

Upon substituting the two expressions in Eq. (4.1) into Eq. (4.3), we get the following expression for the average occupation number of the potential well V_2 after some rearrangement:

$$\eta_2 = \frac{n_e\eta_e k_e^+ k_1^+ - [n_e\eta_e k_e^+ + \gamma_e k_1^- + k_1^+]J}{n_e\eta_e k_e^+ k_1^+ + \gamma_e k_1^- k_2^- + (k_2^- - k_1^+)J} \tag{4.4}$$

One can also obtain from Eq. (4.4), the following expression of $\gamma_2 = 1 - \eta_2$.

$$\gamma_2 = \frac{\gamma_e k_1^- k_2^- + [n_e \eta_e k_e^+ + \gamma_e k_1^- + k_2^-]J}{n_e \eta_e k_e^+ k_1^+ + \gamma_e k_1^- k_2^- + (k_2^- - k_1^+)J} \tag{4.5}$$

The expressions of the net average particle flux across the potential energy barrier between the potential wells V_2 and V_c is given by the third expression in Eq. (3.1).

$$J = \eta_2 \gamma_c k_2^+ - n_c \eta_c \gamma_2 k_c^- \tag{4.6}$$

Upon substituting the expression in Eq. (4.4) and Eq. (4.5) into Eq. (4.6), we get the expressions of the average particle flux through the nano-channel with two internal potential wells:

$$\begin{aligned} J = & \frac{n_e \eta_e \gamma_c k_e^+ k_1^+ k_2^+ - n_c \eta_c \gamma_e k_1^- k_2^- k_c^-}{n_e \eta_e k_e^+ k_1^+ + \gamma_e k_1^- k_2^- + (k_2^- - k_1^+)J} - \\ & - \left\{ \frac{\gamma_c k_2^+ [n_e \eta_e k_e^+ + \gamma_e k_1^- + k_2^-] + n_c \eta_c k_c^- [n_e \eta_e k_e^+ + \gamma_e k_1^- + k_2^-]}{n_e \eta_e k_e^+ k_1^+ + \gamma_e k_1^- k_2^- + (k_2^- - k_1^+)J} \right\} J \end{aligned} \tag{4.7}$$

One can now rearrange Eq. (4.7) and get a second order linear equation for the average particle flux through a nano-channel with two internal potential wells:

$$\begin{aligned} & (k_2^- - k_1^+)J^2 + \{n_e \eta_e k_e^+ k_1^+ + \gamma_e k_1^- k_2^- + n_e \eta_e \gamma_c k_e^+ k_2^+ + \gamma_e \gamma_c k_1^- k_2^+ + \gamma_c k_2^- k_2^+ + n_e n_c \eta_e \eta_c k_e^+ k_c^- + \\ & + n_c \eta_c \gamma_e k_1^- k_c^- + n_c \eta_c k_2^- k_c^- \} J + n_c \eta_c \gamma_e k_1^- k_2^- k_c^- - n_e \eta_e \gamma_c k_e^+ k_1^+ k_2^+ = 0 \end{aligned} \tag{4.8}$$

Eq. (4.8) can be written in a more simple form:

$$aJ^2 + bJ + c = 0 \tag{4.9}$$

where we have defined the following parameters:

$$\begin{aligned} a &= k_2^- - k_1^+ \\ b &= n_e \eta_e k_e^+ k_1^+ + \gamma_e k_1^- k_2^- + n_e \eta_e \gamma_c k_e^+ k_2^+ + \gamma_e \gamma_c k_1^- k_2^+ + \gamma_c k_2^- k_2^+ + n_e n_c \eta_e \eta_c k_e^+ k_c^- + \\ &\quad + n_c \eta_c \gamma_e k_1^- k_c^- + n_c \eta_c k_2^- k_c^- \\ c &= n_c \eta_c \gamma_e k_1^- k_2^- k_c^- - n_e \eta_e \gamma_c k_e^+ k_1^+ k_2^+ \end{aligned} \tag{4.10}$$

Now Eq. (4.9) is a second order linear equation that has two linearly independent solutions which are given by:

$$\begin{aligned} J_+ &= \frac{-b}{a} + \frac{1}{a}\sqrt{b^2 - 4ac} \\ J_- &= \frac{-b}{a} - \frac{1}{a}\sqrt{b^2 - 4ac} \end{aligned} \tag{4.11}$$

Now since the average particle flux through the nano-channel must be finite and real but can be both positive and negative. For the particle flux to be real, the expression in the square root must be greater than or equal to zero, that is $b^2 - 4ac \geq 0$. For the values of the transition rates specified in Eq. (3.14) and for the concentration gradient $\Delta n = 10000\ \mu M$ and $n_c = 1\ \mu M$, the expression in the square root is positive for both solutions and thus the value of the expression in square root is real. We consider only the first solution, that is J_+, as it is physically acceptable in all aspects. The second solution, that is J_-, diverges to large values which aren't experimentally observable. Moreover, the average values of the occupation numbers of the internal potential wells, given by the expressions in Eq. (4.1) and Eq. (4.4), become greater than one, which violates the constraint imposed on the values of these variables as stated in Eq. (1.20) and as a result we neglect the second solution, that is J_-. Therefore, upon substituting the constants in Eq. (4.10) into the expression of the first solution, $J_+ = J_2$, in Eq. (4.11), we get the expression of the average particle flux through a nano-channel with two internal potential wells:

$$J_2 = -\left[\frac{n_e\eta_e k_e^+\{k_1^+ + \gamma_c k_2^+ + \gamma_e\gamma_c k_1^- k_2^+ + \gamma_c k_2^- k_2^+ + n_c\eta_c k_c^-\} + \gamma_e k_1^- k_2^- + n_c\eta_c k_c^-\{\gamma_e k_1^- + k_2^-\}}{2(k_2^- - k_1^+)}\right]$$
$$\left[1 - \sqrt{1 + \frac{4(k_2^- - k_1^+)(n_e\eta_e\gamma_c k_e^+ k_1^+ k_2^+ - n_c\eta_c\gamma_e k_1^- k_2^- k_c^-)}{(n_e\eta_e k_e^+\{k_1^+ + \gamma_c k_2^+ + \gamma_e\gamma_c k_1^- k_2^+ + \gamma_c k_2^- k_2^+ + n_c\eta_c k_c^-\} + \gamma_e k_1^- k_2^- + n_c\eta_c k_c^-\{\gamma_e k_1^- + k_2^-\})^2}}\right] \tag{4.12}$$

Upon substituting the expression of the concentration gradient in Eq. 3.9 into Eq. 4.12, we get:

$$J_2 = -\left[\frac{(1+\Delta n)\eta_e k_e^+\{k_1^+ + \gamma_c k_2^+ + \gamma_e\gamma_c k_1^- k_2^+ + \gamma_c k_2^- k_2^+ + \eta_c k_c^-\} + \gamma_e k_1^- k_2^- + \eta_c k_c^-\{\gamma_e k_1^- + k_2^-\}}{2(k_2^- - k_1^+)}\right] \times$$
$$\left[1 - \right.$$
$$\left.\sqrt{1 + \frac{4(k_2^- - k_1^+)((1+\Delta n)\eta_e\gamma_c k_e^+ k_1^+ k_2^+ - \eta_c\gamma_e k_1^- k_2^- k_c^-)}{((1+\Delta n)\eta_e k_e^+\{k_1^+ + \gamma_c k_2^+ + \gamma_e\gamma_c k_1^- k_2^+ + \gamma_c k_2^- k_2^+ + \eta_c k_c^-\} + \gamma_e k_1^- k_2^- + \eta_c k_c^-\{\gamma_e k_1^- + k_2^-\})^2}}\right] \tag{4.13}$$

Upon substituting Eq. 1.4 and Eq. 3.12 into Eq. 4.13, after some rearrangement, we get the following general expression of the average particle flux through a nano-channel with two internal potential wells:

$$
\begin{aligned}
J_2 = & \frac{1}{2(\nu_1^+ e^{-u_1^+} - \nu_2^- e^{-u_2^-})} \times \\
& \Bigg\{ \nu_1^- \nu_2^- e^{-(u_1^- + u_2^-)} + \nu_1^- \nu_2^+ e^{-(u_1^- + u_2^+)} + \nu_1^+ \nu_2^+ e^{-(u_1^+ + u_2^+)} + \\
& \left[\nu_1^- \nu_c^- e^{-(u_1^- + u_c^-)} + \nu_2^- \nu_c^- e^{-(u_2^- + u_c^-)} - \nu_1^- \nu_2^+ e^{-(u_1^- + u_2^+)} - \nu_1^+ \nu_2^+ e^{-(u_1^+ + u_2^+)} \right] \eta_c + \\
& \left[\nu_1^- \nu_2^- e^{-(u_1^- + u_2^-)} - \nu_1^- \nu_2^+ e^{-(u_1^- + u_2^+)} + \nu_1^+ \nu_e^+ e^{-(u_1^+ + u_2^+)} + \nu_2^+ \nu_e^+ e^{-(u_2^+ + u_2^+)} \right] \eta_e + \\
& \left[\nu_1^- \nu_2^+ e^{-(u_1^- + u_2^+)} - \nu_1^- \nu_c^- e^{-(u_1^- + u_c^-)} - \nu_2^+ \nu_e^+ e^{-(u_2^+ + u_e^+)} + \nu_c^- \nu_e^+ \eta_c e^{-(u_c^- + u_e^+)} \right] \eta_e \eta_c + \\
& \left[\nu_1^+ \nu_e^+ e^{-(u_1^+ + u_2^+)} + \nu_2^+ \nu_e^+ e^{-(u_2^+ + u_e^+)} + \nu_c^- \nu_e^+ \eta_c e^{-(u_c^- + u_e^+)} - \nu_2^+ \nu_e^+ \eta_c e^{-(u_2^+ + u_e^+)} \right] \eta_e \Delta n - \\
& \Bigg\{ -4 \left[\nu_1^+ e^{-u_1^+} - \nu_2^- e^{-u_2^-} \right] \left[\nu_1^+ \nu_2^+ \nu_e^+ \eta_e (1 - \eta_c) e^{-(u_1^+ + u_2^+ + u_e^+)} - \right. \\
& \left. \nu_1^- \nu_2^- \nu_c^- \eta_c (1 - \eta_e) e^{-(u_1^- + u_2^- + u_c^-)} + \nu_1^+ \nu_2^+ \nu_e^+ \eta_e (1 - \eta_c) e^{-(u_1^+ + u_2^+ + u_e^+)} \Delta n \right] + \\
& \Bigg\{ -\nu_1^- \nu_2^- e^{-(u_1^- + u_2^-)} - \nu_1^- \nu_2^+ e^{-(u_1^- + u_2^+)} - \nu_1^+ \nu_2^+ e^{-(u_1^+ + u_2^+)} + \\
& \left[\nu_1^- \nu_2^+ e^{-(u_1^- + u_2^+)} + \nu_1^+ \nu_2^+ e^{-(u_1^+ + u_2^+)} - \nu_1^- \nu_c^- e^{-(u_1^- + u_c^-)} - \nu_2^- \nu_c^- e^{-(u_2^- + u_c^-)} \right] \eta_c + \\
& \left[\nu_1^- \nu_2^+ e^{-(u_1^- + u_2^+)} + \nu_1^- \nu_2^+ e^{-(u_1^- + u_2^+)} - \nu_1^+ \nu_e^+ e^{-(u_1^+ + u_e^+)} - \nu_2^+ \nu_e^+ e^{-(u_2^+ + u_e^+)} \right] \eta_e + \\
& \left[\nu_1^- \nu_c^- e^{-(u_1^- + u_c^-)} + \nu_2^+ \nu_e^+ e^{-(u_2^+ + u_e^+)} - \nu_1^- \nu_2^+ e^{-(u_1^- + u_2^+)} - \nu_c^- \nu_e^+ e^{-(u_c^- + u_e^+)} \right] \eta_c \eta_e + \\
& \left[-\nu_2^+ \nu_e^+ (1 - \eta_c) e^{-(u_2^+ + u_e^+)} - n u_1^+ \nu_e^+ e^{-(u_1^+ + u_e^+)} - \nu_c^- \nu_e^+ \eta_c e^{-(u_c^- + u_e^+)} \right] \eta_e \Delta n \Bigg\}^2 \Bigg\}^{1/2} \Bigg\}
\end{aligned}
\tag{4.14}
$$

Now upon substituting Eq. 4.14 into Eq. 4.1, we get the expression of the average occupation number of the internal potential well V_1 of a nano-channel with two internal potential wells:

$$\eta_{12} = \frac{1}{2\left[\nu_1^+ e^{-u_1^+} - \nu_2^- e^{-u_1^+}\right]\left[\nu_1^-(1-\eta_e)e^{-u_1^-} + \nu_e^+\eta_e e^{-u_e^+}(1+\Delta n)\right]} \times$$
$$\Bigg\{ \left[2\nu_e^+\eta_e e^{-u_e^+}(1+\Delta n)\right]\left[\nu_1^+ e^{-u_1^+} - \nu_2^- e^{-u_2^-}\right]\left[\nu_1^-(1-\eta_e)e^{-u_1^-} + \nu_e^+\eta_e(1+\Delta n)e^{-u_e^+}\right] -$$
$$\Bigg\{ \nu_1^-\nu_2^- e^{-(u_1^-+u_2^-)} + \nu_1^-\nu_2^+ e^{-(u_1^-+u_2^+)} + \nu_1^+\nu_2^+ e^{-(u_1^+ + u_2^+)} +$$
$$\left[\nu_1^-\nu_c^- e^{-(u_1^-+u_c^-)} + \nu_2^-\nu_c^- e^{-(u_2^-+u_c^-)} - \nu_1^-\nu_2^+ e^{-(u_1^-+u_2^+)} - \nu_1^+\nu_2^+ e^{-(u_1^+ + u_2^+)}\right]\eta_c +$$
$$\left[\nu_1^-\nu_2^- e^{-(u_1^-+u_2^-)} - \nu_1^-\nu_2^+ e^{-(u_1^-+u_2^+)} + \nu_1^+\nu_e^+ e^{-(u_1^+ + u_2^+)} + \nu_2^+\nu_e^+ e^{-(u_2^+ + u_2^+)}\right]\eta_e +$$
$$\left[\nu_1^-\nu_2^+ e^{-(u_1^-+u_2^+)} - \nu_1^-\nu_c^- e^{-(u_1^-+u_c^-)} - \nu_2^+\nu_e^+ e^{-(u_2^+ + u_e^+)} + \nu_c^-\nu_e^+\eta_c e^{-(u_c^- + u_e^+)}\right]\eta_e\eta_c +$$
$$\left[\nu_1^+\nu_e^+ e^{-(u_1^+ + u_2^+)} + \nu_2^+\nu_e^+ e^{-(u_2^+ + u_e^+)} + \nu_c^-\nu_e^+\eta_c e^{-(u_c^- + u_e^+)} - \nu_2^+\nu_e^+\eta_c e^{-(u_2^+ + u_e^+)}\right]\eta_e\Delta n -$$
$$\Bigg\{ -4\left[\nu_1^+ e^{-u_1^+} - \nu_2^- e^{-u_2^-}\right]\Big[\nu_1^+\nu_2^+\nu_e^+\eta_e(1-\eta_c)e^{-(u_1^+ + u_2^+ + u_e^+)} -$$
$$\nu_1^-\nu_2^-\nu_c^-\eta_c(1-\eta_e)e^{-(u_1^-+u_2^-+u_c^-)} + \nu_1^+\nu_2^+\nu_e^+\eta_e(1-\eta_c)e^{-(u_1^+ + u_2^+ + u_e^+)}\Delta n\Big] +$$
$$\Bigg\{ -\nu_1^-\nu_2^- e^{-(u_1^-+u_2^-)} - \nu_1^-\nu_2^+ e^{-(u_1^-+u_2^+)} - \nu_1^+\nu_2^+ e^{-(u_1^+ + u_2^+)} +$$
$$\left[\nu_1^-\nu_2^+ e^{-(u_1^-+u_2^+)} + \nu_1^+\nu_2^+ e^{-(u_1^+ + u_2^+)} - \nu_1^-\nu_c^- e^{-(u_1^-+u_c^-)} - \nu_2^-\nu_c^- e^{-(u_2^-+u_c^-)}\right]\eta_c +$$
$$\left[\nu_1^-\nu_2^+ e^{-(u_1^-+u_2^+)} + \nu_1^-\nu_2^+ e^{-(u_1^-+u_2^+)} - \nu_1^+\nu_e^+ e^{-(u_1^+ + u_e^+)} - \nu_2^+\nu_e^+ e^{-(u_2^+ + u_e^+)}\right]\eta_e +$$
$$\left[\nu_1^-\nu_c^- e^{-(u_1^-+u_c^-)} + \nu_2^+\nu_e^+ e^{-(u_2^+ + u_e^+)} - \nu_1^-\nu_2^+ e^{-(u_1^-+u_2^+)} - \nu_c^-\nu_e^+ e^{-(u_c^- + u_e^+)}\right]\eta_c\eta_e +$$
$$\left[-\nu_2^+\nu_e^+(1-\eta_c)e^{-(u_2^+ + u_e^+)} - nu_1^+\nu_e^+ e^{-(u_1^+ + u_e^+)} - \nu_c^-\nu_e^+\eta_c e^{-(u_c^- + u_e^+)}\right]\eta_e\Delta n\Bigg\}^2\Bigg\}^{1/2}\Bigg\}\Bigg\} \tag{4.15}$$

Similarly, upon substituting Eq. 1.4 and the expression of the average particle flux in Eq. 4.14 into Eq. 4.4, we get the expression of the average occupation number of the internal potential well V_2 of a nano-channel with two internal potential wells:

$$\eta_{22} = \Bigg\{ \nu_e^+ \nu_1^+ \eta_e e^{-(u_e^+ + u_1^+)}(1+\Delta n) - \Big[\nu_e^+ \eta_e e^{-u_e^+}(1+\Delta n) + \nu_1^-(1-\eta_e)e^{-u_1^-} + \nu_1^+ e^{-u_1^+} \Big] \times$$

$$\Bigg\{ \frac{1}{2(\nu_1^+ e^{-u_1^+} - \nu_2^- e^{-u_2^-})} \times$$

$$\Bigg\{ \nu_1^- \nu_2^- e^{-(u_1^- + u_2^-)} + \nu_1^- \nu_2^+ e^{-(u_1^- + u_2^+)} + \nu_1^+ \nu_2^+ e^{-(u_1^+ + u_2^+)} +$$

$$\Big[\nu_1^- \nu_c^- e^{-(u_1^- + u_c^-)} + \nu_2^- \nu_c^- e^{-(u_2^- + u_c^-)} - \nu_1^- \nu_2^+ e^{-(u_1^- + u_2^+)} - \nu_1^+ \nu_2^+ e^{-(u_1^+ + u_2^+)} \Big] \eta_c +$$

$$\Big[\nu_1^- \nu_2^- e^{-(u_1^- + u_2^-)} - \nu_1^- \nu_2^+ e^{-(u_1^- + u_2^+)} + \nu_1^+ \nu_e^+ e^{-(u_1^+ + u_2^+)} + \nu_2^+ \nu_e^+ e^{-(u_2^+ + u_2^+)} \Big] \eta_e +$$

$$\Big[\nu_1^- \nu_2^+ e^{-(u_1^- + u_2^+)} - \nu_1^- \nu_c^- e^{-(u_1^- + u_c^-)} - \nu_2^+ \nu_e^+ e^{-(u_2^+ + u_e^+)} + \nu_c^- \nu_e^+ \eta_c e^{-(u_c^- + u_e^+)} \Big] \eta_e \eta_c +$$

$$\Big[\nu_1^+ \nu_e^+ e^{-(u_1^+ + u_2^+)} + \nu_2^+ \nu_e^+ e^{-(u_2^+ + u_e^+)} + \nu_c^- \nu_e^+ \eta_c e^{-(u_c^- + u_e^+)} - \nu_2^+ \nu_e^+ \eta_c e^{-(u_2^+ + u_e^+)} \Big] \eta_e \Delta n -$$

$$\Bigg\{ -4 \Big[\nu_1^+ e^{-u_1^+} - \nu_2^- e^{-u_2^-} \Big] \Big[\nu_1^+ \nu_2^+ \nu_e^+ \eta_e (1-\eta_c) e^{-(u_1^+ + u_2^+ + u_e^+)} -$$

$$\nu_1^- \nu_2^- \nu_c^- \eta_c (1-\eta_e) e^{-(u_1^- + u_2^- + u_c^-)} + \nu_1^+ \nu_2^+ \nu_e^+ \eta_e (1-\eta_c) e^{-(u_1^+ + u_2^+ + u_e^+)} \Delta n \Big] +$$

$$\Bigg\{ -\nu_1^- \nu_2^- e^{-(u_1^- + u_2^-)} - \nu_1^- \nu_2^+ e^{-(u_1^- + u_2^+)} - \nu_1^+ \nu_2^+ e^{-(u_1^+ + u_2^+)} +$$

$$\Big[\nu_1^- \nu_2^+ e^{-(u_1^- + u_2^+)} + \nu_1^+ \nu_2^+ e^{-(u_1^+ + u_2^+)} - \nu_1^- \nu_c^- e^{-(u_1^- + u_c^-)} - \nu_2^- \nu_c^- e^{-(u_2^- + u_c^-)} \Big] \eta_c +$$

$$\Big[\nu_1^- \nu_2^+ e^{-(u_1^- + u_2^+)} + \nu_1^- \nu_2^+ e^{-(u_1^- + u_2^+)} - \nu_1^+ \nu_e^+ e^{-(u_1^+ + u_e^+)} - \nu_2^+ \nu_e^+ e^{-(u_2^+ + u_e^+)} \Big] \eta_e +$$

$$\Big[\nu_1^- \nu_c^- e^{-(u_1^- + u_c^-)} + \nu_2^+ \nu_e^+ e^{-(u_2^+ + u_e^+)} - \nu_1^- \nu_2^+ e^{-(u_1^- + u_2^+)} - \nu_c^- \nu_e^+ e^{-(u_c^- + u_e^+)} \Big] \eta_c \eta_e +$$

$$\Big[-\nu_2^+ \nu_e^+ (1-\eta_c) e^{-(u_2^+ + u_e^+)} - n u_1^+ \nu_e^+ e^{-(u_1^+ + u_e^+)} - \nu_c^- \nu_e^+ \eta_c e^{-(u_c^- + u_e^+)} \Big] \eta_e \Delta n \Bigg\}^2 \Bigg\}^{1/2} \Bigg\} \Bigg\} \Bigg\} \times$$

$$\times \Bigg\{ \nu_e^+ \nu_1^+ \eta_e e^{-(u_e^+ + u_1^+)}(1+\Delta n) + \nu_1^- \nu_2^- (1-\eta_e) e^{-(u_1^- + u_2^-)} + \left[\nu_2^- e^{-u_2^-} - \nu_1^+ e^{-u_1^+} \right]$$

$$\Bigg\{ \frac{1}{2(\nu_1^+ e^{-u_1^+} - \nu_2^- e^{-u_2^-})} \times \Bigg\{ \nu_1^- \nu_2^- e^{-(u_1^- + u_2^-)} + \nu_1^- \nu_2^+ e^{-(u_1^- + u_2^+)} + \nu_1^+ \nu_2^+ e^{-(u_1^+ + u_2^+)} +$$

$$\left[\nu_1^- \nu_c^- e^{-(u_1^- + u_c^-)} + \nu_2^- \nu_c^- e^{-(u_2^- + u_c^-)} - \nu_1^- \nu_2^+ e^{-(u_1^- + u_2^+)} - \nu_1^+ \nu_2^+ e^{-(u_1^+ + u_2^+)} \right] \eta_c +$$

$$\left[\nu_1^- \nu_2^- e^{-(u_1^- + u_2^-)} - \nu_1^- \nu_2^+ e^{-(u_1^- + u_2^+)} + \nu_1^+ \nu_e^+ e^{-(u_1^+ + u_2^+)} + \nu_2^+ \nu_e^+ e^{-(u_2^+ + u_2^+)} \right] \eta_e +$$

$$\left[\nu_1^- \nu_2^+ e^{-(u_1^- + u_2^+)} - \nu_1^- \nu_c^- e^{-(u_1^- + u_c^-)} - \nu_2^+ \nu_e^+ e^{-(u_2^+ + u_e^+)} + \nu_c^- \nu_e^+ \eta_c e^{-(u_c^- + u_e^+)} \right] \eta_e \eta_c +$$

$$\left[\nu_1^+ \nu_e^+ e^{-(u_1^+ + u_2^+)} + \nu_2^+ \nu_e^+ e^{-(u_2^+ + u_e^+)} + \nu_c^- \nu_e^+ \eta_c e^{-(u_c^- + u_e^+)} - \nu_2^+ \nu_e^+ \eta_c e^{-(u_2^+ + u_e^+)} \right] \eta_e \Delta n -$$

$$\Bigg\{ -4 \left[\nu_1^+ e^{-u_1^+} - \nu_2^- e^{-u_2^-} \right] \left[\nu_1^+ \nu_2^+ \nu_e^+ \eta_e (1-\eta_c) e^{-(u_1^+ + u_2^+ + u_e^+)} - \right.$$

$$\left. \nu_1^- \nu_2^- \nu_c^- \eta_c (1-\eta_e) e^{-(u_1^- + u_2^- + u_c^-)} + \nu_1^+ \nu_2^+ \nu_e^+ \eta_e (1-\eta_c) e^{-(u_1^+ + u_2^+ + u_e^+)} \Delta n \right] +$$

$$\Bigg\{ -\nu_1^- \nu_2^- e^{-(u_1^- + u_2^-)} - \nu_1^- \nu_2^+ e^{-(u_1^- + u_2^+)} - \nu_1^+ \nu_2^+ e^{-(u_1^+ + u_2^+)} +$$

$$\left[\nu_1^- \nu_2^+ e^{-(u_1^- + u_2^+)} + \nu_1^+ \nu_2^+ e^{-(u_1^+ + u_2^+)} - \nu_1^- \nu_c^- e^{-(u_1^- + u_c^-)} - \nu_2^- \nu_c^- e^{-(u_2^- + u_c^-)} \right] \eta_c +$$

$$\left[\nu_1^- \nu_2^+ e^{-(u_1^- + u_2^+)} + \nu_1^- \nu_2^+ e^{-(u_1^- + u_2^+)} - \nu_1^+ \nu_e^+ e^{-(u_1^+ + u_e^+)} - \nu_2^+ \nu_e^+ e^{-(u_2^+ + u_e^+)} \right] \eta_e +$$

$$\left[\nu_1^- \nu_c^- e^{-(u_1^- + u_c^-)} + \nu_2^+ \nu_e^+ e^{-(u_2^+ + u_e^+)} - \nu_1^- \nu_2^+ e^{-(u_1^- + u_2^+)} - \nu_c^- \nu_e^+ e^{-(u_c^- + u_e^+)} \right] \eta_c \eta_e +$$

$$\left[-\nu_2^+ \nu_e^+ (1-\eta_c) e^{-(u_2^+ + u_e^+)} - n u_1^+ \nu_e^+ e^{-(u_1^+ + u_e^+)} - \nu_c^- \nu_e^+ \eta_c e^{-(u_c^- + u_e^+)} \right] \eta_e \Delta n \Bigg\}^2 \Bigg\}^{1/2} \Bigg\} \Bigg\} \Bigg\}^{-1} \tag{4.16}$$

In the following section, we present the plot and discussion of the variation of the average particle flux J and the average occupation numbers η_1 and η_2 as a function of the concentration gradient Δn.

4.2 Discussion of the Average Particle Flux Through a Nano-Channel With Two Internal Potential Wells

4.2.1 The Average Particle Flux Through a Nano-Channel with Two Internal Potential Wells as a Function of the Concentration Gradient when the Potential Barriers are Twice of the Thermal Energy

In this section, we will present a detailed discussion of the average particle flux through a nano-channel with two internal potential wells and two external potential wells as a function of the concentration gradient between the emitter and collector baths when the potential barriers are twice of the thermal energy.

Using $\eta_c = 0$, $u_e^+ = 2, u_1^- = 2, u_1^+ = 2, u_2^- = 2, u_2^+ = 2, u_c^- = 2$ and the values of the transition rates specified in Eq. (3.14) into Eq. (4.14), we have plotted the variation of the average particle flux J through a nano-channel with two internal potential wells as a function of the concentration gradient Δn in units of μM for five different values of η_e, that is $\eta_e = 0, \eta_e = 0.25, \eta_e = 0.5, \eta_e = 0.75, \eta_e = 1.0$ on the same graph as shown in Fig. 4.2.

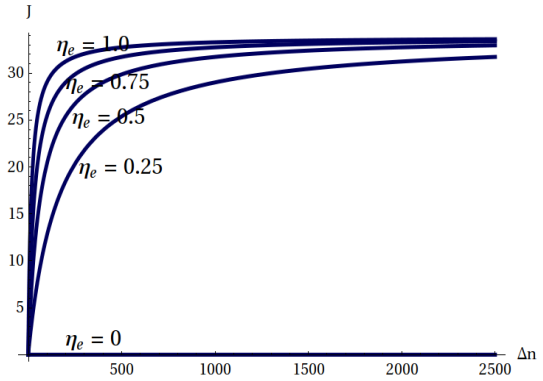

Fig. 4.2: Plot of J as a function of the concentration gradient Δn in units of μM when $s = 2$, $n_c = 1.0\,\mu M$, $\eta_c = 0$, $\nu_e^+ = \nu_c^- = 15\,(\mu M)^{-1}s^{-1}, \nu_1^- = \nu_1^+ = 500\,s^{-1}, \nu_2^- = \nu_2^+ = 500\,s^{-1}$, $u_e^+ = 2, u_1^- = 2, u_1^+ = 2, u_2^- = 2, u_2^+ = 2, u_c^- = 2$ for five different values $\eta_e = 0, \eta_e = 0.25, \eta_e = 0.5, \eta_e = 0.75, \eta_e = 1.0$

Using $\eta_c = 0.5$, $u_e^+ = 2, u_1^- = 2, u_1^+ = 2, u_2^- = 2, u_2^+ = 2, u_c^- = 2$ and the values of the transition rates specified in Eq. (3.14) into Eq. (4.14), we have plotted the variation of the average particle flux J through a nano-channel with two inter-

nal potential wells as a function of concentration gradient Δn in units of μM for five different values of η_e, that is $\eta_e = 0, \eta_e = 0.25, \eta_e = 0.5, \eta_e = 0.75, \eta_e = 1.0$ on the same graph as shown in Fig. 4.3.

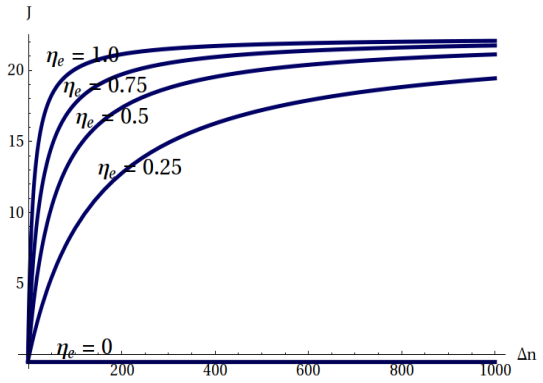

Fig. 4.3: Plot of J as a function of the concentration gradient Δn in units of μM when $s = 2, n_c = 1.0\,\mu M, \eta_c = 0.5, \nu_e^+ = \nu_c^- = 15\,(\mu M)^{-1}s^{-1}, \nu_1^- = \nu_1^+ = 500\,s^{-1}, \nu_2^- = \nu_2^+ = 500\,s^{-1}, u_e^+ = 2, u_1^- = 2, u_1^+ = 2, u_2^- = 2, u_2^+ = 2, u_c^- = 2$ for five different values $\eta_e = 0, \eta_e = 0.25, \eta_e = 0.5, \eta_e = 0.75, \eta_e = 1.0$

Using $\eta_c = 1.0$, $u_e^+ = 2, u_1^- = 2, u_1^+ = 2, u_2^- = 2, u_2^+ = 2, u_c^- = 2$ and the values of the transition rates specified in Eq. (3.14) into Eq. (4.14), we have plotted the variation of the average particle flux J through a nano-channel with two internal potential wells as a function of concentration gradient Δn in units of μM for five different values of η_e, that is $\eta_e = 0, \eta_e = 0.25, \eta_e = 0.5, \eta_e = 0.75, \eta_e = 1.0$ on the same graph as shown in Fig. 4.4.

For the given values of η_e and η_c, the average particle flux J through a nano-channel with two internal potential wells as a function of Δn is again denoted by $J_2(\Delta n|\eta_e, \eta_c)$. Using this notations, one can see from Fig. 4.2 to Fig. 4.4 that: $J_2(\Delta n|\eta_e = 0, \eta_c) < J_2(\Delta n|\eta_e = 0.25, \eta_c) < J_2(\Delta n|\eta_e = 0.5, \eta_c) < J_2(\Delta n|\eta_e = 0.75, \eta_c) < J_2(\Delta n|\eta_e = 1.0, \eta_c)$ for all possible values of Δn and η_c. That is, for the given values of Δn and η_c in their respective ranges, the average particle flux through a nano-channel with two internal potential wells increases as the average value of η_e increases. The average particle flux through a nano-channel is zero even in the presence of a large concentration gradient between the two baths when $\eta_e = \eta_c = 0$ and $\eta_e = \eta_c = 1.0$ as shown in Fig. 4.2 and Fig. 4.4, respectively.

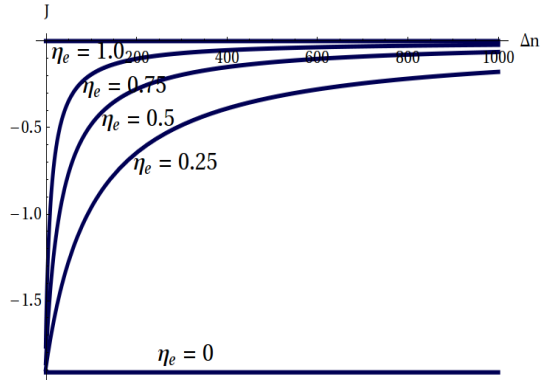

Fig. 4.4: Plot of J as a function of the concentration gradient Δn in units of μM when $s = 2, n_c = 1.0\,\mu M, \eta_c = 1.0, \nu_e^+ = \nu_c^- = 15\,(\mu M)^{-1}s^{-1}, \nu_1^- = \nu_1^+ = 500\,s^{-1}, \nu_2^- = \nu_2^+ = 500\,s^{-1}$, $u_e^+ = 2, u_1^- = 2, u_1^+ = 2, u_2^- = 2, u_2^+ = 2, u_c^- = 2$ for five different values $\eta_e = 0, \eta_e = 0.25, \eta_e = 0.5, \eta_e = 0.75, \eta_e = 1.0$

The flux assumes negative values when $\eta_c = 1.0$ for all possible values of Δn and η_e as shown in Fig. 4.4. When $\Delta n = -1.0\ \mu M$ and $\eta_e = 1.0$, the average particle flux through the nano-channel is zero for all possible values of η_c and for all other values $\eta_e < 1.0$ the flux is negative and its magnitude increases as η_c increases and the flux assumes maximum negative value when $\eta_c = 1.0$ and $\eta_e = 0$. Moreover, $J_2(\Delta n = -1.0\ \mu M|\eta_e, \eta_c = 0) \rightarrow 0$ for all possible values of η_e.

For small values of Δn, the flux increases rapidly as Δn increases and then the flux increases slowly and finally saturates to the same maximum positive value as Δn increases to large positive values. For a given value of η_c, the rate of approach of the flux as a function of Δn to the saturation value is different for different values of η_e. As one can see from the Fig. 4.2 to Fig. 4.4, for a given value of η_c, the value of Δn at which the flux becomes saturated decreases as η_e increases. The flux $J(\Delta n|\eta_e = 1.0, \eta_c)$ saturates more rapidly at small value of Δn and assumes a maximum positive value always for any value of Δn and η_c. For a given value of η_c, the flux associated with different values of η_e converge to each other as $\Delta n \rightarrow -1.0\ \mu M$ and then diverge from each other as Δn increases to intermediate values and finally the flux associated with different values of η_e saturate to the same maximum positive value as Δn increases to large values. These saturation values are: $J_2^{sat}(\Delta n \rightarrow 80\ M|\eta_e > 0, \eta_c = 0) \rightarrow 33.8338\,s^{-1}$, $J_2^{sat}(\Delta n \rightarrow 450\ M|\eta_e > 0, \eta_c = 0.25) \rightarrow 28.8767\,s^{-1}$, $J_2^{sat}(\Delta n \rightarrow 300\ M|\eta_e > 0, \eta_c = 0.5) \rightarrow 22.3326\,s^{-1}$, $J_2^{sat}(\Delta n \rightarrow 25\ M|\eta_e > 0, \eta_c = 0.75) \rightarrow 13.2942\,s^{-1}$

and $J_2^{sat}(\Delta n \rightarrow 20\ M|\eta_e > 0, \eta_c = 1.0) \rightarrow 0$ for all possible values of η_e in the range $0 < \eta_e \leq 1.0$.

Therefore, the average particle flux attains maximum positive value when $\eta_c = 0$ and $\eta_e = 1.0$ for large values of Δn and as a result, the nano-channel behaves as if its gate is closed to conduct particles in the reverse direction. When $\eta_c = 0$, the mean residence time of a particle at the potential well V_c is negligible and thus the occupation probability of V_c is almost zero. Moreover, as η_e increases from zero to one, the mean residence time of a particle in the potential well V_e also increases, which means that the occupation probability of V_e by the particle also increases, and as a result the nano-channel behaves as if its gate is fully closed to conduct particles in the reverse direction. As $\eta_e \rightarrow 1$, the mean residence time of a particle at the potential well V_e is large and as result the occupation probability of this site is almost one. This means that the average particle flux through the nano-channel attains a maximum positive value when V_c is empty, that is $\eta_c = 0$, and when V_e is occupied, that is $\eta_e = 1$.

Using $\eta_e = 0$, $u_e^+ = 2, u_1^- = 2, u_1^+ = 2, u_2^- = 2, u_2^+ = 2, u_c^- = 2$ and the values of the transition rates specified in Eq. (3.14) into Eq. (4.14), we have plotted the variation of the average particle flux J through a nano-channel with two internal potential wells as a function of concentration gradient Δn in units of μM for five different values of η_c, that is $\eta_c = 0, \eta_c = 0.25, \eta_c = 0.5, \eta_c = 0.75, \eta_c = 1.0$ on the same graph as shown in Fig. 4.5.

Using $\eta_e = 0.5$, $u_e^+ = 2, u_1^- = 2, u_1^+ = 2, u_2^- = 2, u_2^+ = 2, u_c^- = 2$ and the values of the transition rates specified in Eq. (3.14) into Eq. (4.14), we have plotted the variation of the average particle flux J through a nano-channel with two internal potential wells as a function of concentration gradient Δn in units of μM for five different values of η_c, that is $\eta_c = 0, \eta_c = 0.25, \eta_c = 0.5, \eta_c = 0.75, \eta_c = 1.0$ on the same graph as shown in Fig. 4.6.

Using $\eta_e = 1.0$, $u_e^+ = 2, u_1^- = 2, u_1^+ = 2, u_2^- = 2, u_2^+ = 2, u_c^- = 2$ and the values of the transition rates specified in Eq. (3.14) into Eq. (4.14), we have plotted the variation of the average particle flux J through a nano-channel with two internal potential wells as a function of concentration gradient Δn in units of μM for five different values of η_c, that is $\eta_c = 0, \eta_c = 0.25, \eta_c = 0.5, \eta_c = 0.75, \eta_c = 1.0$ on the same graph as shown in Fig. 4.7.

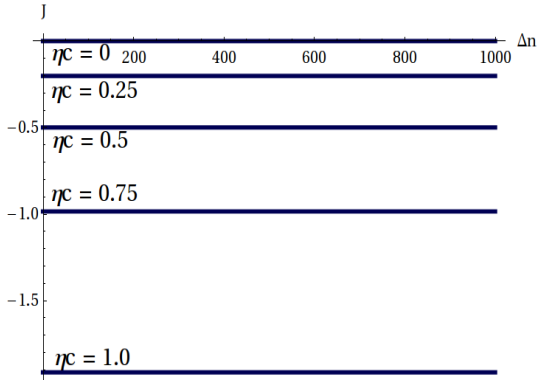

Fig. 4.5: Plot of J as a function of the concentration gradient Δn in units of μM when $s = 2$, $n_c = 1.0\,\mu M$, $\eta_e = 0$, $\nu_e^+ = \nu_c^- = 15\,(\mu M)^{-1}s^{-1}, \nu_1^- = \nu_1^+ = 500\,s^{-1}, \nu_2^- = \nu_2^+ = 500\,s^{-1}$, $u_e^+ = 2, u_1^- = 2, u_1^+ = 2, u_2^- = 2, u_2^+ = 2, u_c^- = 2$ for five different values of η_c, that is, $\eta_c = 0, \eta_c = 0.25, \eta_c = 0.5, \eta_c = 0.75, \eta_c = 1.0$

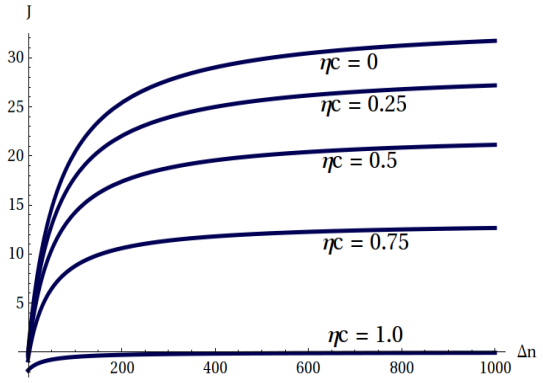

Fig. 4.6: Plot of J as a function of the concentration gradient Δn in units of μM when $s = 2$, $n_c = 1.0\,\mu M$, $\eta_e = 0.5$, $\nu_e^+ = \nu_c^- = 15\,(\mu M)^{-1}s^{-1}, \nu_1^- = \nu_1^+ = 500\,s^{-1}, \nu_2^- = \nu_2^+ = 500\,s^{-1}$, $u_e^+ = 2, u_1^- = 2, u_1^+ = 2, u_2^- = 2, u_2^+ = 2, u_c^- = 2$ for five different values of η_c, that is, $\eta_c = 0, \eta_c = 0.25, \eta_c = 0.5, \eta_c = 0.75, \eta_c = 1.0$

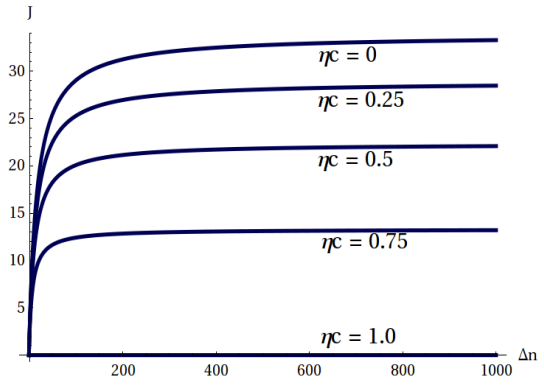

Fig. 4.7: Plot of J as a function of the concentration gradient Δn in units of μM when $s = 2$, $n_c = 1.0\,\mu M$, $\eta_e = 1.0$, $\nu_e^+ = \nu_c^- = 15\,(\mu M)^{-1}s^{-1}, \nu_1^- = \nu_1^+ = 500\,s^{-1}, \nu_2^- = \nu_2^+ = 500\,s^{-1}$, $u_e^+ = 2, u_1^- = 2, u_1^+ = 2, u_2^- = 2, u_2^+ = 2, u_c^- = 2$ for five different values of η_c, that is, $\eta_c = 0, \eta_c = 0.25, \eta_c = 0.5, \eta_c = 0.75, \eta_c = 1.0$

One can see from Fig. 4.5 to Fig. 4.7 that: $J_2(\Delta n|\eta_e, \eta_c = 1.0) < J_2(\Delta n|\eta_e, \eta_c = 0.75) < J_2(\Delta n|\eta_e, \eta_c = 0.5) < J_2(\Delta n|\eta_e, \eta_c = 0.25) < J_2(\Delta n|\eta_e, \eta_c = 0)$ for all possible values of Δn and η_e. That is, for the given values of Δn and η_e in their respective ranges, the average particle flux increases as the average value of η_c increases. As can be seen from Fig. 4.5, when $\eta_e = 0$ the average particle flux through the nano-channel as a function of Δn in the entire range that we have considered in this work has the property that: $J_2(\Delta n|\eta_e = 0, \eta_c = 0) = 0$ and $J_2(\Delta n|\eta_e = 0, \eta_c > 0) < 0$. That is, the average particle flux through the nano-channel associated with each possible value of $\eta_c >$ assumes a constant negative value as Δn increases and as η_c increases from zero to one, the magnitude of the average particle flux increases from zero, which occurs when $J_2(\Delta n|\eta_e = 0, \eta_c = 0) = 0$ to a maximum negative value $J_2(\Delta n|\eta_e = 0, \eta_c = 1.0) = -1.91491\,s^{-1}$, a flux in the negative direction and as a result we conclude that the nano-channel is totally inactivated so as to conduct particles in the positive direction but more activated to conduct particles in the reverse direction.

Fig. 4.7 shows that $J_2(\Delta n|\eta_e = 1.0, \eta_c = 1.0) = 0$ and $J_2(\Delta n|\eta_e = 1.0, \eta_c < 1.0) > 0$ for all possible values of Δn. Moreover, the plots in Fig. 4.5 to Fig. 4.7 shows that $J_2(\Delta n|\eta_e, \eta_c = 1.0) < 0$ for all possible values of Δn and η_e. Therefore, even in the presence of large concentration gradient between the two baths, the average particle flux through the nano-channel is zero when $\eta_e = 0$ and $\eta_c = 0$ and when $\eta_e = 1.0$ and $\eta_c = 1.0$. Moreover, $J_2(\Delta n = -1.0\ \mu M|\eta_e = 1.0, \eta_c) = 0$

for all possible values of η_c.

For small values of Δn, the flux increases rapidly as Δn increases and then the flux increases slowly and finally saturates to the same maximum positive value as Δn increases to large positive values. For a given value of η_e, the rate of approach of the flux as a function of Δn to the saturation value is different for different values of η_c. As one can see from the Fig. 4.5 to Fig. 4.7, for a given value of η_e, the value of Δn at which the flux becomes saturated decreases as η_c increases. The flux $J(\Delta n|\eta_e, \eta_c = 1.0)$ saturates more rapidly at small value of Δn and assumes a minimum positive value and the flux $J(\Delta n|\eta_e, \eta_c = 0)$ saturates more slowly at large value of Δn for any value of Δn and η_e. For a given value of η_e, the flux associated with different values of η_c converge to each other as $\Delta n \rightarrow -1.0\ \mu M$ and then diverge from each other as Δn increases to intermediate values and finally the flux associated with different values of η_c become parallel to each other and saturate to the different maximum positive values as Δn increases to large positive values. The fluxes associated with different values of η_c saturate to the same maximum positive value as η_e increases but the value of Δn at which the saturation occurs decreases as η_e increases. These saturation values are: $J_2^{sat}(\Delta n|\eta_e > 0, \eta_c = 0) \rightarrow 33.8338\, s^{-1}$, $J_2^{sat}(\Delta n\eta_e > 0, \eta_c = 0.25) \rightarrow 28.8767\, s^{-1}$, $J_2^{sat}(\Delta n|\eta_e > 0, \eta_c = 0.5) \rightarrow 22.3326\, s^{-1}$, $J_2^{sat}(\Delta n|\eta_e > 0, \eta_c = 0.75) \rightarrow 13.2942\, s^{-1}$ and $J_2^{sat}(\Delta n|\eta_e > 0, \eta_c = 1.0) \rightarrow 0$ for all possible values of η_e in the range $0 < \eta_e \leq 1.0$. The saturation values of the concentration gradient Δn corresponding to $\eta_e = 0.25$, $\eta_e = 0.5$, $\eta_e = 0.75$ and $\eta_e = 1.0$ are $\Delta n \approx 80\ M$, $\Delta n \approx 35\ M$, $\Delta n \approx 20\ M$, $\Delta n \approx 10\ M$, respectively.

Therefore, when $\eta_c = 1.0$, the average particle flux assumes negative values for all possible values of Δn and η_e and when $\eta_e = 1.0$, the average particle flux assumes positive values for all possible values of Δn and η_c and the nano-channel behaves as if its gate is closed to conduct particles in the reverse direction when $\eta_e = 1.0$ and in the forward direction when $\eta_c = 1.0$. Therefore, as η_e increases from zero to one, the mean residence time of the particle in the potential well V_e also increases, which means that the occupation probability of V_e by a particle increases, and as a result the nano-channel behaves as if its gate is fully closed for reverse flux. In other words, as $\eta_e \rightarrow 1$, the mean residence time of a particle at the external potential well V_e is large and as result the occu-

pation probability of this site is almost one. When $\eta_c = 0$, the mean residence time of a particle at the external potential well V_c is negligible and as a result the occupation probability of this site is almost zero.

Using $\eta_e = 0.1$, $\eta_c = 0.1$, $u_1^- = 2, u_1^+ = 2, u_2^- = 2, u_2^+ = 2, u_c^- = 2$ and the values of the transition rates specified in Eq. 3.14 into Eq. 4.14, we have plotted the variation of the average particle flux J through a nano-channel with two internal potential wells as a function of concentration gradient Δn in units of μM for four different values of u_e^+, that is $u_e^+ \approx 0, u_e^+ = 1.0, u_e^+ = 2.0, u_e^+ = 3.0$ on the same graph as shown in Fig. 4.8.

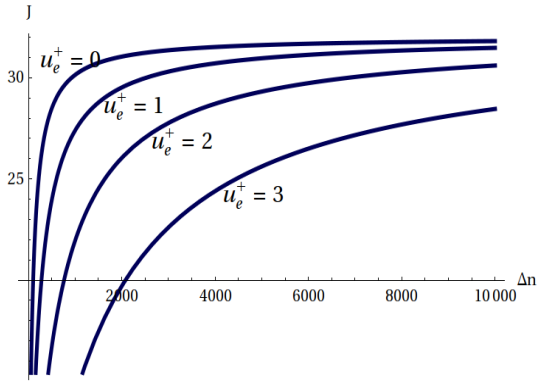

Fig. 4.8: Plot of J as a function of the concentration gradient Δn in units of μM when $s = 2$, $n_c = 1.0\,\mu M$, $\eta_e = 0.1$, $\eta_c = 0.1$, $\nu_e^+ = \nu_c^- = 15\,(\mu M)^{-1}s^{-1}, \nu_1^- = \nu_1^+ = 500\,s^{-1}, \nu_2^- = \nu_2^+ = 500\,s^{-1}$, $u_1^- = 2, u_1^+ = 2, u_2^- = 2, u_2^+ = 2, u_c^- = 2$ for the values $u_e^+ \approx 0, u_e^+ = 1.0, u_e^+ = 2.0, u_e^+ = 3.0$

Using $\eta_e = 0.9$, $\eta_c = 0.9$, $u_1^- = 2, u_1^+ = 2, u_2^- = 2, u_2^+ = 2, u_c^- = 2$ and the values of the transition rates specified in Eq. 3.14 into Eq. 4.14, we have plotted the variation of the average particle flux J through a nano-channel with two internal potential wells as a function of concentration gradient Δn in units of μM for four different values of u_e^+, that is $u_e^+ \approx 0, u_e^+ = 1.0, u_e^+ = 2.0, u_e^+ = 3.0$ on the same graph as shown in Fig. 4.9.

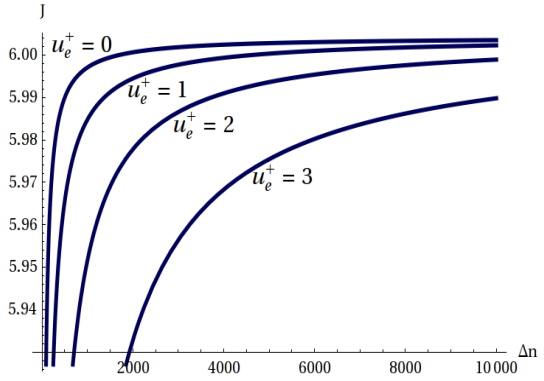

Fig. 4.9: Plot of J as a function of the concentration gradient Δn in units of μM when $s = 2$, $n_c = 1.0\,\mu M$, $\eta_e = 0.9$, $\eta_c = 0.9$, $\nu_e^+ = \nu_c^- = 15\,(\mu M)^{-1}s^{-1}, \nu_1^- = \nu_1^+ = 500\,s^{-1}, \nu_2^- = \nu_2^+ = 500\,s^{-1}$, $u_1^- = 2, u_1^+ = 2, u_2^- = 2, u_2^+ = 2, u_c^- = 2$ for the values $u_e^+ \approx 0, u_e^+ = 1.0, u_e^+ = 2.0, u_e^+ = 3.0$

Using $\eta_e = 1.0$, $\eta_c = 0$, $u_1^- = 2, u_1^+ = 2, u_2^- = 2, u_2^+ = 2, u_c^- = 2$ and the values of the transition rates specified in Eq. 3.14 into Eq. 4.14, we have plotted the variation of the average particle flux J through a nano-channel with two internal potential wells as a function of concentration gradient Δn in units of μM for four different values of u_e^+, that is $u_e^+ \approx 0, u_e^+ = 1.0, u_e^+ = 2.0, u_e^+ = 3.0$ on the same graph as shown in Fig. 4.10.

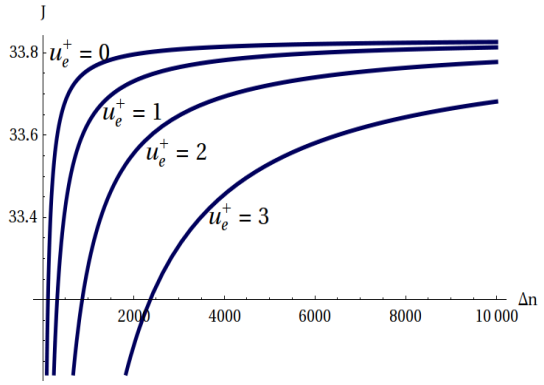

Fig. 4.10: Plot of J as a function of the concentration gradient Δn in units of μM when $s = 2$, $n_c = 1.0\,\mu M$, $\eta_e = 1.0$, $\eta_c = 0$, $\nu_e^+ = \nu_c^- = 15\,(\mu M)^{-1}s^{-1}, \nu_1^- = \nu_1^+ = 500\,s^{-1}, \nu_2^- = \nu_2^+ = 500\,s^{-1}$, $u_1^- = 2, u_1^+ = 2, u_2^- = 2, u_2^+ = 2, u_c^- = 2$ for the values $u_e^+ \approx 0, u_e^+ = 1.0, u_e^+ = 2.0, u_e^+ = 3.0$

Using $\eta_e = 0.1$, $\eta_c = 0.1$, $u_e^+ = 2, u_1^+ = 2, u_2^- = 2, u_2^+ = 2, u_c^- = 2$ and the values of the transition rates specified in Eq. (3.14) into Eq. (4.14), we have plotted the

variation of the average particle flux J through a nano-channel with two internal potential wells as a function of concentration gradient Δn in units of μM for four different values of u_1^-, that is $u_1^- \approx 0, u_1^- = 1.0, u_1^- = 2.0, u_1^- = 3.0$ on the same graph as shown in Fig. 4.11.

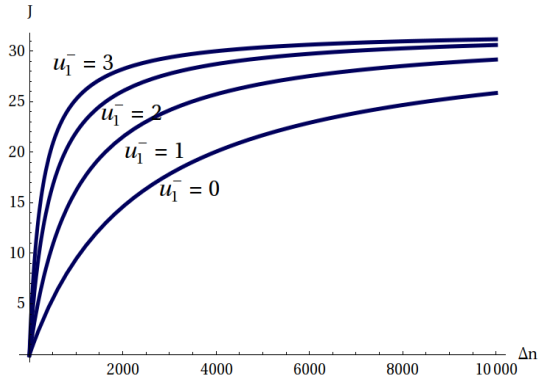

Fig. 4.11: Plot of J as a function of the concentration gradient Δn in units of μM when $s = 2$, $n_c = 1.0\,\mu M$, $\eta_e = 0.1$, $\eta_c = 0.1$, $\nu_e^+ = \nu_c^- = 15\,(\mu M)^{-1}s^{-1}, \nu_1^- = \nu_1^+ = 500\,s^{-1}, \nu_2^- = \nu_2^+ = 500\,s^{-1}$, $u_e^+ = 2, u_1^+ = 2, u_2^- = 2, u_2^+ = 2, u_c^- = 2$ for the values $u_1^- \approx 0, u_1^- = 1.0, u_1^- = 2.0, u_1^- = 3.0$

Using $\eta_e = 0.1$, $\eta_c = 0.1$, $u_e^+ = 2, u_1^- = 2, u_2^- = 2, u_2^+ = 2, u_c^- = 2$ and the values of the transition rates specified in Eq. (3.14) into Eq. (4.14), we have plotted the variation of the average particle flux J through a nano-channel with two internal potential wells as a function of concentration gradient Δn in units of μM for four different values of u_e^+, that is $u_1^+ \approx 0, u_1^+ = 1.0, u_1^+ = 2.0, u_1^+ = 3.0$ on the same graph as shown in Fig. 4.12.

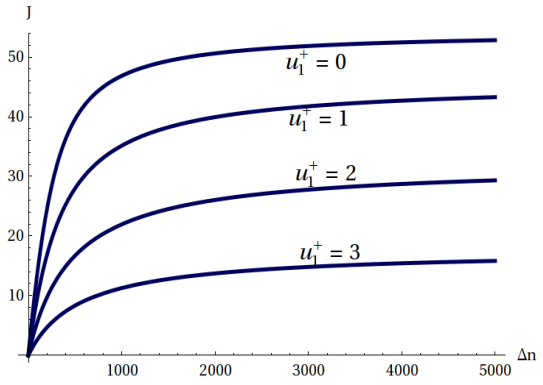

Fig. 4.12: Plot of J as a function of the concentration gradient Δn in units of μM when $s = 2$, $n_c = 1.0\,\mu M$, $\eta_e = 0.1$, $\eta_c = 0.1$, $\nu_e^+ = \nu_c^- = 15\,(\mu M)^{-1}s^{-1}, \nu_1^- = \nu_1^+ = 500\,s^{-1}, \nu_2^- = \nu_2^+ = 500\,s^{-1}$, $u_e^+ = 2, u_1^- = 2, u_2^- = 2, u_2^+ = 2, u_c^- = 2$ for the values $u_1^+ \approx 0, u_1^+ = 1.0, u_1^+ = 2.0, u_1^+ = 3.0$

Using $\eta_e = 0.1$, $\eta_c = 0.1$, $u_e^+ = 2, u_1^- = 2, u_1^+ = 2, u_2^+ = 2, u_c^- = 2$ and the values of the transition rates specified in Eq. 3.14 into Eq. 4.14, we have plotted the variation of the average particle flux J through a nano-channel with two internal potential wells as a function of concentration gradient Δn in units of μM for four different values of u_1^-, that is $u_2^- \approx 0, u_2^- = 1.0, u_2^- = 2.0, u_2^- = 3.0$ on the same graph as shown in Fig. 4.13.

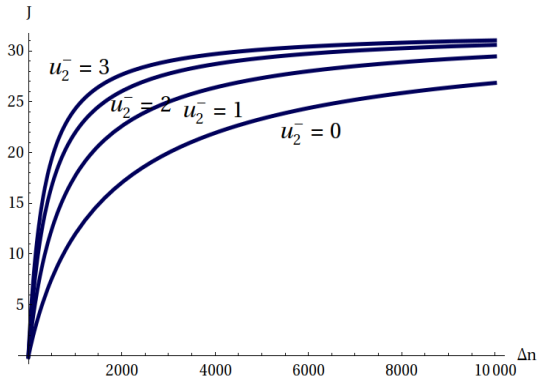

Fig. 4.13: Plot of J as a function of the concentration gradient Δn in units of μM when $s = 2$, $n_c = 1.0\,\mu M$, $\eta_e = 0.1$, $\eta_c = 0.1$, $\nu_e^+ = \nu_c^- = 15\,(\mu M)^{-1}s^{-1}, \nu_1^- = \nu_1^+ = 500\,s^{-1}, \nu_2^- = \nu_2^+ = 500\,s^{-1}$, $u_e^+ = 2, u_1^- = 2, u_1^+ = 2, u_2^+ = 2, u_c^- = 2$ for the values $u_2^- \approx 0, u_2^- = 1.0, u_2^- = 2.0, u_2^- = 3.0$

Using $\eta_e = 0.1$, $\eta_c = 0.1$, $u_e^+ = 2, u_1^- = 2, u_1^+ = 2, u_2^- = 2, u_c^- = 2$ and the values of the transition rates specified in Eq. (3.14) into Eq. (4.14), we have plotted

the variation of the average particle flux J through a nano-channel with two internal potential wells as a function of concentration gradient Δn in units of μM for four different values of u_2^+, that is $u_2^+ \approx 0, u_2^+ = 1.0, u_2^+ = 2.0, u_2^+ = 3.0$ on the same graph as shown in Fig. 4.14.

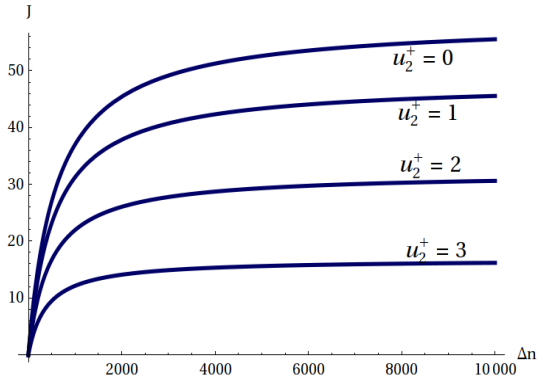

Fig. 4.14: Plot of J as a function of the concentration gradient Δn in units of μM when $s = 2$, $n_c = 1.0\,\mu M$, $\eta_e = 0.1$, $\eta_c = 0.1$, $\nu_e^+ = \nu_c^- = 15\,(\mu M)^{-1}s^{-1}, \nu_1^- = \nu_1^+ = 500\,s^{-1}, \nu_2^- = \nu_2^+ = 500\,s^{-1}$, $u_e^+ = 2, u_1^- = 2, u_1^+ = 2, u_2^- = 2, u_c^- = 2$ for the values $u_2^+ \approx 0, u_2^+ = 1.0, u_2^+ = 2.0, u_2^+ = 3.0$

Using $\eta_e = 0.1$, $\eta_c = 0.1$, $u_e^+ = 2, u_1^- = 2, u_1^+ = 2, u_2^- = 2, u_2^+ = 2$ and the values of the transition rates specified in Eq. (3.14) into Eq. (4.14), we have plotted the variation of the average particle flux J through a nano-channel with two internal potential wells as a function of concentration gradient Δn in units of μM for four different values of u_c^-, that is $u_c^- \approx 0, u_c^- = 1.0, u_c^- = 2.0, u_c^- = 3.0$ on the same graph as shown in Fig. 4.15.

As one can see in Fig. 4.8 to Fig. 4.15, the average particle flux as a function of Δn through a nano-channel with two internal potential wells decreases as the height of the normalized potential barriers u_e^+, u_1^+ and u_2^+ increase from values that are nearly zero to higher values. The average flux approaches the saturation values more quickly when $u_e^+ \approx 0$ than when $u_e^+ = 3$ but the flux approaches the saturation value more quickly when $u_1^+ = 3$ than when $u_1^+ \approx 0$ and when $u_2^+ = 3$ than when $u_2^+ \approx 0$. The average particle flux associated with different values of u_e^+ saturate to the same maximum positive value but that associated with different values of u_1^+ and u_2^+ saturate to different maximum positive values as Δn increases to large positive values.

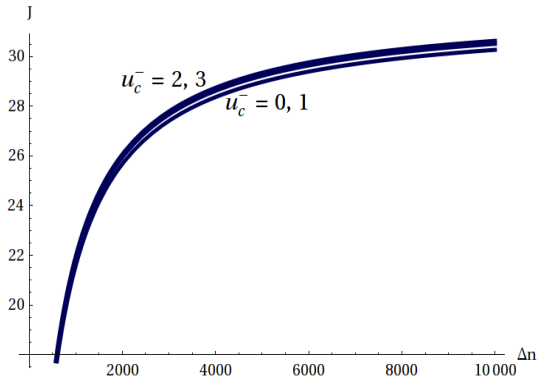

Fig. 4.15: Plot of J as a function of the concentration gradient Δn in units of μM when $s = 2$, $n_c = 1.0\,\mu M$, $\eta_e = 0.1$, $\eta_c = 0.1$, $\nu_e^+ = \nu_c^- = 15\,(\mu M)^{-1}s^{-1}, \nu_1^- = \nu_1^+ = 500\,s^{-1}, \nu_2^- = \nu_2^+ = 500\,s^{-1}$, $u_e^+ = 2, u_1^- = 2, u_1^+ = 2, u_2^- = 2, u_2^+ = 2$ for the values $u_c^- \approx 0, u_c^- = 1.0, u_c^- = 2.0, u_c^- = 3.0$

Therefore, for all possible values of u_e^+, we see that $J_2^{sat}(\Delta n \to 360M|\eta_e = 0.1, \eta_c = 0.1) \to 32.0025\,s^{-1}$. But the fluxes associated with different values of u_1^+ saturate to: $J_2^{sat}(\Delta n \to 10M|\eta_e = 0.1, \eta_c = 0.1, u_1^+ \approx 0) \to 54.2681\,s^{-1}$, $J_2^{sat}(\Delta n \to 10M|\eta_e = 0.1, \eta_c = 0.1, u_1^+ \approx 1.0) \to 45.7134\,s^{-1}$, $J_2^{sat}(\Delta n \to 10M|\eta_e = 0.1, \eta_c = 0.1, u_1^+ \approx 2.0) \to 32.0011\,s^{-1}$, $J_2^{sat}(\Delta n \to 10M|\eta_e = 0.1, \eta_c = 0.1, u_1^+ \approx 3.0) \to 17.6279\,s^{-1}$. Similarly, the fluxes associated with different values of u_2^+ saturate to: $J_2^{sat}(\Delta n \to 30M|\eta_e = 0.1, \eta_c = 0.1, u_2^+ \approx 0) \to 58.7982\,s^{-1}$, $J_2^{sat}(\Delta n \to 30M|\eta_e = 0.1, \eta_c = 0.1, u_2^+ \approx 1.0) \to 47.991\,s^{-1}$, $J_2^{sat}(\Delta n \to 30M|\eta_e = 0.1, \eta_c = 0.1, u_2^+ \approx 2.0) \to 32.0021\,s^{-1}$, $J_2^{sat}(\Delta n \to 10M|\eta_e = 0.1, \eta_c = 0.1, u_2^+ \approx 3.0) \to 16.7934\,s^{-1}$.

However, the average particle flux as a function of Δn through a nano-channel with two internal potential wells increases as the height of the normalized potential barriers u_1^-, u_2^- and u_c^- increase from values that are nearly zero to higher values as shown in Fig. 4.11, Fig. 4.13 and Fig. 4.15. The average particle flux associated with different values of u_1^-, u_2^- and u_c^- saturate to the same maximum positive value as Δn increases to large positive values, that is, $J_2^{sat}(\Delta n \to 300\ M|\eta_e = 0.1, \eta_c = 0.1, u_1^-) = 32.0025 s^{-1}$ for all possible values of u_1^-, $J_1^{sat}(\Delta n \to 300\ M|\eta_e = 0.1, \eta_c = 0.1, u_2^-) \to 32.0025\,s^{-1}$ for all possible values of u_2^- and $J_1^{sat}(\Delta n \to 300\ M|\eta_e = 0.1, \eta_c = 0.1, u_c^-) \to 32.0025\,s^{-1}$ for all possible values of u_c^-.

4.2.2 The Average Particle Flux Through a Nano-Channel With Two Internal Potential Wells as a Function of the Average Occupation Number of the External Potential Wells

Using the positive concentration gradient $\Delta n = 2500\ \mu M$, $u_e^+ = 2, u_1^- = 2, u_1^+ = 2, u_2^- = 2, u_2^+ = 2, u_c^- = 2$ and the values of the transition rates specified in Eq. (3.14) into Eq. (4.14), we have plotted the variation of the average particle flux J through a nano-channel with two internal potential wells as a function of η_c for five different values of η_e, that is $\eta_e = 0, \eta_e = 0.25, \eta_e = 0.5, \eta_e = 0.75, \eta_e = 1.0$ on the same graph as shown in Fig. 4.16.

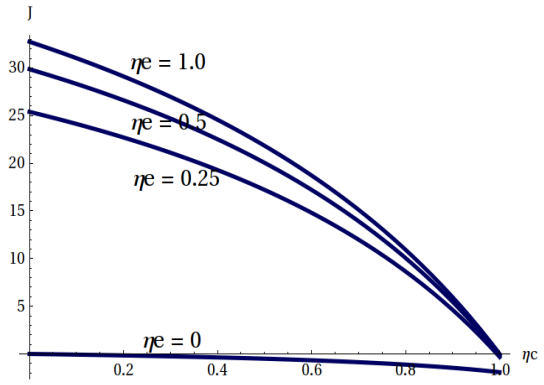

Fig. 4.16: Plot of J as a function of η_c when $s = 2$, $\Delta n = 2500\ \mu M$, $n_c = 1.0 \mu M$, $\nu_e^+ = \nu_c^- = 15\,(\mu M)^{-1} s^{-1}, \nu_1^- = \nu_1^+ = 500\, s^{-1}, \nu_2^- = \nu_2^+ = 500\, s^{-1}$, $u_e^+ = 2, u_1^- = 2, u_1^+ = 2, u_2^- = 2, u_2^+ = 2, u_c^- = 2$ for five different values of η_e, that is: $\eta_e = 0, \eta_e = 0.25, \eta_e = 0.5, \eta_e = 0.75, \eta_e = 1.0$

When there is a positive concentration gradient of $\Delta n = 2500\ \mu M$ the average particle flux as a function of η_c approaches to slightly different maximum positive values as $\eta_c \to 0$ and to slightly different maximum negative values as $\eta_c \to 1.0$. For the given values of Δn and η_e, the average flux decreases as η_c increases from zero to one. The average particle fluxes associated with different values of η_e are far apart from each other as $\eta_c \to 0$ and assume the values $J_2(\Delta n = 2500\ \mu M | \eta_e = 0, \eta_c \to 0) \to 0$, $J_2(\Delta n = 2500\ \mu M | \eta_e = 0.25, \eta_c \to 0) \to 31.7219$, $J_2(\Delta n = 2500\ \mu M | \eta_e = 0.5, \eta_c \to 0) \to 32.9562$, $J_2(\Delta n = 2500\ \mu M | \eta_e = 0.75, \eta_c \to 0) \to 33.3892$ and $J_2(\Delta n = 2500\ \mu M | \eta_e = 1.0, \eta_c \to 0) \to 33.6101$. The Fluxes converge to each other as $\eta_c \to 1.0$ and assume slightly different negative values: $J_2(\Delta n = 2500\ \mu M | \eta_e = 0, \eta_c \to 1.0) \to -1.91491$, $J_2(\Delta n =$

$2500\ \mu M|\eta_e = 0.25, \eta_c \to 1.0) \to -0.0755163$, $J_2(\Delta n = 2500\ \mu M|\eta_e = 0.5, \eta_c \to 1.0) \to -0.0258517$, $J_2(\Delta n = 2500\ \mu M|\eta_e = 0.75, \eta_c \to 1.0) \to -0.0086955$ and $J_2(\Delta n = 2500\ \mu M|\eta_e = 1.0, \eta_c \to 1.0) \to 0$. Moreover, the average fluxes $J_2(\Delta n = 2500\ \mu M|\eta_e = 1.0, \eta_c) > 0$ and $J_2(\Delta n = 2500\ \mu M|\eta_e = 0, \eta_c) < 0$ for all possible values of η_c.

Using zero concentration gradient $\Delta n = 0$, $u_e^+ = 2, u_1^- = 2, u_1^+ = 2, u_2^- = 2, u_2^+ = 2, u_c^- = 2$ and the values of the transition rates specified in Eq. (3.14) into Eq. (4.14), we have plotted the variation of the average particle flux J through a nano-channel with two internal potential wells as a function of η_c for five different values of η_e, that is $\eta_e = 0, \eta_e = 0.25, \eta_e = 0.5, \eta_e = 0.75, \eta_e = 1.0$ on the same graph as shown in Fig. 4.17.

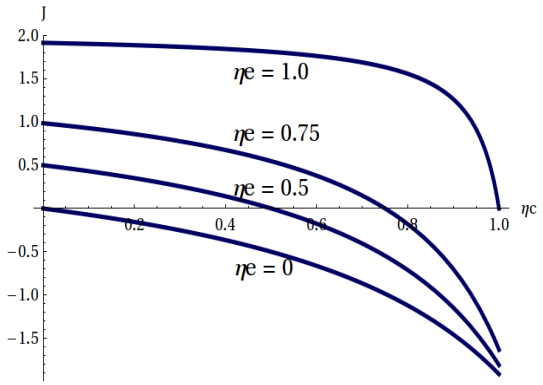

Fig. 4.17: Plot of J as a function of η_c when $s = 2$, $\Delta n = 0$, $n_c = 1.0\mu M$, $\nu_e^+ = \nu_c^- = 15\,(\mu M)^{-1}s^{-1}, \nu_1^- = \nu_1^+ = 500\,s^{-1}, \nu_2^- = \nu_2^+ = 500\,s^{-1}$, $u_e^+ = 2, u_1^- = 2, u_1^+ = 2, u_2^- = 2, u_2^+ = 2, u_c^- = 2$ for five different values of η_e, that is: $\eta_e = 0, \eta_e = 0.25, \eta_e = 0.5, \eta_e = 0.75, \eta_e = 1.0$

When $\Delta n = 0$, the average particle flux as a function of η_c obey that $J_2(\Delta n = 0|\eta_e = 1.0, \eta_c) > J_2(\Delta n = 0|\eta_e = 0.75, \eta_c) > J_2(\Delta n = 0|\eta_e = 0.5, \eta_c) > J_2(\Delta n = 0|\eta_e = 0.25, \eta_c) > J_2(\Delta n = 0|\eta_e = 0, \eta_c)$ and approach to different maximum positive values as $\eta_c \to 0$, that is, $J_2(\Delta n = 0|\eta_e = 0, \eta_c \to 0) \to 0$, $J_2(\Delta n = 0|\eta_e = 0.25, \eta_c \to 0) \to 0.201913s^{-1}$, $J_2(\Delta n = 0|\eta_e = 0.5, \eta_c \to 0) \to 0.500257s^{-1}$, $J_2(\Delta n = 0|\eta_e = 0.75, \eta_c \to 0) \to 0.985789s^{-1}$, $J_2(\Delta n = 0|\eta_e = 1.0, \eta_c \to 0) \to 1.91522s^{-1}$. Moreover, the average particle flux as a function of η_c approach to different maximum negative values as $\eta_c \to 1.0$, that is, $J_2(\Delta n = 0|\eta_e = 0, \eta_c \to 1.0) \to -1.91491s^{-1}$, $J_2(\Delta n = 0|\eta_e = 0.25, \eta_c \to 1.0) \to -1.87887s^{-1}$, $J_2(\Delta n = 0|\eta_e = 0.5, \eta_c \to 1.0) \to -1.8107s^{-1}$, $J_2(\Delta n = 0|\eta_e = 0.75, \eta_c \to 1.0) \to -1.63299s^{-1}$,

$J_2(\Delta n = 0|\eta_e = 1.0, \eta_c \to 1.0) \to 0$. When $\Delta n = 0$, the average particle flux through the nano-channel is positive if $J_2(\Delta n = 0|\eta_e = 0.25, \eta_c < 0.250376) > 0$, $J_2(\Delta n = 0|\eta_e = 0.5, \eta_c < 0.500501) > 0$, $J_2(\Delta n = 0|\eta_e = 0.75, \eta_c < 0.750375) > 0$. Moreover, $J_2(\Delta n = 0|\eta_e = 0, \eta_c) < 0$ and $J_2(\Delta n = 0|\eta_e = 1.0, \eta_c) > 0$ for all possible values of η_c in the range $0 \leq \eta_c \leq 1.0$.

Using the negative concentration gradient $\Delta n = -1.0\ \mu M$, $u_e^+ = 2, u_1^- = 2, u_1^+ = 2, u_2^- = 2, u_2^+ = 2, u_c^- = 2$ and the values of the transition rates specified in Eq. (3.14) into Eq. (4.14), we have plotted the variation of the average particle flux J through a nano-channel with two internal potential wells as a function of η_c for five different values of η_e, that is $\eta_e = 0, \eta_e = 0.25, \eta_e = 0.5, \eta_e = 0.75, \eta_e = 1.0$ on the same graph as shown in Fig. 4.18.

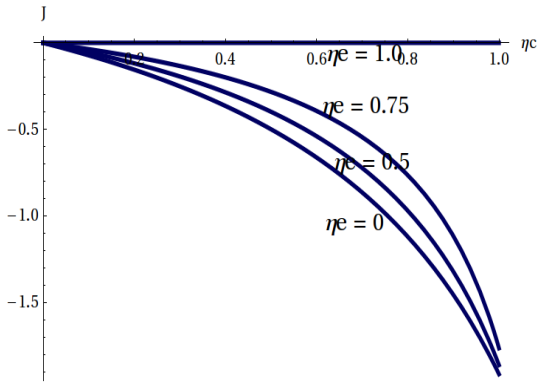

Fig. 4.18: Plot of J as a function of η_c when $s = 2$, $\Delta n = -1.0\ \mu M$, $n_c = 1.0 \mu M$, $\nu_e^+ = \nu_c^- = 15\,(\mu M)^{-1} s^{-1}, \nu_1^- = \nu_1^+ = 500\,s^{-1}, \nu_2^- = \nu_2^+ = 500\,s^{-1}$, $u_e^+ = 2, u_1^- = 2, u_1^+ = 2, u_2^- = 2, u_2^+ = 2, u_c^- = 2$ for five different values of η_e, that is: $\eta_e = 0, \eta_e = 0.25, \eta_e = 0.5, \eta_e = 0.75, \eta_e = 1.0$

When the concentration gradient has the maximum possible negative value, that is, $\Delta n = -1.0\ \mu M$, Fig. 4.18 shows that the average particle flux through the nano-channel as a function of η_c is zero when $\eta_e = 1.0$ for all possible values of η_c in the range $0 \leq \eta_c \leq 1.0$ and is negative for all other possible values of η_e in the range $0 \leq \eta_e < 1.0$ in the entire range $0 \leq \eta_c \leq 1.0$. When $\Delta n = -1.0\ \mu M$, the average particle flux is zero when $\eta_c = 0$ for all possible values of η_e and as $\eta_c \to 1.0$, the average particle flux as a function of η_c approach to different maximum negative values, that is, $J_2(\Delta n = -1.0\ \mu M|\eta_e = 0, \eta_c \to 1.0) \to -1.91491 s^{-1}$, $J_2(\Delta n = -1.0\ \mu M|\eta_e = 0.25, \eta_c \to 1.0) \to -1.89698 s^1$, $J_2(\Delta n = -1.0\ \mu M|\eta_e = 0.5, \eta_c \to 1.0) \to -1.86212 s^{-1}$, $J_2(\Delta n = -1.0\ \mu M|\eta_e = 0.75, \eta_c \to 1.0) \to -1.76483 s^{-1}$,

$J_2(\Delta n = -1.0\ \mu M|\eta_e = 1.0, \eta_c \to 1.0) \to 0$.

Using the positive concentration gradient $\Delta n = 2500\ \mu M$, $u_e^+ = 2, u_1^- = 2, u_1^+ = 2, u_2^- = 2, u_2^+ = 2, u_c^- = 2$ and the values of the transition rates specified in Eq. (3.14) into Eq. (4.14), we have plotted the variation of the average particle flux J through a nano-channel with two internal potential wells as a function of η_e for five different values of η_c, that is, $\eta_c = 0, \eta_c = 0.25, \eta_c = 0.5, \eta_c = 0.75, \eta_c = 1.0$ on the same graph as shown in Fig. 4.19.

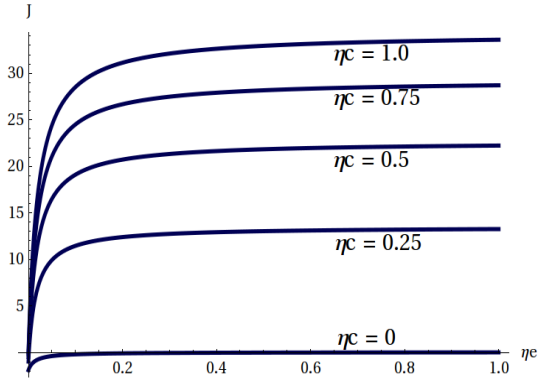

Fig. 4.19: Plot of J as a function of η_e when $s = 2$, $\Delta n = 2500\ \mu M$, $n_c = 1.0\mu M$, $\nu_e^+ = \nu_c^- = 15\,(\mu M)^{-1}s^{-1}, \nu_1^- = \nu_1^+ = 500\,s^{-1}, \nu_2^- = \nu_2^+ = 500\,s^{-1}$, $u_e^+ = 2, u_1^- = 2, u_1^+ = 2, u_2^- = 2, u_2^+ = 2, u_c^- = 2$ for five different values of η_c, that is: $\eta_c = 0, \eta_c = 0.25, \eta_c = 0.5, \eta_c = 0.75, \eta_c = 1.0$

When $\Delta n = 2500\ \mu M$ the average particle flux approach to slightly different negative values as $\eta_e \to 0$ and assume the values: $J_2^{sat}(\Delta n = 2500\ \mu M|\eta_e \to 1.0, \eta_c = 0) \to 0$, $J_2^{sat}(\Delta n = 2500\ \mu M|\eta_e \to 1.0, \eta_c = 0.25) \to -0.20155s^{-1}$, $J_2^{sat}(\Delta n = 2500\ \mu M|\eta_e \to 1.0, \eta_c = 0.5) \to -0.499503s^{-1}$, $J_2^{sat}(\Delta n = 2500\ \mu M|\eta_e \to 1.0, \eta_c = 0.75) \to -0.984765s^{-1}$, $J_2^{sat}(\Delta n = 2500\ \mu M|\eta_e \to 1.0, \eta_c = 1.0) \to -1.91491s^{-1}$. The fluxes diverge from each other and saturate to different maximum positive values as $\eta_e \to 1.0$, that is, $J_2^{sat}(\Delta n = 2500\ \mu M|\eta_e \to 1.0, \eta_c = 0) \to 33.6101s^{-1}$, $J_2^{sat}(\Delta n = 2500\ \mu M|\eta_e \to 1.0, \eta_c = 0.25) \to 28.7119s^{-1}$, $J_2^{sat}(\Delta n = 2500\ \mu M|\eta_e \to 1.0, \eta_c = 0.5) \to 22.232s^{-1}$, $J_2^{sat}(\Delta n = 2500\ \mu M|\eta_e \to 1.0, \eta_c = 0.75) \to 13.2565s^{-1}$, $J_2^{sat}(\Delta n = 2500\ \mu M|\eta_e \to 1.0, \eta_c = 1.0) \to 0$. Moreover, the average particle flux assumes the values when $J_2^{sat}(\Delta n = 2500\ \mu M|\eta_e, \eta_c \to 0) > 0$ and $J_2^{sat}(\Delta n = 2500\ \mu M|\eta_e, \eta_c \to 1.0) < 0$ for all possible values of η_e.

Using zero concentration gradient $\Delta n = 0$, $u_e^+ = 2, u_1^- = 2, u_1^+ = 2, u_2^- =$

$2, u_2^+ = 2, u_c^- = 2$ and the values of the transition rates specified in Eq. (3.14) into Eq. (4.14), we have plotted the variation of the average particle flux J through a nano-channel with two internal potential wells as a function of η_e for five different values of η_c, that is: $\eta_c = 0, \eta_c = 0.25, \eta_c = 0.5, \eta_c = 0.75, \eta_c = 1.0$ on the same graph as shown in Fig. 4.20.

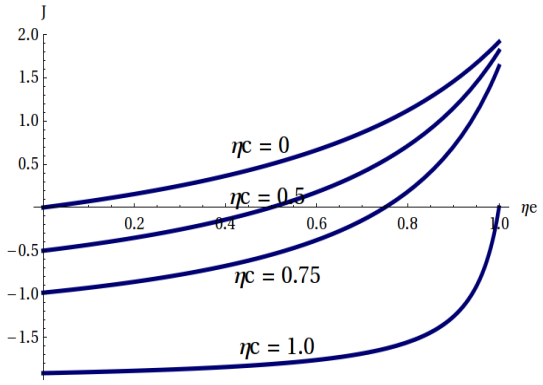

Fig. 4.20: Plot of J as a function of η_e when $s = 2$, $\Delta n = 0$, $n_c = 1.0\ \mu M$, $\nu_e^+ = \nu_c^- = 15\,(\mu M)^{-1}s^{-1}, \nu_1^- = \nu_1^+ = 500\,s^{-1}, \nu_2^- = \nu_2^+ = 500\,s^{-1}$, $u_e^+ = 2, u_1^- = 2, u_1^+ = 2, u_2^- = 2, u_2^+ = 2, u_c^- = 2$ for five different values of η_c, that is: $\eta_c = 0, \eta_c = 0.25, \eta_c = 0.5, \eta_c = 0.75, \eta_c = 1.0$

When $\Delta n = 0$, the average particle flux as a function of η_e obey that $J_2(\Delta n = 0|\eta_e, \eta_c = 0) > J_2(\Delta n = 0|\eta_e, \eta_c = 0.25) > J_2(\Delta n = 0|\eta_e, \eta_c = 0.5) > J_2(\Delta n = 0|\eta_e, \eta_c = 0.75) > J_2(\Delta n = 0|\eta_e, \eta_c = 1.0)$ and approach to different negative values as $\eta_e \to 0$, that is, $J_2(\Delta n = 0|\eta_c = 0, \eta_e \to 0) \to 0$, $J_2(\Delta n = 0|\eta_c = 0.25, \eta_e \to 0) \to -0.20155s^{-1}$, $J_2(\Delta n = 0|\eta_c = 0.5, \eta_e \to 0) \to -0.499503s^{-1}$, $J_2(\Delta n = 0|\eta_c = 0.75, \eta_e \to 0) \to -0.984765s^{-1}$, $J_2(\Delta n = 0|\eta_c = 1.0, \eta_e \to 0) \to -1.91491s^{-1}$. Moreover, the average particle flux as a function of η_e approach to different maximum positive values as $\eta_e \to 1.0$, that is, $J_2(\Delta n = 0|\eta_c = 0, \eta_e \to 1.0) \to 1.91522421s^{-1}$, $J_2(\Delta n = 0|\eta_c = 0.25, \eta_e \to 1.0) \to 1.879298s^{-1}$, $J_2(\Delta n = 0|\eta_c = 0.5, \eta_e \to 1.0) \to 1.81134077s^{-1}$, $J_2(\Delta n = 0|\eta_c = 0.75, \eta_e \to 1.0) \to 1.6340541196s^{-1}$, $J_2(\Delta n = 0|\eta_c = 1.0, \eta_e \to 1.0) \to 0$. When $\Delta n = 0$, the average particle flux through the nano-channel is positive if $J_2(\Delta n = 0|\eta_c = 0.25, \eta_e > 0.25) > 0$, $J_2(\Delta n = 0|\eta_c = 0.5, \eta_e > 0.5) > 0$, $J_2(\Delta n = 0|\eta_c = 0.75, \eta_e > 0.75) > 0$. Moreover, $J_2(\Delta n = 0|\eta_c = 0, \eta_e) > 0$ and $J_2(\Delta n = 0|\eta_c = 1, 0, \eta_e) < 0$ for all possible values of η_e in the range $0 \leq \eta_e \leq 1.0$.

Using the negative concentration gradient $\Delta n = -1.0\ \mu M$, $u_e^+ = 2, u_1^- =$

$2, u_1^+ = 2, u_2^- = 2, u_2^+ = 2, u_c^- = 2$ and the values of the transition rates specified in Eq. (3.14) into Eq. (4.14), we have plotted the variation of the average particle flux J through a nano-channel with two internal potential wells as a function of η_e for five different values of η_c, that is: $\eta_c = 0, \eta_c = 0.25, \eta_c = 0.5, \eta_c = 0.75, \eta_c = 1.0$ on the same graph as shown in Fig. 4.21.

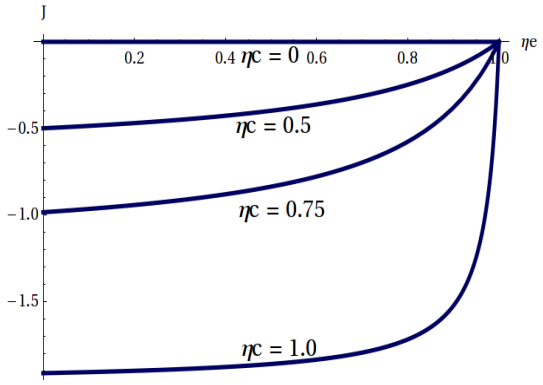

Fig. 4.21: Plot of J as a function of η_e when $s = 2$, $\Delta n = -1.0\ \mu M$, $n_c = 1.0 \mu M$, $\nu_e^+ = \nu_c^- = 15\,(\mu M)^{-1} s^{-1}, \nu_1^- = \nu_1^+ = 500\,s^{-1}, \nu_2^- = \nu_2^+ = 500\,s^{-1}$, $u_e^+ = 2, u_1^- = 2, u_1^+ = 2, u_2^- = 2, u_2^+ = 2, u_c^- = 2$ for the values η_c, that is: $\eta_c = 0, \eta_c = 0.25, \eta_c = 0.5, \eta_c = 0.75, \eta_c = 1.0$

When $\Delta n = -1.0\ \mu M$, Fig. 4.21 shows that the average particle flux through the nano-channel as a function of η_e is zero when $\eta_c = 0$ for all possible values of η_e in the range $0 \leq \eta_e \leq 1.0$ and is negative for all other possible values of η_c in the range $0 < \eta_c \leq 1.0$ in the entire range $0 \leq \eta_e \leq 1.0$. When $\Delta n = -1.0\,\mu M$, the average particle flux is zero when $\eta_e = 1.0$ for all possible values of η_c and as $\eta_e \to 0$, the average particle flux as a function of η_e approach to different maximum negative values, that is, $J_2(\Delta n = -1.0\ \mu M | \eta_c = 0, \eta_e \to 0) \to 0$, $J_2(\Delta n = -1.0\ \mu M | \eta_c = 0.25, \eta_e \to 0) \to -0.20155 s^{-1}$, $J_2(\Delta n = -1.0\ \mu M | \eta_c = 0.5, \eta_e \to 0) \to -0.499503 s^{-1}$, $J_2(\Delta n = -1.0\ \mu M | \eta_c = 0.75, \eta_e \to 0) \to -0.984765 s^{-1}$, $J_2(\Delta n = -1.0\ \mu M | \eta_c = 1.0, \eta_e \to 0) \to -1.91491 s^{-1}$.

Using $\eta_e = 0$, $u_e^+ = 2, u_1^- = 2, u_1^+ = 2, u_2^- = 2, u_2^+ = 2, u_c^- = 2$ and the values of the transition rates specified in Eq. (3.14) into Eq. (4.14), we have plotted the variation of the average particle flux J through a nano-channel with two internal potential wells as a function of η_c for five different values of the concentration gradient Δn in units of μM, that is: $\Delta n = -0.99, \Delta n = 0, \Delta n = 50, \Delta n = 100, \Delta n = 500, \Delta n = 1000$ on the same graph as shown in Fig. 4.22.

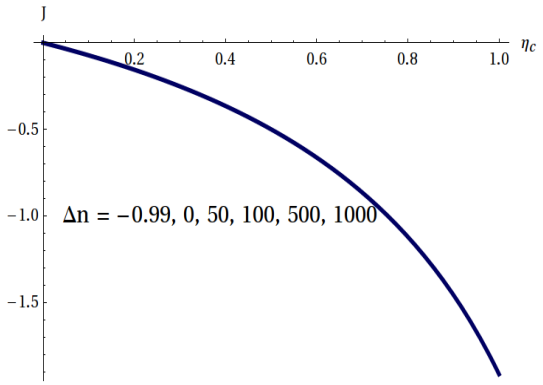

Fig. 4.22: Plot of J as a function of η_c when $s = 2$, $n_c = 1.0\,\mu M$, $\eta_e = 0$, $\nu_e^+ = \nu_c^- = 15\,(\mu M)^{-1}s^{-1}, \nu_1^- = \nu_1^+ = 500\,s^{-1}, \nu_2^- = \nu_2^+ = 500\,s^{-1}$, $u_e^+ = 2, u_1^- = 2, u_1^+ = 2, u_2^- = 2, u_2^+ = 2, u_c^- = 2$ for the values of Δn in units of μM: $\Delta n = -0.99, \Delta n = 0, \Delta n = 35, \Delta n = 100, \Delta n = 500, \Delta n = 1000$

Using $\eta_e = 0.5$, $u_e^+ = 2, u_1^- = 2, u_1^+ = 2, u_2^- = 2, u_2^+ = 2, u_c^- = 2$ and the values of the transition rates specified in Eq. (3.14) into Eq. (4.14), we have plotted the variation of the average particle flux J through a nano-channel with two internal potential wells as a function of η_c for five different values of the concentration gradient Δn in units of μM, that is: $\Delta n = -0.99, \Delta n = 0, \Delta n = 50, \Delta n = 100, \Delta n = 500, \Delta n = 1000$ on the same graph as shown in Fig. 4.23.

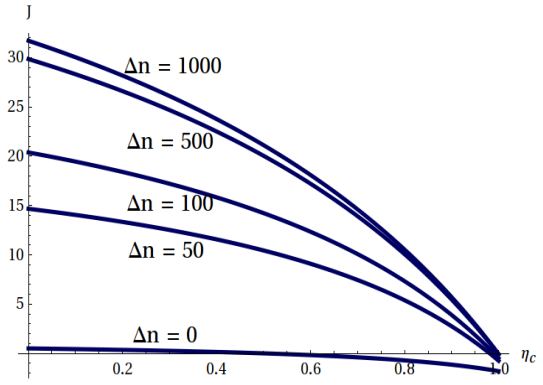

Fig. 4.23: Plot of J as a function of η_c when $s = 2$, $n_c = 1.0\,\mu M$, $\eta_e = 0.5$, $\nu_e^+ = \nu_c^- = 15\,(\mu M)^{-1}s^{-1}, \nu_1^- = \nu_1^+ = 500\,s^{-1}, \nu_2^- = \nu_2^+ = 500\,s^{-1}$, $u_e^+ = 2, u_1^- = 2, u_1^+ = 2, u_2^- = 2, u_2^+ = 2, u_c^- = 2$ for the values of Δn in units of μM: $\Delta n = -0.99, \Delta n = 0, \Delta n = 35, \Delta n = 100, \Delta n = 500, \Delta n = 1000$

Using $\eta_e = 1.0$, $u_e^+ = 2, u_1^- = 2, u_1^+ = 2, u_2^- = 2, u_2^+ = 2, u_c^- = 2$ and the values of the transition rates specified in Eq. (3.14) into Eq. (4.14), we have plotted

the variation of the average particle flux J through a nano-channel with two internal potential wells as a function of η_c for five different values of the concentration gradient Δn in units of μM, that is: $\Delta n = -0.99, \Delta n = 0, \Delta n = 50, \Delta n = 100, \Delta n = 500, \Delta n = 1000$ on the same graph as shown in Fig. 4.24.

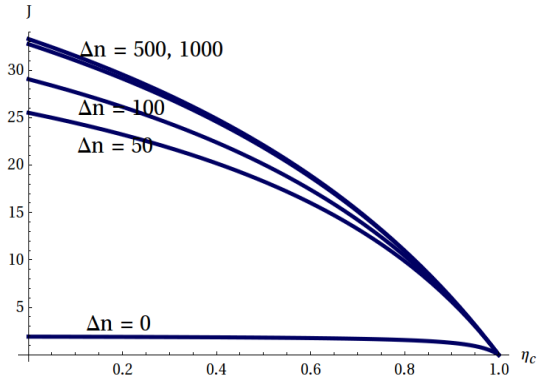

Fig. 4.24: Plot of J as a function of η_c when $s = 2$, $n_c = 1.0\,\mu M$, $\eta_e = 1.0$, $\nu_e^+ = \nu_c^- = 15\,(\mu M)^{-1}s^{-1}, \nu_1^- = \nu_1^+ = 500\,s^{-1}, \nu_2^- = \nu_2^+ = 500\,s^{-1}$, $u_e^+ = 2, u_1^- = 2, u_1^+ = 2, u_2^- = 2, u_2^+ = 2, u_c^- = 2$ for the values of Δn in units of μM: $\Delta n = -0.99, \Delta n = 0, \Delta n = 35, \Delta n = 100, \Delta n = 500, \Delta n = 1000$

When $\eta_e = 0$, as shown in Fig. 4.22 the average particle flux is negative in the entire range $0 \leq \eta_c \leq 1$ and has the same value for all possible values of Δn. The figures Fig. 4.23 and Fig. 4.24 show that as η_e increases the flux associated with different values of Δn become separated from each other, that is, the distance between them increases and the flux increases in the positive direction and finally the flux associated with all the possible values of Δn becomes totally positive as $\eta_e \to 1.0$. Moreover, $J_2(\Delta n = -0.99\ \mu M|\eta_e, \eta_c) < J_2(\Delta n = 0|\eta_e, \eta_c) < J_2(\Delta n = 35\ \mu M|\eta_e, \eta_c) < J_2(\Delta n = 100\ \mu M|\eta_e, \eta_c) < J_2(\Delta n = 500\ \mu M|\eta_e, \eta_c) < J_2(\Delta n = 1000\ \mu M|\eta_e, \eta_c)$ for all possible values of η_e and η_c. The average particle flux assumes a maximum positive value when $\eta_c \to 0$ for all possible values of η_e and Δn and then decreases as η_c increases and finally become minimum when $\eta_c = 1.0$.

Using $\eta_c = 0$, $u_e^+ = 2, u_1^- = 2, u_1^+ = 2, u_2^- = 2, u_2^+ = 2, u_c^- = 2$ and the values of the transition rates specified in Eq. (3.14) into Eq. (4.14), we have plotted the variation of the average particle flux J through a nano-channel with two internal potential wells as a function of η_e for five different values of the concentration gradient Δn in units of μM, that is: $\Delta n = -0.99, \Delta n = 0, \Delta n = 35, \Delta n =$

$100, \Delta n = 500, \Delta n = 1000$ on the same graph as shown in Fig. 4.25.

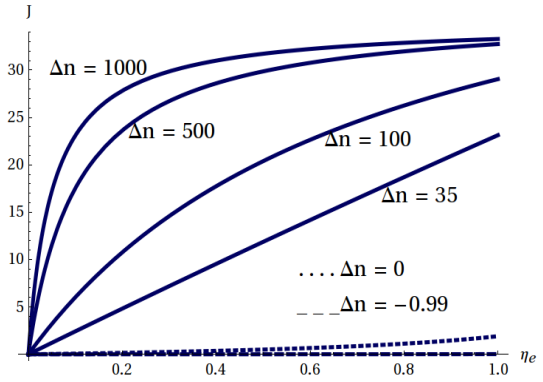

Fig. 4.25: Plot of J as a function of η_e when $s = 2$, $n_c = 1.0\ \mu M$, $\eta_c = 0$, $\nu_e^+ = \nu_c^- = 15\,(\mu M)^{-1}s^{-1}, \nu_1^- = \nu_1^+ = 500\,s^{-1}, \nu_2^- = \nu_2^+ = 500\,s^{-1}$, $u_e^+ = 2, u_1^- = 2, u_1^+ = 2, u_2^- = 2, u_2^+ = 2, u_c^- = 2$ for the values of Δn in units of μM: $\Delta n = -0.99, \Delta n = 0, \Delta n = 35, \Delta n = 100, \Delta n = 500, \Delta n = 1000$

Using $\eta_c = 0.5$,$u_e^+ = 2, u_1^- = 2, u_1^+ = 2, u_2^- = 2, u_2^+ = 2, u_c^- = 2$ and the values of the transition rates specified in Eq. (3.14) into Eq. (4.14), we have plotted the variation of the average particle flux J through a nano-channel with two internal potential wells as a function of η_e for five different values of the concentration gradient Δn in units of μM, that is $\Delta n = -0.99\ \mu M, \Delta n = 0, \Delta n = 35\ \mu M, \Delta n = 100\ \mu M, \Delta n = 500\ \mu M, \Delta n = 1000\ \mu M$ on the same graph as shown in Fig. 4.26.

When $\eta_c = 0$, as shown in Fig. 4.25 the average particle flux is positive in the entire range $0 \leq \eta_e \leq 1$ and when $\eta_c = 1.0$, as shown in Fig. 4.27 the average particle flux is negative in the entire range $0 \leq \eta_e \leq 1$. The average flux increases almost linearly when $\Delta n = 35\ \mu M$ for all possible values of η_e and η_c. The fluxes associated with the different possible values of Δn converge to each other as $\eta_e \to 0$ and as η_e increases to intermediate values the flux associated with different values of Δn diverge from each other to the maximum extent, that is, the distance between them increases and as $\eta_e \to 1.0$ the fluxes associated with different values of Δn converge to each other. Moreover, the magnitudes of the fluxes associated with different values of Δn obey that: $|J_2(\Delta n = -1.0\ \mu M|\eta_c, \eta_e)| < |J_2(\Delta n = 0|\eta_c, \eta_e)| < |J_2(\Delta n = 35\ \mu M|\eta_c, \eta_e)| < |J_2(\Delta n = 100\ \mu M|\eta_c, \eta_e)| < |J_2(\Delta n = 500\ \mu M|\eta_c, \eta_e)| < |J_2(\Delta n = 1000\ \mu M|\eta_c, \eta_e)|$ for all possible values of η_e and η_c.

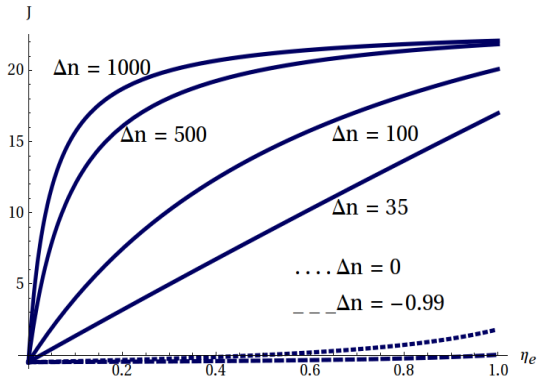

Fig. 4.26: Plot of J as a function of η_e when $s = 2$, $n_c = 1.0\,\mu M$, $\eta_c = 0.5$, $\nu_e^+ = \nu_c^- = 15\,(\mu M)^{-1}s^{-1}, \nu_1^- = \nu_1^+ = 500\,s^{-1}, \nu_2^- = \nu_2^+ = 500\,s^{-1}$, $u_e^+ = 2, u_1^- = 2, u_1^+ = 2, u_2^- = 2, u_2^+ = 2, u_c^- = 2$ for the values of Δn in units of μM: $\Delta n = -0.99, \Delta n = 0, \Delta n = 35, \Delta n = 100, \Delta n = 500, \Delta n = 1000$

Using $\eta_c = 1.0$, $u_e^+ = 2, u_1^- = 2, u_1^+ = 2, u_2^- = 2, u_2^+ = 2, u_c^- = 2$ and the values of the transition rates specified in Eq. (3.14) into Eq. (4.14), we have plotted the variation of the average particle flux J through a nano-channel with two internal potential wells as a function of η_e for five different values of the concentration gradient Δn in units of μM, that is: $\Delta n = -0.99, \Delta n = 0, \Delta n = 35, \Delta n = 100, \Delta n = 500, \Delta n = 1000$ on the same graph as shown in Fig. 4.27.

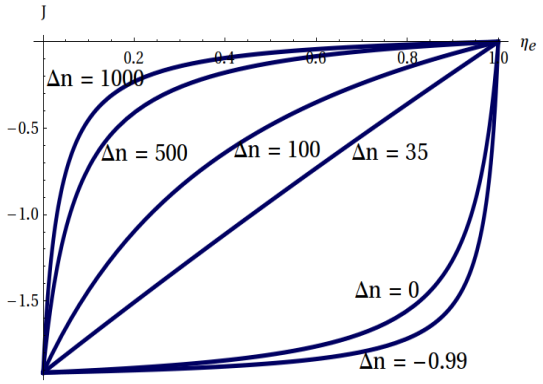

Fig. 4.27: Plot of J as a function of η_e when $s = 2$, $n_c = 1.0\,\mu M$, $\eta_c = 1.0$, $\nu_e^+ = \nu_c^- = 15\,(\mu M)^{-1}s^{-1}, \nu_1^- = \nu_1^+ = 500\,s^{-1}, \nu_2^- = \nu_2^+ = 500\,s^{-1}$, $u_e^+ = 2, u_1^- = 2, u_1^+ = 2, u_2^- = 2, u_2^+ = 2, u_c^- = 2$ for the values of Δn in units of μM: $\Delta n = -0.99, \Delta n = 0, \Delta n = 35, \Delta n = 100, \Delta n = 500, \Delta n = 1000$

4.3 Conclusion of the Average Particle Flux Through a Nano-Channel with Two Internal Potential Wells

1. For one particular given value of η_c, the average particle flux $J_2(\Delta n|\eta_e,\eta_c)$ as a function of Δn associated with the different values of η_e saturate to the same maximum positive value as Δn increases to large positive values.

2. For given values of η_e, the fluxes obey that: $J_2(\Delta n|\eta_e=0,\eta_c) < J_2(\Delta n|\eta_e=0.25,\eta_c) < J_2(\Delta n|\eta_e=0.5,\eta_c) < J_2(\Delta n|\eta_e=0.75,\eta_c) < J_2(\Delta n|\eta_e=1.0,\eta_c)$ for all possible values of $\Delta n > 0$ and η_c.

3. For given values of η_c, the fluxes obey that: $J_2(\Delta n|\eta_e,\eta_c=0) > J_2(\Delta n|\eta_e,\eta_c=0.25) > J_2(\Delta n|\eta_e,\eta_c=0.5) > J_2(\Delta n|\eta_e,\eta_c=0.75) < J_2(\Delta n|\eta_e,\eta_c=1.0)$ for all possible values of $\Delta n > 0$ and η_e.

4. For one particular given value of η_e, the average particle flux $J_2(\Delta n|\eta_e,\eta_c)$ as a function of Δn associated with the different values of η_c saturate to different maximum positive value as Δn increases to large positive values.

5. The average particle flux through a nano-channel is zero even in the presence of a large concentration gradient between the two baths when $\eta_e = \eta_c = 0$ and $\eta_e = \eta_c = 1.0$ as shown in Fig. 4.2 and Fig. 4.4, respectively.

6. The flux assumes negative values when $\eta_c = 1.0$ for all possible values of Δn and η_e as shown in Fig. 4.4.

7. When $\Delta n = -1.0\ \mu M$ and $\eta_e = 1.0$, the average particle flux through the nano-channel is zero for all possible values of η_c and for all values $\eta_e < 1.0$ the flux is negative and its magnitude increases as η_c increases and assumes maximum negative value when $\eta_c = 1.0$ and $\eta_e = 0$.

8. Moreover, $J_2(\Delta n = -1.0\ \mu M|\eta_e,\eta_c=0) \to 0$ for all possible values of η_e.

9. For a given particular value of η_c, the flux $J_2(\Delta n|\eta_e=1.0,\eta_c)$ as a function of Δn approaches its saturation value more rapidly when η_e assumes higher value and more slowly when η_e assumes smaller values.

10. The average particle flux through a nano-channel attains maximum positive value when V_c is empty, that is $\eta_c = 0$, and when V_e is occupied, that is $\eta_e = 1$.

11. For the given values of Δn, η_e and η_c, the average particle flux $J_2(\Delta n|\eta_e, \eta_c)$ is a monotonically decreasing function of the height of the forward potential barriers u_e^+, u_1^+ and u_2^+. That is, $J_2(\Delta n|\eta_e, \eta_c)$ assumes large values when these potentia barriers are small as compared to thermal energy, that is, $u_e^+ < 1$, $u_1^+ < 1.0$ and $u_2^+ < 1.0$.

12. For the given values of Δn, η_e and η_c, the average particle flux $J_2(\Delta n|\eta_e, \eta_c)$ is a monotonically increasing function of the height of the backward potential barriers u_1^-, u_2^- and u_c^-. That is, $J_2(\Delta n|\eta_e, \eta_c)$ assumes large values when these potentia barriers are large as compared to thermal energy, that is, $u_1^- \gg 1.0$, $u_2^- \gg 1.0$ and $u_c^- \gg 1.0$.

13. For the given values of Δn, η_e and η_c, the average particle fluxes associated with the different values of u_e^+ saturate to the same value as Δn increases to large positive values. The average particle fluxes associated with the different values of u_1^-, u_2^- and u_c^- also have similar saturation property.

14. For the given values of Δn, η_e and η_c, the average particle fluxes associated with the different values of u_1^+ saturate to different saturation values as Δn increases to large positive values and those associated with different values of u_2^+ also saturate to different values.

4.4 Discussion of the Average Occupation Numbers of the Internal Potential Wells of a Nano-Channel With Two Internal Potential Wells

In this section, we will present a detailed description of the dependence of the average occupation numbers of the internal potential wells of the nano-channel on the concentration gradient and the Average occupation numbers of the external potential wells. The nano-channel has two internal potential wells and two external potential wells and the heights of the potential barriers are twice of the thermal energy. The expression of the average occupation numbers of the internal potential wells V_1 and V_2 as a function of the concentration gradient Δn are given in Eq. 4.15 and Eq. 4.16, respectively.

4.4.1 Discussion of the Average Occupation Number of the Internal Potential Well V_1 of a Nano-Channel

4.4.1.1 The Average Occupation Number of the Internal Potential Well V_1 of a Nano-Channel as a Function of the concentration gradient

Using $\eta_c = 0$, $u_e^+ = 2, u_1^- = 2, u_1^+ = 2, u_2^- = 2, u_2^+ = 2, u_c^- = 2$ and the values of the transition rates specified in Eq. (3.14) into Eq. (4.15), we have plotted the variation of the average occupation number η_1 of the internal potential well V_1 of a nano-channel with two internal potential wells as a function of the concentration gradient Δn in units of μM for five different values of η_e, that is, $\eta_e = 0, \eta_e = 0.25, \eta_e = 0.5, \eta_e = 0.75, \eta_e = 1.0$ on the same graph as shown in Fig. 4.28.

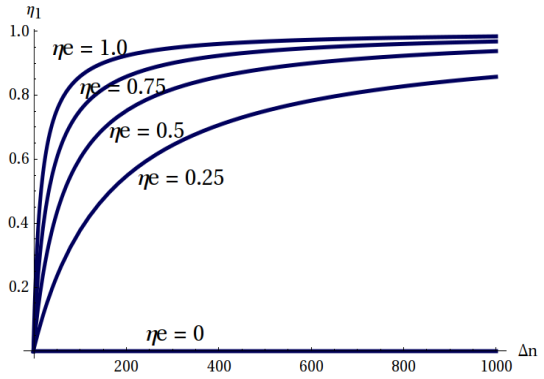

Fig. 4.28: Plot of η_1 as a function of the concentration gradient Δn in units of μM when $s = 2, n_c = 1.0\mu M, \eta_c = 0, \nu_e^+ = \nu_c^- = 15\,(\mu M)^{-1}s^{-1}, \nu_1^- = \nu_1^+ = 500\,s^{-1}, \nu_2^- = \nu_2^+ = 500\,s^{-1}, u_e^+ = 2, u_1^- = 2, u_1^+ = 2, u_2^- = 2, u_2^+ = 2, u_c^- = 2$ for the values $\eta_e = 0, \eta_e = 0.25, \eta_e = 0.5, \eta_e = 0.75, \eta_e = 1.0$

Using $\eta_c = 0.5, u_e^+ = 2, u_1^- = 2, u_1^+ = 2, u_2^- = 2, u_2^+ = 2, u_c^- = 2$ and the values of the transition rates specified in Eq. (3.14) into Eq. (4.15), we have plotted the variation of the average occupation number η_1 of the internal potential well V_1 of a nano-channel with two internal potential wells as a function of the concentration gradient Δn in units of μM for five different values of η_e, that is $\eta_e = 0, \eta_e = 0.25, \eta_e = 0.5, \eta_e = 0.75, \eta_e = 1.0$ on the same graph as shown in Fig. 4.29.

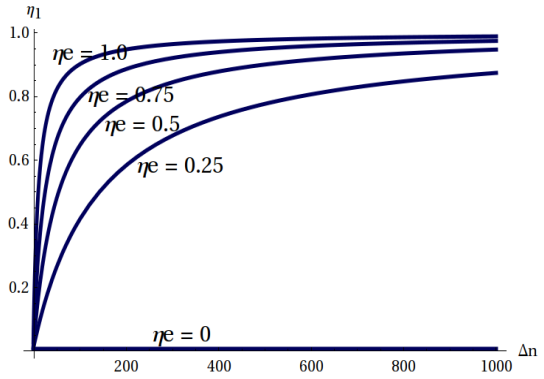

Fig. 4.29: Plot of η_1 as a function of the concentration gradient Δn in units of μM when $s = 2, n_c = 1.0\mu M, \eta_c = 0.5, \nu_e^+ = \nu_c^- = 15\,(\mu M)^{-1}s^{-1}, \nu_1^- = \nu_1^+ = 500\,s^{-1}, \nu_2^- = \nu_2^+ = 500\,s^{-1}, u_e^+ = 2, u_1^- = 2, u_1^+ = 2, u_2^- = 2, u_2^+ = 2, u_c^- = 2$ for the values $\eta_e = 0, \eta_e = 0.25, \eta_e = 0.5, \eta_e = 0.75, \eta_e = 1.0$

Using $\eta_c = 1.0, u_e^+ = 2, u_1^- = 2, u_1^+ = 2, u_2^- = 2, u_2^+ = 2, u_c^- = 2$ and the val-

ues of the transition rates specified in Eq. (3.14) into Eq. (4.15), we have plotted the variation of the average occupation number η_1 of the internal potential well V_1 of a nano-channel with two internal potential wells as a function of the concentration gradient Δn in units of μM for five different values of η_e, that is $\eta_e = 0, \eta_e = 0.25, \eta_e = 0.5, \eta_e = 0.75, \eta_e = 1.0$ on the same graph as shown in Fig. 4.30.

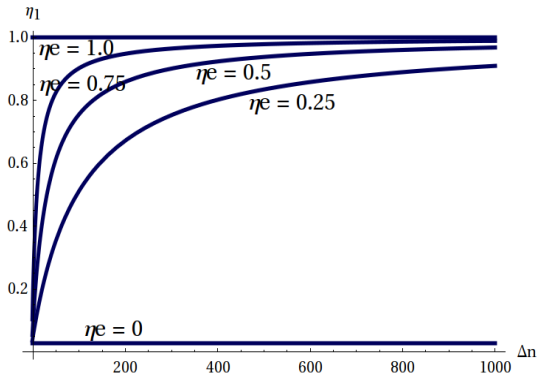

Fig. 4.30: Plot of η_1 as a function of the concentration gradient Δn in units of μM when $s = 2$, $n_c = 1.0\mu M$, $\eta_c = 1.0$, $\nu_e^+ = \nu_c^- = 15\,(\mu M)^{-1}s^{-1}, \nu_1^- = \nu_1^+ = 500\,s^{-1}, \nu_2^- = \nu_2^+ = 500\,s^{-1}$, $u_e^+ = 2, u_1^- = 2, u_1^+ = 2, u_2^- = 2, u_2^+ = 2, u_c^- = 2$ for the values $\eta_e = 0, \eta_e = 0.25, \eta_e = 0.5, \eta_e = 0.75, \eta_e = 1.0$

For the given values of η_e and η_c, the average occupation number of the internal potential well V_1 of a nano-channel with two internal potential wells as a function of Δn is denoted by $\eta_{12}(\Delta n|\eta_e, \eta_c)$. The plots in Fig. 4.28 to Fig. 4.30 show that $\eta_{12}(\Delta n|\eta_e = 0, \eta_c) < \eta_{12}(\Delta n|\eta_e = 0.25, \eta_c) < \eta_{12}(\Delta n|\eta_e = 0.5, \eta_c) < \eta_{12}(\Delta n|\eta_e = 0.75, \eta_c) < \eta_{12}(\Delta n|\eta_e = 1.0, \eta_c)$ for all possible values of Δn and η_c. The average value of the occupation number assumes the values $\eta_{12}(\Delta n|\eta_e = 1.0, \eta_c = 1.0) = 1.0$ and $\eta_{12}(\Delta n|\eta_e = 0, \eta_c = 0) = 0$ for all possible values of Δn. Moreover, $\eta_{12}(\Delta n \to 10M|\eta_e, \eta_c) \to 1.0$ for all possible values of $\eta_e > 0$ and η_c and $\eta_{12}(\Delta n|\eta_e = 1.0, \eta_c)$ approaches its saturation or maximum positive value more rapidly than the other possible values. For small values of Δn, that is, $\Delta n < 400\mu M$, the average occupation number of V_1 of the nano-channel increases very rapidly as Δn increases and then it increases slowly and finally as Δn increases to large positive values, $\eta_{12}(\Delta n|\eta_e, \eta_c)$ saturates to its maximum constant value of one, that is $\eta_{12}(\Delta n|\eta_e, \eta_c) \to 1.0$.

For a given value of η_c, the rate of approach of $\eta_{12}(\Delta n|\eta_e, \eta_c)$ as a function of

Δn to the saturation value is different for different values of η_e. That is, $\eta_{12}(\Delta n|\eta_e = 1.0, \eta_c)$ saturates more quickly at a small value of Δn and $\eta_{12}(\Delta n|\eta_e = 0, \eta_c)$ saturates more slowly at large value of Δn. Thus, as η_e increases from zero to one, the value of Δn at which $\eta_{12}(\Delta n|\eta_e, \eta_c)$ becomes saturated decreases from the largest value, which occurs when $\eta_e = 0$ to the smallest one, which occurs when $\eta_e = 1.0$. In other words, for a given value of η_c, the value of Δn at which $\eta_{12}(\Delta n|\eta_e, \eta_c)$ saturates increases as η_e decreases from one to zero. For a given value of η_c, the average value of $\eta_{12}(\Delta n|\eta_e, \eta_c)$ associated with different values of η_e converge to each other as $\Delta n \rightarrow -1.0\ \mu M$ and then diverge from each other as Δn increases to intermediate values and after that the average value of $\eta_{12}(\Delta n|\eta_e, \eta_c)$ associated with different values of η_e began to converge to each other and finally saturate to the same maximum value $\eta_{12}(\Delta n|\eta_e, \eta_c) \rightarrow 1.0$ as Δn increases to large positive values.

Therefore, the average value of $\eta_{12}(\Delta n|\eta_e, \eta_c)$ attains its maximum value of one when $\eta_c = 1.0$ and $\eta_e = 1.0$ at very small value of Δn as shown in Fig. 4.30. Therefore, when $\eta_c = 1.0$, the mean residence time of a particle at the potential well V_c is large and as result the occupation probability of V_c is almost one. Moreover, as $\eta_e \rightarrow 1.0$, the mean residence time of a particle at the potential well V_e is large and as result the occupation probability of this site is almost one. This means that the average value of $\eta_{12}(\Delta n|\eta_e, \eta_c)$ attains its maximum value when V_c is occupied, that is $\eta_c = 1.0$, and when V_e is occupied, that is $\eta_e = 1$.

Using $\eta_e = 0$, $u_e^+ = 2, u_1^- = 2, u_1^+ = 2, u_2^- = 2, u_2^+ = 2, u_c^- = 2$ and the values of the transition rates specified in Eq. (3.14) into Eq. (4.15), we have plotted the variation of the average occupation number η_1 of the internal potential well V_1 of a nano-channel with two internal potential wells as a function of the concentration gradient Δn in units of μM for five different values of η_c, that is $\eta_c = 0, \eta_c = 0.25, \eta_c = 0.5, \eta_c = 0.75, \eta_c = 1.0$ on the same graph as shown in Fig. 4.31.

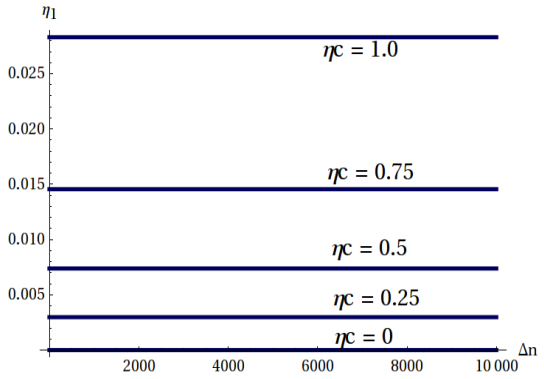

Fig. 4.31: Plot of η_1 as a function of the concentration gradient Δn in units of μM when $s = 2, n_c = 1.0\mu M, \eta_e = 0, \nu_e^+ = \nu_c^- = 15\,(\mu M)^{-1}s^{-1}, \nu_1^- = \nu_1^+ = 500\,s^{-1}, \nu_2^- = \nu_2^+ = 500\,s^{-1}, u_e^+ = 2, u_1^- = 2, u_1^+ = 2, u_2^- = 2, u_2^+ = 2, u_c^- = 2$ for the values $\eta_c = 0, \eta_c = 0.25, \eta_c = 0.5, \eta_c = 0.75, \eta_c = 1.0$

Using $\eta_e = 0.5$, $u_e^+ = 2, u_1^- = 2, u_1^+ = 2, u_2^- = 2, u_2^+ = 2, u_c^- = 2$ and the values of the transition rates specified in Eq. (3.14) into Eq. (4.15), we have plotted the variation of the average occupation number η_1 of the internal potential well V_1 of a nano-channel with two internal potential wells as a function of the concentration gradient Δn in units of μM for five different values of η_c, that is $\eta_c = 0, \eta_c = 0.25, \eta_c = 0.5, \eta_c = 0.75, \eta_c = 1.0$ on the same graph as shown in Fig. 4.32.

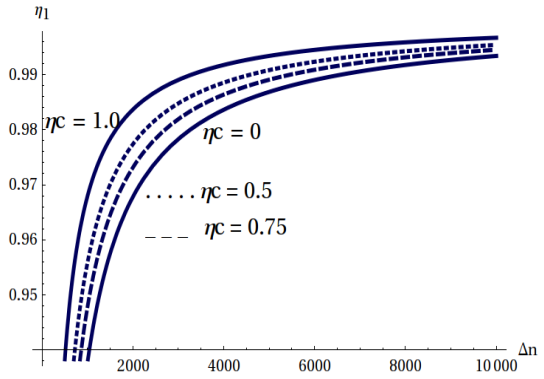

Fig. 4.32: Plot of η_1 as a function of the concentration gradient Δn in units of μM when $s = 2, n_c = 1.0\mu M, \eta_e = 0.5, \nu_e^+ = \nu_c^- = 15\,(\mu M)^{-1}s^{-1}, \nu_1^- = \nu_1^+ = 500\,s^{-1}, \nu_2^- = \nu_2^+ = 500\,s^{-1}, u_e^+ = 2, u_1^- = 2, u_1^+ = 2, u_2^- = 2, u_2^+ = 2, u_c^- = 2$ for five different values $\eta_c = 0, \eta_c = 0.25, \eta_c = 0.5, \eta_c = 0.75, \eta_c = 1.0$

Using $\eta_e = 1.0$, $u_e^+ = 2, u_1^- = 2, u_1^+ = 2, u_2^- = 2, u_2^+ = 2, u_c^- = 2$ and the val-

ues of the transition rates specified in Eq. (3.14) into Eq. (4.15), we have plotted the variation of the average occupation number η_1 of the internal potential well V_1 of a nano-channel with two internal potential wells as a function of the concentration gradient Δn in units of μM for five different values of η_c, that is $\eta_c = 0, \eta_c = 0.25, \eta_c = 0.5, \eta_c = 0.75, \eta_c = 1.0$ on the same graph as shown in Fig. 4.33.

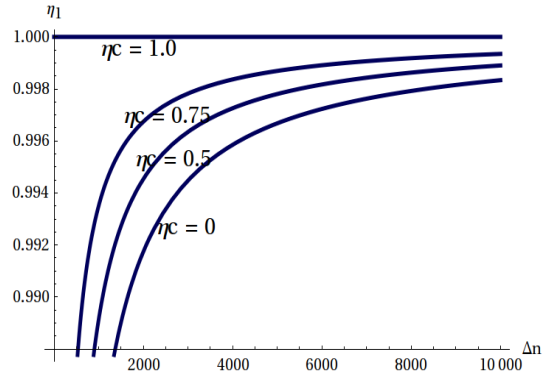

Fig. 4.33: Plot of η_1 as a function of the concentration gradient Δn in units of μM when $s = 2$, $n_c = 1.0\mu M$, $\eta_e = 1.0$, $\nu_e^+ = \nu_c^- = 15\,(\mu M)^{-1}s^{-1}, \nu_1^- = \nu_1^+ = 500\,s^{-1}, \nu_2^- = \nu_2^+ = 500\,s^{-1}$, $u_e^+ = 2, u_1^- = 2, u_1^+ = 2, u_2^- = 2, u_2^+ = 2, u_c^- = 2$ for five different values $\eta_c = 0, \eta_c = 0.25, \eta_c = 0.5, \eta_c = 0.75, \eta_c = 1.0$

As shown in Fig. 4.31, for the given values of η_c, the average value of $\eta_{12}(\Delta n|\eta_e = 0, \eta_c)$ as a function of Δn assumes small constant values that don't change as Δn increases. The plots shown in Fig. 4.31 to Fig. 4.33 imply that: $\eta_{12}(\Delta n|\eta_e, \eta_c = 0) < \eta_{12}(\Delta n|\eta_e, \eta_c = 0.25) < \eta_{12}(\Delta n|\eta_e, \eta_c = 0.5) < \eta_{12}(\Delta n|\eta_e, \eta_c = 0.75) < \eta_{12}(\Delta n|\eta_e, \eta_c = 1.0)$ for all possible values of Δn and η_e. Moreover, $\eta_{12}(\Delta n|\eta_e = 1.0, \eta_c = 1.0) = 1.0$ and $\eta_{12}(\Delta n|\eta_e = 0, \eta_c = 0) = 0$ for all possible values of Δn. Furthermore, $\eta_{12}(\Delta n \to 10\ M|\eta_e, \eta_c) \to 1.0$ for all possible values of $\eta_e > 0$ and η_c and $\eta_{12}(\Delta n|\eta_e, \eta_c = 1.0)$ approaches its saturation value more rapidly. For small values of Δn, that is, $\Delta n < 4000\ \mu M$ the average occupation number of V_1 of the nano-channel increases very rapidly as Δn increases and then it increases slowly and finally as Δn increases to large positive values, $\eta_{12}(\Delta n|\eta_e, \eta_c)$ saturates to its maximum constant value, that is, $\eta_{12}(\Delta n|\eta_e, \eta_c) \to 1.0$.

Using $\eta_e = 0.1$, $\eta_c = 0.1$, $u_1^- = 2, u_1^+ = 2, u_2^- = 2, u_2^+ = 2, u_c^- = 2$ and the values of the transition rates specified in Eq. (3.14) into Eq. (4.15), we have plotted the variation of the average occupation number η_1 of the internal potential well V_1 of

a nano-channel with two internal potential wells as a function of concentration gradient Δn in units of μM for four different values of u_e^+, that is $u_e^+ \approx 0, u_e^+ = 1.0, u_e^+ = 2.0, u_e^+ = 3.0$ on the same graph as shown in Fig. 4.34.

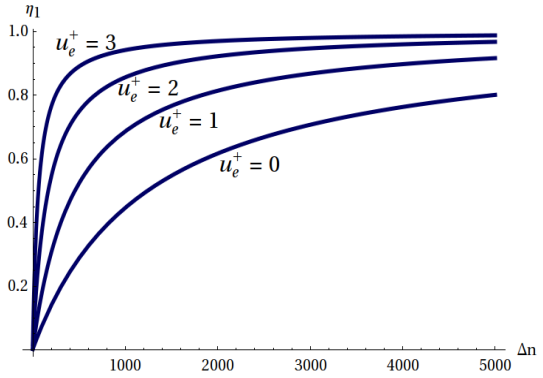

Fig. 4.34: Plot ofη_1 as a function of the concentration gradient Δn in units of μM when $s = 2$, $n_c = 1.0\,\mu M$, $\eta_e = 0.1$, $\eta_c = 0.1$, $\nu_e^+ = \nu_c^- = 15\,(\mu M)^{-1}s^{-1}, \nu_1^- = \nu_1^+ = 500\,s^{-1}, \nu_2^- = \nu_2^+ = 500\,s^{-1}$, $u_1^- = 2, u_1^+ = 2, u_2^- = 2, u_2^+ = 2, u_c^- = 2$ for the values $u_e^+ \approx 0, u_e^+ = 1.0, u_e^+ = 2.0, u_e^+ = 3.0$

Using $\eta_e = 0.95$, $\eta_c = 0.95$, $u_1^- = 2, u_1^+ = 2, u_2^- = 2, u_2^+ = 2, u_c^- = 2$ and the values of the transition rates specified in Eq. (3.14) into Eq. (4.15), we have plotted the variation of the average occupation number η_1 of the internal potential well V_1 of a nano-channel with two internal potential wells as a function of concentration gradient Δn in units of μM for four different values of u_e^+, that is $u_e^+ \approx 0, u_e^+ = 1.0, u_e^+ = 2.0, u_e^+ = 3.0$ on the same graph as shown in Fig. 4.35.

Using $\eta_e = 1.0$, $\eta_c = 0$, $u_1^- = 2, u_1^+ = 2, u_2^- = 2, u_2^+ = 2, u_c^- = 2$ and the values of the transition rates specified in Eq. (3.14) into Eq. (4.15), we have plotted the variation of the average occupation number η_1 of the internal potential well V_1 of a nano-channel with two internal potential wells as a function of concentration gradient Δn in units of μM for four different values of u_e^+, that is $u_e^+ \approx 0, u_e^+ = 1.0, u_e^+ = 2.0, u_e^+ = 3.0$ on the same graph as shown in Fig. 4.36.

Using $\eta_e = 0$, $\eta_c = 1.0$, $u_1^- = 2, u_1^+ = 2, u_2^- = 2, u_2^+ = 2, u_c^- = 2$ and the values of the transition rates specified in Eq. (3.14) into Eq. (4.15), we have plotted the variation of the average occupation number η_1 of the internal potential well V_1 of a nano-channel with two internal potential wells as a function of concentration gradient Δn in units of μM for four different values of u_e^+, that

is $u_e^+ \approx 0, u_e^+ = 1.0, u_e^+ = 2.0, u_e^+ = 3.0$ on the same graph as shown in Fig. 4.37.

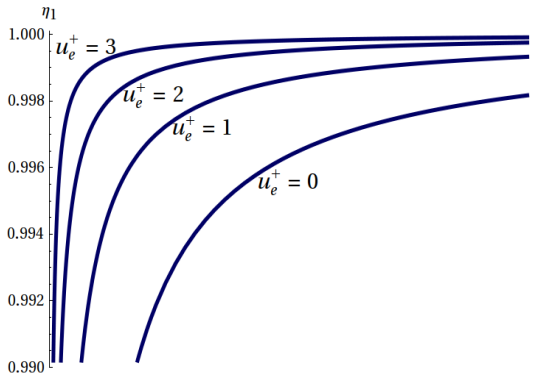

Fig. 4.35: Plot of η_1 as a function of the concentration gradient Δn in units of μM when $s = 2$, $n_c = 1.0\,\mu M$, $\eta_e = 0.95$, $\eta_c = 0.95$, $\nu_e^+ = \nu_c^- = 15\,(\mu M)^{-1}s^{-1}, \nu_1^- = \nu_1^+ = 500\,s^{-1}, \nu_2^- = \nu_2^+ = 500\,s^{-1}$, $u_1^- = 2, u_1^+ = 2, u_2^- = 2, u_2^+ = 2, u_c^- = 2$ for the values $u_e^+ \approx 0, u_e^+ = 1.0, u_e^+ = 2.0, u_e^+ = 3.0$

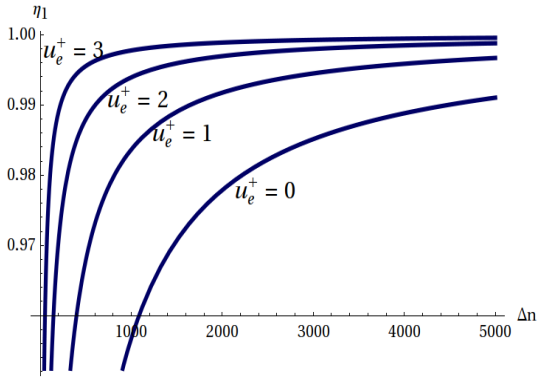

Fig. 4.36: Plot of η_1 as a function of the concentration gradient Δn in units of μM when $s = 2$, $n_c = 1.0\,\mu M$, $\eta_e = 1.0$, $\eta_c = 0$, $\nu_e^+ = \nu_c^- = 15\,(\mu M)^{-1}s^{-1}, \nu_1^- = \nu_1^+ = 500\,s^{-1}, \nu_2^- = \nu_2^+ = 500\,s^{-1}$, $u_1^- = 2, u_1^+ = 2, u_2^- = 2, u_2^+ = 2, u_c^- = 2$ for the values $u_e^+ \approx 0, u_e^+ = 1.0, u_e^+ = 2.0, u_e^+ = 3.0$

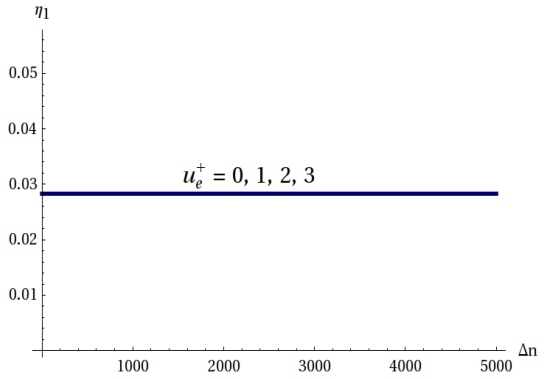

Fig. 4.37: Plot of η_1 as a function of the concentration gradient Δn in units of μM when $s = 2$, $n_c = 1.0\,\mu M$, $\eta_e = 0$, $\eta_c = 1.0$, $\nu_e^+ = \nu_c^- = 15\,(\mu M)^{-1}s^{-1}, \nu_1^- = \nu_1^+ = 500\,s^{-1}, \nu_2^- = \nu_2^+ = 500\,s^{-1}$, $u_1^- = 2, u_1^+ = 2, u_2^- = 2, u_2^+ = 2, u_c^- = 2$ for the values $u_e^+ \approx 0, u_e^+ = 1.0, u_e^+ = 2.0, u_e^+ = 3.0$

Using $\eta_e = 1.0$, $\eta_c = 1.0$, $u_1^- = 2, u_1^+ = 2, u_2^- = 2, u_2^+ = 2, u_c^- = 2$ and the values of the transition rates specified in Eq. (3.14) into Eq. (4.15), we have plotted the variation of the average occupation number η_1 of the internal potential well V_1 of a nano-channel with two internal potential wells as a function of concentration gradient Δn in units of μM for four different values of u_e^+, that is $u_e^+ \approx 0, u_e^+ = 1.0, u_e^+ = 2.0, u_e^+ = 3.0$ on the same graph as shown in Fig. 4.38.

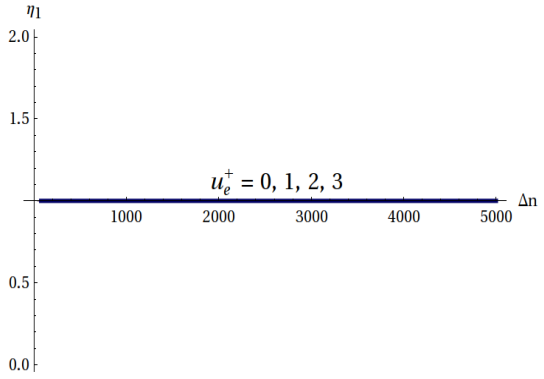

Fig. 4.38: Plot of η_1 as a function of the concentration gradient Δn in units of μM when $s = 2$, $n_c = 1.0\,\mu M$, $\eta_e = 1.0$, $\eta_c = 1.0$, $\nu_e^+ = \nu_c^- = 15\,(\mu M)^{-1}s^{-1}, \nu_1^- = \nu_1^+ = 500\,s^{-1}, \nu_2^- = \nu_2^+ = 500\,s^{-1}$, $u_1^- = 2, u_1^+ = 2, u_2^- = 2, u_2^+ = 2, u_c^- = 2$ for the values $u_e^+ \approx 0, u_e^+ = 1.0, u_e^+ = 2.0, u_e^+ = 3.0$

The plots shown in Fig. 4.37 and Fig. 4.38 show that the average value of $\eta_{12}(\Delta n|\eta_e, \eta_c, u_e^+)$ as a function of Δn assumes the same constant values that don't change as Δn

increases for each possible value of u_e^+. That is, $\eta_{12}(\Delta n|\eta_e = 0, \eta_c = 1.0, u_e^+) = 0.0282988$ and $\eta_{12}(\Delta n|\eta_e = 1.0, \eta_c = 1.0, u_e^+) = 1.0$ for each possible value of u_e^+. The plots shown in Fig. 4.34 to Fig. 4.36 show the property that: $\eta_{12}(\Delta n|\eta_e, \eta_c, u_e^+ \approx 0) > \eta_{12}(\Delta n|\eta_e, \eta_c, u_e^+ \approx 1.0) > \eta_{12}(\Delta n|\eta_e, \eta_c, u_e^+ \approx 2.0) > \eta_{12}(\Delta n|\eta_e, \eta_c, u_e^+ \approx 3.0)$ for all possible values of Δn, η_e and η_c. Moreover, $\eta_{12}(\Delta n|\eta_e, \eta_c, u_e^+)$ approaches its saturation value more rapidly when u_e^+ is small, that is $u_e^+ \approx 0$ than when u_e^+ assumes higher values. Therefore, as the normalized potential barrier u_e^+ increases, the transition rate from the external potential well V_e to the internal potential well V_1 decreases and as result the occupation probability of V_1 is small, which means that the average value of the occupation number η_1 of V_1 of a nano-channel with two internal potential wells decreases.

Using $\eta_e = 0.1$, $\eta_c = 0.1$, $u_e^+ = 2, u_1^+ = 2, u_2^- = 2, u_2^+ = 2, u_c^- = 2$ and the values of the transition rates specified in Eq. (3.14) into Eq. (4.15), we have plotted the variation of the average occupation number η_1 of the internal potential well V_1 of a nano-channel with two internal potential wells as a function of concentration gradient Δn in units of μM for four different values of u_1^-, that is $u_1^- \approx 0, u_1^- = 1.0, u_1^- = 2.0, u_1^- = 3.0$ on the same graph as shown in Fig. 4.39.

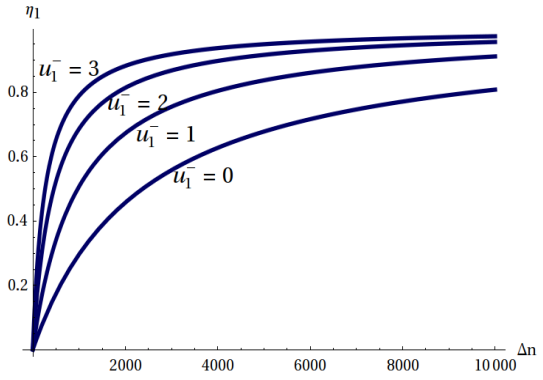

Fig. 4.39: Plot of η_1 as a function of the concentration gradient Δn in units of μM when $s = 2$, $n_c = 1.0\,\mu M$, $\eta_e = 0.1$, $\eta_c = 0.1$, $\nu_e^+ = \nu_c^- = 15\,(\mu M)^{-1}s^{-1}, \nu_1^- = \nu_1^+ = 500\,s^{-1}, \nu_2^- = \nu_2^+ = 500\,s^{-1}$, $u_e^+ = 2, u_1^+ = 2, u_2^- = 2, u_2^+ = 2, u_c^- = 2$ for the values $u_1^- \approx 0, u_1^- = 1.0, u_1^- = 2.0, u_1^- = 3.0$

Using $\eta_e = 0.1$, $\eta_c = 0.1$, $u_e^+ = 2, u_1^- = 2, u_2^- = 2, u_2^+ = 2, u_c^- = 2$ and the values of the transition rates specified in Eq. (3.14) into Eq. (4.15), we have plotted the variation of the average occupation number η_1 of the internal potential well V_1 of

a nano-channel with two internal potential wells as a function of concentration gradient Δn in units of μM for four different values of u_e^+, that is $u_1^+ \approx 0, u_1^+ = 1.0, u_1^+ = 2.0, u_1^+ = 3.0$ on the same graph as shown in Fig. 4.40.

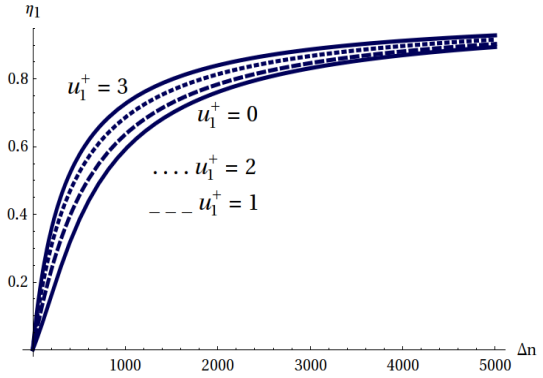

Fig. 4.40: Plot of η_1 as a function of the concentration gradient Δn in units of μM when $s = 2$, $n_c = 1.0\,\mu M$, $\eta_e = 0.1$, $\eta_c = 0.1$, $\nu_e^+ = \nu_c^- = 15\,(\mu M)^{-1}s^{-1}, \nu_1^- = \nu_1^+ = 500\,s^{-1}, \nu_2^- = \nu_2^+ = 500\,s^{-1}$, $u_e^+ = 2, u_1^- = 2, u_2^- = 2, u_2^+ = 2, u_c^- = 2$ for the values $u_1^+ \approx 0, u_1^+ = 1.0, u_1^+ = 2.0, u_1^+ = 3.0$

Using $\eta_e = 0.5$, $\eta_c = 0.5$, $u_e^+ = 2, u_1^- = 2, u_1^+ = 2, u_2^+ = 2, u_c^- = 2$ and the values of the transition rates specified in Eq. (3.14) into Eq. (4.15), we have plotted the variation of the average occupation number η_1 of the internal potential well V_1 of a nano-channel with two internal potential wells as a function of concentration gradient Δn in units of μM for four different values of u_2^-, that is $u_2^- \approx 0, u_2^- = 1.0, u_2^- = 2.0, u_2^- = 3.0$ on the same graph as shown in Fig. 4.41.

Using $\eta_e = 0.1$, $\eta_c = 0.1$, $u_e^+ = 2, u_1^- = 2, u_1^+ = 2, u_2^- = 2, u_c^- = 2$ and the values of the transition rates specified in Eq. (3.14) into Eq. (4.15), we have plotted the variation of the average occupation number η_1 of the internal potential well V_1 of a nano-channel with two internal potential wells as a function of concentration gradient Δn in units of μM for four different values of u_2^+, that is $u_2^+ \approx 0, u_2^+ = 1.0, u_2^+ = 2.0, u_2^+ = 3.0$ on the same graph as shown in Fig. 4.42.

Using $\eta_e = 0.5$, $\eta_c = 0.5$, $u_e^+ = 2, u_1^- = 2, u_1^+ = 2, u_2^- = 2, u_2^+ = 2$ and the values of the transition rates specified in Eq. (3.14) into Eq. (4.15), we have plotted the variation of the average occupation number η_1 of the internal potential well V_1 of a nano-channel with two internal potential wells as a function of concentration gradient Δn in units of μM for four different values of u_c^-, that

is $u_c^- \approx 0, u_c^- = 1.0, u_c^- = 2.0, u_c^- = 3.0$ on the same graph as shown in Fig. 4.43.

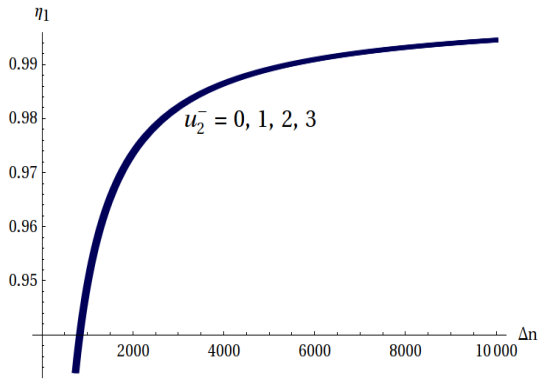

Fig. 4.41: Plot of η_1 as a function of the concentration gradient Δn in units of μM when $s = 2$, $n_c = 1.0\,\mu M$, $\eta_e = 0.5$, $\eta_c = 0.5$, $\nu_e^+ = \nu_c^- = 15\,(\mu M)^{-1}s^{-1}, \nu_1^- = \nu_1^+ = 500\,s^{-1}, \nu_2^- = \nu_2^+ = 500\,s^{-1}$, $u_e^+ = 2, u_1^- = 2, u_1^+ = 2, u_2^+ = 2, u_c^- = 2$ for the values $u_2^- \approx 0, u_2^- = 1.0, u_2^- = 2.0, u_2^- = 3.0$

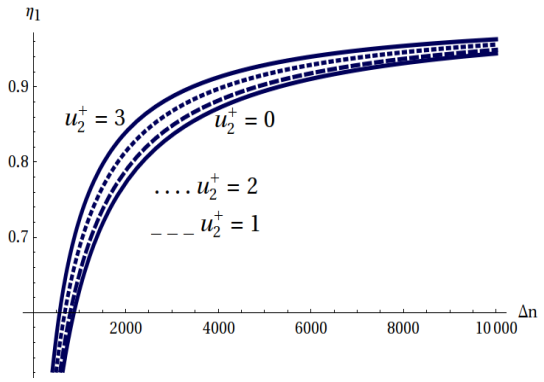

Fig. 4.42: Plot of η_1 as a function of the concentration gradient Δn in units of μM when $s = 2$, $n_c = 1.0\ \mu M$, $\eta_e = 0.1$, $\eta_c = 0.1$, $\nu_e^+ = \nu_c^- = 15\,(\mu M)^{-1}s^{-1}, \nu_1^- = \nu_1^+ = 500\,s^{-1}, \nu_2^- = \nu_2^+ = 500\,s^{-1}$, $u_e^+ = 2, u_1^- = 2, u_1^+ = 2, u_2^- = 2, u_c^- = 2$ for the values $u_2^+ \approx 0, u_2^+ = 1.0, u_2^+ = 2.0, u_2^+ = 3.0$

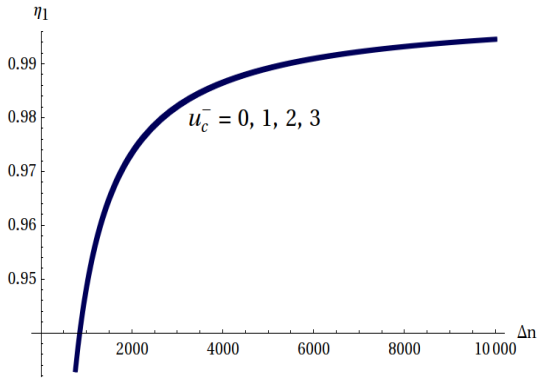

Fig. 4.43: Plot of η_1 as a function of the concentration gradient Δn in units of μM when $s = 2$, $n_c = 1.0\,\mu M$, $\eta_e = 0.5$, $\eta_c = 0.5$, $\nu_e^+ = \nu_c^- = 15\,(\mu M)^{-1}s^{-1}, \nu_1^- = \nu_1^+ = 500\,s^{-1}, \nu_2^- = \nu_2^+ = 500\,s^{-1}$, $u_e^+ = 2, u_1^- = 2, u_1^+ = 2, u_2^- = 2, u_2^+ = 2$ for the values $u_c^- \approx 0, u_c^- = 1.0, u_c^- = 2.0, u_c^- = 3.0$

The average value of $\eta_{12}(\Delta n|\eta_e, \eta_c)$ becomes large when u_1^- and u_1^+ assume large values as shown in Fig. 4.39 and Fig. 4.40, respectively. That is, when u_1^- and u_1^+ assume large values the escape rate from the internal potential well V_1 is small and as a result the mean residence time of the particle in V_1 becomes large, which in turn imply that the occupation probability of V_1 by a particle increases and thus the average value of $\eta_{12}(\Delta n|\eta_e, \eta_c)$ increases as u_1^- and u_1^+ increase. The average value of $\eta_{12}(\Delta n|\eta_e, \eta_c)$ saturates more quickly to its maximum value when u_1^- and u_1^+ assume large values. Moreover, the average value of $\eta_{12}(\Delta n|\eta_e, \eta_c)$ assumes the same value for each possible value of u_2^- and u_c^- as shown in Fig. 4.41 and Fig. 4.43, respectively. However, average value of $\eta_{12}(\Delta n|\eta_e, \eta_c)$ becomes large when u_2^+ assume large values as shown in Fig. 4.42. This is because as u_2^+ increases the escape rate from the internal potential well V_2 decreases and as a result the mean residence time of a particle in V_2 becomes large, which in turn imply that the probability that V_2 is found to be in the vacant state becomes very small and as a result a particle in V_1 can't jump to V_2. Therefore as a particle stays for a long time in V_2, it forces the particle V_1 to stay there longer and thus the occupation probability of V_1 by a particle increases and thus the average value of $\eta_{12}(\Delta n|\eta_e, \eta_c)$ increases as u_2^+ increases.

4.4.1.2 The Average Occupation Number of the Internal Potential Well V_1 of a Nano-Channel as a Function of the Average Occupation Number of the External Potential Wells when the Potential Barriers are Twice of Thermal Energy

Using the positive concentration gradient $\Delta n = 1000\ \mu M$, $u_e^+ = 2, u_1^- = 2, u_1^+ = 2, u_2^- = 2, u_2^+ = 2, u_c^- = 2$ and the values of the transition rates specified in Eq. (3.14) into Eq. (4.15), we have plotted the variation of the average occupation number η_1 of the internal potential well V_1 of a nano-channel with two internal potential wells as a function of η_c for five different possible values of η_e, that is $\eta_e = 0, \eta_e = 0.25, \eta_e = 0.5, \eta_e = 0.75, \eta_e = 1.0$ on the same graph as shown in Fig. 4.44.

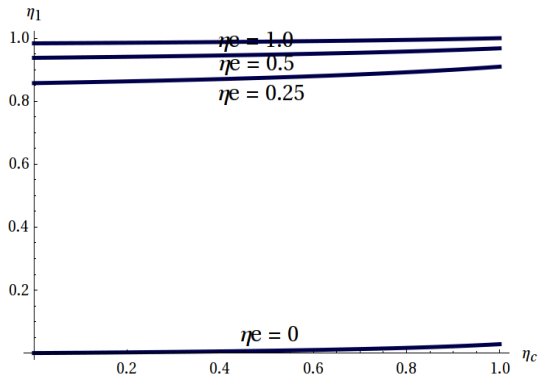

Fig. 4.44: Plot of η_1 as a function of η_c when $s = 2$, $\Delta n = 1000\ \mu M$, $n_c = 1.0\ \mu M$, $\nu_e^+ = \nu_c^- = 15\,(\mu M)^{-1}s^{-1}, \nu_1^- = \nu_1^+ = 500\,s^{-1}, \nu_2^- = \nu_2^+ = 500\,s^{-1}$, $u_e^+ = 2, u_1^- = 2, u_1^+ = 2, u_2^- = 2, u_2^+ = 2, u_c^- = 2$ for five values of η_e, that is $\eta_e = 0, \eta_e = 0.25, \eta_e = 0.5, \eta_e = 0.75, \eta_e = 1.0$

When $\Delta n = 1000\ \mu M$, the plot in in Fig. 4.44 show that the average value of $\eta_{12}(\Delta n|\eta_e, \eta_c)$ as a function of η_c obey that: $\eta_{12}(\Delta n = 1000\ \mu M|\eta_e = 1.0, \eta_c) > \eta_{12}(\Delta n = 1000\ \mu M|\eta_e = 0.75, \eta_c) > \eta_{12}(\Delta n = 1000\ \mu M|\eta_e = 0.5, \eta_c) > \eta_{12}(\Delta n = 1000\ \mu M|\eta_e = 0.25, \eta_c) > \eta_{12}(\Delta n = 1000\ \mu M|\eta_e = 0, \eta_c)$ for all possible values of η_c. The average value of $\eta_{12}(\Delta n = 1000\ \mu M|\eta_e, \eta_c)$ associated with the different values of η_e increase very slowly as η_c increases from zero to one. As η_e becomes slightly greater than zero, the average value of $\eta_{12}(\Delta n = 1000\ \mu M|\eta_e, \eta_c)$ jumps rapidly to slightly different values that are closer to one and are almost parallel to each other as shown in Fig. 4.44.

Using zero concentration gradient $\Delta n = 0$, $u_e^+ = 2, u_1^- = 2, u_1^+ = 2, u_2^- =$

$2, u_2^+ = 2, u_c^- = 2$ and the values of the transition rates specified in Eq. (3.14) into Eq. (4.15), we have plotted the variation of the average occupation number η_1 of the internal potential well V_1 of a nano-channel with two internal potential wells as a function of η_c for five possible values of η_e, that is $\eta_e = 0, \eta_e = 0.25, \eta_e = 0.5, \eta_e = 0.75, \eta_e = 1.0$ on the same graph as shown in Fig. 4.45.

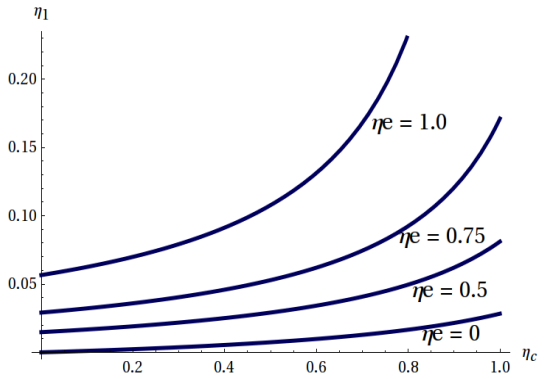

Fig. 4.45: Plot of η_1 as a function of η_c when $s = 2$, $\Delta n = 0$, $n_c = 1.0\ \mu M$, $\nu_e^+ = \nu_c^- = 15\,(\mu M)^{-1}s^{-1}, \nu_1^- = \nu_1^+ = 500\,s^{-1}, \nu_2^- = \nu_2^+ = 500\,s^{-1}$, $u_e^+ = 2, u_1^- = 2, u_1^+ = 2, u_2^- = 2, u_2^+ = 2, u_c^- = 2$ for five values of η_e, that is $\eta_e = 0, \eta_e = 0.25, \eta_e = 0.5, \eta_e = 0.75, \eta_e = 1.0$

When $\Delta n = 0$, the average value of $\eta_{12}(\Delta n|\eta_e, \eta_c)$ as a function of η_c obey that: $\eta_{12}(\Delta n = 0|\eta_e = 1.0, \eta_c) > \eta_{12}(\Delta n = 0|\eta_e = 0.75, \eta_c) > \eta_{12}(\Delta n = 0|\eta_e = 0.5, \eta_c) > \eta_{12}(\Delta n = 0|\eta_e = 0.25, \eta_c) > \eta_{12}(\Delta n = 0|\eta_e = 0, \eta_c)$. The average value of $\eta_{12}(\Delta n|\eta_e, \eta_c)$ approach to different minimum values as $\eta_c \to 0$, that is, $\eta_{12}(\Delta n = 0|\eta_e = 0, \eta_c \to 0) \to 0$, $\eta_{12}(\Delta n = 0|\eta_e = 0.25, \eta_c \to 0) \to 0.00596186$, $\eta_{12}(\Delta n = 0|\eta_e = 0.5, \eta_c \to 0) \to 0.0147711$, $\eta_{12}(\Delta n = 0|\eta_e = 0.75, \eta_c \to 0) \to 0.0291079$, $\eta_{12}(\Delta n = 0|\eta_e = 1.0, \eta_c \to 0) \to 0.0565534$. Moreover, the average occupation number $\eta_{12}(\Delta n|\eta_e, \eta_c)$ as a function of η_c approach to different maximum values as as $\eta_c \to 1.0$, that is, $\eta_{12}(\Delta n = 0|\eta_e = 0, \eta_c \to 1.0) \to 0.0282988$, $\eta_{12}(\Delta n = 0|\eta_e = 0.25, \eta_c \to 1.0) \to 0.0465559$, $\eta_{12}(\Delta n = 0|\eta_e = 0.5, \eta_c \to 1.0) \to 0.0810849$, $\eta_{12}(\Delta n = 0|\eta_e = 0.75, \eta_c \to 1.0) \to 0.171128$, $\eta_{12}(\Delta n = 0|\eta_e = 1.0, \eta_c \to 1.0) \to 1.0$.

Using the negative concentration gradient $\Delta n = -1.0\ \mu M$, $u_e^+ = 2, u_1^- = 2, u_1^+ = 2, u_2^- = 2, u_2^+ = 2, u_c^- = 2$ and the values of the transition rates specified in Eq. (3.14) into Eq. (4.15), we have plotted the variation of the average occupation number η_1 of the internal potential well V_1 of a nano-channel with two internal potential wells as a function of η_c for five possible values of η_e, that is

$\eta_e = 0, \eta_e = 0.25, \eta_e = 0.5, \eta_e = 0.75, \eta_e = 1.0$ on the same graph as shown in Fig. 4.46.

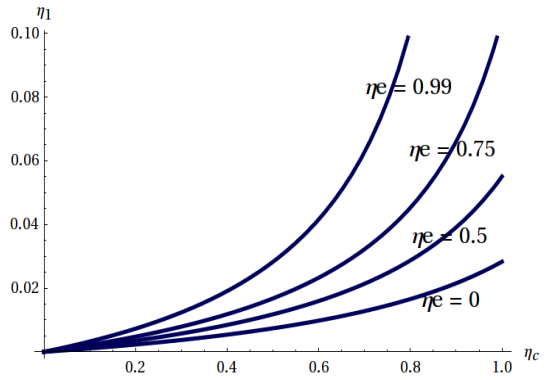

Fig. 4.46: Plot of η_1 as a function of η_c when $s = 2$, $\Delta n = -1.0\ \mu M$, $n_c = 1.0\ \mu M$, $\nu_e^+ = \nu_c^- = 15\,(\mu M)^{-1}s^{-1}, \nu_1^- = \nu_1^+ = 500\,s^{-1}, \nu_2^- = \nu_2^+ = 500\,s^{-1}$, $u_e^+ = 2, u_1^- = 2, u_1^+ = 2, u_2^- = 2, u_2^+ = 2, u_c^- = 2$ for five values of η_e, that is $\eta_e = 0, \eta_e = 0.25, \eta_e = 0.5, \eta_e = 0.75, \eta_e = 1.0$

When $\Delta n = -1.0\ \mu M$, the average occupation number $\eta_{12}(\Delta n|\eta_e, \eta_c)$ as a function of η_c obey that $\eta_{12}(\Delta n = -1.0\ \mu M|\eta_e = 0.99, \eta_c) > \eta_{12}(\Delta n = -1.0\ \mu M|\eta_e = 0.75, \eta_c) > \eta_{12}(\Delta n = -1.0\ \mu M|\eta_e = 0.5, \eta_c) > \eta_{12}(\Delta n = -1.0\ \mu M|\eta_e = 0, \eta_c)$. The average value of $\eta_{12}(\Delta n|\eta_e, \eta_c)$ approach to the same minimum zero value as $\eta_c \to 0$. Moreover, the average value of $\eta_{12}(\Delta n|\eta_e, \eta_c)$ approach to different maximum values as $\eta_c \to 1.0$, that is, $\eta_{12}(\Delta n = -1.0\ \mu M|\eta_e = 0, \eta_c \to 1.0) \to 0.0282988$, $\eta_{12}(\Delta n = -1.0\ \mu M|\eta_e = 0.5, \eta_c \to 1.0) \to 0.0373785$, $\eta_{12}(\Delta n = -1.0\ \mu M|\eta_e = 0.5, \eta_c \to 1.0) \to 0.0550373$, $\eta_{12}(\Delta n = -1.0\ \mu M|\eta_e = 0.75, \eta_c \to 1.0) \to 0.104323$, $\eta_{12}(\Delta n = -1.0\ \mu M|\eta_e = 1.0, \eta_c \to 1.0) \to 0.74413$.

Using the positive concentration gradient $\Delta n = 10000\ \mu M$, $u_e^+ = 2, u_1^- = 2, u_1^+ = 2, u_2^- = 2, u_2^+ = 2, u_c^- = 2$ and the values of the transition rates specified in Eq. (3.14) into Eq. (4.15), we have plotted the variation of the average occupation number η_1 of the internal potential well V_1 of a nano-channel with two internal potential wells as a function of η_e for five possible values of η_c, that is $\eta_c = 0, \eta_c = 0.25, \eta_c = 0.5, \eta_c = 0.75, \eta_c = 1.0$ on the same graph as shown in Fig. 4.47.

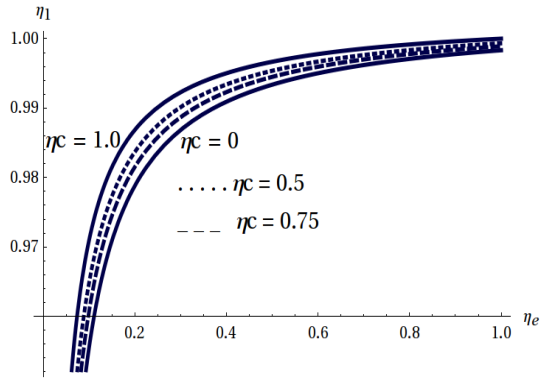

Fig. 4.47: Plot of η_1 as a function of η_e when $s = 2$, $\Delta n = 10000\ \mu M$, $n_c = 1.0\ \mu M$, $\nu_e^+ = \nu_c^- = 15\,(\mu M)^{-1}s^{-1}, \nu_1^- = \nu_1^+ = 500\,s^{-1}, \nu_2^- = \nu_2^+ = 500\,s^{-1}$, $u_e^+ = 2, u_1^- = 2, u_1^+ = 2, u_2^- = 2, u_2^+ = 2, u_c^- = 2$ for five values of η_c, that is, $\eta_c = 0, \eta_c = 0.25, \eta_c = 0.5, \eta_c = 0.75, \eta_c = 1.0$

Using the positive concentration gradient $\Delta n = 35\ \mu M$ and $u_e^+ = 2, u_1^- = 2, u_1^+ = 2, u_2^- = 2, u_2^+ = 2, u_c^- = 2$ and the values of the transition rates specified in Eq. (3.14) into Eq. (4.15), we have plotted the variation of the average occupation number η_1 of the internal potential well V_1 of a nano-channel with two internal potential wells as a function of η_e for five possible values of η_c, that is $\eta_c = 0, \eta_c = 0.25, \eta_c = 0.5, \eta_c = 0.75, \eta_c = 1.0$ on the same graph as shown in Fig. 4.48.

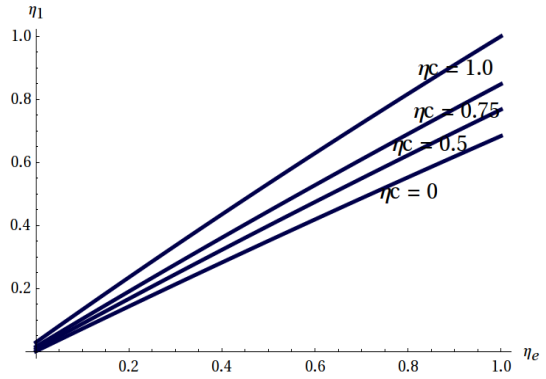

Fig. 4.48: Plot of η_1 as a function of η_e when $s = 2$, $\Delta n = 35\ \mu M$, $n_c = 1.0\ \mu M$, $\nu_e^+ = \nu_c^- = 15\,(\mu M)^{-1}s^{-1}, \nu_1^- = \nu_1^+ = 500\,s^{-1}, \nu_2^- = \nu_2^+ = 500\,s^{-1}$, $u_e^+ = 2, u_1^- = 2, u_1^+ = 2, u_2^- = 2, u_2^+ = 2, u_c^- = 2$ for five values of η_c, that is, $\eta_c = 0, \eta_c = 0.25, \eta_c = 0.5, \eta_c = 0.75, \eta_c = 1.0$

The plots in Fig. 4.47 and Fig. 4.48 show that the average value of $\eta_{12}(\Delta n|\eta_e,\eta_c)$ as a function of η_e obey that: $\eta_{12}(\Delta n|\eta_e,\eta_c=1.0) > \eta_{12}(\Delta n|\eta_e,\eta_c=0.75) > \eta_{12}(\Delta n|\eta_e,\eta_c=0.5) > \eta_{12}(\Delta n|\eta_e,\eta_c=0.25) > \eta_{12}(\Delta n|\eta_e,\eta_c=0)$ for all possible values of Δn and η_e. For a given value of $\Delta n = 10000\ \mu M$ and η_c, the average value of $\eta_{12}(\Delta n|\eta_e,\eta_c)$ increases as the average value of η_e increases. The average value of $\eta_{12}(\Delta n = 10000\ \mu M|\eta_e,\eta_c)$ approach to slightly different minimum values as $\eta_e \to 0$, that is, $\eta_{12}(\Delta n = 10000\ \mu M|\eta_e \to 0,\eta_c = 0) \to 0$, $\eta_{12}(\Delta n = 10000\ \mu M|\eta_e \to 0,\eta_c = 0.25) \to 0.00297852$, $\eta_1(\Delta n = 10000\ \mu M|\eta_e \to 0,\eta_c = 0.5) \to 0.00738171$, $\eta_{12}(\Delta n = 10000\ \mu M|\eta_e \to 0,\eta_c = 0.75) \to 0.014553$, $\eta_1(\Delta n = 10000\ \mu M|\eta_e \to 0,\eta_c = 1.0) \to 0.0282988$. The average value of $\eta_{12}(\Delta n = 10000\ \mu M|\eta_e,\eta_c)$ diverge from each other as η_e increases to intermediate values and after that they began to converge to each other and finally saturate to approximately the same maximum values of one as $\eta_e \to 1.0$. Moreover, when $\Delta n = 35\ \mu M$, the average value of $\eta_{12}(\Delta n|\eta_e,\eta_c)$ increases linearly as η_e increases for each possible value of η_c as shown in Fig. 4.48.

Using zero concentration gradient $\Delta n = 0$, $u_e^+ = 2, u_1^- = 2, u_1^+ = 2, u_2^- = 2, u_2^+ = 2, u_c^- = 2$ and the values of the transition rates specified in Eq. (3.14) into Eq. (4.15), we have plotted the variation of the average occupation number η_1 of the internal potential well V_1 of a nano-channel with two internal potential wells as a function of η_e for five possible values of η_c, that is $\eta_c = 0, \eta_c = 0.25, \eta_c = 0.5, \eta_c = 0.75, \eta_c = 1.0$ on the same graph as shown in Fig. 4.49.

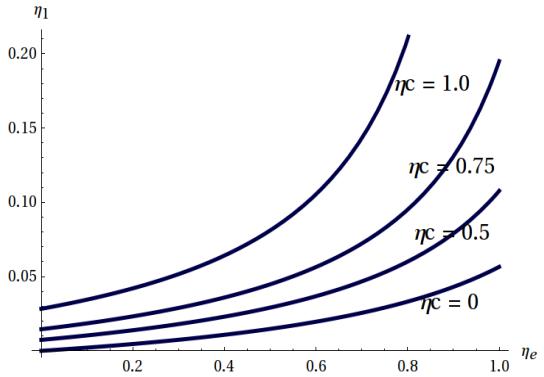

Fig. 4.49: Plot of η_1 as a function of η_e when $s = 2$, $\Delta n = 0$, $n_c = 1.0\ \mu M$, $\nu_e^+ = \nu_c^- = 15\,(\mu M)^{-1}s^{-1}, \nu_1^- = \nu_1^+ = 500\,s^{-1}, \nu_2^- = \nu_2^+ = 500\,s^{-1}$, $u_e^+ = 2, u_1^- = 2, u_1^+ = 2, u_2^- = 2, u_2^+ = 2, u_c^- = 2$ for five values of η_c, that is, $\eta_c = 0, \eta_c = 0.25, \eta_c = 0.5, \eta_c = 0.75, \eta_c = 1.0$

When $\Delta n = 0$, the plots in Fig. 4.49 show that the average value of $\eta_{12}(\Delta n|\eta_e, \eta_c)$ as a function of η_e obey that: $\eta_{12}(\Delta n = 0|\eta_e, \eta_c = 1.0) > \eta_{12}(\Delta n = 0|\eta_e, \eta_c = 0.75) > \eta_{12}(\Delta n = 0|\eta_e, \eta_c = 0.5) > \eta_{12}(\Delta n = 0|\eta_e, \eta_c = 0.25) > \eta_{12}(\Delta n = 0|\eta_e, \eta_c = 0)$. The average value of $\eta_{12}(\Delta n|\eta_e, \eta_c)$ approach to different minimum values as $\eta_e \to 0$, that is, $\eta_{12}(\Delta n = 0|\eta_c = 0, \eta_e \to 0) \to 0$, $\eta_{12}(\Delta n = 0|\eta_c = 0.25, \eta_e \to 0) \to 0.00297852$, $\eta_{12}(\Delta n = 0|\eta_c = 0.5, \eta_e \to 0) \to 0.00738171$, $\eta_{12}(\Delta n = 0|\eta_c = 0.75, \eta_e \to 0) \to 0.014553$, $\eta_{12}(\Delta n = 0|\eta_c = 1.0, \eta_e \to 0) \to 0.0282988$. Moreover, the average value of $\eta_{12}(\Delta n|\eta_e, \eta_c)$ approach to different maximum values as $\eta_e \to 1.0$, that is, $\eta_{12}(\Delta n = 0|\eta_c = 0, \eta_e \to 1.0) \to 0.0565534$, $\eta_{12}(\Delta n = 0|\eta_c = 0.25, \eta_e \to 1.0) \to 0.0742506$, $\eta_{12}(\Delta n = 0|\eta_c = 0.5, \eta_e \to 1.0) \to 0.107727$, $\eta_{12}(\Delta n = 0|\eta_c = 0.75, \eta_e \to 1.0) \to 0.195059$, $\eta_{12}(\Delta n = 0|\eta_c = 1.0, \eta_e \to 1.0) \to 1.0$.

Using negative concentration gradient $\Delta n = -1.0\ \mu M$, $u_e^+ = 2, u_1^- = 2, u_1^+ = 2, u_2^- = 2, u_2^+ = 2, u_c^- = 2$ and the values of the transition rates specified in Eq. (3.14) into Eq. (4.15), we have plotted the variation of the average occupation number η_1 of the internal potential well V_1 of a nano-channel with two internal potential wells as a function of η_e for five possible values of η_c, that is $\eta_c = 0, \eta_c = 0.25, \eta_c = 0.5, \eta_c = 0.75, \eta_c = 1.0$ on the same graph as shown in Fig. 4.50.

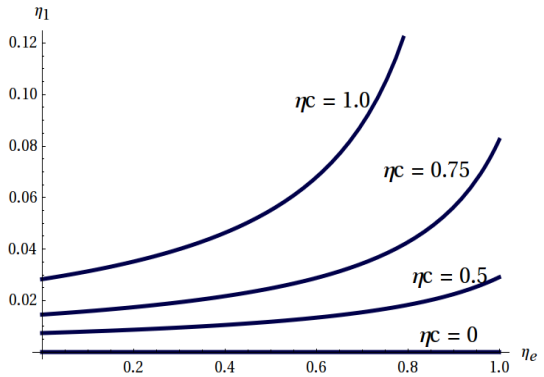

Fig. 4.50: Plot of η_1 as a function of η_e when $s = 2$, $\Delta n = -1.0\ \mu M$, $n_c = 1.0\ \mu M$, $\nu_e^+ = \nu_c^- = 15\,(\mu M)^{-1}s^{-1}, \nu_1^- = \nu_1^+ = 500\,s^{-1}, \nu_2^- = \nu_2^+ = 500\,s^{-1}$, $u_e^+ = 2, u_1^- = 2, u_1^+ = 2, u_2^- = 2, u_2^+ = 2, u_c^- = 2$ for five values of η_c, that is $\eta_c = 0, \eta_c = 0.25, \eta_c = 0.5, \eta_c = 0.75, \eta_c = 1.0$

When $\Delta n = -1.0\ \mu M$, the plots in Fig. 4.50 show that the average value of $\eta_{12}(\Delta n|\eta_e, \eta_c)$ as a function of η_e obey that: $\eta_{12}(\Delta n = -1.0\ \mu M|\eta_e, \eta_c = 1.0) > \eta_{12}(\Delta n = -1.0\ \mu M|\eta_e, \eta_c = 0.75) > \eta_{12}(\Delta n = -1.0\ \mu M|\eta_e, \eta_c = 0.5) > \eta_{12}(\Delta n =$

$-1.0\ \mu M|\eta_e, \eta_c = 0.25) > \eta_{12}(\Delta n = -1.0\ \mu M|\eta_e, \eta_c = 0)$. We see that $\eta_{12}(\Delta n|\eta_e, \eta_c)$ approach to different minimum values as $\eta_e \to 0$, that is, $\eta_{12}(\Delta n = -1.0\,\mu M|\eta_c = 0, \eta_e \to 0) \to 0$, $\eta_{12}(\Delta n = -1.0\ \mu M|\eta_c = 0.25, \eta_e \to 0) \to 0.00297852$, $\eta_1(\Delta n = -1.0\ \mu M|\eta_c = 0.5, \eta_e \to 0) \to 0.00738171$, $\eta_1(\Delta n = -1.0\ \mu M|\eta_c = 0.75, \eta_e \to 0) \to 0.014553$, $\eta_1(\Delta n = -1.0\ \mu M|\eta_c = 1.0, \eta_e \to 0) \to 0.0282988$. Moreover, $\eta_{12}(\Delta n|\eta_e, \eta_c)$ approach to different maximum values as $\eta_e \to 1.0$, that is, $\eta_{12}(\Delta n = -1.0\ \mu M|\eta_c = 0, \eta_e \to 1.0) \to 0$, $\eta_{12}(\Delta n = -1.0\ \mu M|\eta_c = 0.25, \eta_e \to 1.0) \to 0.009886349$, $\eta_1(\Delta n = -1.0\ \mu M|\eta_c = 0.5, \eta_e \to 1.0) \to 0.02906965$, $\eta_1(\Delta n = -1.0\ \mu M|\eta_c = 0.75, \eta_e \to 1.0) \to 0.08242224$, $\eta_{12}(\Delta n = -1.0\ \mu M|\eta_c = 1.0, \eta_e \to 1.0) \to 1.0$.

Using $\eta_e = 0$, $u_e^+ = 2, u_1^- = 2, u_1^+ = 2, u_2^- = 2, u_2^+ = 2, u_c^- = 2$ and the values of the transition rates specified in Eq. (3.14) into Eq. (4.15), we have plotted the variation of the average occupation number η_1 of the internal potential well V_1 of a nano-channel with two internal potential wells as a function of η_c for five different values of the concentration gradient Δn in units of μM: $\Delta n = -0.99, \Delta n = 0, \Delta n = 35, \Delta n = 100, \Delta n = 500, \Delta n = 1000$ on the same graph as shown in Fig. 4.51.

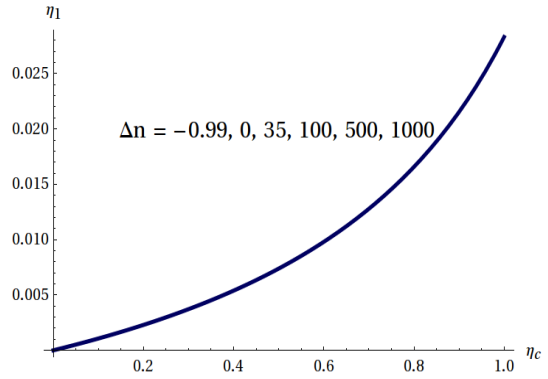

Fig. 4.51: Plot of η_1 as a function of η_c when $s = 2$, $n_c = 1.0\,\mu M$, $\eta_e = 0$, $\nu_e^+ = \nu_c^- = 15\,(\mu M)^{-1}s^{-1}, \nu_1^- = \nu_1^+ = 500\,s^{-1}, \nu_2^- = \nu_2^+ = 500\,s^{-1}$, $u_e^+ = 2, u_1^- = 2, u_1^+ = 2, u_2^- = 2, u_2^+ = 2, u_c^- = 2$ for the values of Δn in units of μM: $\Delta n = -0.99, \Delta n = 0, \Delta n = 35, \Delta n = 100, \Delta n = 500, \Delta n = 1000$

Using $\eta_e = 0.5$,$u_e^+ = 2, u_1^- = 2, u_1^+ = 2, u_2^- = 2, u_2^+ = 2, u_c^- = 2$ and the values of the transition rates specified in Eq. (3.14) into Eq. (4.15), we have plotted the variation of the average occupation number η_1 of the internal potential well V_1 of a nano-channel with two internal potential wells as a function

of η_c for five different values of the concentration gradient Δn in units of μM: $\Delta n = -0.99, \Delta n = 0, \Delta n = 35, \Delta n = 100, \Delta n = 500, \Delta n = 1000$ on the same graph as shown in Fig. 4.52.

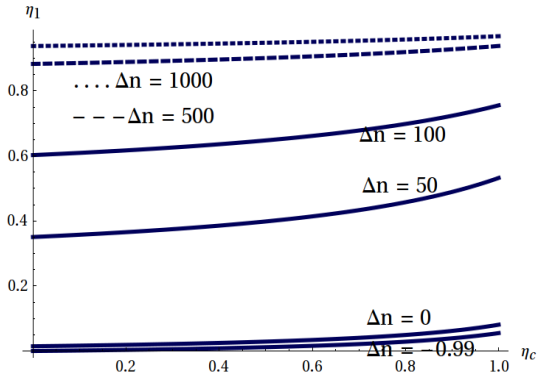

Fig. 4.52: Plot of η_1 as a function of η_c when $s = 2$, $n_c = 1.0\,\mu M$, $\eta_e = 0.5$, $\nu_e^+ = \nu_c^- = 15\,(\mu M)^{-1}s^{-1}, \nu_1^- = \nu_1^+ = 500\,s^{-1}, \nu_2^- = \nu_2^+ = 500\,s^{-1}$, $u_e^+ = 2, u_1^- = 2, u_1^+ = 2, u_2^- = 2, u_2^+ = 2, u_c^- = 2$ for the values of Δn in units of μM: $\Delta n = -0.99, \Delta n = 0, \Delta n = 35, \Delta n = 100, \Delta n = 500, \Delta n = 1000$

Using $\eta_e = 1.0$, $u_e^+ = 2, u_1^- = 2, u_1^+ = 2, u_2^- = 2, u_2^+ = 2, u_c^- = 2$ and the values of the transition rates specified in Eq. (3.14) into Eq. (4.15), we have plotted the variation of the average occupation number η_1 of the internal potential well V_1 of a nano-channel with two internal potential wells as a function of η_c for five different values of the concentration gradient Δn in units of μM: $\Delta n = -0.99, \Delta n = 0, \Delta n = 35, \Delta n = 100, \Delta n = 500, \Delta n = 1000$ on the same graph as shown in Fig. 4.53.

The average value of $\eta_{12}(\Delta n|\eta_e, \eta_c)$ as a function of η_c associated with different values of Δn coincide with each other in the entire range $0 \leq \eta_c \leq 1.0$ when $\eta_e = 0$ and increase rapidly to its maximum value $\eta_{12}(\Delta n|\eta_e, \eta_c) = 0.0282988$ as $\eta_c = 1.0$ as shown in Fig. 4.51. The average value of $\eta_{12}(\Delta n|\eta_e, \eta_c)$ associated with different values of Δn separate from each other as η_e increases to intermediate values, that is $\eta_e \to 0.5$ and increase slowly to their maximum values as η_c increases as the plot in Fig. 4.52 shows. Finally when $\eta_e \to 1.0$, the average value of $\eta_{12}(\Delta n|\eta_e, \eta_c)$ associated with different values of Δn approach to different values as $\eta_c \to 0$, that is, $\eta_{12}(\Delta n = -0.99\ \mu M|\eta_e = 1.0, \eta_c \to 0) \to 0.000599041$, $\eta_{12}(\Delta n = 0|\eta_e = 1.0, \eta_c \to 0) \to 0.0565534$, $\eta_{12}(\Delta n = 35\ \mu M|\eta_e =$

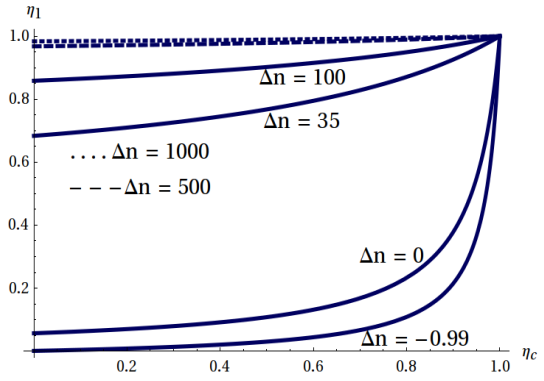

Fig. 4.53: Plot ofη_1 as a function of η_c when $s = 2$, $n_c = 1.0\,\mu M$, $\eta_e = 1.0$, $\nu_e^+ = \nu_c^- = 15\,(\mu M)^{-1}s^{-1}, \nu_1^- = \nu_1^+ = 500\,s^{-1}, \nu_2^- = \nu_2^+ = 500\,s^{-1}$, $u_e^+ = 2, u_1^- = 2, u_1^+ = 2, u_2^- = 2, u_2^+ = 2, u_c^- = 2$ for the values of Δn in units of μM: $\Delta n = -0.99, \Delta n = 0, \Delta n = 35, \Delta n = 100, \Delta n = 500, \Delta n = 1000$

$1.0, \eta_c \to 0) \to 0.683476$, $\eta_{12}(\Delta n = 100\ \mu M|\eta_e = 1.0, \eta_c \to 0) \to 0.85834$, $\eta_{12}(\Delta n = 500\ \mu M|\eta_e = 1.0, \eta_c \to 0) \to 0.967803$, $\eta_{12}(\Delta n = 1000\ \mu M|\eta_e = 1.0, \eta_c \to 0) \to$ and $\eta_{12}(\Delta n = 10000\ \mu M|\eta_e = 1.0, \eta_c \to 0) \to 0.983622$. As η_c increases the average values of $\eta_{12}(\Delta n|\eta_e, \eta_c)$ associated with different values of Δn approach to each other and finally all of them converge to the same saturation value of $\eta_{12}(\Delta n|\eta_e = 1.0, \eta_c) \to 1.0$ as $\eta_c \to 1.0$ as shown in Fig. 4.53.

Using $\eta_c = 0$, $u_e^+ = 2, u_1^- = 2, u_1^+ = 2, u_2^- = 2, u_2^+ = 2, u_c^- = 2$ and the values of the transition rates specified in Eq. (3.14) into Eq. (4.15), we have plotted the variation of the average occupation number η_1 of the internal potential well V_1 of a nano-channel with two internal potential wells as a function of η_e for five different values of the concentration gradient Δn in units of μM: $\Delta n = -0.99, \Delta n = 0, \Delta n = 35, \Delta n = 100, \Delta n = 500, \Delta n = 1000$ on the same graph as shown in Fig. 4.54.

Using $\eta_c = 1.0$, $u_e^+ = 2, u_1^- = 2, u_1^+ = 2, u_2^- = 2, u_2^+ = 2, u_c^- = 2$ and the values of the transition rates specified in Eq. (3.14) into Eq. (4.15), we have plotted the variation of the average occupation number η_1 of the internal potential well V_1 of a nano-channel with two internal potential wells as a function of η_e for five different values of the concentration gradient Δn in units of μM: $\Delta n = -0.99, \Delta n = 0, \Delta n = 35, \Delta n = 100, \Delta n = 500, \Delta n = 1000$ on the same graph as shown in Fig. 4.55.

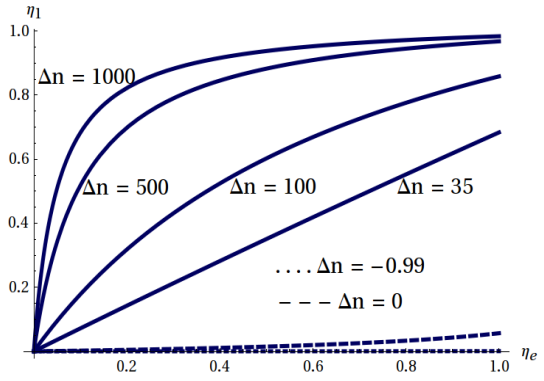

Fig. 4.54: Plot of η_1 as a function of η_e when $s = 2$, $n_c = 1.0\,\mu M$, $\eta_c = 0$, $\nu_e^+ = \nu_c^- = 15\,(\mu M)^{-1}s^{-1}, \nu_1^- = \nu_1^+ = 500\,s^{-1}, \nu_2^- = \nu_2^+ = 500\,s^{-1}$, $u_e^+ = 2, u_1^- = 2, u_1^+ = 2, u_2^- = 2, u_2^+ = 2, u_c^- = 2$ for the values of Δn in units of μM: $\Delta n = -0.99, \Delta n = 0, \Delta n = 35, \Delta n = 100, \Delta n = 500, \Delta n = 1000$

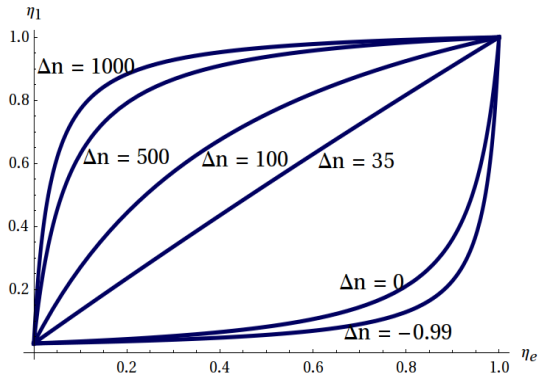

Fig. 4.55: Plot of η_1 as a function of η_e when $s = 2$, $n_c = 1.0\,\mu M$, $\eta_c = 1.0$, $\nu_e^+ = \nu_c^- = 15\,(\mu M)^{-1}s^{-1}, \nu_1^- = \nu_1^+ = 500\,s^{-1}, \nu_2^- = \nu_2^+ = 500\,s^{-1}$, $u_e^+ = 2, u_1^- = 2, u_1^+ = 2, u_2^- = 2, u_2^+ = 2, u_c^- = 2$ for the values of Δn in units of μM: $\Delta n = -0.99, \Delta n = 0, \Delta n = 35, \Delta n = 100, \Delta n = 500, \Delta n = 1000$

The plots in Fig. 4.54 and Fig. 4.55 show that the average value of $\eta_{12}(\Delta n = 35\ \mu M|\eta_e, \eta_c)$ as a function of η_e increases linearly as η_e increases for each possible value of η_c. The average value of $\eta_{12}(\Delta n|\eta_e, \eta_c = 0)$ as a function of η_e associated with different values of Δn coincide with each other and assume the same value $\eta_{12}(\Delta n|\eta_e, \eta_c = 0) = 0$ as $\eta_e \to 0$ and then as η_e increases to intermediate values, that is $\eta_e \to 0.5$, the deviation between the values of $\eta_{12}(\Delta n|\eta_e, \eta_c = 0)$ associated with different values of Δn becomes maximum and then as $\eta_e \to 1.0$

they approach to each other but assume different values as shown in Fig. 4.54. These values are: $\eta_{12}(\Delta n = -0.99\ \mu M|\eta_e \rightarrow 1.0, \eta_c = 0) \rightarrow 0.000599041$, $\eta_{12}(\Delta n = 0|\eta_e \rightarrow 1.0, \eta_c = 0) \rightarrow 0.0565534$, $\eta_{12}(\Delta n = 35\ \mu M|\eta_e \rightarrow 1.0, \eta_c = 0) \rightarrow 0.683476$, $\eta_{12}(\Delta n = 100\ \mu M|\eta_e \rightarrow 1.0, \eta_c = 0) \rightarrow 0.85834$, $\eta_{12}(\Delta n = 500\ \mu M|\eta_e \rightarrow 1.0, \eta_c = 0) \rightarrow 0.967803$, $\eta_{12}(\Delta n = 1000\ \mu M|\eta_e \rightarrow 1.0, \eta_c = 0) \rightarrow 0.983622$ and $\eta_{12}(\Delta n = 10000\ \mu M|\eta_e \rightarrow 1.0, \eta_c = 0) \rightarrow 0.998336$. When $\eta_c = 1.0$, the average value of $\eta_{12}(\Delta n|\eta_e, \eta_c = 1.0)$ associated with different values of Δn converge to each other and assume the same value $\eta_{12}(\Delta n|\eta_e, \eta_c = 1.0) = 0$ as $\eta_e \rightarrow 0$ and as η_e increases to intermediate values the deviation between the values of $\eta_{12}(\Delta n|\eta_e, \eta_c = 1.0)$ associated with different values of Δn becomes maximum and then as $\eta_e \rightarrow 1.0$ they converge to the same saturation value of $\eta_{12}(\Delta n|\eta_e, \eta_c = 1.0) = 1.0$ as shown in Fig. 4.55.

4.4.2 Discussion of the Average Occupation Number of the Internal Potential Well V_2 of a Nano-Channel with Two Internal Potential Wells

4.4.2.1 The Average Occupation Number of the Internal Potential Well V_2 of a Nano-Channel as a Function of the Concentration Gradient

Using $\eta_c = 0$, $u_e^+ = 2, u_1^- = 2, u_1^+ = 2, u_2^- = 2, u_2^+ = 2, u_c^- = 2$ and the values of the transition rates specified in Eq. (3.14) into Eq. (4.16), we have plotted the variation of the average occupation number η_2 of the internal potential well V_2 of a nano-channel with two internal potential wells as a function of the concentration gradient Δn in units of μM for five different values of η_e, that is $\eta_e = 0, \eta_e = 0.25, \eta_e = 0.5, \eta_e = 0.75, \eta_e = 1.0$ on the same graph as shown in Fig. 4.56.

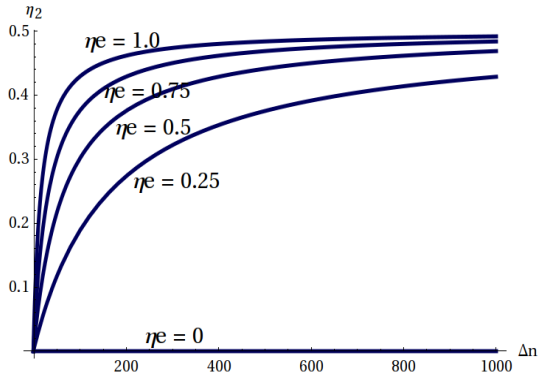

Fig. 4.56: Plot of η_2 as a function of the concentration gradient Δn in units of μM when $s = 2, n_c = 1.0\ \mu M, \eta_c = 0, \nu_e^+ = \nu_c^- = 15\,(\mu M)^{-1}s^{-1}, \nu_1^- = \nu_1^+ = 500\,s^{-1}, \nu_2^- = \nu_2^+ = 500\,s^{-1}, u_e^+ = 2, u_1^- = 2, u_1^+ = 2, u_2^- = 2, u_2^+ = 2, u_c^- = 2$ for five different values: $\eta_e = 0, \eta_e = 0.25, \eta_e = 0.5, \eta_e = 0.75, \eta_e = 1.0$

Using $\eta_c = 0.5$, $u_e^+ = 2, u_1^- = 2, u_1^+ = 2, u_2^- = 2, u_2^+ = 2, u_c^- = 2$ and the values of the transition rates specified in Eq. (3.14) into Eq. (4.16), we have plotted the variation of the average occupation number η_2 of the internal potential well V_2 of the nano-channel with two internal potential wells as a function of the concentration gradient Δn in units of μM for five different values of η_e, that is $\eta_e = 0, \eta_e = 0.25, \eta_e = 0.5, \eta_e = 0.75, \eta_e = 1.0$ on the same graph as shown in Fig. 4.57.

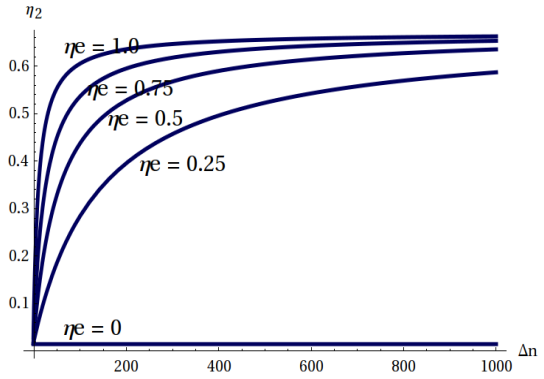

Fig. 4.57: Plot of η_2 as a function of the concentration gradient Δn in units of μM when $s = 2$, $n_c = 1.0\ \mu M$, $\eta_c = 0.5$, $\nu_e^+ = \nu_c^- = 15\,(\mu M)^{-1}s^{-1}, \nu_1^- = \nu_1^+ = 500\,s^{-1}, \nu_2^- = \nu_2^+ = 500\,s^{-1}$, $u_e^+ = 2, u_1^- = 2, u_1^+ = 2, u_2^- = 2, u_2^+ = 2, u_c^- = 2$ for five different values: $\eta_e = 0, \eta_e = 0.25, \eta_e = 0.5, \eta_e = 0.75, \eta_e = 1.0$

Using $\eta_c = 1.0$, $u_e^+ = 2, u_1^- = 2, u_1^+ = 2, u_2^- = 2, u_2^+ = 2, u_c^- = 2$ and the values of the transition rates specified in Eq. (3.14) into Eq. (4.16), we have plotted the variation of the average occupation number η_2 of the internal potential well V_2 of the nano-channel with two internal potential wells as a function of the concentration gradient Δn in units of μM for five different values of η_e, that is $\eta_e = 0, \eta_e = 0.25, \eta_e = 0.5, \eta_e = 0.75, \eta_e = 1.0$ on the same graph as shown in Fig. 4.58.

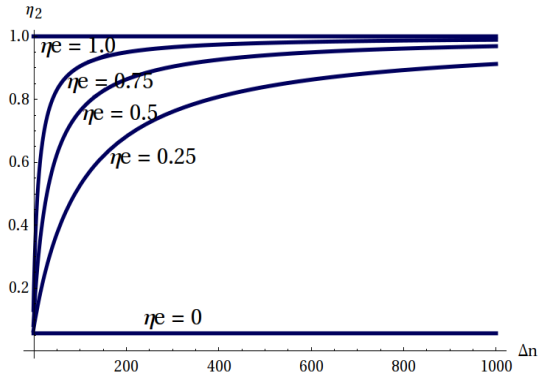

Fig. 4.58: Plot of η_2 as a function of the concentration gradient Δn in units of μM when $s = 2$, $n_c = 1.0\ \mu M$, $\eta_c = 1.0$, $\nu_e^+ = \nu_c^- = 15\,(\mu M)^{-1}s^{-1}, \nu_1^- = \nu_1^+ = 500\,s^{-1}, \nu_2^- = \nu_2^+ = 500\,s^{-1}$, $u_e^+ = 2, u_1^- = 2, u_1^+ = 2, u_2^- = 2, u_2^+ = 2, u_c^- = 2$ for five different values: $\eta_e = 0, \eta_e = 0.25, \eta_e = 0.5, \eta_e = 0.75, \eta_e = 1.0$

For the given values of η_e and η_c, the average value of the occupation number of the internal potential well V_1 of a nano-channel with two internal potential wells as a function of Δn is denoted by $\eta_{22}(\Delta n|\eta_e, \eta_c)$. The plots in Fig. 4.56 to Fig. 4.58 show that $\eta_{22}(\Delta n|\eta_e = 0, \eta_c) < \eta_{22}(\Delta n|\eta_e = 0.25, \eta_c) < \eta_{22}(\Delta n|\eta_e = 0.5, \eta_c) < \eta_{22}(\Delta n|\eta_e = 0.75, \eta_c) < \eta_{22}(\Delta n|\eta_e = 1.0, \eta_c)$ for all possible values of Δn and η_c. The average value of $\eta_{22}(\Delta n|\eta_e, \eta_c)$ assumes the values $\eta_{22}(\Delta n|\eta_e = 1.0, \eta_c = 1.0) = 1.0$ and $\eta_{22}(\Delta n|\eta_e = 0, \eta_c = 0) = 0$ for all possible values of Δn. For small values of Δn, that is, $\Delta n < 400\ \mu M$, the average value of $\eta_{22}(\Delta n|\eta_e, \eta_c)$ of the nano-channel increases very rapidly as Δn increases and then it increases slowly and finally as Δn increases to large positive values, $\eta_{22}(\Delta n|\eta_e, \eta_c)$ saturates to its maximum constant value. Moreover, for one particular given value of η_c, the average values of $\eta_{22}(\Delta n|\eta_e, \eta_c)$ associated with different values of η_e saturate to the same values. The saturation value of $\eta_{22}(\Delta n|\eta_e, \eta_c)$ and the corresponding concentration gradient where the saturation occurs are: $\eta_{22}(\Delta n \rightarrow 100\ M|\eta_e, \eta_c = 0) \rightarrow 0.5$, $\eta_{22}(\Delta n \rightarrow 85\ M|\eta_e, \eta_c = 0.5) \rightarrow 0.669967$, $\eta_{22}(\Delta n \rightarrow 40\ M|\eta_e, \eta_c = 1.0) \rightarrow 1.0$ for all possible values of $\eta_e > 0$. The average value of $\eta_{22}(\Delta n|\eta_e, \eta_c)$ with the higher value of η_e approaches its saturation value more quickly than that at a smaller value as the plots in Fig. 4.56 to Fig. 4.58 show. That is, $\eta_{22}(\Delta n|\eta_e = 1.0, \eta_c)$ saturates more quickly at a small value of Δn and $\eta_{22}(\Delta n|\eta_e = 0, \eta_c)$ saturates more slowly at large value of Δn.

Thus, as η_e increases from zero to one, the value of Δn at which $\eta_{22}(\Delta n|\eta_e, \eta_c)$ becomes saturated decreases from the largest value, which occurs when $\eta_e = 0$ to the smallest one, which occurs when $\eta_e = 1.0$. In other words, for a given value of η_c, the value of Δn at which $\eta_{22}(\Delta n|\eta_e, \eta_c)$ saturates increases as η_e decreases from one to zero. For a given value of η_c, the average value of $\eta_{22}(\Delta n|\eta_e, \eta_c)$ associated with different values of η_e converge to each other as $\Delta n \rightarrow -1.0\ \mu M$ and then diverge from each other as Δn increases to intermediate values and after that the average value of $\eta_{22}(\Delta n|\eta_e, \eta_c)$ associated with different values of η_e began to converge to each other and finally saturate to the same maximum value as Δn increases to large positive values.

Therefore, the average value of $\eta_{22}(\Delta n|\eta_e, \eta_c)$ attains its maximum value of one when $\eta_c = 1.0$ and $\eta_e = 1.0$ at very small value of Δn as shown in Fig. 4.58. Therefore, when $\eta_c = 1.0$, the mean residence time of a particle at the poten-

tial well V_c is large and as result the occupation probability of V_c is almost one. Moreover, as $\eta_e \rightarrow 1.0$, the mean residence time of a particle at the potential well V_e is large and as result the occupation probability of this site is almost one. This means that the average value of $\eta_{22}(\Delta n|\eta_e, \eta_c)$ attains its maximum value when V_c is occupied, that is $\eta_c = 1.0$, and when V_e is occupied, that is $\eta_e = 1$.

Using $\eta_e = 0$, $u_e^+ = 2, u_1^- = 2, u_1^+ = 2, u_2^- = 2, u_2^+ = 2, u_c^- = 2$ and the values of the transition rates specified in Eq. (3.14) into Eq. (4.16), we have plotted the variation of the average occupation number η_2 of the internal potential well V_2 of the nano-channel with two internal potential wells as a function of the concentration gradient Δn in units of μM for five different values of η_c, that is $\eta_c = 0, \eta_c = 0.25, \eta_c = 0.5, \eta_c = 0.75, \eta_c = 1.0$ on the same graph as shown in Fig. 4.59.

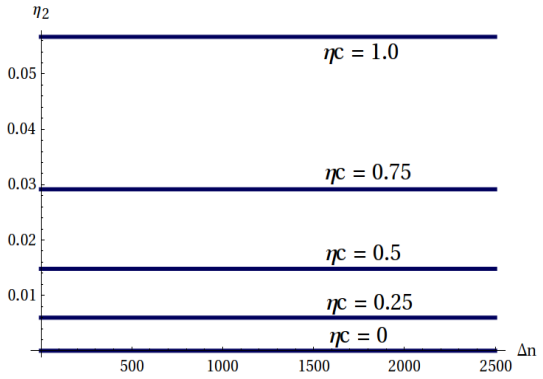

Fig. 4.59: Plot of η_2 as a function of the concentration gradient Δn in units of μM when $s = 2, n_c = 1.0\ \mu M, \eta_e = 0, \nu_e^+ = \nu_c^- = 15\,(\mu M)^{-1}s^{-1}, \nu_1^- = \nu_1^+ = 500\,s^{-1}, \nu_2^- = \nu_2^+ = 500\,s^{-1}, u_e^+ = 2, u_1^- = 2, u_1^+ = 2, u_2^- = 2, u_2^+ = 2, u_c^- = 2$ for five different values: $\eta_c = 0, \eta_c = 0.25, \eta_c = 0.5, \eta_c = 0.75, \eta_c = 1.0$

Using $\eta_e = 0.5$, $u_e^+ = 2, u_1^- = 2, u_1^+ = 2, u_2^- = 2, u_2^+ = 2, u_c^- = 2$ and the values of the transition rates specified in Eq. (3.14) into Eq. (4.16), we have plotted the variation of the average occupation number η_2 of the internal potential well V_2 of the nano-channel with two internal potential wells as a function of the concentration gradient Δn in units of μM for five different values of η_c, that is $\eta_c = 0, \eta_c = 0.25, \eta_c = 0.5, \eta_c = 0.75, \eta_c = 1.0$ on the same graph as shown in Fig. 4.60.

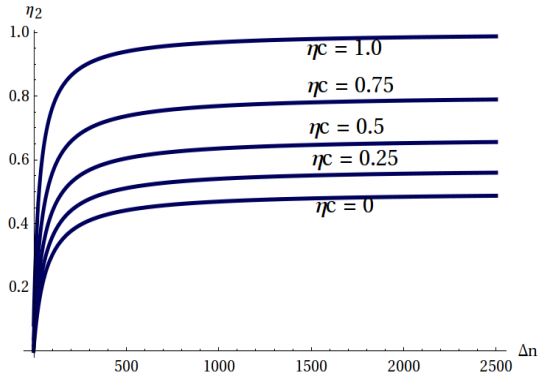

Fig. 4.60: Plot of η_2 as a function of the concentration gradient Δn in units of μM when $s = 2$, $n_c = 1.0\ \mu M$, $\eta_e = 0.5$, $\nu_e^+ = \nu_c^- = 15\,(\mu M)^{-1}s^{-1}, \nu_1^- = \nu_1^+ = 500\,s^{-1}, \nu_2^- = \nu_2^+ = 500\,s^{-1}$, $u_e^+ = 2, u_1^- = 2, u_1^+ = 2, u_2^- = 2, u_2^+ = 2, u_c^- = 2$ for five different values: $\eta_c = 0, \eta_c = 0.25, \eta_c = 0.5, \eta_c = 0.75, \eta_c = 1.0$

Using $\eta_e = 1.0$, $u_e^+ = 2, u_1^- = 2, u_1^+ = 2, u_2^- = 2, u_2^+ = 2, u_c^- = 2$ and the values of the transition rates specified in Eq. (3.14) into Eq. (4.16), we have plotted the variation of the average occupation number η_2 of the internal potential well V_2 of the nano-channel with two internal potential wells as a function of the concentration gradient Δn in units of μM for five different values of η_c, that is $\eta_c = 0, \eta_c = 0.25, \eta_c = 0.5, \eta_c = 0.75, \eta_c = 1.0$ on the same graph as shown in Fig. 4.61.

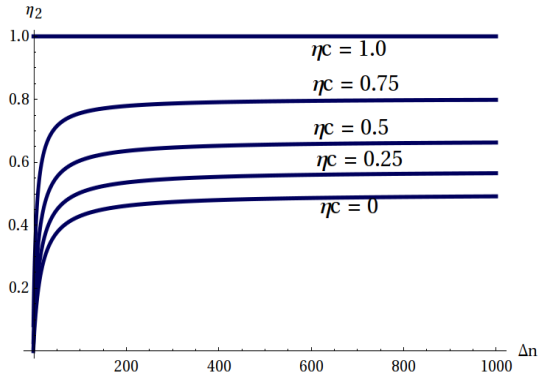

Fig. 4.61: Plot of η_2 as a function of the concentration gradient Δn in units of μM when $s = 2$, $n_c = 1.0\ \mu M$, $\eta_e = 1.0$, $\nu_e^+ = \nu_c^- = 15\,(\mu M)^{-1}s^{-1}, \nu_1^- = \nu_1^+ = 500\,s^{-1}, \nu_2^- = \nu_2^+ = 500\,s^{-1}$, $u_e^+ = 2, u_1^- = 2, u_1^+ = 2, u_2^- = 2, u_2^+ = 2, u_c^- = 2$ for five different values: $\eta_c = 0, \eta_c = 0.25, \eta_c = 0.5, \eta_c = 0.75, \eta_c = 1.0$

The plots shown in Fig. 4.59 to Fig. 4.61 imply that: $\eta_{22}(\Delta n|\eta_e, \eta_c = 0) < \eta_{22}(\Delta n|\eta_e, \eta_c = 0.25) < \eta_{22}(\Delta n|\eta_e, \eta_c = 0.5) < \eta_{22}(\Delta n|\eta_e, \eta_c = 0.75) < \eta_{22}(\Delta n|\eta_e, \eta_c = 1.0)$ for all possible values of Δn and η_e. As shown in Fig. 4.59, for the given values of η_c, the average value of $\eta_{22}(\Delta n|\eta_e = 0, \eta_c)$ as a function of Δn assumes small constant values that don't change as Δn increases in the positive direction. These small values are: $\eta_{22}(\Delta n|\eta_e = 0, \eta_c = 0) = 0$, $\eta_{22}(\Delta n|\eta_e = 0, \eta_c = 0.25) = 0.00596895$, $\eta_{22}(\Delta n|\eta_e = 0, \eta_c = 0.5) = 0.0147928$, $\eta_{22}(\Delta n|\eta_e = 0, \eta_c = 0.75) = 0.0291634$, $\eta_{22}(\Delta n|\eta_e = 0, \eta_c = 1.0) = 0.0567077$. Moreover, $\eta_{22}(\Delta n|\eta_e = 1.0, \eta_c = 1.0) = 1.0$ and $\eta_{22}(\Delta n|\eta_e = 0, \eta_c = 0) = 0$ for all possible values of Δn. Furthermore, the average value of $\eta_{22}(\Delta n|\eta_e, \eta_c)$ associated with the different values of η_c saturate to different values when η_e has different values. When $\eta_e = 0.5$, these saturation values are: $\eta_{22}(\Delta n \rightarrow 70\ M|\eta_e = 0.5, \eta_c = 0) \rightarrow 0.5$, $\eta_{22}(\Delta n \rightarrow 70\ M|\eta_e = 0.5, \eta_c = 0.25) \rightarrow 0.573257$, $\eta_{22}(\Delta n \rightarrow 70\ M|\eta_e = 0.5, \eta_c = 0.5) \rightarrow 0.669966$, $\eta_{22}(\Delta n \rightarrow 70\ M|\eta_e = 0.5, \eta_c = 0.75) \rightarrow 0.803536$, $\eta_{22}(\Delta n \rightarrow 70\ M|\eta_e = 0.5, \eta_c = 1.0) \rightarrow 1.0$. When $\eta_e = 1.0$, these saturation values are: $\eta_{22}(\Delta n \rightarrow 10\ M|\eta_e = 0.5, \eta_c = 0) \rightarrow 0.5$, $\eta_{22}(\Delta n \rightarrow 10\ M|\eta_e = 0.5, \eta_c = 0.25) \rightarrow 0.573257$, $\eta_{22}(\Delta n \rightarrow 10\ M|\eta_e = 0.5, \eta_c = 0.5) \rightarrow 0.669966$, $\eta_{22}(\Delta n \rightarrow 10\ M|\eta_e = 0.5, \eta_c = 0.75) \rightarrow 0.803536$, $\eta_{22}(\Delta n \rightarrow 10\ M|\eta_e = 0.5, \eta_c = 1.0) \rightarrow 1.0$.

For small values of Δn, that is, $\Delta n < 500\ \mu M$ when $\eta_e = 0.5$ and $\Delta n < 200\ \mu M$ when $\eta_e = 1.0$, the average value of $\eta_{22}(\Delta n|\eta_e, \eta_c)$ increases very rapidly as Δn increases and then it increases slowly and finally as Δn increases to large positive values, $\eta_{22}(\Delta n|\eta_e, \eta_c)$ saturates to different maximum values. The average value of $\eta_{22}(\Delta n|\eta_e, \eta_c)$ with the higher value of η_c approaches its saturation value more quickly than that at a smaller value as the plots in Fig. 4.59 to Fig. 4.61 show. That is, $\eta_{22}(\Delta n|\eta_e, \eta_c = 1.0)$ saturates more quickly at a small value of Δn and $\eta_{22}(\Delta n|\eta_e, \eta_c = 0)$ saturates more slowly at large value of Δn. For a given value of η_e, the average value of $\eta_{22}(\Delta n|\eta_e, \eta_c)$ associated with different values of η_e converge to each other as $\Delta n \rightarrow -1.0\ \mu M$ and then diverge from each other as Δn increases to intermediate values and after that the average value of $\eta_{22}(\Delta n|\eta_e, \eta_c)$ associated with different values of η_e become parallel to each other and saturate to different maximum values as Δn increases to large positive values. Therefore, the average value of $\eta_{22}(\Delta n|\eta_e, \eta_c)$ attains its maximum value of one when $\eta_c = 1.0$ and $\eta_e = 1.0$ at very small value of Δn as shown in Fig. 4.61.

Using $\eta_e = 0.1$, $\eta_c = 0.1$, $u_1^- = 2, u_1^+ = 2, u_2^- = 2, u_2^+ = 2, u_c^- = 2$ and the values of the transition rates specified in Eq. (3.14) into Eq. (4.16), we have plotted the variation of the average occupation number η_2 of a nano-channel with two internal potential wells as a function of concentration gradient Δn in units of μM for four different values of u_e^+, that is $u_e^+ \approx 0, u_e^+ = 1.0, u_e^+ = 2.0, u_e^+ = 3.0$ on the same graph as shown in Fig. 4.62.

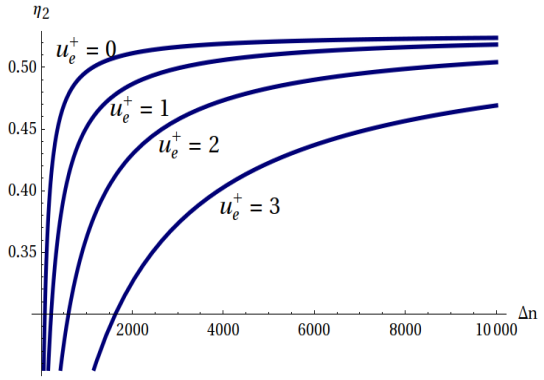

Fig. 4.62: Plot of η_2 as a function of the concentration gradient Δn in units of μM when $s = 2$, $n_c = 1.0\ \mu M$, $\eta_e = 0.1$, $\eta_c = 0.1$, $\nu_e^+ = \nu_c^- = 15\,(\mu M)^{-1}s^{-1}, \nu_1^- = \nu_1^+ = 500\,s^{-1}, \nu_2^- = \nu_2^+ = 500\,s^{-1}$, $u_1^- = 2, u_1^+ = 2, u_2^- = 2, u_2^+ = 2, u_c^- = 2$ for the values: $u_e^+ \approx 0, u_e^+ = 1.0, u_e^+ = 2.0, u_e^+ = 3.0$

The plot shown in Fig. 4.62 shows that the fluxes associated with different values of u_e^+ obey: $\eta_{22}(\Delta n|\eta_e, \eta_c, u_e^+ \approx 0) > \eta_{22}(\Delta n|\eta_e, \eta_c, u_e^+ \approx 1.0) > \eta_{22}(\Delta n|\eta_e, \eta_c, u_e^+ \approx 2.0) > \eta_{22}(\Delta n|\eta_e, \eta_c, u_e^+ \approx 3.0)$ for all possible values of Δn, η_e and η_c. Moreover, $\eta_{22}(\Delta n|\eta_e, \eta_c)$ approaches its saturation value more rapidly when $u_e^+ \approx 0$ than when $u_e^+ \approx 3.0$. The average value of $\eta_{22}(\Delta n|\eta_e, \eta_c)$ associated with the different values of u_e^+ saturate to the same maximum value: $\eta_{22}(\Delta n \to 100\ M|\eta_e = 0.1, \eta_c = 0.1, u_e^+) \to 0.527062$ for all possible values of u_e^+. Therefore, as the normalized potential barrier u_e^+ increases, the transition rate from the external potential well V_e to the internal potential well V_1 decreases and as a result the occupation probability of V_1 is small which means that the average value of $\eta_{12}(\Delta n|\eta_e, \eta_c$ decreases. Therefore, when $\eta_{12}(\Delta n|\eta_e, \eta_c$ is nearly empty, the transition rate of a particle from V_1 to V_2 is negligible and as a result the occupation probability of V_2 is small and thus the average value of $\eta_{22}(\Delta n|\eta_e, \eta_c)$ decreases as u_e^+ increases.

Using $\eta_e = 0.1$, $\eta_c = 0.1$, $u_e^+ = 2, u_1^+ = 2, u_2^- = 2, u_2^+ = 2, u_c^- = 2$ and the values of the transition rates specified in Eq. (3.14) into Eq. (4.16), we have plotted the variation of the average occupation number η_2 of a nano-channel with two internal potential wells as a function of concentration gradient Δn in units of μM for four different values of u_1^-, that is $u_1^- \approx 0, u_1^- = 1.0, u_1^- = 2.0, u_1^- = 3.0$ on the same graph as shown in Fig. 4.63.

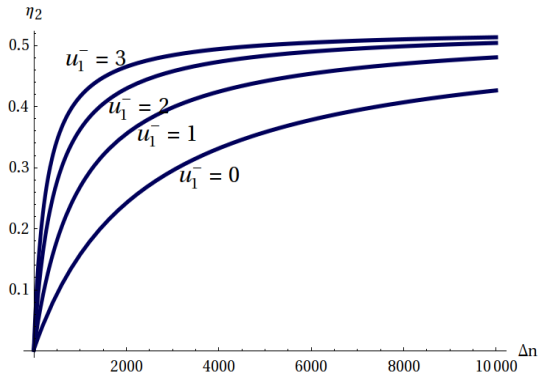

Fig. 4.63: Plot of η_2 as a function of the concentration gradient Δn in units of μM when $s = 2$, $n_c = 1.0\,\mu M$, $\eta_e = 0.1$, $\eta_c = 0.1$, $\nu_e^+ = \nu_c^- = 15\,(\mu M)^{-1}s^{-1}, \nu_1^- = \nu_1^+ = 500\,s^{-1}, \nu_2^- = \nu_2^+ = 500\,s^{-1}$, $u_e^+ = 2, u_1^+ = 2, u_2^- = 2, u_2^+ = 2, u_c^- = 2$ for the values: $u_1^- \approx 0, u_1^- = 1.0, u_1^- = 2.0, u_1^- = 3.0$

The plot shown in Fig. 4.63 shows that the fluxes associated with different values of u_1^- obey: $\eta_{22}(\Delta n|\eta_e, \eta_c, u_1^- \approx 0) < \eta_{22}(\Delta n|\eta_e, \eta_c, u_1^- \approx 1.0) < \eta_{22}(\Delta n|\eta_e, \eta_c, u_1^- \approx 2.0) < \eta_{22}(\Delta n|\eta_e, \eta_c, u_1^- \approx 3.0)$ for all possible values of Δn, η_e and η_c. Moreover, $\eta_{22}(\Delta n|\eta_e, \eta_c)$ approaches its saturation value more rapidly when $u_1^- \approx 3.0$ than when $u_1^- \approx 0$. The average value of $\eta_{22}(\Delta n|\eta_e, \eta_c)$ associated with the different values of u_1^- saturate to the same maximum value: $\eta_{22}(\Delta n \to 150\ M|\eta_e = 0.1, \eta_c = 0.1, u_1^-) \to 0.527062$ for all possible values of u_1^-. Therefore, as the normalized potential barrier u_1^- increases, the transition rate from the internal potential well V_1 to the external potential well V_e decreases and as a result the occupation probability of V_1 is large which means that the average value of $\eta_{12}(\Delta n|\eta_e, \eta_c$ is large. Therefore, when $\eta_{12}(\Delta n|\eta_e, \eta_c$ is nearly occupied, the transition rate of a particle from V_2 to V_1 is negligible as transition from V_2 to V_1 takes place as long as V_1 is empty and as a result the mean residence time of a particle in V_2 is large which implies that the occupation probability of V_2 is enhanced and thus the average value of $\eta_{22}(\Delta n|\eta_e, \eta_c)$ increases as u_1^- increases.

Using $\eta_e = 0.1$, $\eta_c = 0.1$, $u_e^+ = 2, u_1^- = 2, u_2^- = 2, u_2^+ = 2, u_c^- = 2$ and the values of the transition rates specified in Eq. (3.14) into Eq. (4.16), we have plotted the variation of the average occupation number η_2 of a nano-channel with two internal potential wells as a function of concentration gradient Δn in units of μM for four different values of u_e^+, that is $u_1^+ \approx 0, u_1^+ = 1.0, u_1^+ = 2.0, u_1^+ = 3.0$ on the same graph as shown in Fig. 4.64.

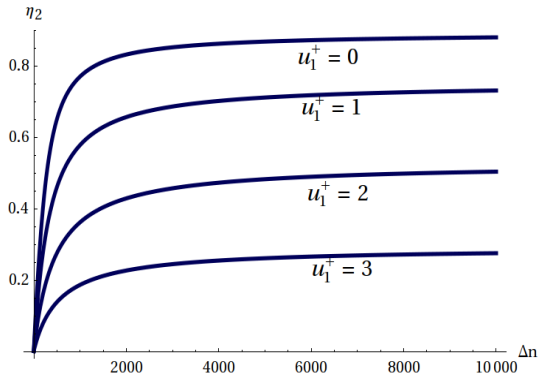

Fig. 4.64: Plot of η_2 as a function of the concentration gradient Δn in units of μM when $s = 2$, $n_c = 1.0\ \mu M$, $\eta_e = 0.1$, $\eta_c = 0.1$, $\nu_e^+ = \nu_c^- = 15\,(\mu M)^{-1}s^{-1}, \nu_1^- = \nu_1^+ = 500\,s^{-1}, \nu_2^- = \nu_2^+ = 500\,s^{-1}$, $u_e^+ = 2, u_1^- = 2, u_2^- = 2, u_2^+ = 2, u_c^- = 2$ for the values: $u_1^+ \approx 0, u_1^+ = 1.0, u_1^+ = 2.0, u_1^+ = 3.0$

The plot shown in Fig. 4.64 shows that the flux associated with different values of u_1^+ obey: $\eta_{22}(\Delta n|\eta_e, \eta_c, u_1^+ \approx 0) > \eta_{22}(\Delta n|\eta_e, \eta_c, u_1^+ \approx 1.0) > \eta_{22}(\Delta n|\eta_e, \eta_c, u_1^+ \approx 2.0) > \eta_{22}(\Delta n|\eta_e, \eta_c, u_1^+ \approx 3.0)$ for all possible values of Δn, η_e and η_c. Moreover, $\eta_{22}(\Delta n|\eta_e, \eta_c)$ approaches its saturation value more rapidly when $u_1^+ \approx 0$ than when $u_1^+ \approx 3.0$. The average value of $\eta_{22}(\Delta n|\eta_e, \eta_c)$ associated with the different values of u_1^+ saturate to different maximum values: $\eta_{22}(\Delta n \to 100\ M|\eta_e = 0.1, \eta_c = 0.1, u_1^- \approx 0) \to 0.891461$, $\eta_{22}(\Delta n \to 100\ M|\eta_e = 0.1, \eta_c = 0.1, u_1^- \approx 1.0) \to 0.751467$, $\eta_{22}(\Delta n \to 100\ M|\eta_e = 0.1, \eta_c = 0.1, u_1^- \approx 2.0) \to 0.52706$, $\eta_{22}(\Delta n \to 100\ M|\eta_e = 0.1, \eta_c = 0.1, u_1^- \approx 3.0) \to 0.291827$. Therefore, as the normalized potential barrier u_1^+ increases, the transition rate from V_1 to V_2 decreases and as a result the average value of $\eta_{22}(\Delta n|\eta_e, \eta_c$ decreases.

Using $\eta_e = 0.1$, $\eta_c = 0.1$, $u_e^+ = 2, u_1^- = 2, u_1^+ = 2, u_2^+ = 2, u_c^- = 2$ and the values of the transition rates specified in Eq. (3.14) into Eq. (4.16), we have plotted the variation of the average occupation number η_2 of a nano-channel with two in-

ternal potential wells as a function of concentration gradient Δn in units of μM for four different values of u_2^-, that is $u_2^- \approx 0, u_2^- = 1.0, u_2^- = 2.0, u_2^- = 3.0$ on the same graph as shown in Fig. 4.65.

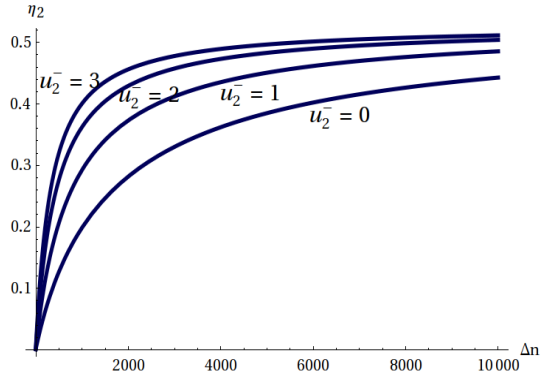

Fig. 4.65: Plot of η_2 as a function of the concentration gradient Δn in units of μM when $s = 2$, $n_c = 1.0\ \mu M$, $\eta_e = 0.1$, $\eta_c = 0.1$, $\nu_e^+ = \nu_c^- = 15\,(\mu M)^{-1}s^{-1}, \nu_1^- = \nu_1^+ = 500\,s^{-1}, \nu_2^- = \nu_2^+ = 500\,s^{-1}$, $u_e^+ = 2, u_1^- = 2, u_1^+ = 2, u_2^+ = 2, u_c^- = 2$ for the values: $u_2^- \approx 0, u_2^- = 1.0, u_2^- = 2.0, u_2^- = 3.0$

The plot shown in Fig. 4.65 shows that the fluxes associated with different values of u_2^- obey: $\eta_{22}(\Delta n|\eta_e, \eta_c, u_2^- \approx 0) < \eta_{22}(\Delta n|\eta_e, \eta_c, u_2^- \approx 1.0) < \eta_{22}(\Delta n|\eta_e, \eta_c, u_2^- \approx 2.0) < \eta_{22}(\Delta n|\eta_e, \eta_c, u_2^- \approx 3.0)$ for all possible values of Δn, η_e and η_c. Moreover, $\eta_{22}(\Delta n|\eta_e, \eta_c)$ approaches its saturation value more rapidly when $u_2^- \approx 3.0$ than when $u_2^- \approx 0$. The average value of $\eta_{22}(\Delta n|\eta_e, \eta_c)$ associated with the different values of u_2^- saturate to the same maximum value: $\eta_{22}(\Delta n \to 150\ M|\eta_e = 0.1, \eta_c = 0.1, u_2^-) \to 0.527061$ for all possible values of u_2^-. Therefore, as the normalized potential barrier u_2^- increases, the transition rate from V_2 to V_1 decreases and as a result the average value of $\eta_{22}(\Delta n|\eta_e, \eta_c$ increases.

Using $\eta_e = 0.1$, $\eta_c = 0.1$, $u_e^+ = 2, u_1^- = 2, u_1^+ = 2, u_2^- = 2, u_c^- = 2$ and the values of the transition rates specified in Eq. (3.14) into Eq. (4.16), we have plotted the variation of the average occupation number η_2 of a nano-channel with two internal potential wells as a function of concentration gradient Δn in units of μM for four different values of u_2^+, that is $u_2^+ \approx 0, u_2^+ = 1.0, u_2^+ = 2.0, u_2^+ = 3.0$ on the same graph as shown in Fig. 4.66.

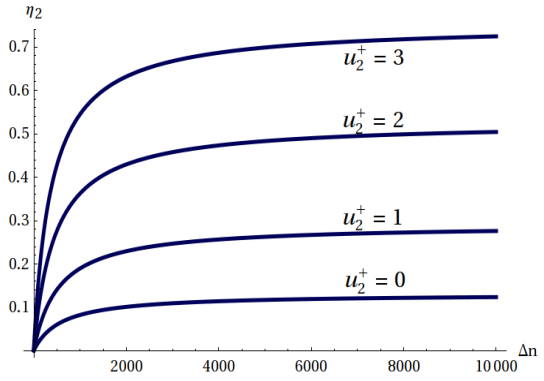

Fig. 4.66: Plot of η_2 as a function of the concentration gradient Δn in units of μM when $s = 2$, $n_c = 1.0\,\mu M$, $\eta_e = 0.1$, $\eta_c = 0.1$, $\nu_e^+ = \nu_c^- = 15\,(\mu M)^{-1}s^{-1}, \nu_1^- = \nu_1^+ = 500\,s^{-1}, \nu_2^- = \nu_2^+ = 500\,s^{-1}$, $u_e^+ = 2, u_1^- = 2, u_1^+ = 2, u_2^- = 2, u_c^- = 2$ for the values: $u_2^+ \approx 0, u_2^+ = 1.0, u_2^+ = 2.0, u_2^+ = 3.0$

The plot shown in Fig. 4.66 shows that the fluxes associated with different values of u_2^+ obey: $\eta_{22}(\Delta n|\eta_e, \eta_c, u_2^+ \approx 0) < \eta_{22}(\Delta n|\eta_e, \eta_c, u_2^+ \approx 1.0) < \eta_{22}(\Delta n|\eta_e, \eta_c, u_2^+ \approx 2.0) < \eta_{22}(\Delta n|\eta_e, \eta_c, u_2^+ \approx 3.0)$ for all possible values of Δn, η_e and η_c. Moreover, $\eta_{22}(\Delta n|\eta_e, \eta_c)$ approaches its saturation value more rapidly when $u_2^+ \approx 0$ than when $u_2^+ \approx 3.0$. The average value of $\eta_{22}(\Delta n|\eta_e, \eta_c)$ associated with the different values of u_2^+ saturate to different maximum values: $\eta_{22}(\Delta n \to 150\ M|\eta_e = 0.1, \eta_c = 0.1, u_2^+ \approx 0) \to 0.131057$, $\eta_{22}(\Delta n \to 150\ M|\eta_e = 0.1, \eta_c = 0.1, u_2^+ \approx 1.0) \to 0.29077$, $\eta_{22}(\Delta n \to 150\ M|\eta_e = 0.1, \eta_c = 0.1, u_2^+ \approx 2.0) \to 0.527061$, $\eta_{22}(\Delta n \to 150\ M|\eta_e = 0.1, \eta_c = 0.1, u_2^+ \approx 3.0) \to 0.751821$. Therefore, as the normalized potential barrier u_2^+ increases, the transition rate from V_2 to V_c decreases and as a result the average value of $\eta_{22}(\Delta n|\eta_e, \eta_c$ increases.

Using $\eta_e = 0.1$, $\eta_c = 0.1$, $u_e^+ = 2, u_1^- = 2, u_1^+ = 2, u_2^- = 2, u_2^+ = 2$ and the values of the transition rates specified in Eq. (3.14) into Eq. (4.16), we have plotted the variation of the average occupation number η_2 of a nano-channel with two internal potential wells as a function of concentration gradient Δn in units of μM for four different values of u_c^-, that is $u_c^- \approx 0, u_c^- = 1.0, u_c^- = 2.0, u_c^- = 3.0$ on the same graph as shown in Fig. 4.67. The average value of $\eta_{22}(\Delta n|\eta_e, \eta_c, u_c^-)$ associated with different values of u_c^- assume the same value for all possible values of Δn.

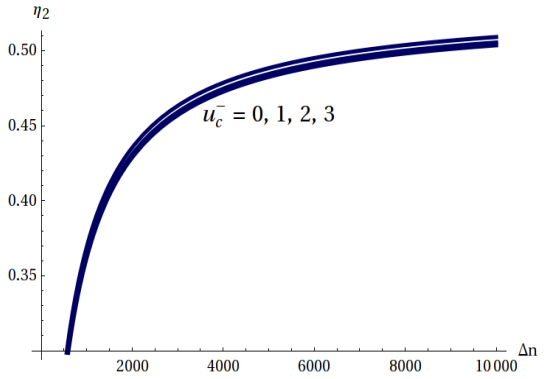

Fig. 4.67: Plot of η_2 as a function of the concentration gradient Δn in units of μM when $s = 2$, $n_c = 1.0\ \mu M$, $\eta_e = 0.1$, $\eta_c = 0.1$, $\nu_e^+ = \nu_c^- = 15\,(\mu M)^{-1}s^{-1}, \nu_1^- = \nu_1^+ = 500\,s^{-1}, \nu_2^- = \nu_2^+ = 500\,s^{-1}$, $u_e^+ = 2, u_1^- = 2, u_1^+ = 2, u_2^- = 2, u_2^+ = 2$ for the values: $u_c^- \approx 0, u_c^- = 1.0, u_c^- = 2.0, u_c^- = 3.0$

4.4.2.2 The Average Occupation Number of the Internal Potential Well V_2 of a Nano-Channel as a Function of the Occupation Number of the external Potential Wells when the Potential Barriers are Twice of Thermal Energy

Using the positive concentration gradient $\Delta n = 10000\ \mu M$ and the values of the transition rates specified in Eq. (3.14) into Eq. (4.16), we have plotted the variation of the average occupation number η_2 of the internal potential well V_2 of the nano-channel with two internal potential wells as a function of η_c for five possible values of η_e, that is $\eta_e = 0, \eta_e = 0.25, \eta_e = 0.5, \eta_e = 0.75, \eta_e = 1.0$ on the same graph as shown in Fig. 4.68.

When $\Delta n = 400\ \mu M$, the plot in Fig. 4.69 show that the average value of $\eta_{22}(\Delta n|\eta_e, \eta_c)$ as a function of η_c obey that: $\eta_{22}(\Delta n = 400\ \mu M|\eta_e = 1.0, \eta_c) > \eta_{22}(\Delta n = 400\ \mu M|\eta_e = 0.75, \eta_c) > \eta_{22}(\Delta n = 400\ \mu M|\eta_e = 0.5, \eta_c) > \eta_{22}(\Delta n = 400\ \mu M|\eta_e = 0.25, \eta_c) > \eta_{22}(\Delta n = 400\ \mu M|\eta_e = 0, \eta_c)$ for all possible values of η_c. The average value of $\eta_{22}(\Delta n = 10000\ \mu M|\eta_e, \eta_c)$ associated with the different values of η_e coincide with each other and assume the same value for all possible values of η_c as shown in Fig. 4.68. The average value of $\eta_{22}(\Delta n|\eta_e, \eta_c)$ associated with the different values of η_e increase very slowly as η_c increases from zero to one for all possible values of Δn and η_e. As η_e becomes slightly greater than zero, the average value of $\eta_{22}(\Delta n = 400\ \mu M|\eta_e, \eta_c)$ jumps rapidly to slightly different values that are closer to one and are almost parallel to each other as shown in

Fig. 4.69.

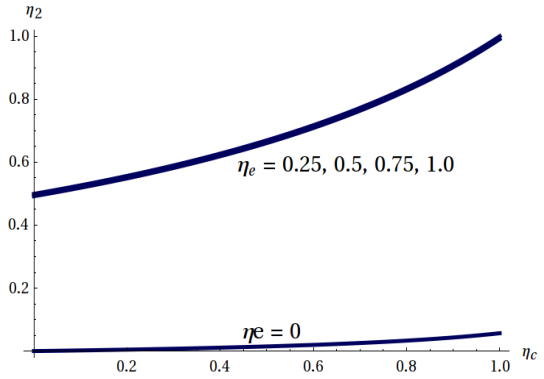

Fig. 4.68: Plot of η_2 as a function of η_c when $s = 2$, $\Delta n = 10000\ \mu M$, $n_c = 1.0 \mu M$, $\nu_e^+ = \nu_c^- = 15\,(\mu M)^{-1} s^{-1}, \nu_1^- = \nu_1^+ = 500\,s^{-1}, \nu_2^- = \nu_2^+ = 500\,s^{-1}$, $u_e^+ = 2, u_1^- = 2, u_1^+ = 2, u_2^- = 2, u_2^+ = 2, u_c^- = 2$ for five values of η_e, that is: $\eta_e = 0, \eta_e = 0.25, \eta_e = 0.5, \eta_e = 0.75, \eta_e = 1.0$

Using the positive concentration gradient $\Delta n = 400\ \mu M$ and the values of the transition rates specified in Eq. (3.14) into Eq. (4.16), we have plotted the variation of the average occupation number η_2 of the internal potential well V_2 of the nano-channel with two internal potential wells as a function of η_c for five possible values of η_e, that is $\eta_e = 0, \eta_e = 0.25, \eta_e = 0.5, \eta_e = 0.75, \eta_e = 1.0$ on the same graph as shown in Fig. 4.69.

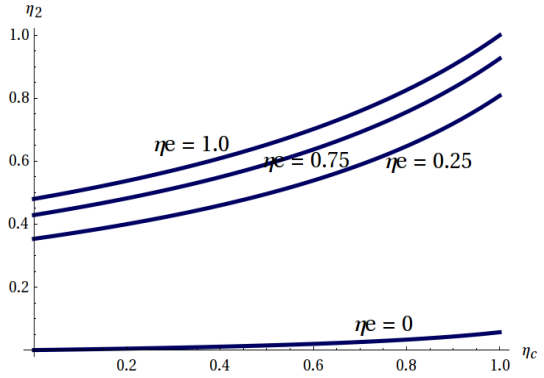

Fig. 4.69: Plot of η_2 as a function of η_c when $s = 2$, $\Delta n = 400\ \mu M$, $n_c = 1.0 \mu M$, $\nu_e^+ = \nu_c^- = 15\,(\mu M)^{-1} s^{-1}, \nu_1^- = \nu_1^+ = 500\,s^{-1}, \nu_2^- = \nu_2^+ = 500\,s^{-1}$, $u_e^+ = 2, u_1^- = 2, u_1^+ = 2, u_2^- = 2, u_2^+ = 2, u_c^- = 2$ for five values of η_e, that is: $\eta_e = 0, \eta_e = 0.25, \eta_e = 0.5, \eta_e = 0.75, \eta_e = 1.0$

Using zero concentration gradient $\Delta n = 0$ and the values of the transition rates

specified in Eq. (3.14) into Eq. (4.16), we have plotted the variation of the average occupation number η_2 of the internal potential well V_2 of the nano-channel with two internal potential wells as a function of η_c for five possible values of η_e, that is $\eta_e = 0, \eta_e = 0.25, \eta_e = 0.5, \eta_e = 0.75, \eta_e = 1.0$ on the same graph as shown in Fig. 4.70.

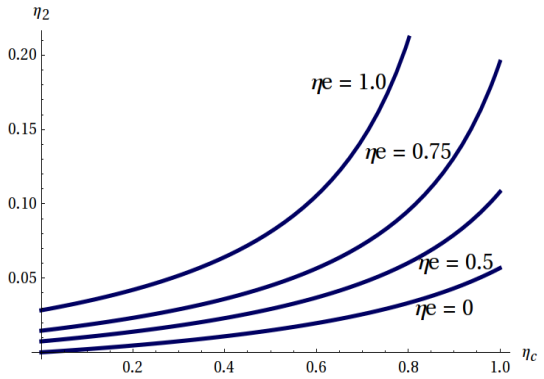

Fig. 4.70: Plot of η_2 as a function of η_c when $s = 2$, $\Delta n = 0$, $n_c = 1.0\ \mu M$, $\nu_e^+ = \nu_c^- = 15\,(\mu M)^{-1}s^{-1}, \nu_1^- = \nu_1^+ = 500\,s^{-1}, \nu_2^- = \nu_2^+ = 500\,s^{-1}$, $u_e^+ = 2, u_1^- = 2, u_1^+ = 2, u_2^- = 2, u_2^+ = 2, u_c^- = 2$ for five values of η_e, that is: $\eta_e = 0, \eta_e = 0.25, \eta_e = 0.5, \eta_e = 0.75, \eta_e = 1.0$

When $\Delta n = 0$, the average value of $\eta_{22}(\Delta n|\eta_e, \eta_c)$ as a function of η_c obey that: $\eta_{22}(\Delta n = 0|\eta_e = 1.0, \eta_c) > \eta_{22}(\Delta n = 0|\eta_e = 0.75, \eta_c) > \eta_{22}(\Delta n = 0|\eta_e = 0.5, \eta_c) > \eta_{22}(\Delta n = 0|\eta_e = 0.25, \eta_c) > \eta_{22}(\Delta n = 0|\eta_e = 0, \eta_c)$. The average value of $\eta_{22}(\Delta n|\eta_e, \eta_c)$ approach to different minimum values as $\eta_c \to 0$, that is, $\eta_{22}(\Delta n = 0|\eta_e = 0, \eta_c \to 0) \to 0$, $\eta_{22}(\Delta n = 0|\eta_e = 0.25, \eta_c \to 0) \to 0.00298389$, $\eta_{22}(\Delta n = 0|\eta_e = 0.5, \eta_c \to 0) \to 0.00739286$, $\eta_{22}(\Delta n = 0|\eta_e = 0.75, \eta_c \to 0) \to 0.0145681$, $\eta_{22}(\Delta n = 0|\eta_e = 1.0, \eta_c \to 0) \to 0.0283034$. Moreover, the average value of $\eta_{22}(\Delta n|\eta_e, \eta_c)$ as a function of η_c approach to different maximum values as $\eta_c \to 1.0$, that is, $\eta_{22}(\Delta n = 0|\eta_e = 0, \eta_c \to 1.0) \to 0.0567077$, $\eta_{12}(\Delta n = 0|\eta_e = 0.25, \eta_c \to 1.0) \to 0.074464$, $\eta_{22}(\Delta n = 0|\eta_e = 0.5, \eta_c \to 1.0) \to 0.108042$, $\eta_{12}(\Delta n = 0|\eta_e = 0.75, \eta_c \to 1.0) \to 0.195585$, $\eta_{12}(\Delta n = 0|\eta_e = 1.0, \eta_c \to 1.0) \to 1.0$.

Using the negative concentration gradient $\Delta n = -1.0\ \mu M$ and the values of the transition rates specified in Eq. (3.14) into Eq. (4.16), we have plotted the variation of the average occupation number η_2 of the internal potential well V_2 of the nano-channel with two internal potential wells as a function of η_c for five possible values of η_e, that is $\eta_e = 0, \eta_e = 0.25, \eta_e = 0.5, \eta_e = 0.75, \eta_e = 1.0$ on the

same graph as shown in Fig. 4.71.

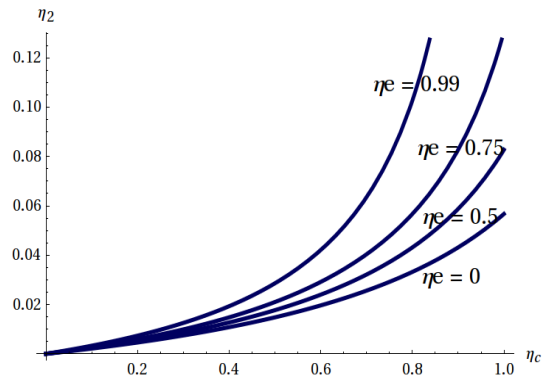

Fig. 4.71: Plot of η_2 as a function of η_c when $s = 2$, $\Delta n = -1.0\ \mu M$, $n_c = 1.0\mu M$, $\nu_e^+ = \nu_c^- = 15\,(\mu M)^{-1}s^{-1}, \nu_1^- = \nu_1^+ = 500\,s^{-1}, \nu_2^- = \nu_2^+ = 500\,s^{-1}$, $u_e^+ = 2, u_1^- = 2, u_1^+ = 2, u_2^- = 2, u_2^+ = 2, u_c^- = 2$ for five values of η_e, that is: $\eta_e = 0, \eta_e = 0.25, \eta_e = 0.5, \eta_e = 0.75, \eta_e = 1.0$

When $\Delta n = -1.0\ \mu M$, the average occupation number $\eta_{22}(\Delta n|\eta_e, \eta_c)$ as a function of η_c obey that $\eta_{22}(\Delta n = -1.0\ \mu M|\eta_e = 0.99, \eta_c) > \eta_{22}(\Delta n = -1.0\ \mu M|\eta_e = 0.75, \eta_c) > \eta_{22}(\Delta n = -1.0\ \mu M|\eta_e = 0.5, \eta_c) > \eta_{22}(\Delta n = -1.0\ \mu M|\eta_e = 0, \eta_c)$. The average value of $\eta_{22}(\Delta n|\eta_e, \eta_c)$ approach to the same minimum zero value as $\eta_c \to 0$. Moreover, the average value of $\eta_{22}(\Delta n|\eta_e, \eta_c)$ approach to different maximum values as $\eta_c \to 1.0$, that is, $\eta_{12}(\Delta n = -1.0\ \mu M|\eta_e = 0, \eta_c \to 1.0) \to 0.0282988$, $\eta_1(\Delta n = -1.0\ \mu M|\eta_e = 0.5, \eta_c \to 1.0) \to 0.0373785$, $\eta_1(\Delta n = -1.0\ \mu M|\eta_e = 0.5, \eta_c \to 1.0) \to 0.0550373$, $\eta_1(\Delta n = -1.0\ \mu M|\eta_e = 0.75, \eta_c \to 1.0) \to 0.104323$, $\eta_1(\Delta n = -1.0\ \mu M|\eta_e = 1.0, \eta_c \to 1.0) \to 0.74413$.

Using the positive concentration gradient $\Delta n = 2500\ \mu M$, $u_e^+ = 2, u_1^- = 2, u_1^+ = 2, u_2^- = 2, u_2^+ = 2, u_c^- = 2$ and the values of the transition rates specified in Eq. (3.14) into Eq. (4.16), we have plotted the variation of the average occupation number η_2 of the internal potential well V_2 of the nano-channel with two internal potential wells as a function of η_e for five possible values of η_c, that is $\eta_c = 0, \eta_c = 0.25, \eta_c = 0.5, \eta_c = 0.75, \eta_c = 1.0$ on the same graph as shown in Fig. 4.72.

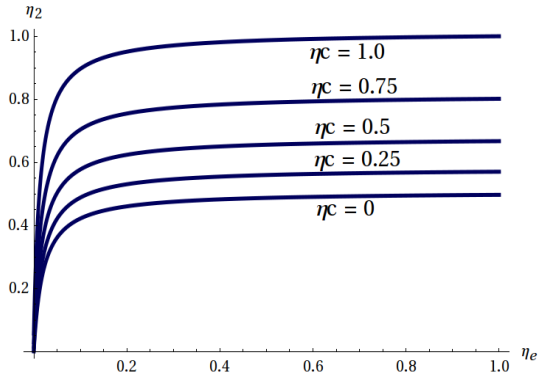

Fig. 4.72: Plot of η_2 as a function of η_e when $s = 2$, $\Delta n = 2500\ \mu M$, $n_c = 1.0\ \mu M$, $\nu_e^+ = \nu_c^- = 15\,(\mu M)^{-1}s^{-1}, \nu_1^- = \nu_1^+ = 500\,s^{-1}, \nu_2^- = \nu_2^+ = 500\,s^{-1}$, $u_e^+ = 2, u_1^- = 2, u_1^+ = 2, u_2^- = 2, u_2^+ = 2, u_c^- = 2$ for the values of η_c, that is: $\eta_c = 0, \eta_c = 0.25, \eta_c = 0.5, \eta_c = 0.75, \eta_c = 1.0$

Using the positive concentration gradient $\Delta n = 35\ \mu M$ and the values of the transition rates specified in Eq. (3.14) into Eq. (4.16), we have plotted the variation of the average occupation number η_2 of the internal potential well V_2 of the nano-channel with two internal potential wells as a function of η_e for five possible values of η_c, that is $\eta_c = 0, \eta_c = 0.25, \eta_c = 0.5, \eta_c = 0.75, \eta_c = 1.0$ on the same graph as shown in Fig. 4.73.

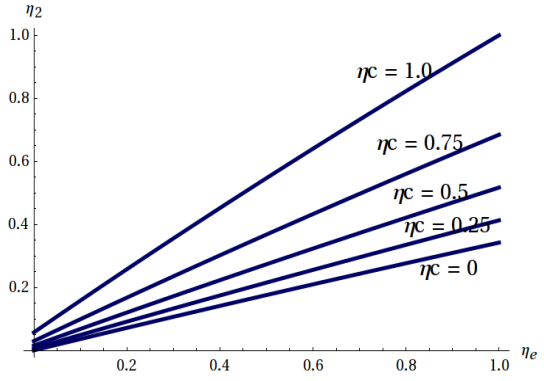

Fig. 4.73: Plot of η_2 as a function of η_e when $s = 2$, $\Delta n = 35\ \mu M$, $n_c = 1.0\ \mu M$, $\nu_e^+ = \nu_c^- = 15\,(\mu M)^{-1}s^{-1}, \nu_1^- = \nu_1^+ = 500\,s^{-1}, \nu_2^- = \nu_2^+ = 500\,s^{-1}$, $u_e^+ = 2, u_1^- = 2, u_1^+ = 2, u_2^- = 2, u_2^+ = 2, u_c^- = 2$ for the five values of η_c, that is: $\eta_c = 0, \eta_c = 0.25, \eta_c = 0.5, \eta_c = 0.75, \eta_c = 1.0$

The plots in Fig. 4.72 and Fig. 4.73 show that the average value of $\eta_{22}(\Delta n|\eta_e, \eta_c)$ as a function of η_e obey that: $\eta_{22}(\Delta n|\eta_e, \eta_c = 1.0) > \eta_{22}(\Delta n|\eta_e, \eta_c = 0.75) >$

$\eta_{22}(\Delta n|\eta_e, \eta_c = 0.5) > \eta_{22}(\Delta n|\eta_e, \eta_c = 0.25) > \eta_{22}(\Delta n|\eta_e, \eta_c = 0)$ for all possible values of Δn and η_e. For a given value of $\Delta n = 2500\ \mu M$ and η_c, the average value of $\eta_{22}(\Delta n|\eta_e, \eta_c)$ increases as the average value of η_e increases. The average value of $\eta_{22}(\Delta n = 2500\ \mu M|\eta_e, \eta_c)$ converge to each other and assume nearly the same zero value as $\eta_e \to 0$, that is, $\eta_{22}(\Delta n = 2500\ \mu M|\eta_e \to 0, \eta_c) \to 0$ for all possible values of η_c. The average values of $\eta_{22}(\Delta n = 2500\ \mu M|\eta_e, \eta_c)$ increase rapidly as η_e increases, particularly in the small range $0 < \eta_e < 0.2$, and after that the average value of $\eta_{22}(\Delta n = 2500\ \mu M|\eta_e, \eta_c)$ become constant and saturate to the different maximum values, which are parallel to each other as shown in Fig. 4.72. As $\eta_e \to 1.0$, the $\eta_{22}(\Delta n = 2500\ \mu M|\eta_e, \eta_c)$ approach to the different saturation values, which are given by, $\eta_{22}(\Delta n = 2500\ \mu M|\eta_e \to 1.0, \eta_c = 0) \to 0.496693$, $\eta_{22}(\Delta n = 2500\ \mu M|\eta_e \to 1.0, \eta_c = 0.25) \to 0.570043$, $\eta_{22}(\Delta n = 2500\ \mu M|\eta_e \to 1.0, \eta_c = 0.5) \to 0.667081$, $\eta_{22}(\Delta n = 2500\ \mu M|\eta_e \to 1.0, \eta_c = 0.75) \to 0.801488$, $\eta_{22}(\Delta n = 2500\ \mu M|\eta_e \to 1.0, \eta_c = 1.0) \to 1.0$. Moreover, when $\Delta n = 35\ \mu M$, the average value of $\eta_{22}(\Delta n|\eta_e, \eta_c)$ increases linearly as η_e increases for each possible value of η_c as shown in Fig. 4.73.

Using zero concentration gradient $\Delta n = 0$ and the values of the transition rates specified in Eq. (3.14) into Eq. (4.16), we have plotted the variation of the average occupation number η_2 of the internal potential well V_2 of the nanochannel with two internal potential wells as a function of η_e for five possible values of η_c, that is $\eta_c = 0, \eta_c = 0.25, \eta_c = 0.5, \eta_c = 0.75, \eta_c = 1.0$ on the same graph as shown in Fig. 4.74.

When $\Delta n = 0$, the plots in Fig. 4.74 show that the average value of $\eta_{22}(\Delta n|\eta_e, \eta_c)$ as a function of η_e obey that: $\eta_{22}(\Delta n = 0|\eta_e, \eta_c = 1.0) > \eta_{22}(\Delta n = 0|\eta_e, \eta_c = 0.75) > \eta_{22}(\Delta n = 0|\eta_e, \eta_c = 0.5) > \eta_{22}(\Delta n = 0|\eta_e, \eta_c = 0.25) > \eta_{22}(\Delta n = 0|\eta_e, \eta_c = 0)$. The average value of $\eta_{22}(\Delta n|\eta_e, \eta_c)$ approach to different minimum values as $\eta_e \to 0$, that is, $\eta_{22}(\Delta n = 0|\eta_e \to 0, \eta_c = 0) \to 0$, $\eta_{22}(\Delta n = 0|\eta_e \to 0, \eta_c = 0.25) \to 0.00596895$, $\eta_{22}(\Delta n = 0|\eta_e \to 0, \eta_c = 0.5) \to 0.0147928$, $\eta_{22}(\Delta n = 0|\eta_e \to 0, \eta_c = 0.75) \to 0.0291634$, $\eta_{22}(\Delta n = 0|\eta_e \to 0, \eta_c = 1.0) \to 0.0567077$. Moreover, the average value of $\eta_{22}(\Delta n|\eta_e, \eta_c)$ approach to different maximum values as $\eta_e \to 1.0$, that is, $\eta_{22}(\Delta n = 0|\eta_e \to 0, \eta_c = 0) \to 0.0283034$, $\eta_{22}(\Delta n = 0|\eta_e \to 0, \eta_c = 0.25) \to 0.0465643$, $\eta_{22}(\Delta n = 0|\eta_e \to 0, \eta_c = 0.5) \to 0.0811033$, $\eta_{22}(\Delta n = 0|\eta_e \to 0, \eta_c = 0.75) \to 0.171186$, $\eta_{22}(\Delta n = 0|\eta_e \to 0, \eta_c = 1.0) \to 1.0$.

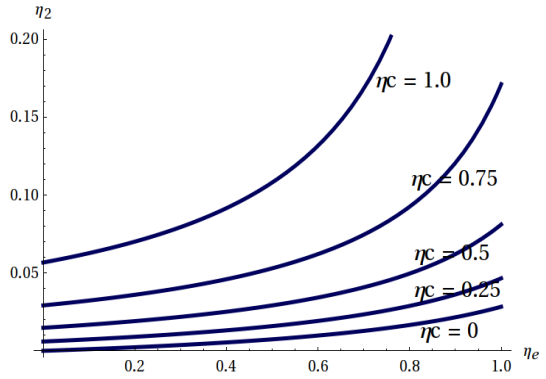

Fig. 4.74: Plot of η_2 as a function of η_e when $s = 2$, $\Delta n = 0$, $n_c = 1.0\ \mu M$, $\nu_e^+ = \nu_c^- = 15\,(\mu M)^{-1}s^{-1}, \nu_1^- = \nu_1^+ = 500\,s^{-1}, \nu_2^- = \nu_2^+ = 500\,s^{-1}$, $u_e^+ = 2, u_1^- = 2, u_1^+ = 2, u_2^- = 2, u_2^+ = 2, u_c^- = 2$ for five values of η_c, that is: $\eta_c = 0, \eta_c = 0.25, \eta_c = 0.5, \eta_c = 0.75, \eta_c = 1.0$

Using negative concentration gradient $\Delta n = -1.0\ \mu M$ and the values of the transition rates specified in Eq. (3.14) into Eq. (4.16), we have plotted the variation of the average occupation number η_2 of the internal potential well V_2 of the nano-channel with two internal potential wells as a function of η_e for five possible values of η_c, that is $\eta_c = 0, \eta_c = 0.25, \eta_c = 0.5, \eta_c = 0.75, \eta_c = 1.0$ on the same graph as shown in Fig. 4.75.

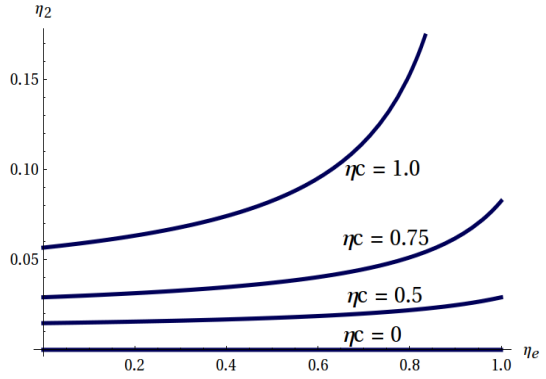

Fig. 4.75: Plot of η_2 as a function of η_c when $s = 2$, $\Delta n = -1.0\ \mu M$, $n_c = 1.0\ \mu M$, $\nu_e^+ = \nu_c^- = 15\,(\mu M)^{-1}s^{-1}, \nu_1^- = \nu_1^+ = 500\,s^{-1}, \nu_2^- = \nu_2^+ = 500\,s^{-1}$, $u_e^+ = 2, u_1^- = 2, u_1^+ = 2, u_2^- = 2, u_2^+ = 2, u_c^- = 2$ for five values of η_e, that is: $\eta_e = 0, \eta_e = 0.25, \eta_e = 0.5, \eta_e = 0.75, \eta_e = 1.0$

When $\Delta n = -1.0\ \mu M$, the plots in Fig. 4.75 show that the average value of $\eta_{22}(\Delta n|\eta_e, \eta_c)$ as a function of η_e obey that: $\eta_{22}(\Delta n = -1.0\ \mu M|\eta_e, \eta_c = 1.0) >$

$\eta_{22}(\Delta n = -1.0\ \mu M|\eta_e, \eta_c = 0.75) > \eta_{22}(\Delta n = -1.0\ \mu M|\eta_e, \eta_c = 0.5) > \eta_{22}(\Delta n = -1.0\ \mu M|\eta_e, \eta_c = 0.25) > \eta_{22}(\Delta n = -1.0\ \mu M|\eta_e, \eta_c = 0)$. We see that $\eta_{22}(\Delta n|\eta_e, \eta_c)$ approach to different minimum values as $\eta_e \to 0$, that is, $\eta_{22}(\Delta n = -1.0\,\mu M|\eta_e \to 0, \eta_c = 0) \to$, $\eta_{22}(\Delta n = -1.0\ \mu M|\eta_e \to 0, \eta_c = 0.25) \to$, $\eta_{22}(\Delta n = -1.0\ \mu M|\eta_e \to 0, \eta_c = 0.5) \to$, $\eta_{22}(\Delta n = -1.0\ \mu M|\eta_e \to 0, \eta_c = 0.75) \to$, $\eta_{22}(\Delta n = -1.0\ \mu M|\eta_e \to 0, \eta_c = 1.0) \to$. Moreover, $\eta_{22}(\Delta n|\eta_e, \eta_c)$ approach to different maximum values as $\eta_e \to 1.0$, that is, $\eta_{22}(\Delta n = -1.0\,\mu M|\eta_e \to 1.0, \eta_c = 0) \to$, $\eta_{22}(\Delta n = -1.0\ \mu M|\eta_e \to 1.0, \eta_c = 0.25) \to$, $\eta_{22}(\Delta n = -1.0\ \mu M|\eta_e \to 1.0, \eta_c = 0.5) \to$, $\eta_{22}(\Delta n = -1.0\ \mu M|\eta_e \to 1.0, \eta_c = 0.75) \to$, $\eta_{22}(\Delta n = -1.0\ \mu M|\eta_e \to 1.0, \eta_c = 1.0) \to$.

Using $\eta_e = 0$, $u_e^+ = 2, u_1^- = 2, u_1^+ = 2, u_2^- = 2, u_2^+ = 2, u_c^- = 2$ and the values of the transition rates specified in Eq. (3.14) into Eq. (4.16), we have plotted the variation of the average occupation number η_2 of the internal potential well V_2 of a nano-channel with two internal potential wells as a function of η_c for five different values of the concentration gradient Δn in units of μM, that is $\Delta n = -0.99, \Delta n = 0, \Delta n = 35, \Delta n = 100, \Delta n = 500, \Delta n = 1000$ on the same graph as shown in Fig. 4.76.

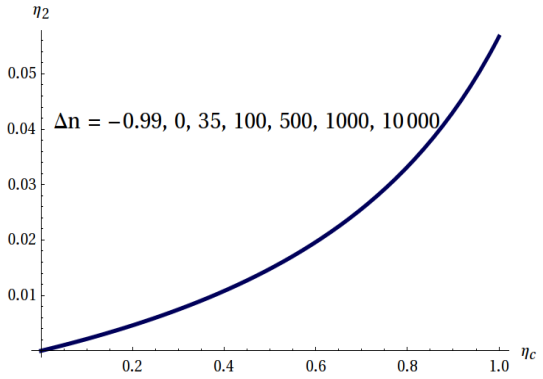

Fig. 4.76: Plot of η_2 as a function of η_c when $s = 2$, $n_c = 1.0\ \mu M$, $\eta_e = 0$, $\nu_e^+ = \nu_c^- = 15\,(\mu M)^{-1}s^{-1}, \nu_1^- = \nu_1^+ = 500\,s^{-1}, \nu_2^- = \nu_2^+ = 500\,s^{-1}$, $u_e^+ = 2, u_1^- = 2, u_1^+ = 2, u_2^- = 2, u_2^+ = 2, u_c^- = 2$ for the values of Δn in units of μM: $\Delta n = -0.99, \Delta n = 0, \Delta n = 35, \Delta n = 100, \Delta n = 500, \Delta n = 1000$

Using $\eta_e = 0.1$,$u_e^+ = 2, u_1^- = 2, u_1^+ = 2, u_2^- = 2, u_2^+ = 2, u_c^- = 2$ and the values of the transition rates specified in Eq. (3.14) into Eq. (4.16), we have plotted the variation of the average occupation number η_2 of the internal potential well V_2 of a nano-channel with two internal potential wells as a function of η_c

for five different values of the concentration gradient Δn in units of μM, that is $\Delta n = -0.99, \Delta n = 0, \Delta n = 35, \Delta n = 100, \Delta n = 500, \Delta n = 1000$ on the same graph as shown in Fig. 4.77.

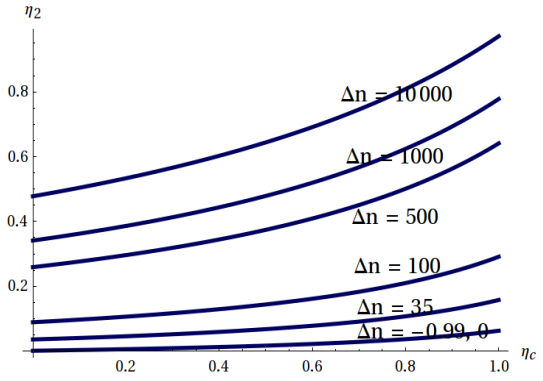

Fig. 4.77: Plot of η_2 as a function of η_c when $s = 2$, $n_c = 1.0\ \mu M$, $\eta_e = 0.1$, $\nu_e^+ = \nu_c^- = 15\,(\mu M)^{-1}s^{-1}, \nu_1^- = \nu_1^+ = 500\,s^{-1}, \nu_2^- = \nu_2^+ = 500\,s^{-1}$, $u_e^+ = 2, u_1^- = 2, u_1^+ = 2, u_2^- = 2, u_2^+ = 2, u_c^- = 2$ for the values of Δn in units of μM: $\Delta n = -0.99, \Delta n = 0, \Delta n = 35, \Delta n = 100, \Delta n = 500, \Delta n = 1000$

The average value of $\eta_{22}(\Delta n|\eta_e, \eta_c)$ as a function of η_c associated with different values of Δn coincide with each other in the entire range $0 \leq \eta_c \leq 1.0$ when $\eta_e = 0$ and increase rapidly to its maximum value $\eta_{22}(\Delta n|\eta_e, \eta_c) = 0.0567077$ as $\eta_c = 1.0$ as shown in Fig. 4.76. The average value of $\eta_{22}(\Delta n|\eta_e, \eta_c)$ associated with different values of Δn separate from each other as η_e increases to values $\eta_e \to 0.1$ and increase slowly to their maximum values as η_c increases as shown in Fig. 4.76 to Fig. 4.78. Finally when $\eta_e \to 1.0$, the average value of $\eta_{22}(\Delta n|\eta_e, \eta_c)$ associated with different values of Δn approach to different values as $\eta_c \to 0$, that is, $\eta_{22}(\Delta n = -0.99\ \mu M|\eta_e = 1.0, \eta_c \to 0) \to 0.00029982$, $\eta_{22}(\Delta n = 0|\eta_e = 1.0, \eta_c \to 0) \to 0.0283034$, $\eta_{22}(\Delta n = 35\ \mu M|\eta_e = 1.0, \eta_c \to 0) \to 0.341846$, $\eta_{12}(\Delta n = 100\ \mu M|\eta_e = 1.0, \eta_c \to 0) \to 0.429231$, $\eta_{22}(\Delta n = 500\ \mu M|\eta_e = 1.0, \eta_c \to 0) \to 0.483917$, $\eta_1(\Delta n = 1000\ \mu M|\eta_e = 1.0, \eta_c \to 0) \to 0.491819$ and $\eta_{22}(\Delta n = 10000\ \mu M|\eta_e = 1.0, \eta_c \to 0) \to 0.499169$. As η_c increases the average values of $\eta_{22}(\Delta n|\eta_e, \eta_c)$ associated with different values of Δn approach to each other and finally all of them converge to the same saturation value of $\eta_{22}(\Delta n|\eta_e = 1.0, \eta_c) \to 1.0$ as $\eta_c \to 1.0$ as shown in Fig. 4.78.

Using $\eta_e = 1.0$, $u_e^+ = 2, u_1^- = 2, u_1^+ = 2, u_2^- = 2, u_2^+ = 2, u_c^- = 2$ and the values of the transition rates specified in Eq. (3.14) into Eq. (4.16), we have plot-

ted the variation of the average occupation number η_2 of the internal potential well V_2 of a nano-channel with two internal potential wells as a function of η_c for five different values of the concentration gradient Δn in units of μM, that is $\Delta n = -0.99, \Delta n = 0, \Delta n = 50, \Delta n = 100, \Delta n = 500, \Delta n = 1000$ on the same graph as shown in Fig. 4.78.

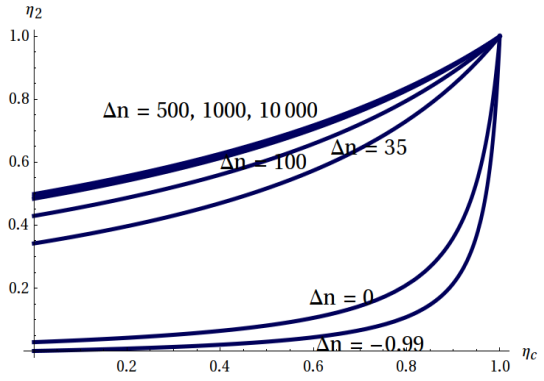

Fig. 4.78: Plot of η_2 as a function of η_c when $s = 2$, $n_c = 1.0\ \mu M$, $\eta_e = 1.0$, $\nu_e^+ = \nu_c^- = 15\,(\mu M)^{-1}s^{-1}, \nu_1^- = \nu_1^+ = 500\,s^{-1}, \nu_2^- = \nu_2^+ = 500\,s^{-1}$, $u_e^+ = 2, u_1^- = 2, u_1^+ = 2, u_2^- = 2, u_2^+ = 2, u_c^- = 2$ for the values of Δn in units of μM: $\Delta n = -0.99, \Delta n = 0, \Delta n = 35, \Delta n = 100, \Delta n = 500, \Delta n = 1000$

Using $\eta_c = 0$, $u_e^+ = 2, u_1^- = 2, u_1^+ = 2, u_2^- = 2, u_2^+ = 2, u_c^- = 2$ and the values of the transition rates specified in Eq. (3.14) into Eq. (4.16), we have plotted the variation of the average occupation number η_2 of the internal potential well V_2 of a nano-channel with two internal potential wells as a function of η_e for five different values of the concentration gradient Δn in units of μM, that is $\Delta n = -0.99, \Delta n = 0, \Delta n = 35, \Delta n = 100, \Delta n = 500, \Delta n = 1000$ on the same graph as shown in Fig. 4.79.

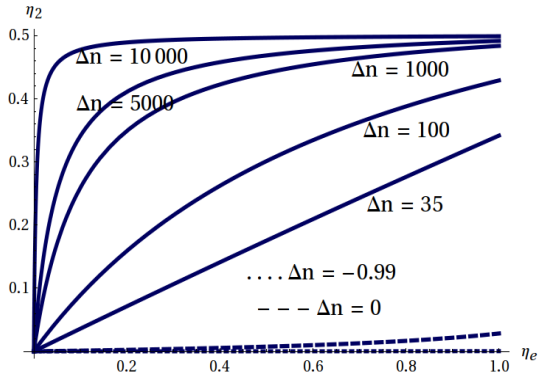

Fig. 4.79: Plot of η_2 as a function of η_e when $s = 2$, $n_c = 1.0\,\mu M$, $\eta_c = 0$, $\nu_e^+ = \nu_c^- = 15\,(\mu M)^{-1}s^{-1}, \nu_1^- = \nu_1^+ = 500\,s^{-1}, \nu_2^- = \nu_2^+ = 500\,s^{-1}$, $u_e^+ = 2, u_1^- = 2, u_1^+ = 2, u_2^- = 2, u_2^+ = 2, u_c^- = 2$ for the values of Δn in units of μM: $\Delta n = -0.99, \Delta n = 0, \Delta n = 35, \Delta n = 100, \Delta n = 500, \Delta n = 1000$

Using $\eta_c = 1.0$, $u_e^+ = 2, u_1^- = 2, u_1^+ = 2, u_2^- = 2, u_2^+ = 2, u_c^- = 2$ and the values of the transition rates specified in Eq. (3.14) into Eq. (4.16), we have plotted the variation of the average occupation number η_2 of the internal potential well V_2 of a nano-channel with two internal potential wells as a function of η_e for five different values of the concentration gradient Δn in units of μM, that is $\Delta n = -0.99, \Delta n = 0, \Delta n = 35, \Delta n = 100, \Delta n = 500, \Delta n = 1000$ on the same graph as shown in Fig. 4.80.

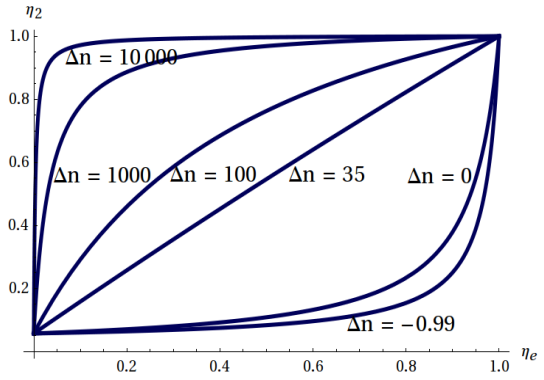

Fig. 4.80: Plot of η_2 as a function of η_e when $s = 2$, $n_c = 1.0\,\mu M$, $\eta_c = 1.0$, $\nu_e^+ = \nu_c^- = 15\,(\mu M)^{-1}s^{-1}, \nu_1^- = \nu_1^+ = 500\,s^{-1}, \nu_2^- = \nu_2^+ = 500\,s^{-1}$, $u_e^+ = 2, u_1^- = 2, u_1^+ = 2, u_2^- = 2, u_2^+ = 2, u_c^- = 2$ for the values of Δn in units of μM: $\Delta n = -0.99, \Delta n = 0, \Delta n = 35, \Delta n = 100, \Delta n = 500, \Delta n = 1000$

The plots in Fig. 4.79 and Fig. 4.80 show that the average value of $\eta_{22}(\Delta n =$

$35\ \mu M|\eta_e, \eta_c)$ is a linearly increasing function of η_e for each possible value of η_c. The average values of $\eta_{22}(\Delta n|\eta_e, \eta_c = 0)$ as a function of η_e associated with different values of Δn coincide with each other and assume the same value $\eta_{22}(\Delta n|\eta_e, \eta_c = 0) = 0$ as $\eta_e \to 0$ and then as $\eta_e \to 0.5$, the deviation between the values of $\eta_{22}(\Delta n|\eta_e, \eta_c = 0)$ associated with different values of Δn becomes maximum and then as $\eta_e \to 1.0$ they approach to each other and assume the values: $\eta_{22}(\Delta n = -0.99\ \mu M|\eta_e \to 1.0, \eta_c = 0) \to 0.00029982$, $\eta_{22}(\Delta n = 0|\eta_e \to 1.0, \eta_c = 0) \to 0.0283034$, $\eta_{22}(\Delta n = 35\ \mu M|\eta_e \to 1.0, \eta_c = 0) \to 0.341846$, $\eta_{22}(\Delta n = 100\ \mu M|\eta_e \to 1.0, \eta_c = 0) \to 0.429231$, $\eta_{22}(\Delta n = 1000\ \mu M|\eta_e \to 1.0, \eta_c = 0) \to 0.491819$ and $\eta_{22}(\Delta n = 10000\ \mu M|\eta_e \to 1.0, \eta_c = 0) \to 0.499169$ as shown in Fig. 4.79. When $\eta_c = 1.0$, the average value of $\eta_{22}(\Delta n|\eta_e, \eta_c = 1.0)$ associated with different values of Δn converge to each other and assume the same value $\eta_{22}(\Delta n|\eta_e, \eta_c = 1.0) = 0$ as $\eta_e \to 0$ and as η_e increases to intermediate values the deviation between the values of $\eta_{22}(\Delta n|\eta_e, \eta_c = 1.0)$ associated with different values of Δn becomes maximum and then as $\eta_e \to 1.0$ they converge to the same saturation value of $\eta_{22}(\Delta n|\eta_e, \eta_c = 1.0) = 1.0$ as shown in Fig. 4.80.

4.4.3 Conclusion of the Average Occupation number of the Internal Potential Wells V_1 and V_2 of a Nano-Channel With Two Internal Potential Wells

1. For one particular given value of η_c, the average occupation numbers of the Internal Potential Wells V_1 and V_2, denoted by $\eta_{12}(\Delta n|\eta_e, \eta_c)$ and $\eta_{22}(\Delta n|\eta_e, \eta_c)$, respectively as a function of Δn associated with the different values of η_e saturate to the same maximum positive value of one as Δn increases to large positive values.

2. For the given possible values of η_e, the average occupation numbers $\eta_{12}(\Delta n|\eta_e, \eta_c)$ associated with different values of η_e obey that: $\eta_{12}(\Delta n|\eta_e = 0, \eta_c) < \eta_{12}(\Delta n|\eta_e = 0.25, \eta_c) < \eta_{12}(\Delta n|\eta_e = 0.5, \eta_c) < \eta_{12}(\Delta n|\eta_e = 0.75, \eta_c) < \eta_{12}(\Delta n|\eta_e = 1.0, \eta_c)$ for all possible values of $\Delta n > 0$ and η_c.

3. For the given possible values of η_e, the average occupation numbers $\eta_{22}(\Delta n|\eta_e, \eta_c)$ associated with different values of η_e obey that: $\eta_{22}(\Delta n|\eta_e = 0, \eta_c) < \eta_{22}(\Delta n|\eta_e = 0.25, \eta_c) < \eta_{22}(\Delta n|\eta_e = 0.5, \eta_c) < \eta_{22}(\Delta n|\eta_e = 0.75, \eta_c) < \eta_{22}(\Delta n|\eta_e = 1.0, \eta_c)$

for all possible values of $\Delta n > 0$ and η_c.

4. For the given values of η_c, the average occupation numbers $\eta_{12}(\Delta n|\eta_e, \eta_c)$ associated with different values of η_c obey that: $\eta_{12}(\Delta n|\eta_e, \eta_c = 0) > \eta_{12}(\Delta n|\eta_e, \eta_c = 0.25) > \eta_{12}(\Delta n|\eta_e, \eta_c = 0.5) > \eta_{12}(\Delta n|\eta_e, \eta_c = 0.75) < \eta_{12}(\Delta n|\eta_e, \eta_c = 1.0)$ for all possible values of $\Delta n > 0$ and η_e.

5. For the given values of η_c, the average occupation numbers $\eta_{22}(\Delta n|\eta_e, \eta_c)$ associated with different values of η_c obey that: $\eta_{22}(\Delta n|\eta_e, \eta_c = 0) > \eta_{22}(\Delta n|\eta_e, \eta_c = 0.25) > \eta_{22}(\Delta n|\eta_e, \eta_c = 0.5) > \eta_{22}(\Delta n|\eta_e, \eta_c = 0.75) < \eta_{22}(\Delta n|\eta_e, \eta_c = 1.0)$ for all possible values of $\Delta n > 0$ and η_e.

6. For one particular given value of η_e, the average occupation numbers $\eta_{12}(\Delta n|\eta_e, \eta_c)$ and $\eta_{22}(\Delta n|\eta_e, \eta_c)$ as functions of Δn associated with the different values of η_c saturate to different maximum positive values as Δn increases to large positive values.

7. The average values of $\eta_{12}(\Delta n|\eta_e, \eta_c)$ and $\eta_{22}(\Delta n|\eta_e, \eta_c)$ as functions of Δn are one for all possible values of Δn when $\eta_e = \eta_c = 1.0$.

8. When $\eta_e = 0$, the average values of $\eta_{12}(\Delta n|\eta_e, \eta_c)$ and $\eta_{22}(\Delta n|\eta_e, \eta_c)$ associated with different values of η_c are constant and don't change as Δn increases.

9. For the given value of η_c, the average values of $\eta_{12}(\Delta n|\eta_e = 1.0, \eta_c)$ and $\eta_{22}(\Delta n|\eta_e = 1.0, \eta_c)$ as functions of Δn approach their saturation values more rapidly when η_e assumes higher values than when η_e assumes smaller values.

10. The average values of $\eta_{12}(\Delta n|\eta_e, \eta_c)$ and $\eta_{22}(\Delta n|\eta_e, \eta_c)$ attain maximum positive values when V_e and V_c are occupied, that is $\eta_e = 1$ and $\eta_c = 1$.

11. For the given values of Δn, η_e and η_c, the average values of $\eta_{12}(\Delta n|\eta_e, \eta_c)$ decrease as the height of the potential barriers u_e^+, u_2^- and u_c^- increases. This because as the potential barriers u_e^+, u_2^- and u_c^- increase the transition rate into the internal potential well V_1 decreases and thus the occupation probability of V_1 also decreases.

12. For the given values of Δn, η_e and η_c, the average values of $\eta_{22}(\Delta n|\eta_e,\eta_c)$ decrease as the height of the potential barriers u_e^+, u_1^- and u_c^- increases. This because as the potential barriers u_e^+, u_1^- and u_c^- increase the transition rate into the internal potential well V_2 decreases and thus the occupation probability of V_2 also decreases.

13. The average value of $\eta_{12}(\Delta n|\eta_e,\eta_c)$ increases as the height of the potential barriers u_1^-, u_1^+ and u_2^+ increases. This because as the potential barriers u_1^-, u_1^+ and u_2^+ increase the mean residence time of a particle in the internal potential well V_1 increases, which means that the occupation probability of V_1 also increases.

14. The average value of $\eta_{22}(\Delta n|\eta_e,\eta_c)$ increases as the height of the potential barriers u_2^-, u_2^+ and u_1^- increases. This because as the potential barriers u_2^-, u_2^+ and u_1^- increase the mean residence time of a particle in the internal potential well V_2 increases, which means that the occupation probability of V_2 also increases.

15. For the given values of Δn, η_e and η_c, the average occupation numbers $\eta_{12}(\Delta n|\eta_e,\eta_c)$ and $\eta_{22}(\Delta n|\eta_e,\eta_c)$ associated with different values of u_j^- and u_e^+ saturate to the same maximum value as Δn increases to large positive values and those associated with different values of u_j^+ saturate to different maximum values, where $j = 1, 2$.

16. For the given values of Δn and η_c, the average occupation numbers $\eta_{12}(\Delta n = 35\ \mu M|\eta_e,\eta_c)$ and $\eta_{22}(\Delta n = 35\ \mu M|\eta_e,\eta_c)$ as functions of η_e increase almost linearly as η_e increases for all possible values of η_c.

17. The average occupation numbers $\eta_{12}(\Delta n|\eta_e,\eta_c)$ and $\eta_{22}(\Delta n|\eta_e,\eta_c)$ are monotonically increasing function of both η_e and η_c for all possible values of Δn.

5

SUMMARY AND CONCLUSION OF THE PROPERTIES OF A NANO-CHANNEL WITH ONE AND TWO INTERNAL POTENTIAL WELLS

5.1 Comparison of the Average Occupation Numbers of the Internal Potential Wells of a Nano-Channel with Two Internal Potential Wells

Using $\eta_e = 0.1$, $\eta_c = 0.1$, $u_e^+ = 2, u_1^- = 2, u_1^+ = 2, u_2^- = 2.0, u_2^+ = 2, u_c^- = 2$ and the values of the transition rates specified in Eq. 3.14 into Eq. 4.15 and Eq. 4.16 so as to get the average occupation numbers of the internal potential wells V_1 and V_2 of a nano-channel with two internal potential wells denoted by $\eta_{12}(\Delta n|\eta_e, \eta_c)$ and $\eta_{22}(\Delta n|\eta_e, \eta_c)$, respectively. The plot of the variation of $\eta_{12}(\Delta n|\eta_e, \eta_c)$ and $\eta_{22}(\Delta n|\eta_e, \eta_c)$ as a function of Δn in units of μM on the same graph are shown in Fig. 5.1.

Using $\eta_e = 1.0$, $\eta_c = 0$, $u_e^+ = 2, u_1^- = 2, u_1^+ = 2, u_2^- = 2.0, u_2^+ = 2, u_c^- = 2$ and the values of the transition rates specified in Eq. 3.14 into Eq. 4.15 and Eq. 4.16 so as to get the average occupation numbers of the internal potential wells V_1 and V_2 of a nano-channel with two internal potential wells denoted by $\eta_{12}(\Delta n|\eta_e, \eta_c)$ and $\eta_{22}(\Delta n|\eta_e, \eta_c)$, respectively. The plot of the variation of $\eta_{12}(\Delta n|\eta_e, \eta_c)$ and $\eta_{22}(\Delta n|\eta_e, \eta_c)$ as a function of the concentration gradient Δn in units of μM on the same graph are shown in Fig. 5.2.

Using $\eta_e = 0, \eta_c = 1.0, u_e^+ = 2, u_1^- = 2, u_1^+ = 2, u_2^- = 2.0, u_2^+ = 2, u_c^- = 2$ and the values of the transition rates specified in Eq. 3.14 into Eq. 4.15 and Eq. 4.16 so as to get the average occupation numbers of the internal potential wells V_1 and V_2 of a nano-channel with two internal potential wells denoted by $\eta_{12}(\Delta n|\eta_e, \eta_c)$ and $\eta_{22}(\Delta n|\eta_e, \eta_c)$, respectively. The plot of the variation of $\eta_{12}(\Delta n|\eta_e, \eta_c)$ and $\eta_{22}(\Delta n|\eta_e, \eta_c)$ as a function of the concentration gradient Δn in units of μM on the same graph are shown in Fig. 5.3.

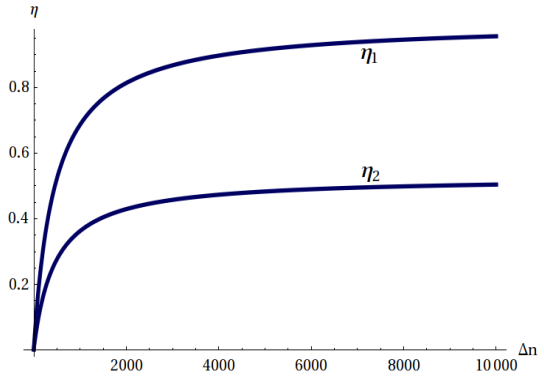

Fig. 5.1: Plot of $\eta_{12}(\Delta n|\eta_e, \eta_c)$ and $\eta_{22}(\Delta n|\eta_e, \eta_c)$ as a function of the concentration gradient Δn in units of μM when $s = 2$, $n_c = 1.0\,\mu M$, $\eta_e = 0.1$, $\eta_c = 0.1$, $\nu_e^+ = \nu_c^- = 15\,(\mu M)^{-1}s^{-1}, \nu_1^- = \nu_1^+ = 500\,s^{-1}, \nu_2^- = \nu_2^+ = 500\,s^{-1}$, $u_e^+ = 2, u_1^- = 2, u_1^+ = 2, u_2^- = 2, u_2^+ = 2, u_c^- = 2$

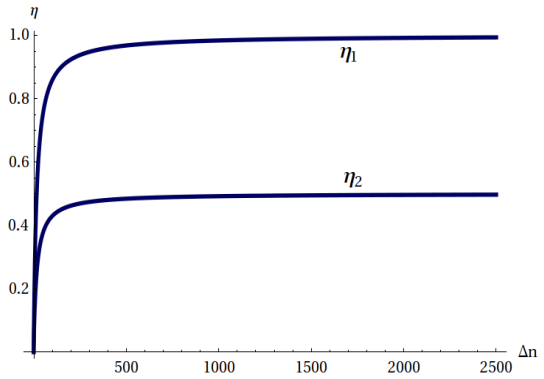

Fig. 5.2: Plot of $\eta_{12}(\Delta n|\eta_e, \eta_c)$ and $\eta_{22}(\Delta n|\eta_e, \eta_c)$ as a function of the concentration gradient Δn in units of μM when $s = 2$, $n_c = 1.0\,\mu M$, $\eta_e = 1.0$, $\eta_c = 0$, $\nu_e^+ = \nu_c^- = 15\,(\mu M)^{-1}s^{-1}, \nu_1^- = \nu_1^+ = 500\,s^{-1}, \nu_2^- = \nu_2^+ = 500\,s^{-1}$, $u_e^+ = 2, u_1^- = 2, u_1^+ = 2, u_2^- = 2.0, u_2^+ = 2, u_c^- = 2$

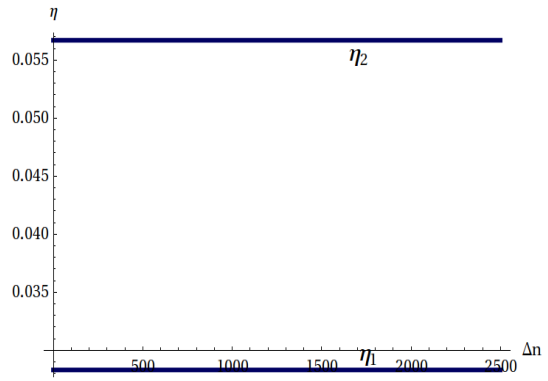

Fig. 5.3: Plot of $\eta_{12}(\Delta n|\eta_e,\eta_c)$ and $\eta_{22}(\Delta n|\eta_e,\eta_c)$ as a function of the concentration gradient Δn in units of μM when $s = 2$, $n_c = 1.0\,\mu M$, $\eta_e = 0$, $\eta_c = 1.0$, $\nu_e^+ = \nu_c^- = 15\,(\mu M)^{-1}s^{-1}, \nu_1^- = \nu_1^+ = 500\,s^{-1}, \nu_2^- = \nu_2^+ = 500\,s^{-1}$, $u_e^+ = 2, u_1^- = 2, u_1^+ = 2, u_2^- = 2.0, u_2^+ = 2, u_c^- = 2$

For all possible given average values of the external occupation numbers η_e and η_c, the average values of the internal occupation number as a function of Δn, that is, $\eta_{12}(\Delta n|\eta_e,\eta_c)$ and $\eta_{22}(\Delta n|\eta_e,\eta_c)$ obey that: $\eta_{12}(\Delta n|\eta_e,\eta_c < 1.0) > \eta_{22}(\Delta n|\eta_e,\eta_c < 1.0)$, for all possible values of Δn, η_e and $\eta_c < 1.0$. As $\eta_e \to 1.0$, $\eta_{12}(\Delta n|\eta_e,\eta_c) \to 1.0$ and also as η_c increases, $\eta_{22}(\Delta n|\eta_e,\eta_c)$ also increases and thus $\eta_{22}(\Delta n|\eta_e = 0,\eta_c = 1.0) > \eta_{12}(\Delta n|\eta_e = 0,\eta_c = 1.0)$ as shown in Fig. 5.2. The maximum value of both $\eta_{12}(\Delta n|\eta_e,\eta_c)$ and $\eta_{22}(\Delta n|\eta_e,\eta_c < 1.0)$ occurs when $\eta_e = 1.0$ and $\eta_c = 0$ as shown in Fig. 5.2. The average values of $\eta_{12}(\Delta n|\eta_e,\eta_c)$ and $\eta_{22}(\Delta n|\eta_e,\eta_c)$ increase rapidly in the range of the concentration gradient $\Delta n < 2000\ \mu M$ when $\eta_e = 0.1$, $\eta_c = 0.1$ as shown in Fig. 5.1 and in the range $\Delta n < 500\ \mu M$ when $\eta_e = 1.0$, $\eta_c = 0$ as shown in Fig. 5.2 and after that both saturate to different saturation values values. On the other hand when $\eta_e = 0$, $\eta_c = 1.0$, the average values of $\eta_{12}(\Delta n|\eta_e,\eta_c)$ and $\eta_{22}(\Delta n|\eta_e,\eta_c)$ assume constant average values that don't change as the concentration gradient increases as shown in Fig. 5.3.

Using $\Delta n = 5000\ \mu M$, $\eta_e = 0$, $u_e^+ = 2, u_1^- = 2, u_1^+ = 2, u_2^- = 2.0, u_2^+ = 2, u_c^- = 2$ and the values of the transition rates specified in Eq. 3.14 into Eq. 4.15 and Eq. 4.16 so as to get the average occupation numbers of the internal potential wells V_1 and V_2 of a nano-channel with two internal potential wells denoted by $\eta_{12}(\Delta n|\eta_e,\eta_c)$ and $\eta_{22}(\Delta n|\eta_e,\eta_c)$, respectively. The plot of the varia-

tion of $\eta_{12}(\Delta n|\eta_e,\eta_c)$ and $\eta_{22}(\Delta n|\eta_e,\eta_c)$ as a function of η_c on the same graph are shown in Fig. 5.4.

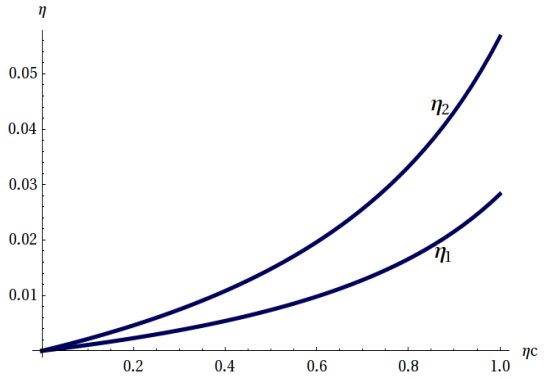

Fig. 5.4: Plot of $\eta_{12}(\Delta n|\eta_e,\eta_c)$ and $\eta_{22}(\Delta n|\eta_e,\eta_c)$ as a function of η_c when $s=2$, $n_c=1.0\ \mu M$, $\Delta n=5000\ \mu M$, $\eta_e=0$, $\nu_e^+=\nu_c^-=15\,(\mu M)^{-1}s^{-1}, \nu_1^-=\nu_1^+=500\,s^{-1}, \nu_2^-=\nu_2^+=500\,s^{-1}$, $u_e^+=2, u_1^-=2, u_1^+=2, u_2^-=2.0, u_2^+=2, u_c^-=2$

Using $\Delta n=5000\ \mu M$, $\eta_e=1.0$, $u_e^+=2, u_1^-=2, u_1^+=2, u_2^-=2.0, u_2^+=2, u_c^-=2$ and the values of the transition rates specified in Eq. 3.14 into Eq. 4.15 and Eq. 4.16 so as to get the average occupation numbers of the internal potential wells V_1 and V_2 of a nano-channel with two internal potential wells denoted by $\eta_{12}(\Delta n|\eta_e,\eta_c)$ and $\eta_{22}(\Delta n|\eta_e,\eta_c)$, respectively. The plot of the variation of $\eta_{12}(\Delta n|\eta_e,\eta_c)$ and $\eta_{22}(\Delta n|\eta_e,\eta_c)$ as a function of η_c on the same graph are shown in Fig. 5.5.

For the given possible values of Δn and η_e, the average values of the internal occupation numbers as a function of η_c, that is, $\eta_{12}(\Delta n|\eta_e,\eta_c)$ and $\eta_{22}(\Delta n|\eta_e,\eta_c)$ obey that: $\eta_{22}(\Delta n=5000\ \mu M|\eta_e=0,\eta_c)>\eta_{12}(\Delta n=5000\ \mu M|\eta_e=0,\eta_c)$ for all possible values of η_c and both increase continuously in the entire range $0<\eta_c<1.0$ as shown in Fig. 5.4. This implies that when $\eta_e=0$, the occupation of the potential well V_1 is less likely and as η_c increases the occupation probability of V_2 increases and as a result the average value of $\eta_{22}(\Delta n|\eta_e,\eta_c)$ dominates as $\eta_c\to 1.0$. But, when $\eta_e>0$, the average value of $\eta_{12}(\Delta n=5000\ \mu M|\eta_e>0,\eta_c)$ jumps rapidly to its saturation value, that is, $\eta_{12}(\Delta n=5000\ \mu M|\eta_e>0,\eta_c)\to 1.0$ and becomes dominant, that is, $\eta_{12}(\Delta n=5000\ \mu M|\eta_e>0,\eta_c)>\eta_{22}(\Delta n=$

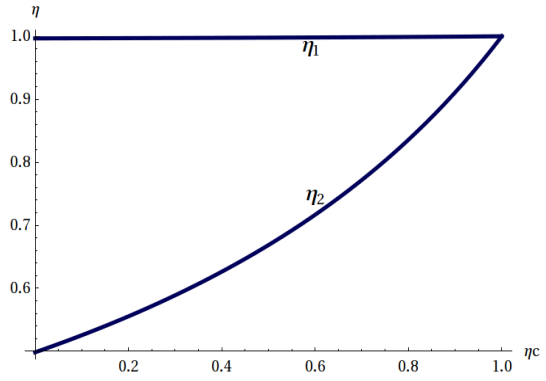

Fig. 5.5: Plot of $\eta_{12}(\Delta n|\eta_e,\eta_c)$ and $\eta_{22}(\Delta n|\eta_e,\eta_c)$ as a function of η_c when $s=2$, $n_c=1.0\ \mu M$, $\Delta n=5000\ \mu M$, $\eta_e=1.0$, $\nu_e^+=\nu_c^-=15\,(\mu M)^{-1}s^{-1},\nu_1^-=\nu_1^+=500\,s^{-1},\nu_2^-=\nu_2^+=500\,s^{-1}$, $u_e^+=2,u_1^-=2,u_1^+=2,u_2^-=2.0,u_2^+=2,u_c^-=2$

$5000\ \mu M|\eta_e>0,\eta_c)$ in the entire range $0<\eta_c<1.0$ for all possible values of $\eta_e>0$. However, $\eta_{22}(\Delta n|\eta_e,\eta_c)$ increase continuously in the entire range $0<\eta_c<1.0$ as shown in Fig. 5.5.

Using $\Delta n=2500\ \mu M$, $\eta_c=0$, $u_e^+=2,u_1^-=2,u_1^+=2,u_2^-=2.0,u_2^+=2,u_c^-=2$ and the values of the transition rates specified in Eq. 3.14 into Eq. 4.15 and Eq. 4.16 so as to get the average occupation numbers of the internal potential wells V_1 and V_2 of a nano-channel with two internal potential wells denoted by $\eta_{12}(\Delta n|\eta_e,\eta_c)$ and $\eta_{22}(\Delta n|\eta_e,\eta_c)$, respectively. The plot of the variation of $\eta_{12}(\Delta n|\eta_e,\eta_c)$ and $\eta_{22}(\Delta n|\eta_e,\eta_c)$ as a function of η_e on the same graph are shown in Fig. 5.6.

For the given possible values Δn and η_c, the average values of the internal occupation numbers as a function of the eternal occupation number η_e, that is, $\eta_{12}(\Delta n|\eta_e,\eta_c)$ and $\eta_{22}(\Delta n|\eta_e,\eta_c)$ obey that: $\eta_{12}(\Delta n=5000\ \mu M|\eta_e,\eta_c=0)>\eta_{22}(\Delta n=5000\ \mu M|\eta_e,\eta_c=0)$ for all possible values of η_e and both increase rapidly in the small range $0<\eta_e<0.2$ and after that both assume their saturation values as shown in Fig. 5.6. But as the average value of η_c increases, the average values of $\eta_{12}(\Delta n=5000\ \mu M|\eta_e,\eta_c)$ and $\eta_{22}(\Delta n=5000\ \mu M|\eta_e,\eta_c)$ approach each other and finally when $\eta_c\to 1.0$, the plots of coincide with each other as shown in Fig. 5.7.

Using $\Delta n=2500\ \mu M$, $\eta_c=1.0$, $u_e^+=2,u_1^-=2,u_1^+=2,u_2^-=2.0,u_2^+=2,u_c^-=2$ and the values of the transition rates specified in Eq. 3.14 into Eq.

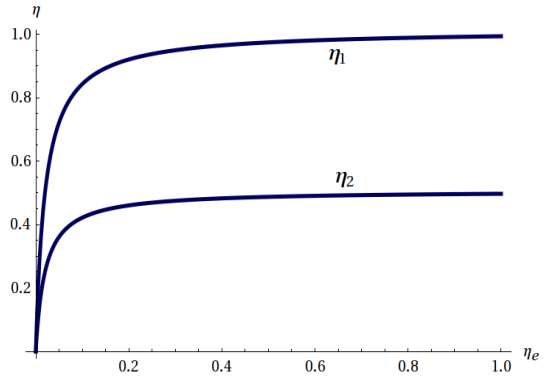

Fig. 5.6: Plot of $\eta_{12}(\Delta n|\eta_e,\eta_c)$ and $\eta_{22}(\Delta n|\eta_e,\eta_c)$ as a function of η_e when $s=2$, $n_c=1.0\ \mu M$, $\Delta n=2500\ \mu M$, $\eta_c=0$, $\nu_e^+=\nu_c^-=15\,(\mu M)^{-1}s^{-1}, \nu_1^-=\nu_1^+=500\,s^{-1}, \nu_2^-=\nu_2^+=500\,s^{-1}$, $u_e^+=2, u_1^-=2, u_1^+=2, u_2^-=2.0, u_2^+=2, u_c^-=2$

4.15 and Eq. 4.16 so as to get the average occupation numbers of the internal potential wells V_1 and V_2 of a nano-channel with two internal potential wells denoted by $\eta_{12}(\Delta n|\eta_e,\eta_c)$ and $\eta_{22}(\Delta n|\eta_e,\eta_c)$, respectively. The plot of the variation of $\eta_{12}(\Delta n|\eta_e,\eta_c)$ and $\eta_{22}(\Delta n|\eta_e,\eta_c)$ as a function of η_e on the same graph are shown in Fig. 5.7.

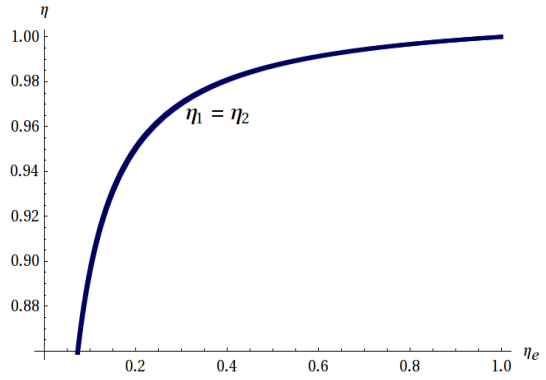

Fig. 5.7: Plot of $\eta_{12}(\Delta n|\eta_e,\eta_c)$ and $\eta_{22}(\Delta n|\eta_e,\eta_c)$ as a function of η_e when $s=2$, $n_c=1.0\ \mu M$, $\Delta n=2500\ \mu M$, $\eta_c=1.0$, $\nu_e^+=\nu_c^-=15\,(\mu M)^{-1}s^{-1}, \nu_1^-=\nu_1^+=500\,s^{-1}, \nu_2^-=\nu_2^+=500\,s^{-1}$, $u_e^+=2, u_1^-=2, u_1^+=2, u_2^-=2.0, u_2^+=2, u_c^-=2$

Using $\Delta n=0$, $\eta_e=0$, $u_e^+=2, u_1^-=2, u_1^+=2, u_2^-=2.0, u_2^+=2, u_c^-=2$ and the values of the transition rates specified in Eq. 3.14 into Eq. 4.15 and Eq. 4.16 so as to get the average occupation numbers of the internal potential wells V_1 and V_2 of a nano-channel with two internal potential wells denoted by $\eta_{12}(\Delta n|\eta_e,\eta_c)$ and $\eta_{22}(\Delta n|\eta_e,\eta_c)$, respectively. The plot of the variation of $\eta_{12}(\Delta n|\eta_e,\eta_c)$ and

$\eta_{22}(\Delta n|\eta_e,\eta_c)$ as a function of η_c on the same graph are shown in Fig. 5.8.

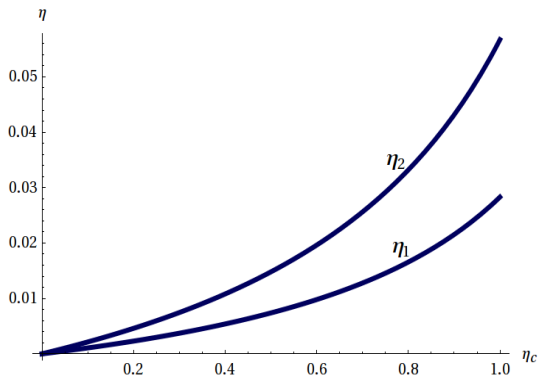

Fig. 5.8: Plot of $\eta_{12}(\Delta n|\eta_e,\eta_c)$ and $\eta_{22}(\Delta n|\eta_e,\eta_c)$ as a function of η_c when $s=2$, $n_c=1.0\ \mu M$, $\Delta n=0$, $\eta_e=0$, $\nu_e^+=\nu_c^-=15\,(\mu M)^{-1}s^{-1}, \nu_1^-=\nu_1^+=500\,s^{-1}, \nu_2^-=\nu_2^+=500\,s^{-1}$, $u_e^+=2, u_1^-=2, u_1^+=2, u_2^-=2.0, u_2^+=2, u_c^-=2$

Using $\Delta n=0$, $\eta_e=0.5$, $u_e^+=2, u_1^-=2, u_1^+=2, u_2^-=2.0, u_2^+=2, u_c^-=2$ and the values of the transition rates specified in Eq. 3.14 into Eq. 4.15 and Eq. 4.16 so as to get the average occupation numbers of the internal potential wells V_1 and V_2 of a nano-channel with two internal potential wells denoted by $\eta_{12}(\Delta n|\eta_e,\eta_c)$ and $\eta_{22}(\Delta n|\eta_e,\eta_c)$, respectively. The plot of the variation of $\eta_{12}(\Delta n|\eta_e,\eta_c)$ and $\eta_{22}(\Delta n|\eta_e,\eta_c)$ as a function of η_c on the same graph are shown in Fig. 5.9.

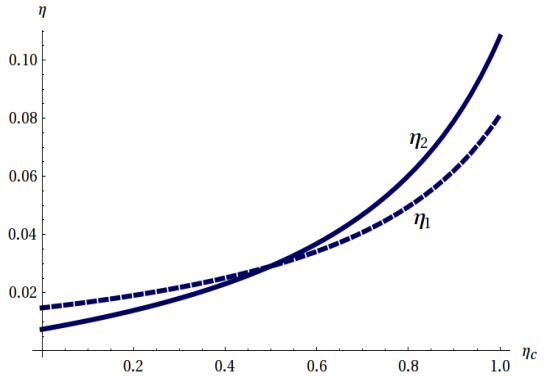

Fig. 5.9: Plot of $\eta_{12}(\Delta n|\eta_e,\eta_c)$ and $\eta_{22}(\Delta n|\eta_e,\eta_c)$ as a function of η_c when $s=2$, $n_c=1.0\ \mu M$, $\Delta n=0$, $\eta_e=0.5$, $\nu_e^+=\nu_c^-=15\,(\mu M)^{-1}s^{-1}, \nu_1^-=\nu_1^+=500\,s^{-1}, \nu_2^-=\nu_2^+=500\,s^{-1}$, $u_e^+=2, u_1^-=2, u_1^+=2, u_2^-=2.0, u_2^+=2, u_c^-=2$

For the given possible values of Δn and η_e, the average values of the internal occupation numbers as a function of η_c, that is, $\eta_{12}(\Delta n|\eta_e,\eta_c)$ and $\eta_{22}(\Delta n|\eta_e,\eta_c)$

obey that: $\eta_{22}(\Delta n = 0|\eta_e = 0, \eta_c) > \eta_{12}(\Delta n = 0|\eta_e = 0, \eta_c)$ for all possible values of η_c and both increase continuously in the entire range $0 < \eta_c < 1.0$ as shown in Fig. 5.8. But, as the average value of η_e increases the occupation probability of the potential well V_1 increases and thus the average value of $\eta_{12}(\Delta n = 0|\eta_e > 0, \eta_c)$ increases and thus began to shift upward and intersects with the plot of $\eta_{22}(\Delta n = 0|\eta_e, \eta_c)$ as shown in Fig. 5.9 and when $\eta_e = 1.0$, the average value of $\eta_{12}(\Delta n = 0|\eta_e = 1.0, \eta_c)$ dominates the average value of $\eta_{22}(\Delta n = 0|\eta_e = 1.0, \eta_c)$, that is, $\eta_{12}(\Delta n = 0|\eta_e = 1.0, \eta_c) > \eta_{22}(\Delta n = 0|\eta_e = 1.0, \eta_c)$ in the entire range $0 < \eta_c < 1.0$ as shown in Fig. 5.10. Finally, when $\eta_e = 1.0$ and $\eta_c = 1.0$, the occupation probability of both V_1 and V_2 increases and as a result even when the concentration gradient is zero, $\eta_{12}(\Delta n = 0|\eta_e = 1.0, \eta_c = 1.0) = \eta_{22}(\Delta n = 0|\eta_e = 1.0, \eta_c = 1.0) = 1.0$ as shown in Fig. 5.10.

Using $\Delta n = 0$, $\eta_e = 1.0$, $u_e^+ = 2, u_1^- = 2, u_1^+ = 2, u_2^- = 2.0, u_2^+ = 2, u_c^- = 2$ and the values of the transition rates specified in Eq. 3.14 into Eq. 4.15 and Eq. 4.16 so as to get the average occupation numbers of the internal potential wells V_1 and V_2 of a nano-channel with two internal potential wells denoted by $\eta_{12}(\Delta n|\eta_e, \eta_c)$ and $\eta_{22}(\Delta n|\eta_e, \eta_c)$, respectively. The plot of the variation of $\eta_{12}(\Delta n|\eta_e, \eta_c)$ and $\eta_{22}(\Delta n|\eta_e, \eta_c)$ as a function of η_c on the same graph are shown in Fig. 5.10.

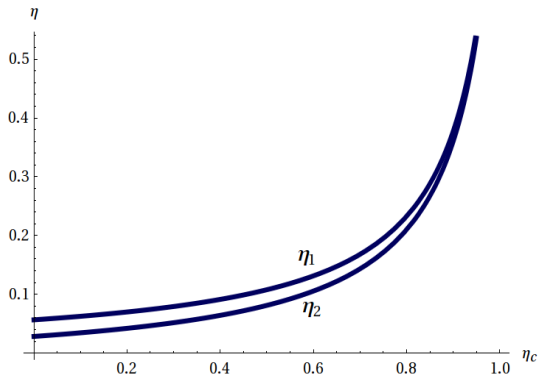

Fig. 5.10: Plot of $\eta_{12}(\Delta n|\eta_e, \eta_c)$ and $\eta_{22}(\Delta n|\eta_e, \eta_c)$ as a function of η_c when $s = 2$, $n_c = 1.0\ \mu M$, $\Delta n = 0$, $\eta_e = 1.0$, $\nu_e^+ = \nu_c^- = 15\,(\mu M)^{-1}s^{-1}, \nu_1^- = \nu_1^+ = 500\,s^{-1}, \nu_2^- = \nu_2^+ = 500\,s^{-1}$, $u_e^+ = 2, u_1^- = 2, u_1^+ = 2, u_2^- = 2.0, u_2^+ = 2, u_c^- = 2$

Using $\Delta n = 0$, $\eta_c = 0$, $u_e^+ = 2, u_1^- = 2, u_1^+ = 2, u_2^- = 2.0, u_2^+ = 2, u_c^- = 2$ and the values of the transition rates specified in Eq. 3.14 into Eq. 4.15 and Eq. 4.16 so as to get the average occupation numbers of the internal potential wells V_1 and

V_2 of a nano-channel with two internal potential wells denoted by $\eta_{12}(\Delta n|\eta_e,\eta_c)$ and $\eta_{22}(\Delta n|\eta_e,\eta_c)$, respectively. The plot of the variation of $\eta_{12}(\Delta n|\eta_e,\eta_c)$ and $\eta_{22}(\Delta n|\eta_e,\eta_c)$ as a function of η_e on the same graph are shown in Fig. 5.11.

Using $\Delta n = 0$, $\eta_c = 0.5$, $u_e^+ = 2, u_1^- = 2, u_1^+ = 2, u_2^- = 2.0, u_2^+ = 2, u_c^- = 2$ and the values of the transition rates specified in Eq. 3.14 into Eq. 4.15 and Eq. 4.16 so as to get the average occupation numbers of the internal potential wells V_1 and V_2 of a nano-channel with two internal potential wells denoted by $\eta_{12}(\Delta n|\eta_e,\eta_c)$ and $\eta_{22}(\Delta n|\eta_e,\eta_c)$, respectively. The plot of the variation of $\eta_{12}(\Delta n|\eta_e,\eta_c)$ and $\eta_{22}(\Delta n|\eta_e,\eta_c)$ as a function of η_e on the same graph are shown in Fig. 5.12.

Using $\Delta n = 0$, $\eta_c = 1.0$, $u_e^+ = 2, u_1^- = 2, u_1^+ = 2, u_2^- = 2.0, u_2^+ = 2, u_c^- = 2$ and the values of the transition rates specified in Eq. 3.14 into Eq. 4.15 and Eq. 4.16 so as to get the average occupation numbers of the internal potential wells V_1 and V_2 of a nano-channel with two internal potential wells denoted by $\eta_{12}(\Delta n|\eta_e,\eta_c)$ and $\eta_{22}(\Delta n|\eta_e,\eta_c)$, respectively. The plot of the variation of $\eta_{12}(\Delta n|\eta_e,\eta_c)$ and $\eta_{22}(\Delta n|\eta_e,\eta_c)$ as a function of η_e on the same graph are shown in Fig. 5.13.

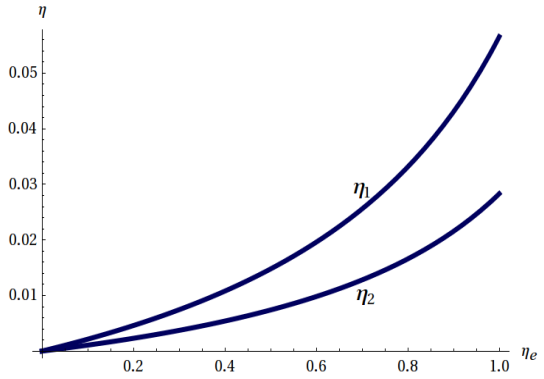

Fig. 5.11: Plot of $\eta_{12}(\Delta n|\eta_e,\eta_c)$ and $\eta_{22}(\Delta n|\eta_e,\eta_c)$ as a function of η_e when $s = 2$, $n_c = 1.0\ \mu M$, $\Delta n = 0$, $\eta_c = 0$, $\nu_e^+ = \nu_c^- = 15\,(\mu M)^{-1}s^{-1}, \nu_1^- = \nu_1^+ = 500\,s^{-1}, \nu_2^- = \nu_2^+ = 500\,s^{-1}$, $u_e^+ = 2, u_1^- = 2, u_1^+ = 2, u_2^- = 2.0, u_2^+ = 2, u_c^- = 2$

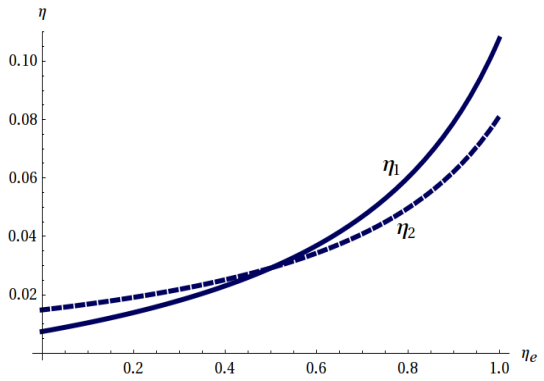

Fig. 5.12: Plot of $\eta_{12}(\Delta n|\eta_e,\eta_c)$ and $\eta_{22}(\Delta n|\eta_e,\eta_c)$ as a function of η_e when $s=2$, $n_c=1.0\ \mu M$, $\Delta n=0$, $\eta_c=0.5$, $\nu_e^+=\nu_c^-=15\,(\mu M)^{-1}s^{-1}, \nu_1^-=\nu_1^+=500\,s^{-1}, \nu_2^-=\nu_2^+=500\,s^{-1}$, $u_e^+=2, u_1^-=2, u_1^+=2, u_2^-=2.0, u_2^+=2, u_c^-=2$

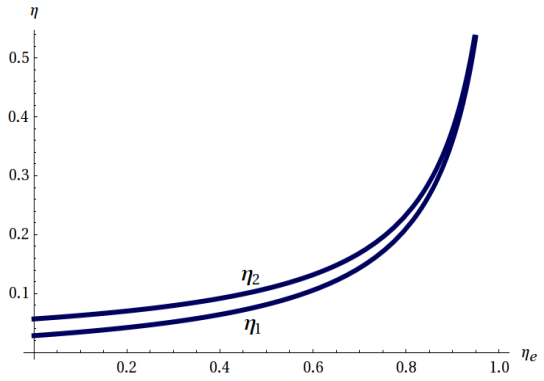

Fig. 5.13: Plot of $\eta_{12}(\Delta n|\eta_e,\eta_c)$ and $\eta_{22}(\Delta n|\eta_e,\eta_c)$ as a function of η_e when $s=2$, $n_c=1.0\ \mu M$, $\Delta n=0$, $\eta_c=1.0$, $\nu_e^+=\nu_c^-=15\,(\mu M)^{-1}s^{-1}, \nu_1^-=\nu_1^+=500\,s^{-1}, \nu_2^-=\nu_2^+=500\,s^{-1}$, $u_e^+=2, u_1^-=2, u_1^+=2, u_2^-=2.0, u_2^+=2, u_c^-=2$

For the given possible values of Δn and η_c, the average values of the internal occupation numbers as a function of η_e, that is, $\eta_{12}(\Delta n|\eta_e,\eta_c)$ and $\eta_{22}(\Delta n|\eta_e,\eta_c)$ obey that: $\eta_{12}(\Delta n=0|\eta_e,\eta_c=0)>\eta_{22}(\Delta n=0|\eta_e,\eta_c=0)$ for all possible values of η_e and both increase continuously in the entire range $0<\eta_e<1.0$ as shown in Fig. 5.11. But, as the average value of η_c increases the occupation probability of the potential well V_2 increases and thus the average value of $\eta_{22}(\Delta n=0|\eta_e,\eta_c>0)$ increases and thus began to shift upward and intersects with the plot of $\eta_{12}(\Delta n=0|\eta_e,\eta_c)$ as shown in Fig. 5.12 and when $\eta_c=1.0$, the average value of $\eta_{22}(\Delta n=0|\eta_e,\eta_c=1.0)$ dominates the average value of $\eta_{12}(\Delta n=0|\eta_e,\eta_c=1.0)$, that is, $\eta_{22}(\Delta n=0|\eta_e,\eta_c=1.0)>\eta_{12}(\Delta n=0|\eta_e,\eta_c=1.0)$

in the entire range $0 < \eta_e < 1.0$ as shown in Fig. 5.13. Finally, when $\eta_e = 1.0$ and $\eta_c = 1.0$, the occupation probability of both V_1 and V_2 increases and as a result even when the concentration gradient is zero, $\eta_{12}(\Delta n = 0|\eta_e = 1.0, \eta_c = 1.0) = \eta_{22}(\Delta n = 0|\eta_e = 1.0, \eta_c = 1.0) = 1.0$ as shown in Fig. 5.13.

Using $\Delta n = -1.0\ \mu M$, $\eta_e = 0$, $u_e^+ = 2, u_1^- = 2, u_1^+ = 2, u_2^- = 2.0, u_2^+ = 2, u_c^- = 2$ and the values of the transition rates specified in Eq. 3.14 into Eq. 4.15 and Eq. 4.16 so as to get the average occupation numbers of the internal potential wells V_1 and V_2 of a nano-channel with two internal potential wells denoted by $\eta_{12}(\Delta n|\eta_e, \eta_c)$ and $\eta_{22}(\Delta n|\eta_e, \eta_c)$, respectively. The plot of the variation of $\eta_{12}(\Delta n|\eta_e, \eta_c)$ and $\eta_{22}(\Delta n|\eta_e, \eta_c)$ as a function of η_c on the same graph are shown in Fig. 5.14.

Using $\Delta n = -1.0\ \mu M$, $\eta_e = 1.0$, $u_e^+ = 2, u_1^- = 2, u_1^+ = 2, u_2^- = 2.0, u_2^+ = 2, u_c^- = 2$ and the values of the transition rates specified in Eq. 3.14 into Eq. 4.15 and Eq. 4.16 so as to get the average occupation numbers of the internal potential wells V_1 and V_2 of a nano-channel with two internal potential wells denoted by $\eta_{12}(\Delta n|\eta_e, \eta_c)$ and $\eta_{22}(\Delta n|\eta_e, \eta_c)$, respectively. The plot of the variation of $\eta_{12}(\Delta n|\eta_e, \eta_c)$ and $\eta_{22}(\Delta n|\eta_e, \eta_c)$ as a function of η_c on the same graph are shown in Fig. 5.15.

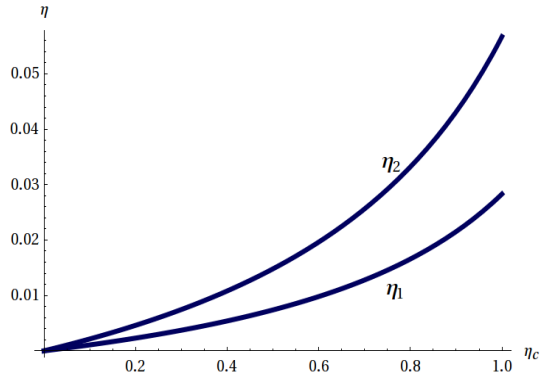

Fig. 5.14: Plot of $\eta_{12}(\Delta n|\eta_e, \eta_c)$ and $\eta_{22}(\Delta n|\eta_e, \eta_c)$ as a function of η_c when $s = 2$, $n_c = -1.0\ \mu M$, $\Delta n = -1.0\ \mu M$, $\eta_e = 0$, $\nu_e^+ = \nu_c^- = 15\,(\mu M)^{-1}s^{-1}, \nu_1^- = \nu_1^+ = 500\,s^{-1}, \nu_2^- = \nu_2^+ = 500\,s^{-1}$, $u_e^+ = 2, u_1^- = 2, u_1^+ = 2, u_2^- = 2.0, u_2^+ = 2, u_c^- = 2$

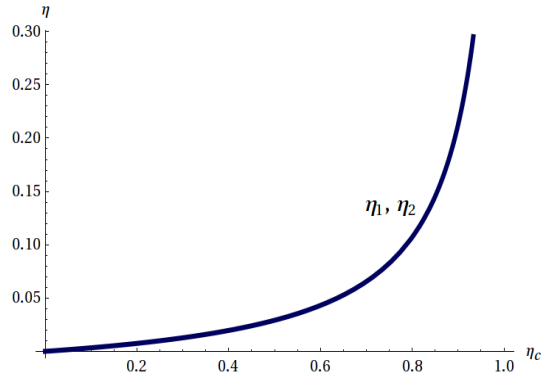

Fig. 5.15: Plot of $\eta_{12}(\Delta n|\eta_e,\eta_c)$ and $\eta_{22}(\Delta n|\eta_e,\eta_c)$ as a function of η_c when $s=2$, $n_c=1.0\ \mu M$, $\Delta n=-1.0\ \mu M$, $\eta_e=0.9999$, $\nu_e^+=\nu_c^-=15\,(\mu M)^{-1}s^{-1}, \nu_1^-=\nu_1^+=500\,s^{-1}, \nu_2^-=\nu_2^+=500\,s^{-1}$, $u_e^+=2, u_1^-=2, u_1^+=2, u_2^-=2.0, u_2^+=2, u_c^-=2$

For the given possible values of Δn and η_e, the average values of $\eta_{12}(\Delta n|\eta_e,\eta_c)$ and $\eta_{22}(\Delta n|\eta_e,\eta_c)$ obey that: $\eta_{22}(\Delta n=-1.0\ \mu M|\eta_e=0,\eta_c)>\eta_{12}(\Delta n=-1.0\ \mu M|\eta_e=0,\eta_c)$ for all possible values of η_c and both increase continuously in the entire range $0<\eta_c<1.0$ as shown in Fig. 5.14. But, as the average value of η_e increases the occupation probability of the potential well V_1 increases and thus the average value of $\eta_{12}(\Delta n=0|\eta_e>0,\eta_c)$ increases and thus began to shift upward and approaches the plot of $\eta_{22}(\Delta n=0|\eta_e,\eta_c)$ and when $\eta_e=1.0$, the average value of $\eta_{12}(\Delta n=0|\eta_e=1.0,\eta_c)$ coincides with the average value of $\eta_{22}(\Delta n=-1.0\ \mu M|\eta_e=1.0,\eta_c)$ and assume the same value in the entire range $0<\eta_c<1.0$ as shown in Fig. 5.15. When $\eta_e=1.0$, where $\eta_{12}(\Delta n|\eta_e,\eta_c)$ and $\eta_{22}(\Delta n|\eta_e,\eta_c)$ coincide with each other, the common average value increases slowly for small values of η_c and when $\eta_c>0.8$, it increases rapidly to its maximum common value of $\eta_{12}(\Delta n=-1.0\ \mu M|\eta_e=1.0,\eta_c=1.0)=\eta_{22}(\Delta n=-1.0\ \mu M|\eta_e=1.0,\eta_c=1.0)\rightarrow 1.0$.

Using $\Delta n=-1.0\ \mu M$, $\eta_c=0$, $u_e^+=2, u_1^-=2, u_1^+=2, u_2^-=2.0, u_2^+=2, u_c^-=2$ and the values of the transition rates specified in Eq. 3.14 into Eq. 4.15 and Eq. 4.16 so as to get the average occupation numbers of the internal potential wells V_1 and V_2 of a nano-channel with two internal potential wells denoted by $\eta_{12}(\Delta n|\eta_e,\eta_c)$ and $\eta_{22}(\Delta n|\eta_e,\eta_c)$, respectively. The plot of the variation of $\eta_{12}(\Delta n|\eta_e,\eta_c)$ and $\eta_{22}(\Delta n|\eta_e,\eta_c)$ as a function of η_e on the same graph are shown in Fig. 5.16.

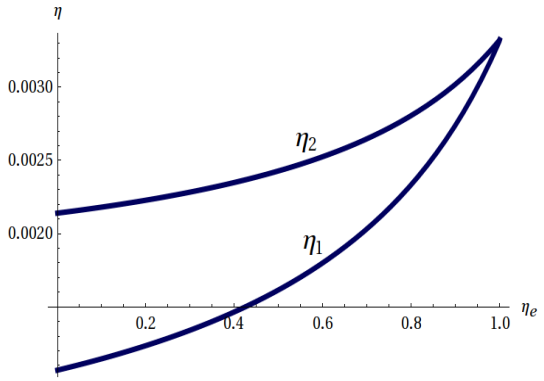

Fig. 5.16: Plot of $\eta_{12}(\Delta n|\eta_e,\eta_c)$ and $\eta_{22}(\Delta n|\eta_e,\eta_c)$ as a function of η_e when $s = 2$, $n_c = 1.0\ \mu M$, $\Delta n = -1.0\ \mu M$, $\eta_c = 0$, $\nu_e^+ = \nu_c^- = 15\,(\mu M)^{-1}s^{-1}, \nu_1^- = \nu_1^+ = 500\,s^{-1}, \nu_2^- = \nu_2^+ = 500\,s^{-1}$, $u_e^+ = 2, u_1^- = 2, u_1^+ = 2, u_2^- = 2.0, u_2^+ = 2, u_c^- = 2$

Using $\Delta n = -1.0\ \mu M$, $\eta_c = 1.0$, $u_e^+ = 2, u_1^- = 2, u_1^+ = 2, u_2^- = 2.0, u_2^+ = 2, u_c^- = 2$ and the values of the transition rates specified in Eq. 3.14 into Eq. 4.15 and Eq. 4.16 so as to get the average occupation numbers of the internal potential wells V_1 and V_2 of a nano-channel with two internal potential wells denoted by $\eta_{12}(\Delta n|\eta_e,\eta_c)$ and $\eta_{22}(\Delta n|\eta_e,\eta_c)$, respectively. The plot of the variation of $\eta_{12}(\Delta n|\eta_e,\eta_c)$ and $\eta_{22}(\Delta n|\eta_e,\eta_c)$ as a function of η_e on the same graph are shown in Fig. 5.17.

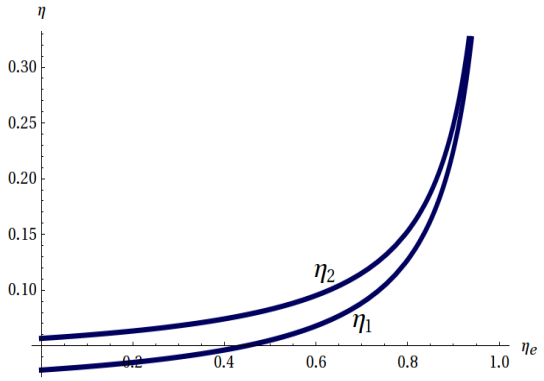

Fig. 5.17: Plot of $\eta_{12}(\Delta n|\eta_e,\eta_c)$ and $\eta_{22}(\Delta n|\eta_e,\eta_c)$ as a function of η_e when $s = 2$, $n_c = 1.0\ \mu M$, $\Delta n = -1.0\ \mu M$, $\eta_c = 1.0$, $\nu_e^+ = \nu_c^- = 15\,(\mu M)^{-1}s^{-1}, \nu_1^- = \nu_1^+ = 500\,s^{-1}, \nu_2^- = \nu_2^+ = 500\,s^{-1}$, $u_e^+ = 2, u_1^- = 2, u_1^+ = 2, u_2^- = 2.0, u_2^+ = 2, u_c^- = 2$

For the given possible values of Δn and η_c, the average values of $\eta_{12}(\Delta n|\eta_e,\eta_c)$ and $\eta_{22}(\Delta n|\eta_e,\eta_c)$ obey that: $\eta_{22}(\Delta n=-1.0\ \mu M|\eta_e,\eta_c)>\eta_{12}(\Delta n=-1.0\ \mu M|\eta_e,\eta_c)$ for all possible values of η_e and η_c and both increase continuously in the entire range $0<\eta_c<1.0$ as shown in Fig. 5.16 and Fig. 5.17 and approach the same value of 0.0033 as $\eta_e\rightarrow 1.0$ when $\eta_c=1.0$.

5.2 Comparison of the Average Particle Flux Through a Nano-Channel With One and Two Internal Potential Wells

Using $\eta_e = 0.1$, $\eta_c = 0.1$, $u_e^+ = 2, u_1^- = 2, u_1^+ = 2, u_2^- = 2.0, u_2^+ = 2, u_c^- = 2$ and the values of the transition rates specified in Eq. 3.14 into Eq. 3.15 and Eq. 4.14 so as to get the average particle flux through a nano-channel with a single internal potential well denoted by $J_1(\Delta n|\eta_e, \eta_c)$ and the average particle flux through a nano-channel with two internal potential wells denoted by $J_2(\Delta n|\eta_e, \eta_c)$, respectively. The plot of the variation of $J_1(\Delta n|\eta_e, \eta_c)$ and $J_2(\Delta n|\eta_e, \eta_c)$ as a function of Δn on the same graph are shown in Fig. 5.18.

Using $\eta_e = 0.95$, $\eta_c = 0.95$, $u_e^+ = 2, u_1^- = 2, u_1^+ = 2, u_2^- = 2.0, u_2^+ = 2, u_c^- = 2$ and the values of the transition rates specified in Eq. 3.14 into Eq. 3.15 and Eq. 4.14 so as to get the average particle flux through a nano-channel with a single internal potential well denoted by $J_1(\Delta n|\eta_e, \eta_c)$ and the average particle flux through a nano-channel with two internal potential wells denoted by $J_2(\Delta n|\eta_e, \eta_c)$, respectively. The plot of the variation of $J_1(\Delta n|\eta_e, \eta_c)$ and $J_2(\Delta n|\eta_e, \eta_c)$ as a function of Δn on the same graph are shown in Fig. 5.19.

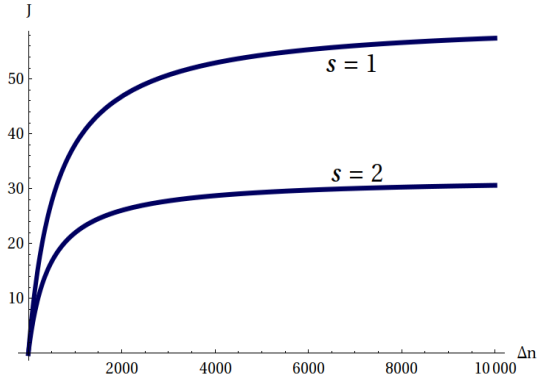

Fig. 5.18: Plot of $J_1(\Delta n|\eta_e, \eta_c)$ and $J_2(\Delta n|\eta_e, \eta_c)$ as a function of the concentration gradient Δn in units of μM when $n_c = 1.0\ \mu M$, $\eta_e = 0.1$, $\eta_c = 0.1$, $\nu_e^+ = \nu_c^- = 15\,(\mu M)^{-1}s^{-1}, \nu_1^- = \nu_1^+ = 500\,s^{-1}, \nu_2^- = \nu_2^+ = 500\,s^{-1}$, $u_e^+ = 2, u_1^- = 2, u_1^+ = 2, u_2^- = 2.0, u_2^+ = 2, u_c^- = 2$

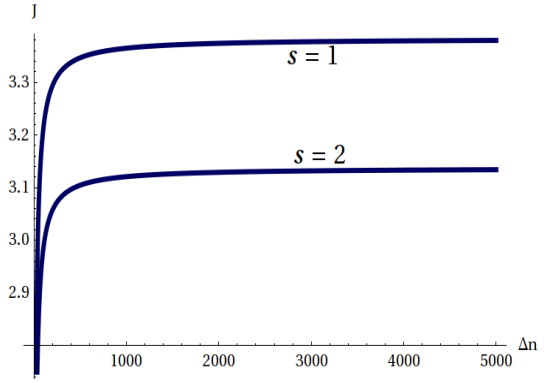

Fig. 5.19: Plot of $J_1(\Delta n|\eta_e,\eta_c)$ and $J_2(\Delta n|\eta_e,\eta_c)$ as a function of the concentration gradient Δn in units of μM when $n_c = 1.0\ \mu M$, $\eta_e = 0.95$, $\eta_c = 0.95$, $\nu_e^+ = \nu_c^- = 15\,(\mu M)^{-1}s^{-1}, \nu_1^- = \nu_1^+ = 500\,s^{-1}, \nu_2^- = \nu_2^+ = 500\,s^{-1}$, $u_e^+ = 2, u_1^- = 2, u_1^+ = 2, u_2^- = 2.0, u_2^+ = 2, u_c^- = 2$

For all possible given average values of η_e and η_c, the average particle fluxes as a function of Δn, that is, $J_1(\Delta n|\eta_e,\eta_c)$ and $J_2(\Delta n|\eta_e,\eta_c)$ obey that: $J_1(\Delta n|\eta_e > 0,\eta_c < 1.0) > J_2(\Delta n|\eta_e > 0,\eta_c < 1.0)$, for all possible values of Δn, $\eta_e > 0$ and $\eta_c < 1.0$. That is, for the same given values of Δn, η_e, η_c and transition rates, a nano-channel with a single internal potential well is more permeable to particles than that with two internal potential wells. In other words, the rate of translocation of particles through a nano-channel with a single internal potential well is greater than that with two internal potential wells. When both η_e and η_c increase to higher values both average particle fluxes decrease and finally become zero when $J_1(\Delta n|\eta_e = 1.0,\eta_c = 1.0) = J_2(\Delta n|\eta_e = 1.0,\eta_c = 1.0) = 0$, which implies that the nano-channel becomes totally impermeable or totally inactivated. The average particle fluxes assume maximum saturation values when $J_1(\Delta n = 1\ M|\eta_e = 1.0,\eta_c = 0) = 67.6674^{-1}$ and $J_2(\Delta n = 1\ M|\eta_e = 1.0,\eta_c = 0) = 33.8338s^{-1}$, which implies that the nano-channel is fully activated and hence the rate of translocation of particles through the nano-channel is maximum. Therefore, the gate of the nano-channel is fully open to conduct particles in the positive direction. Both $J_1(\Delta n|\eta_e,\eta_c)$ and $J_2(\Delta n|\eta_e,\eta_c)$ increase rapidly and saturate quickly to different saturation values and become parallel to each other in the small range of the concentration gradient Δn as shown in Fig. 5.18 to Fig. 5.20. This property reflects the fact that a rapid process occurs that changes the gate of the nano-channel from fully being closed state to fully open open state.

Using $\eta_e = 1.0$, $\eta_c = 0$, $u_e^+ = 2, u_1^- = 2, u_1^+ = 2, u_2^- = 2.0, u_2^+ = 2, u_c^- = 2$ and the values of the transition rates specified in Eq. 3.14 into Eq. 3.15 and Eq. 4.14 so as to get the average particle flux through a nano-channel with a single internal potential well denoted by $J_1(\Delta n|\eta_e, \eta_c)$ and the average particle flux through a nano-channel with two internal potential wells denoted by $J_2(\Delta n|\eta_e, \eta_c)$, respectively. The plot of the variation of $J_1(\Delta n|\eta_e, \eta_c)$ and $J_2(\Delta n|\eta_e, \eta_c)$ as a function of Δn on the same graph are shown in Fig. 5.20.

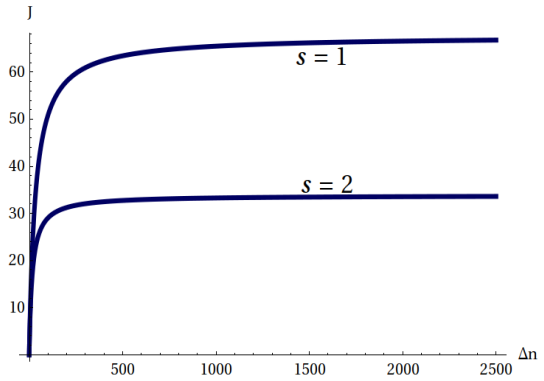

Fig. 5.20: Plot of $J_1(\Delta n|\eta_e, \eta_c)$ and $J_2(\Delta n|\eta_e, \eta_c)$ as a function of the concentration gradient Δn in units of μM when $n_c = 1.0\ \mu M$, $\eta_e = 1.0$, $\eta_c = 0$, $\nu_e^+ = \nu_c^- = 15\,(\mu M)^{-1}s^{-1}, \nu_1^- = \nu_1^+ = 500\,s^{-1}, \nu_2^- = \nu_2^+ = 500\,s^{-1}$, $u_e^+ = 2, u_1^- = 2, u_1^+ = 2, u_2^- = 2.0, u_2^+ = 2, u_c^- = 2$

Using $\Delta n = 10000\ \mu M$, $\eta_e = 1.0$, $u_e^+ = 2, u_1^- = 2, u_1^+ = 2, u_2^- = 2.0, u_2^+ = 2, u_c^- = 2$ and of the transition rates specified in Eq. 3.14 into Eq. 3.15 and Eq. 4.14 so as to get the average particle flux through a nano-channel with a single internal potential well denoted by $J_1(\Delta n|\eta_e, \eta_c)$ and the average particle flux through a nano-channel with two internal potential wells denoted by $J_2(\Delta n|\eta_e, \eta_c)$, respectively. The plot of the variation of $J_1(\Delta n|\eta_e, \eta_c)$ and $J_2(\Delta n|\eta_e, \eta_c)$ as a function of η_c on the same graph are shown in Fig. 5.21.

For all possible given average values of Δn and η_e, the average particle flux as a function of η_c, that is, $J_1(\Delta n|\eta_e, \eta_c)$ and $J_2(\Delta n|\eta_e, \eta_c)$, obey that: $J_1(\Delta n = 10000\ \mu M|\eta_e = 1.0, \eta_c) > J_2(\Delta n = 10000\ \mu M|\eta_e = 1.0, \eta_c)$ for all possible values of η_c. This property hold for all possible values of $\eta_e > 0$ and η_c. As the average value of η_c increases, the average particle flux through a nano-channel with a single internal potential well, $J_1(\Delta n|\eta_e, \eta_c)$ decreases almost linearly but

the average particle flux through a nano-channel with two internal potential wells, $J_2(\Delta n|\eta_e,\eta_c)$ decreases slowly just like an inverted parabola as shown in Fig. 5.21. As $\eta_c \rightarrow 1.0$, both average particle fluxes become zero, that is, $J_1(\Delta n = 10000\ \mu M|\eta_e = 1.0,\eta_c = 1.0) = J_2(\Delta n = 10000\ \mu M|\eta_e = 1.0,\eta_c = 1.0) = 0$, which implies that the nano-channel behaves as if its gate is in the fully closed state. As $\eta_c \rightarrow 0$, both fluxes assume maximum values, that is, $J_1(\Delta n = 10000\ \mu M|\eta_e = 1.0,\eta_c = 0) = 67.4429 s^{-1}$ and $J_2(\Delta n = 10000\ \mu M|\eta_e = 1.0,\eta_c = 0) = 33.7776 s^{-1}$, which implies that the nano-channel behaves as if its gate is fully open, and hence the rate of translocation of particles through the nano-channel is maximum.

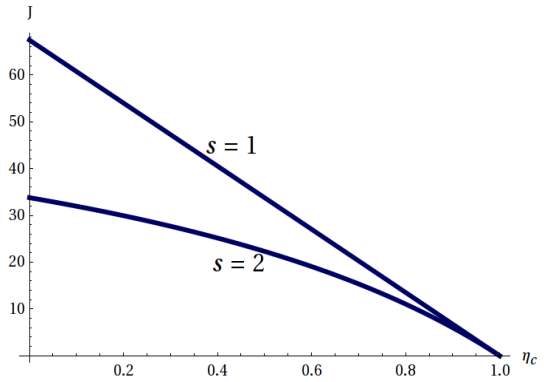

Fig. 5.21: Plot of $J_1(\Delta n|\eta_e,\eta_c)$ and $J_2(\Delta n|\eta_e,\eta_c)$ as a function of η_c when $n_c = 1.0\ \mu M$, $\Delta n = 10000\ \mu M$, $\eta_e = 1.0$, $\nu_e^+ = \nu_c^- = 15\,(\mu M)^{-1}s^{-1}, \nu_1^- = \nu_1^+ = 500\,s^{-1}, \nu_2^- = \nu_2^+ = 500\,s^{-1}$, $u_e^+ = 2, u_1^- = 2, u_1^+ = 2, u_2^- = 2.0, u_2^+ = 2, u_c^- = 2$

Using $\Delta n = 10000\ \mu M$, $\eta_c = 0$, $u_e^+ = 2, u_1^- = 2, u_1^+ = 2, u_2^- = 2.0, u_2^+ = 2, u_c^- = 2$ and of the transition rates specified in Eq. 3.14 into Eq. 3.15 and Eq. 4.14 so as to get the average particle flux through a nano-channel with a single internal potential well denoted by $J_1(\Delta n|\eta_e,\eta_c)$ and the average particle flux through a nano-channel with two internal potential wells denoted by $J_2(\Delta n|\eta_e,\eta_c)$, respectively. The plot of the variation of $J_1(\Delta n|\eta_e,\eta_c)$ and $J_2(\Delta n|\eta_e,\eta_c)$ as a function of η_e on the same graph are shown in Fig. 5.22.

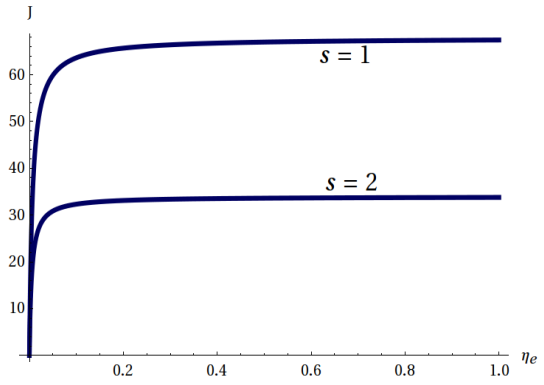

Fig. 5.22: Plot of $J_1(\Delta n|\eta_e,\eta_c)$ and $J_2(\Delta n|\eta_e,\eta_c)$ as a function of η_e when $n_c = 1.0\ \mu M$, $\Delta n = 10000\ \mu M$, $\eta_c = 0$, $\nu_e^+ = \nu_c^- = 15\,(\mu M)^{-1}s^{-1}, \nu_1^- = \nu_1^+ = 500\,s^{-1}, \nu_2^- = \nu_2^+ = 500\,s^{-1}$, $u_e^+ = 2, u_1^- = 2, u_1^+ = 2, u_2^- = 2.0, u_2^+ = 2, u_c^- = 2$

Using $\Delta n = 10000\ \mu M$, $\eta_c = 0.95$, $u_e^+ = 2, u_1^- = 2, u_1^+ = 2, u_2^- = 2.0, u_2^+ = 2, u_c^- = 2$ and of the transition rates specified in Eq. 3.14 into Eq. 3.15 and Eq. 4.14 so as to get the average particle flux through a nano-channel with a single internal potential well denoted by $J_1(\Delta n|\eta_e,\eta_c)$ and the average particle flux through a nano-channel with two internal potential wells denoted by $J_2(\Delta n|\eta_e,\eta_c)$, respectively. The plot of the variation of $J_1(\Delta n|\eta_e,\eta_c)$ and $J_2(\Delta n|\eta_e,\eta_c)$ as a function of η_e on the same graph are shown in Fig. 5.23.

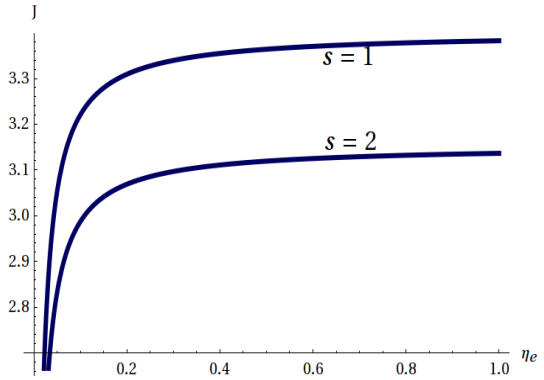

Fig. 5.23: Plot of $J_1(\Delta n|\eta_e,\eta_c)$ and $J_2(\Delta n|\eta_e,\eta_c)$ as a function of η_e when $n_c = 1.0\ \mu M$, $\Delta n = 10000\ \mu M$, $\eta_c = 0.95$, $\nu_e^+ = \nu_c^- = 15\,(\mu M)^{-1}s^{-1}, \nu_1^- = \nu_1^+ = 500\,s^{-1}, \nu_2^- = \nu_2^+ = 500\,s^{-1}$, $u_e^+ = 2, u_1^- = 2, u_1^+ = 2, u_2^- = 2.0, u_2^+ = 2, u_c^- = 2$

For all possible given average values of Δn and η_c, the average particle fluxes as functions of η_e, that is, $J_1(\Delta n|\eta_e,\eta_c)$ and $J_2(\Delta n|\eta_e,\eta_c)$ obey that: $J_1(\Delta n = 10000\ \mu M|\eta_e,\eta_c = 0) > J_2(\Delta n = 10000\ \mu M|\eta_e,\eta_c = 0)$, for all possible val-

ues of η_e. Both $J_1(\Delta n|\eta_e,\eta_c)$ and $J_2(\Delta n|\eta_e,\eta_c)$ increase rapidly in the range of $0 < \eta_e < 0.1$ and after that they saturate to different average values as shown in Fig. 5.22 and Fig. 5.23. However as η_c increases, both fluxes $J_1(\Delta n|\eta_e,\eta_c)$ and $J_2(\Delta n|\eta_e,\eta_c)$ decrease and the difference between them decreases and finally when $\eta_c = 1.0$, both fluxes coincide and assume the same negative flux as shown in Fig. 5.24.

Using $\Delta n = 10000\ \mu M$, $\eta_c = 1.0$, $u_e^+ = 2, u_1^- = 2, u_1^+ = 2, u_2^- = 2.0, u_2^+ = 2, u_c^- = 2$ and of the transition rates specified in Eq. 3.14 into Eq. 3.15 and Eq. 4.14 so as to get the average particle flux through a nano-channel with a single internal potential well denoted by $J_1(\Delta n|\eta_e,\eta_c)$ and the average particle flux through a nano-channel with two internal potential wells denoted by $J_2(\Delta n|\eta_e,\eta_c)$, respectively. The plot of the variation of $J_1(\Delta n|\eta_e,\eta_c)$ and $J_2(\Delta n|\eta_e,\eta_c)$ as a function of η_e on the same graph are shown in Fig. 5.24.

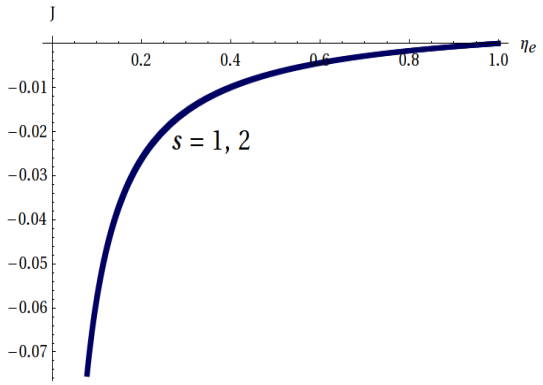

Fig. 5.24: Plot of $J_1(\Delta n|\eta_e,\eta_c)$ and $J_2(\Delta n|\eta_e,\eta_c)$ as a function of η_e when $n_c = 1.0\ \mu M$, $\Delta n = 10000\ \mu M$, $\eta_c = 1.0$, $\nu_e^+ = \nu_c^- = 15\,(\mu M)^{-1}s^{-1}, \nu_1^- = \nu_1^+ = 500\,s^{-1}, \nu_2^- = \nu_2^+ = 500\,s^{-1}$, $u_e^+ = 2, u_1^- = 2, u_1^+ = 2, u_2^- = 2.0, u_2^+ = 2, u_c^- = 2$

Using $\Delta n = 1000\ \mu M$, $\eta_c = 0$, $u_e^+ = 2, u_1^- = 2, u_1^+ = 2, u_2^- = 2.0, u_2^+ = 2, u_c^- = 2$ and of the transition rates specified in Eq. 3.14 into Eq. 3.15 and Eq. 4.14 so as to get the average particle flux through a nano-channel with a single internal potential well denoted by $J_1(\Delta n|\eta_e,\eta_c)$ and the average particle flux through a nano-channel with two internal potential wells denoted by $J_2(\Delta n|\eta_e,\eta_c)$, respectively. The plot of the variation of $J_1(\Delta n|\eta_e,\eta_c)$ and $J_2(\Delta n|\eta_e,\eta_c)$ as a function of η_e on the same graph are shown in Fig. 5.25.

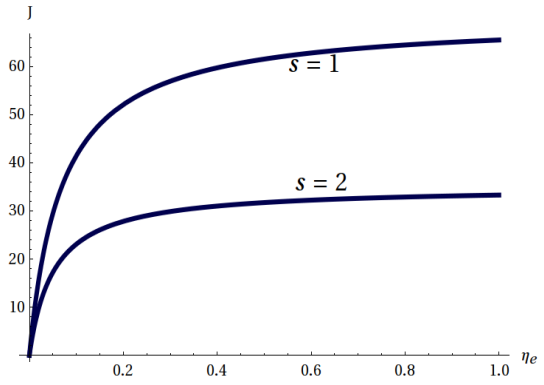

Fig. 5.25: Plot of $J_1(\Delta n|\eta_e,\eta_c)$ and $J_2(\Delta n|\eta_e,\eta_c)$ as a function of η_e when $n_c = 1.0\ \mu M$, $\Delta n = 1000\ \mu M$, $\eta_c = 0$, $\nu_e^+ = \nu_c^- = 15\,(\mu M)^{-1}s^{-1}, \nu_1^- = \nu_1^+ = 500\,s^{-1}, \nu_2^- = \nu_2^+ = 500\,s^{-1}$, $u_e^+ = 2, u_1^- = 2, u_1^+ = 2, u_2^- = 2.0, u_2^+ = 2, u_c^- = 2$

Using $\Delta n = 0$, $\eta_c = 0$, $u_e^+ = 2, u_1^- = 2, u_1^+ = 2, u_2^- = 2.0, u_2^+ = 2, u_c^- = 2$ and of the transition rates specified in Eq. 3.14 into Eq. 3.15 and Eq. 4.14 so as to get the average particle flux through a nano-channel with a single internal potential well denoted by $J_1(\Delta n|\eta_e,\eta_c)$ and the average particle flux through a nano-channel with two internal potential wells denoted by $J_2(\Delta n|\eta_e,\eta_c)$, respectively. The plot of the variation of $J_1(\Delta n|\eta_e,\eta_c)$ and $J_2(\Delta n|\eta_e,\eta_c)$ as a function of η_e on the same graph are shown in Fig. 5.26.

Using $\Delta n = 0$, $\eta_c = 0.5$, $u_e^+ = 2, u_1^- = 2, u_1^+ = 2, u_2^- = 2.0, u_2^+ = 2, u_c^- = 2$ and of the transition rates specified in Eq. 3.14 into Eq. 3.15 and Eq. 4.14 so as to get the average particle flux through a nano-channel with a single internal potential well denoted by $J_1(\Delta n|\eta_e,\eta_c)$ and the average particle flux through a nano-channel with two internal potential wells denoted by $J_2(\Delta n|\eta_e,\eta_c)$, respectively. The plot of the variation of $J_1(\Delta n|\eta_e,\eta_c)$ and $J_2(\Delta n|\eta_e,\eta_c)$ as a function of η_e on the same graph are shown in Fig. 5.27.

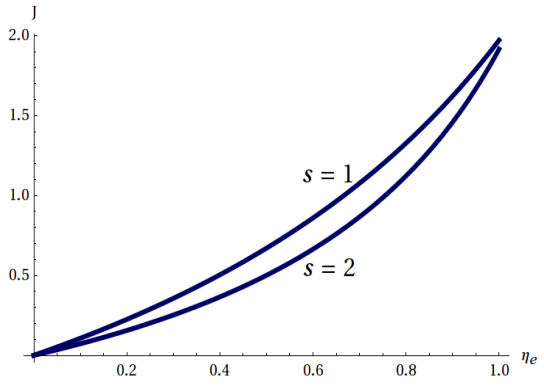

Fig. 5.26: Plot of $J_1(\Delta n|\eta_e,\eta_c)$ and $J_2(\Delta n|\eta_e,\eta_c)$ as a function of η_e when $n_c = 1.0\ \mu M$, $\Delta n = 0$, $\eta_c = 0$, $\nu_e^+ = \nu_c^- = 15\,(\mu M)^{-1}s^{-1}, \nu_1^- = \nu_1^+ = 500\,s^{-1}, \nu_2^- = \nu_2^+ = 500\,s^{-1}$, $u_e^+ = 2, u_1^- = 2, u_1^+ = 2, u_2^- = 2.0, u_2^+ = 2, u_c^- = 2$

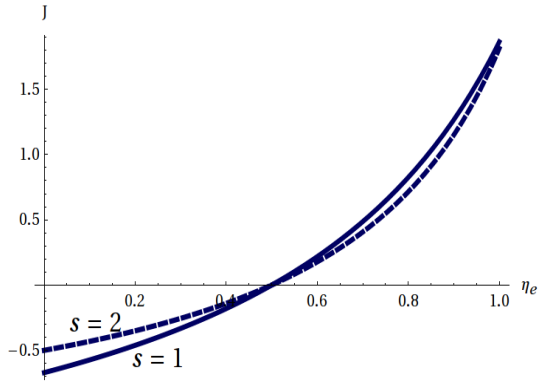

Fig. 5.27: Plot of $J_1(\Delta n|\eta_e,\eta_c)$ and $J_2(\Delta n|\eta_e,\eta_c)$ as a function of η_e when $n_c = 1.0\ \mu M$, $\Delta n = 0$, $\eta_c = 0.5$, $\nu_e^+ = \nu_c^- = 15\,(\mu M)^{-1}s^{-1}, \nu_1^- = \nu_1^+ = 500\,s^{-1}, \nu_2^- = \nu_2^+ = 500\,s^{-1}$, $u_e^+ = 2, u_1^- = 2, u_1^+ = 2, u_2^- = 2.0, u_2^+ = 2, u_c^- = 2$

For the given possible values of Δn and η_c, the average particle fluxes as a function of η_e, that is, $J_1(\Delta n|\eta_e,\eta_c)$ and $J_2(\Delta n|\eta_e,\eta_c)$ obey that: $J_1(\Delta n = 0|\eta_e,\eta_c = 0) > J_2(\Delta n = 0|\eta_e,\eta_c = 0)$ for all possible values of η_e and both increase continuously in the entire range $0 < \eta_e < 1.0$ as shown in Fig. 5.26. But, the plot of $J_2(\Delta n = 0|\eta_e,\eta_c > 0)$ began to shift upward, that is, it increases as η_c increases and intersects with the plot of $J_1(\Delta n = 0|\eta_e,\eta_c)$ as shown in Fig. 5.27 and finally when $\eta_c = 1.0$, the plot of $J_2(\Delta n = 0|\eta_e,\eta_c = 1.0)$ exceeds that of $J_1(\Delta n = 0|\eta_e,\eta_c = 1.0)$, that is, $J_2(\Delta n = 0|\eta_e,\eta_c = 1.0) > J_1(\Delta n = 0|\eta_e,\eta_c = 1.0)$ in the entire range $0 < \eta_e < 1.0$ and both become negative as shown in Fig. 5.28.

Using $\Delta n = 0$, $\eta_c = 1.0$, $u_e^+ = 2, u_1^- = 2, u_1^+ = 2, u_2^- = 2.0, u_2^+ = 2, u_c^- = 2$ and

of the transition rates specified in Eq. 3.14 into Eq. 3.15 and Eq. 4.14 so as to get the average particle flux through a nano-channel with a single internal potential well denoted by $J_1(\Delta n|\eta_e,\eta_c)$ and the average particle flux through a nano-channel with two internal potential wells denoted by $J_2(\Delta n|\eta_e,\eta_c)$, respectively. The plot of the variation of $J_1(\Delta n|\eta_e,\eta_c)$ and $J_2(\Delta n|\eta_e,\eta_c)$ as a function of η_e on the same graph are shown in Fig. 5.28.

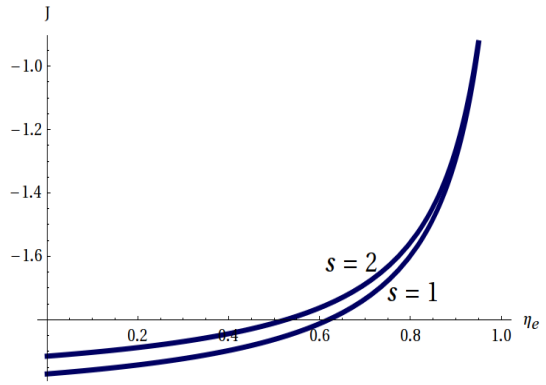

Fig. 5.28: Plot of $J_1(\Delta n|\eta_e,\eta_c)$ and $J_2(\Delta n|\eta_e,\eta_c)$ as a function of η_e when $n_c = 1.0\ \mu M$, $\Delta n = 0$, $\eta_c = 1.0$, $\nu_e^+ = \nu_c^- = 15\,(\mu M)^{-1}s^{-1}, \nu_1^- = \nu_1^+ = 500\,s^{-1}, \nu_2^- = \nu_2^+ = 500\,s^{-1}$, $u_e^+ = 2, u_1^- = 2, u_1^+ = 2, u_2^- = 2.0, u_2^+ = 2, u_c^- = 2$

Using $\Delta n = -0.99\ \mu M$, $\eta_c = 0$, $u_e^+ = 2, u_1^- = 2, u_1^+ = 2, u_2^- = 2.0, u_2^+ = 2, u_c^- = 2$ and of the transition rates specified in Eq. 3.14 into Eq. 3.15 and into Eq. 4.14 so as to get the average particle flux through a nano-channel with a single internal potential well denoted by $J_1(\Delta n|\eta_e,\eta_c)$ and the average particle flux through a nano-channel with two internal potential wells denoted by $J_2(\Delta n|\eta_e,\eta_c)$, respectively. The plot of the variation of $J_1(\Delta n|\eta_e,\eta_c)$ and $J_2(\Delta n|\eta_e,\eta_c)$ as a function of η_e on the same graph are shown in Fig. 5.29.

Using $\Delta n = -0.99\ \mu M$, $\eta_c = 0.5$, $u_e^+ = 2, u_1^- = 2, u_1^+ = 2, u_2^- = 2.0, u_2^+ = 2, u_c^- = 2$ and of the transition rates specified in Eq. 3.14 into Eq. 3.15 and Eq. 4.14 so as to get the average particle flux through a nano-channel with a single internal potential well denoted by $J_1(\Delta n|\eta_e,\eta_c)$ and the average particle flux through a nano-channel with two internal potential wells denoted by $J_2(\Delta n|\eta_e,\eta_c)$, respectively. The plot of the variation of $J_1(\Delta n|\eta_e,\eta_c)$ and $J_2(\Delta n|\eta_e,\eta_c)$ as a function of η_e on the same graph are shown in Fig. 5.30.

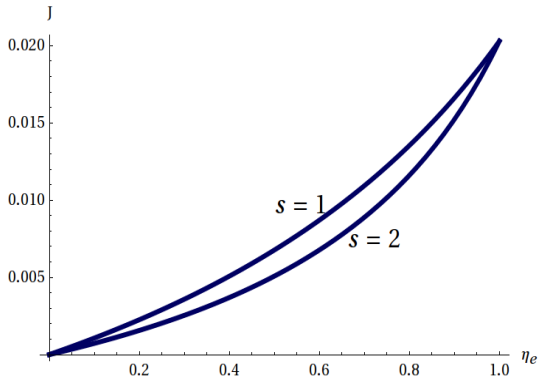

Fig. 5.29: Plot of $J_1(\Delta n|\eta_e,\eta_c)$ and $J_2(\Delta n|\eta_e,\eta_c)$ as a function of η_e when $n_c = 1.0\ \mu M$, $\Delta n = -0.99\ \mu M$, $\eta_c = 0$, $\nu_e^+ = \nu_c^- = 15\,(\mu M)^{-1}s^{-1}, \nu_1^- = \nu_1^+ = 500\,s^{-1}, \nu_2^- = \nu_2^+ = 500\,s^{-1}$, $u_e^+ = 2, u_1^- = 2, u_1^+ = 2, u_2^- = 2.0, u_2^+ = 2, u_c^- = 2$

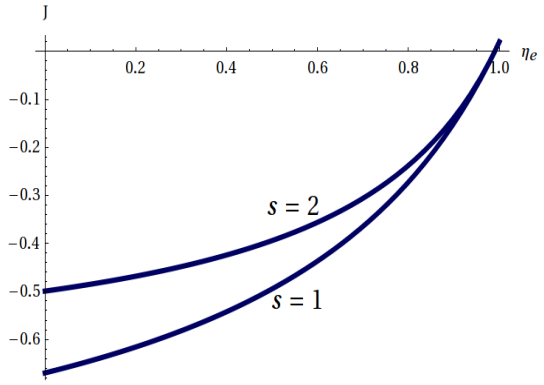

Fig. 5.30: Plot of $J_1(\Delta n|\eta_e,\eta_c)$ and $J_2(\Delta n|\eta_e,\eta_c)$ as a function of η_e when $n_c = 1.0\ \mu M$, $\Delta n = -0.99\ \mu M$, $\eta_c = 0.5$, $\nu_e^+ = \nu_c^- = 15\,(\mu M)^{-1}s^{-1}, \nu_1^- = \nu_1^+ = 500\,s^{-1}, \nu_2^- = \nu_2^+ = 500\,s^{-1}$, $u_e^+ = 2, u_1^- = 2, u_1^+ = 2, u_2^- = 2.0, u_2^+ = 2, u_c^- = 2$

For the given possible values of Δn and η_c, the average particle fluxes as a function of η_e, that is, $J_1(\Delta n|\eta_e,\eta_c)$ and $J_2(\Delta n|\eta_e,\eta_c)$ obey that: $J_1(\Delta n = -0.99\ \mu M|\eta_e,\eta_c = 0) > J_2(\Delta n = -0.99\ \mu M|\eta_e,\eta_c = 0)$ for all possible values of η_e and both increase continuously in the entire range $0 < \eta_e < 1.0$ as shown in Fig. 5.29. But, the plot of $J_2(\Delta n = -0.99\ \mu M|\eta_e,\eta_c > 0)$ began to shift upward, that is, it increases as η_c increases and approaches the plot of $J_1(\Delta n = -0.99\ \mu M|\eta_e,\eta_c)$ as shown in Fig. 5.30 and finally when $\eta_c = 1.0$, the plot of $J_2(\Delta n = -0.99\ \mu M|\eta_e,\eta_c = 1.0)$ exceeds that of $J_1(\Delta n = -0.99\ \mu M|\eta_e,\eta_c = 1.0)$, that is, $J_2(\Delta n = 0|\eta_e,\eta_c = 1.0)$ becomes less negative while $J_1(\Delta n = 0|\eta_e,\eta_c = 1.0)$ becomes more negative in the entire range $0 < \eta_e < 1.0$ as shown in Fig. 5.31.

Using $\Delta n = -0.99\ \mu M$, $\eta_c = 1.0$, $u_e^+ = 2, u_1^- = 2, u_1^+ = 2, u_2^- = 2.0, u_2^+ = 2, u_c^- = 2$ and of the transition rates specified in Eq. 3.14 into Eq. 3.15 and Eq. 4.14 so as to get the average particle flux through a nano-channel with a single internal potential well denoted by $J_1(\Delta n|\eta_e, \eta_c)$ and the average particle flux through a nano-channel with two internal potential wells denoted by $J_2(\Delta n|\eta_e, \eta_c)$, respectively. The plot of the variation of $J_1(\Delta n|\eta_e, \eta_c)$ and $J_2(\Delta n|\eta_e, \eta_c)$ as a function of η_e on the same graph are shown in Fig. 5.31.

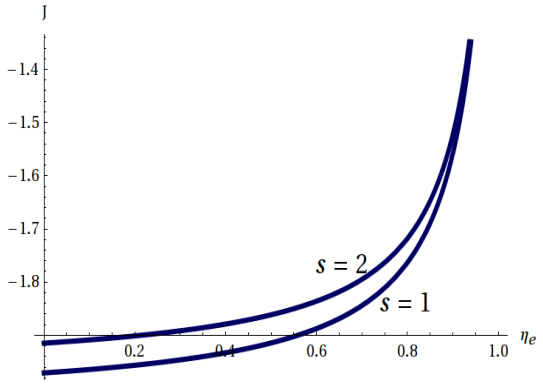

Fig. 5.31: Plot of $J_1(\Delta n|\eta_e, \eta_c)$ and $J_2(\Delta n|\eta_e, \eta_c)$ as a function of η_e when $n_c = 1.0\ \mu M$, $\Delta n = -0.99\ \mu M$, $\eta_c = 1.0$, $\nu_e^+ = \nu_c^- = 15\,(\mu M)^{-1}s^{-1}, \nu_1^- = \nu_1^+ = 500\,s^{-1}, \nu_2^- = \nu_2^+ = 500\,s^{-1}$, $u_e^+ = 2, u_1^- = 2, u_1^+ = 2, u_2^- = 2.0, u_2^+ = 2, u_c^- = 2$

5.3 Discussion of the Average Occupation Number of the Internal Potential Wells and the Average Particle Flux Through a Nano-Channel With One and Two Internal Potential Wells

The average particle flux through a nano-channel as a function of Δn, for the specified values of the other parameters, is a rapidly increasing function of Δn for small and intermediate values. When $\Delta n = 0$, the average flux has a minimum value and as Δn increases to large values, the average particle flux through a nano-channel with both one and two internal potential wells increases slowly and finally enters into the saturation region in which it no longer increase as the concentration gradient increases. For most cases, the range of the concentration gradient in which the average particle flux becomes saturated lies between

$1.0\ M$ and $10\ M$ for the specified values of the other parameters. Moreover, the average particle flux approaches more rapidly to its saturation value when the external potential well V_e is occupied and the external potential well V_c is empty. The average particle flux as a function of Δn, through a nano-channel with a single internal potential well is greater than the average particle flux through a nano-channel with two internal potential wells, that is $J_1(\Delta n|\eta_e,\eta_c) > J_2(\Delta n|\eta_e,\eta_c)$.

The average particle flux through a nano-channel with one and two internal potential wells as a function of η_e, for the given values of the other parameters, has a minimum value when $\eta_e = 0$, which implies that the nano-channel is in the inactivated state and hence the gate of the nano-channel is closed to conduct particles in the positive direction. For all the three possible ranges of concentration gradients and number of internal sites, the average particle flux through a nano-channel is a rapidly increasing function of η_e. Therefore, the rate of translocation of particles through the nano-channel increases as η_e increases, for the given values of the other parameters. Moreover, as $\eta_e \to 1$, the flux attains a maximum positive value which implies that the nano-channel becomes fully activated and hence behaves as if its gate is fully open to conduct particles in the positive direction. The average particle flux has a maximum positive value when V_e is occupied, that is $\eta_e = 1$ and the average particle flux is minimum when V_e is empty, that is $\eta_e = 0$. Therefore, as the mean residence time of particles in V_e increases, which means that the occupation probability of the site increases, the nano-channel becomes more activated and thus the rate of translocation of particles through the nano-channel increases. In general, the optimized particle flux as a function of η_e, for $s = 1$ and $s = 2$, for the specified values of the other parameters, could be negative, zero and positive and as a result η_e acts as a gating variable that controls both magnitude and direction of the average particle flux through the nano-channel.

For all possible ranges of concentration gradient, that is, $\Delta n > 0$, $\Delta n = 0$ and $\Delta n < 0$ and for all possible number of internal sites $s = 1$ and $s = 2$, the average particle flux as a function of η_c, for the specified values of the other parameters, has a maximum positive value when $\eta_c = 0$, which implies that the nano-channel is fully activated and behaves as if its gate is fully open to conduct particles in the positive direction and blocks flux in the reverse direction.

The average particle flux has a maximum positive value when V_c is empty, that is $\eta_c = 0$ and as η_c increases, the average particle flux decreases and finally attains a small negative value when V_c is occupied, that is $\eta_c = 1$. Therefore, the rate of translocation of particles through the nano-channel decreases as η_c increases, for the specified values of the other parameters. Moreover, the nano-channel becomes totally inactivated and behaves as if its gate is totally closed and as a result the flux as a function of η_c attains a small negative value when $\eta_c = 1$, which implies that the gate of the nano-channel is fully closed to conduct particles in the positive direction. Therefore, as the mean residence time of particles in V_c increases, which means that the occupation probability of the site increases, the nano-channel becomes less activated and thus the rate of translocation of particles through the nano-channel decreases. In general, the average particle flux as a function of η_c (when $s = 1$, $s = 2$, for the specified values of the other parameters, could be negative, zero and positive and as a result η_c also acts as a gating variable that controls both magnitude and direction of the average particle flux through the nano-channel.

Based on our model of nano-channels, we have generated a positive particle flux through the nano-channel when $\Delta n > 0$, $\Delta n = 0$ and $\Delta n < 0$ for the given values of the transition rates and number of internal sites, which has a maximum positive saturation value. Moreover, the occupation numbers η_e and η_c act as gate variables that control and change the direction and magnitude of the average particle flux through the nano-channel. That is, the flux through the nano-channel could be positive, zero or negative depending on the values of these variables. Maximum negative flux occurs as $\eta_e \to 0$, $\eta_c \to 1$ but maximum positive flux occurs as $\eta_e \to 1$, $\eta_c \to 0$.

The average values of the occupation numbers of the internal potential wells as a function of Δn, for the specified values of the other parameters, are rapidly increasing functions of Δn for small and intermediate values. When $\Delta n \to 0$, the average occupation numbers have small positive values and as Δn increases to large values, the average occupation numbers of the internal potential wells of a nano-channel with both one and two internal potential wells increase slowly and finally approach the saturation region in which they no longer increase as the concentration gradient increases. For most cases, the range of the con-

centration gradient in which these average occupation numbers become saturated lies between $1.0\ M$ and $10\ M$ for the specified values of the other parameters. Moreover, the average occupation numbers approach more rapidly to the saturation value when the external potential wells V_e and V_c are occupied. For a nano-channel with two internal potential wells, the average occupation number as functions of Δn of the internal potential well V_1 is greater than the average occupation number of the internal potential well V_2, that is $\eta_{12}(\Delta n|\eta_e,\eta_c) > \eta_{22}(\Delta n|\eta_e,\eta_c)$.

The average value of the occupation number of the internal potential well V_1 increases more rapidly as η_e increases and slowly as η_c increases. Similarly, the average value of the occupation number of the internal potential well V_2 increases more rapidly as η_c increases and slowly as η_e increases. As the average value of the occupation number of V_1 increases, the average value of the occupation number of V_2 also increases, and vice versa. The average value of the occupation number of V_1 increases as the values of the normalized potential barriers u_1^-, u_1^+ and u_2^+ increase and as u_e^+, u_2^- and u_c^- decrease. Similarly, the average value of the occupation number of V_2 increases as the values of the normalized potential barriers u_2^-, u_2^+ and u_1^- increase and as u_e^+, u_1^+ and u_c^- decrease.

5.4 Conclusion of the Properties of a Nano-Channel with One and Two Internal Potential Wells

1. The maximum average value of the internal occupation numbers are one and occurs when $\eta_{12}(\Delta n|\eta_e = 1.0, \eta_c = 1.0) = \eta_{22}(\Delta n|\eta_e = 1.0, \eta_c = 1.0) = 1.0$.

2. The occupation probability of V_1 increases as the average value of η_e increases and as a result the average value of $\eta_{12}(\Delta n|\eta_e, \eta_c)$ increases as η_e increases.

3. The occupation probability of V_2 increases as the average value of η_c increases and as a result the average value of $\eta_{22}(\Delta n|\eta_e, \eta_c)$ increases as η_c increases.

4. For the given values of $\eta_e > 0, \eta_c < 1.0$, the average values of $\eta_{12}(\Delta n|\eta_e, \eta_c)$ and $\eta_{22}(\Delta n|\eta_e, \eta_c)$ increase rapidly in the small range of the concentration gradient Δn and then saturate to different maximum saturation values.

5. For the given values of $\eta_e > 0, \eta_c < 1.0$, after saturation plots of the average values of $\eta_{12}(\Delta n|\eta_e, \eta_c)$ and $\eta_{22}(\Delta n|\eta_e, \eta_c)$ as functions of Δn become parallel to each other and $\eta_{12}(\Delta n|\eta_e, \eta_c) > \eta_{22}(\Delta n|\eta_e, \eta_c)$.

6. When $\eta_e = 0, \eta_c = 1.0$, the average values of $\eta_{12}(\Delta n|\eta_e, \eta_c)$ and $\eta_{22}(\Delta n|\eta_e, \eta_c)$ assume constant values that don't change as the concentration gradient increases to large positive values.

7. For the given values of $\Delta n > 0$ and $\eta_e > 0$, the average values of $\eta_{12}(\Delta n|\eta_e, \eta_c)$ and $\eta_{22}(\Delta n|\eta_e, \eta_c)$ as a function of η_c increase slowly as an upward parabola and $\eta_{12}(\Delta n|\eta_e, \eta_c)$ is less sensitive to the variation of η_c but $\eta_{22}(\Delta n|\eta_e, \eta_c)$ is more sensitive to the variation of η_c as shown in Fig. 5.5.

8. For the given values of $\Delta n > 0$ and $\eta_c < 1.0$, the average values of $\eta_{12}(\Delta n|\eta_e, \eta_c)$ and $\eta_{22}(\Delta n|\eta_e, \eta_c)$ as a function of η_e increase rapidly in the small range $0 < \eta_e < 0.2$ and the become saturated to different saturation values and become parallel to each other. As the average value of $\eta_c \to 1.0$, the two fluxes coincide with each other as shown in Fig. 5.7.

9. For the given values of $\Delta n > 0$ and $\eta_c < 1.0$, the average value of both $\eta_{12}(\Delta n|\eta_e, \eta_c)$ and $\eta_{22}(\Delta n|\eta_e, \eta_c)$ are more sensitive to the variation of η_e when η_e is small, that is $\eta_e \approx 0.2$, where saturation began to occur, and after that they become less sensitive to the variation of η_e as shown in Fig. 5.6.

10. For the given values of $\Delta n = 0$ and $\eta_e = 0$, the average values of the fluxes as a function of η_c obey that: $\eta_{12}(\Delta n = 0|\eta_e = 0, \eta_c) < \eta_{22}(\Delta n = 0|\eta_e = 0, \eta_c)$ and as $\eta_e \to 1.0$, we have $\eta_{12}(\Delta n = 0|\eta_e = 1.0, \eta_c) > \eta_{22}(\Delta n = 0|\eta_e = 1.0, \eta_c)$.

11. For the given values of $\Delta n = 0$ and $\eta_c = 0$, the average values of the fluxes as a function of η_e obey that: $\eta_{12}(\Delta n = 0|\eta_e, \eta_c = 0) > \eta_{22}(\Delta n = 0|\eta_e, \eta_c = 0)$ and as $\eta_c \to 1.0$, we have $\eta_{12}(\Delta n = 0|\eta_e, \eta_c = 1.0) < \eta_{22}(\Delta n = 0|\eta_e, \eta_c = 1.0)$.

12. For the given values of $\Delta n = -1.0$ and η_e or η_c, the average values of the fluxes as a function of η_e or η_e obey that: $\eta_{12}(\Delta n = -1.0\ \mu M|\eta_e, \eta_c) < \eta_{22}(\Delta n = -1.0\ \mu M|\eta_e, \eta_c)$ for all possible values of η_e and η_c.

13. For the same given values of Δn, η_e, η_c and transition rates, a nano-channel with a single internal potential well is more permeable to particles than that with two internal potential wells.

14. The rate of translocation of particles through a nano-channel with a single internal potential well is greater than that with two internal potential wells.

15. When $\eta_e = 0$ and $\eta_c = 0$, both fluxes are zero and when η_e and η_c are slightly greater than zero, the average fluxes assume large values as shown in Fig. 5.18. As η_e and η_c increase to higher values, that is $\eta_e = 0.95$ and $\eta_c = 0.95$ both fluxes decrease and finally become zero when $J_1(\Delta n|\eta_e = 1.0, \eta_c = 1.0) = J_2(\Delta n|\eta_e = 1.0, \eta_c = 1.0) = 0$.

16. Therefore, the nano-channel becomes totally impermeable or totally inactivated when $\eta_e = 0$ and $\eta_c = 0$ and $\eta_e = 1.0$ and $\eta_c = 1.0$.

17. The average particle fluxes assume maximum saturation values when $J_1(\Delta n \to 1\ M|\eta_e = 1.0, \eta_c = 0) = 67.6674^{-1}$ and $J_2(\Delta n \to 1\ M|\eta_e = 1.0, \eta_c = 0) = 33.8338 s^{-1}$, which implies that the nano-channel is fully activated and hence

the rate of translocation of particles through the nano-channel is maximum.

18. Therefore, the gate of a nano-channel is fully open to conduct particles in the positive direction when $\eta_e = 1.0, \eta_c = 0$.

19. Both $J_1(\Delta n|\eta_e, \eta_c)$ and $J_2(\Delta n|\eta_e, \eta_c)$ increase rapidly, saturate quickly to different saturation values and become parallel to each other in the small range of the concentration gradient Δn as shown in Fig. 5.18 to Fig. 5.20. This property reflects the fact that a rapid process occurs that changes the gate of the nano-channel from fully being closed state to fully being open open state.

20. Both average particle fluxes, $J_1(\Delta n|\eta_e, \eta_c)$ and $J_2(\Delta n|\eta_e, \eta_c)$, are more sensitive to the variation of the value of Δn in the small range and as Δn increases to higher values the quickly saturate to maximum positive values after which the fluxes become less sensitive to the variation of Δn.

21. For all possible given values of Δn and η_e, the average particle fluxes $J_1(\Delta n|\eta_e, \eta_c)$ and $J_2(\Delta n|\eta_e, \eta_c)$ are monotonically decreasing functions of η_c and as $\eta_c \rightarrow 0$ both fluxes assume maximum positive values which implies that the nano-channel behaves as if its gate is fully open and hence the rate of translocation of particles through the nano-channel is maximum.

22. For all possible given values of $\Delta n > 0$ and η_c, the average particle fluxes $J_1(\Delta n|\eta_e, \eta_c)$ and $J_2(\Delta n|\eta_e, \eta_c)$ are monotonically increasing functions of η_e.

23. For the given value of $\Delta n > 0$, the average particle fluxes $J_1(\Delta n|\eta_e, \eta_c)$ and $J_2(\Delta n|\eta_e, \eta_c)$ as functions of η_e become saturated at a small value of η_e when $\eta_c \rightarrow 0$ and the value of η_e at which $J_1(\Delta n|\eta_e, \eta_c)$ and $J_2(\Delta n|\eta_e, \eta_c)$ become saturated increases as η_c increases and finally when $\eta_c \rightarrow 1.0$, the saturation value of η_e becomes maximum.

24. As the value of the concentration gradient increases, the value of η_e at which the fluxes $J_1(\Delta n|\eta_e, \eta_c)$ and $J_2(\Delta n|\eta_e, \eta_c)$ as functions of η_e become saturated decreases as shown in Fig. 5.22 and Fig. 5.25.

25. For the values of η_e less than their saturation values both $J_1(\Delta n|\eta_e,\eta_c)$ and $J_2(\Delta n|\eta_e,\eta_c)$ increases rapidly and are thus more sensitive to the variation of η_e in that small range.

26. When η_e increases to its saturation values both $J_1(\Delta n|\eta_e,\eta_c)$ and $J_2(\Delta n|\eta_e,\eta_c)$ become saturated to their maximum positive values which implies that the nano-channel behaves as if its gate is fully open and hence the rate of translocation of particles through the nano-channel is maximum and after saturation both fluxes are less sensitive to the variation η_e.

27. For the given possible value of $\Delta n > 0$, the fluxes $J_1(\Delta n|\eta_e,\eta_c)$ and $J_2(\Delta n|\eta_e,\eta_c)$ as functions of η_e coincide with each other as $\eta_c \rightarrow 1.0$ as shown in Fig. 5.24.

28. For the given possible values of $\Delta n = 0$ and η_c, the fluxes as a function of η_e obey that: $J_1(\Delta n = 0|\eta_e,\eta_c = 0) > J_2(\Delta n = 0|\eta_e,\eta_c = 0)$ for all possible values of η_e and as $\eta_c \rightarrow 1.0$, we see that $J_2(\Delta n = 0|\eta_e,\eta_c = 1.0) > J_1(\Delta n = 0|\eta_e,\eta_c = 1.0)$ in the entire range $0 < \eta_e < 1.0$ and both become negative as shown in Fig. 5.28.

29. For the given possible values of $\Delta n = -0.99$ and η_c, the fluxes as a function of η_e obey that: $J_1(\Delta n = -0.99|\eta_e,\eta_c = 0) > J_2(\Delta n = -0.99|\eta_e,\eta_c = 0)$ for all possible values of η_e and as $\eta_c \rightarrow 1.0$, we see that $J_2(\Delta n = -0.99|\eta_e,\eta_c = 1.0) > J_1(\Delta n = -0.99|\eta_e,\eta_c = 1.0)$ in the entire range $0 < \eta_e < 1.0$ as shown in Fig. 5.31.

Bibliography

[1] Gerhard Schwarz, et al, On translocation through membrane channels via an internal binding site: Kinetics and voltage dependence, Biophys. J. 84, 2990-2998 (2003)

[2] Anatoly B. Kolomeisky, Channel facilitated molecular transport across membrane attraction, repulsion and asymmetry, Phys. Rev. Lett. 98, (2007)

[3] P.C. Bressloff and J.M. Newby, Stochastic models of intracellular transport, Rev. Mod. Phys. 85,135-196 (2013)

[4] Joan Kosztin and Klaus Schulten, Fluctuation driven molecular transport through an asymmetric membrane channel, Phys. Rev. Lett. 93, 238102 (2004)

[5] Alexander M. Berezhkovsii and Sergey M. Bezrukove, Optimizing transport of Metabolites through large channels: Molecular sieves with and without binding, Biophys. Lett. L17-L19 (2005)

[6] Alexander M. Berezhkovsii and et al, Channel facilitated membrane transport: Transit probability and interaction with the channel J. Chem. Phys 116, 22 (2002)

[7] Kullman, L., M. Winterhalter, and S. M. Bezrukov. 2002. Transport of maltodextrins through maltoporin: a single channel study. Biophys. J. 82:803812.

[8] J.W. Hous Diffusion in regular and disordered lattices, Physsics reports, 150, No. 5/6, 263-416 (1987)

[9] Peter Hanggi and et al, Reaction-rate theory: fifty years after Kramers, Rev. Mod. Phys. , Vol. 62, No. 2, 1990

[10] S. KH. Aityan, Single-File Diffusion of Uncharged Particles, Gen. Physiol. Biophys. (1985), 4,314

[11] Dani, J. A, and D. G. Levitt, Diffusion and kinetic approaches to describe permeation in ionic channels J. Theor. Biol. 146: 289-301, 1990.

[12] Nara Guisoni and et al. The lattice model for calcium dynamics, Phys. Rev. E, 71, 061910 (2005)

[13] Alan Gabel and et al, Facilitated asymmetric exclusion, Phys. Rev. Lett. 19, 210603 (2010)

[14] A. Parmeggiani and et al, Phase coexistence in driven one dimesional transport, Phys. Rev. Lett. 90, 8 (2003)

[15] Sheldon Katz, Joel Lebowitz, and Herbert Spohn, Nonequilibrium steady states of stochastic lattice gas models of fast ionic conductors, J. Stat. Phys. Vol. 34, Nos. 3, 1984

[16] B. Derrida, E. Domany, and D. MukameP, An Exact Solution of a One-Dimensional Asymmetric Exclusion Model with Open Boundaries, J. Stat. Phys. Vol. 69, Nos. 3/4, 1992

[17] Hangjun Lu and et al. Controllable transport of water through nanochannel by rachet-like mechanism, J. Chem. Phys. 136, 174511 (2012)

[18] A. A. Gurtovenko and I. Vattulainen, calculation of the electrostatic potential of lipid bilayers from molecular dynamics simulation, J. Chem. Phys. 130, 215107 (2009)

[19] Andrey A. Gurtovenko and Ilpo Vattulainen, Lipid Transmembrane Asymmetry and Intrinsic Membrane Potential: Two Sides of the Same Coin, J. AM. CHEM. SOC. Vol. 129, NO. 17, 2007, 5358-5359

[20] Andrey A. Gurtovenko and Ilpo Vattulainen, Intrinsic Potential of Cell Membranes: Opposite Effects of Lipid Transmembrane Asymmetry and Asymmetric Salt Ion Distribution, J. Phys. Chem. B 2009, 113, 71947198

[21] D. Peter Tieleman, Computer simulations of transport through membranes: passive diffusion, pores, channels and transporters, Proceedings of the Australian Physiological Society (2006) 37, 15-27

[22] Hwang, Schatz, and Ratner, Kinetic lattice grand canonical Monte Carlo simulation for ion current calculations in a model ion channel system, J. Chem. Phys. 127, 024706 (2007)

[23] Wolfgang R.Baur and Walter Nadler, Molecular transport through channels and pores: effects of in-channel interactions and blocking, PNAS,August 1, 2006, Vol. 103, no. 31

[24] J Zhang, A. Kamenev, and B.I. Shklovskii, Conductance of ion channels with charged walls: A toy model, Phys. Rev. Lett. PRL. 95, 148101 (2005)

[25] R Dean Astumian Peter Hanggi, Brownian motors, Physics Today 33, 2002

[26] G Lattanzi and A Maritan, Master equation approach to molecular motors, arXiv:cond-mat/0108427 v1, 27 Aug. 2001

[27] Kohler, HL-H, and K. Hec 1979. Unidirectional fluxes in saturated single-file pores of biological and artificial membranes. I Pores containing no more than one vacancy. J. Theor. Biol. 79381-401.

[28] Kohler, H. H., and K. Heckmann. 1980. Unidirectional fluxes m saturated e-file pores of biological and artificial membrane IL Asymptotic behavior at high degrees of saturation J. Theor. Biol. 85-575-595.

[29] Schultz, S. G. 1980. Basic Principles of Membrane Transport, Cambridge University Press, Cambridge. 33-41, 85, 95, 96.

[30] Schumaker, M. F., and R. MacKinnon 1990. A simple model for multi-ion permeation. Single-vacancy conduction in a simple pore model, Biophys. J. 58:975-984.

[31] Stein, W. D. 1986. Transport and Diffusion across Cell Membranes. Academic Press, Orlando, FL. 337-361,613-616.

[32] Walmsley, A. R. 1988. The dynamics of the glucose transporter. TIBS. 13:226-231.

[33] Heckmann K. (1965): Zur Theorie der "Single-File" Diffusion. Z. Physik. Chem. Neue Folge 46, 1-10

[34] Heckmann K. (1972): Sigle-file diffusion. In: Biomembranes, vol. 3: Passive Permeability of Cell Membranes (Ed. K. Kreuzer and F. G. Siegers), pp. 127153, Plenum Publishing Corp., New York

[35] Kohler H. H., Heckmann K. (1979): Unidirectional fluxes in saturated single-file pores of biological and artificial membranes. I. Pores containing no more than one vacancy. J. Theor. Biol. 79, 381401

[36] Markin V. S., Chizmadzhev Yu. A. (1974): Induced Ion Transport. Nauka, Moscow (in Russian) Received January 17, 1984, Accepted May 14, 1984

[37] R. M. Sok and H. J. C. Berendsen, Molecular dynamics simulation of the transport of small molecules across a polymer membrane,J. Chem. Phys., Vol. 96, No.6, 15 March 1992

[38] Aityan S. Kh., Chizmadzhev Yu. A. (1973): The theory of ion transport through the potassium channel of biomembranes. Dokl. Akad. Nauk SSSR 213, 14271430 (in Russian)

[39] Aityan S. Kh., Kalandadze I. L. (1977): The influence of Coulomb effects on the interactions between unidirectional fluxes in the potassium channel of biomembranes. Bioelechem. Bioenergetics 4, 4553

[40] Chizmadzhev Yu. A., Aityan S. Kh. (1977): Ion transport across sodium channels in biological membranes. J. Theor. Biol. 64, 429453

[41] Chizmadzhev Yu. A., Aityan S. Kh. (1982): Ion transport through the selective channels of biological membranes. In: Itogi Nauki i Tekhniki. Biofizika Membrn (Ed. P. G. Kostyuk), v. 2, pp. 581, Nauka, Moscow (in Russian)

[42] Thomas Fischer Weiss, Cellular Biophysics volume 1, MIT press, Cambridge, MA, 1995

[43] Thomas Fischer Weiss, Cellular Biophysics, volume 2, MIT press, Cambridge, MA, 1995

[44] Alwyn Scott, Neuroscience, A mathematical primer, Springer-Verlag, New York, 2002

[45] Peter Dayan and L.F. Abbott, Theoretical Neuroscience, 2000

[46] W.H. Philip C. Nelson, Biological Physics, Energy, Information, and Life, Freeman and Company, 2004

[47] Meyer B. Jackson, Molecular and cellular Biophysics, Cambridge University Press, 2006

[48] Handbook of Modern Biophysics, Fundamental Concepts in Biophysics, Volume I, Humana Press, 2009

[49] Structure and Biophysics, New Technologies for Current Challenges in Biology and Beyond, Erice Italy, 22 June - 3 July 2005, Springer, 2007

[50] Robert Plonsey and Roger C. Barr, Bioelectricity, A Quantitative Approach, Duke University Durham, North Carolina, USA, Third Edition, Springer, 2007

[51] Joel Keizer, Statistical Thermodynamics of Non-equilibrium Processes, Springer-Verlag, 1987

[52] Gerard D.C. Kuiken, Thermodynamics of Irreversible Processes, John Wiley and Sons, 1994,

[53] Mathematical Models in Biology Leah Edelstein-Keshet University of British Columbia Vancouver, British Columbia, Canada

[54] Voltage-Sensitive Ion Channels Biophysics of Molecular Excitability By H. RICHARD LEUCHTAG, 2008 Springer

[55] Sensing with Ion Channels, Springer Series in Biophysics 11, Boris Martinac Editor, 2008 Springer-Verlag Berlin Heidelberg

[56] Ionic Channels of Excitable Membranes, second edition, by Sinauer, Associates INC, 1992, USA

[57] THE ION CHANNEL FactsBook IV Voltage-Gated Channels, Edward C. Conley, William J. Brammar, Academic Press, LONDON, 1999